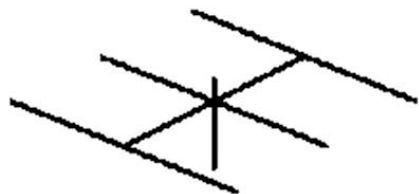
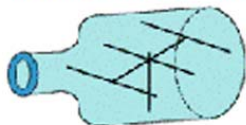


# Antenna Modeling Notes



**Volume 7**

*Final Volume of Series*



**L. B. Cebik, W4RNL**

---

# **Antenna Modeling Notes**

**Volume 7**  
***Final Volume of Series***

**L. B. Cebik, W4RNL**

---

---

***Published by  
antenneX Online Magazine***

**<http://www.antennex.com/>**

**POB 271229**

**Corpus Christi, Texas 78427-1229 USA**

---

---

Copyright 2010 by ***antenneX Online Magazine***. All rights reserved. No part of this book may be reproduced or transmitted in any form, by any means (electronic, photocopying, recording, or otherwise) without the prior written permission of the publisher.

ISBN: 1-877992-59-3

---

## Table of Contents

Preface-----	5
Chapter 133: AM BC Modeling with NEC III-----	7
Chapter 134: AM BC Modeling with NEC IV-----	25
Chapter 135: AM BC Modeling with NEC V-----	41
Chapter 136: AM BC Modeling with NEC VI-----	70
Chapter 137: NEC Implementations, Cores, Limits and Work-Arounds-----	87
Chapter 138: Types of Substitute Models-----	103
Chapter 139: Antenna Matching with EZNEC Version 5: Part 1-----	125
Chapter 140: Antenna Matching with EZNEC Version 5: Part 2-----	148
Chapter 141: Circular R-X Graphs-----	171
Chapter 142: VOACAP Type 13 Files-----	193
Chapter 143: Modeling Radiating Surfaces-----	217
Chapter 144: Receiving Directivity-----	243
Chapter 145: Serial Feedline Connections-----	259
Chapter 146: Unequal Serial Feedline Connections-----	281
Chapter 147: Warnings and Errors of NEC & What to Do-----	302
Other Publications-----	322

## Preface

This collection of antenna modeling notes continues the compilation of the series that I began in 1998 in *antenneX* at the suggestion and encouragement of the publisher, Jack L. Stone. This Volume 7 contains numbers 133 through 147 of the long-running series that continues even today. The time came to collect these columns into a more convenient form for the reader. There is just too much material for a single volume, so the collection is broken into numerous units. I have reviewed the text and graphics for each column to ensure as much accuracy as I can muster. I have also reviewed the sample models used in each column. That process permitted me to add something to these volumes that is not available in *antenneX* or at my own web site. Some models require elements of the command set not included in entry-level programs such as EZNEC. Others require NEC-4

At the time of writing some of the columns, reference was made to the use of NEC-Win Plus for some of the models presented. However, since then, software maker Nittany-Scientific appears to have drifted into a state of instability and with an unknown future. The reader should not rely on the use of that software referred to herein. The software was written for MS Win95, but appeared to work okay through MS Win2k. MS operating systems later than Win2k are known to have issues with NSI software. It is not compatible with VISTA at all as of this writing and has not been tested with the recent Windows 7.

Along the way, we shall explore some basic NEC calculations, including electric fields at a distance. We shall also learn how to supplement NEC calculations by using its output data to arrive at circular gain. Finally, we shall explore the relationship between the EX command and the PT command for special receiving-mode models. The NEC-2 and NEC-4 manuals provide fundamental collections of sample models designed to illustrate in the most compact way possible as many NEC features as possible. These models appear only in print form. In this volume, we shall examine the models, and the model collection will include them in .NEC format.

The adequacy of our models is, as it should be, a continuing challenge. Therefore, we shall revisit the convergence test with particular reference to its use with NEC. In addition, we shall take a look at some of the correctives that we use to work around some of the core's limitations. However, finding limitations and faults is not our goal. Rather, the goal is to make effective use of the program. Toward that end, we shall look at a techniques that will let us in NEC-2 handle insulated wires in a way that is comparable to the IS command in NEC-4. We shall also examine the various ground calculation systems that appear in NEC (and MININEC) software.

Although the list of topics seems to grow more advanced and complete, the appearance is an illusion. The command set is far too large for full coverage even in 4 volumes. As well, good antenna simulations depend as much on the ingenuity of modelers as they do on simply knowing how to apply various commands. Hence, the list of techniques by which to improve our models may well be endless. Mastering antenna modeling software has a further benefit: the use of the software to educate ourselves on the capabilities of various types of antennas. If we add this dimension of the use of NEC and MININEC to further mastery of the command structures and additional modeling techniques, then we may fairly predict that the series is far from its final episode.

***ED: L.B. Passed away in April 2008, but is immortalized in his writings.***

## Chapter 133: AM BC Modeling with NEC

### 3. The Long and the Short of It

Our examination of the use of NEC in modeling towers intended for AM BC service rests on the foundation that the desired ground for such structures is a perfectly reflecting surface. All field-strength measurements are predicated on this ground, used for various theoretical reasons of considerable historical interest. So far, we have examined the steps required to obtain from the NEC modeling core the same results obtained from selected MININEC programs. In addition, we have looked for differences that may exist between models that use the NEC-recommended single-wire substitute towers and those using to one or another degree relatively completely detailed tower structures.

For a certain class of towers, the substitutes and the more detailed geometries showed either a remarkably good correlation or deviations that we could not ascribe to a single cause due to slight deviations from the ideal Average Gain Test (AGT) score. The class of towers included only resonant or near resonant towers, considering the 1-MHz design frequency and the use of lossless conductors. Whether the close correlations hold for other tower lengths remains indeterminate, at least within this sequence of notes.

In this portion of our trek through the maze of towers, we shall explore the consequences of modeling towers having considerable, but not radical amounts of, reactance. We shall begin by going long, using a standard FCC length of 273' for a so-called 90-degree

tower. Then we shall try a short tower, only 201' high. Both towers show source reactance values well above 50 Ohms, but much less than 100 Ohms. The heights are arbitrary with respect to the degree to which each departs from resonance. However, both heights are divisible by 3, setting the length of the sections into which we shall subdivide them for one type of model.

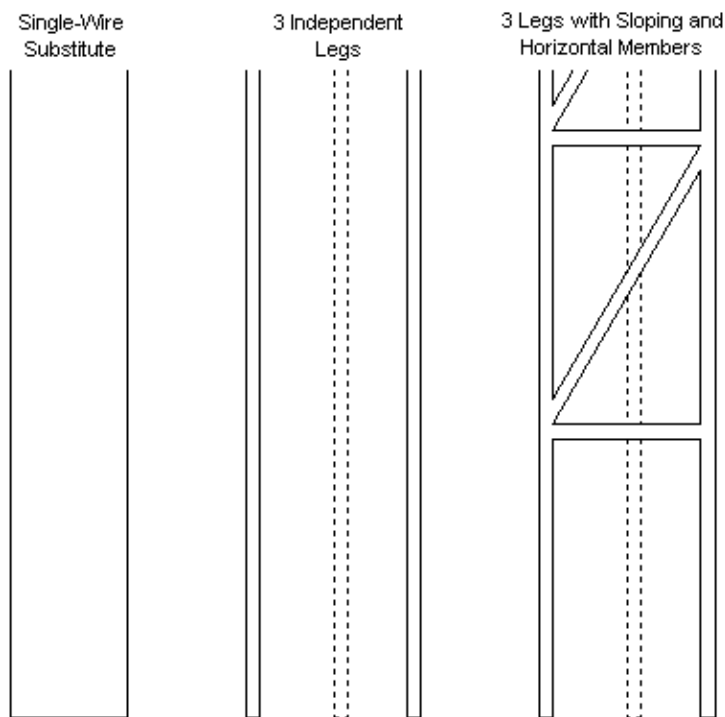


Fig. 1

Tower Types Used in This Episode



In each case, we shall look at three model types, as shown in **Fig.**

**1.** One will use the single-wire substitute model using NAB recommended diameter adjustment factors. In fact, all of the towers in this episode will presume a face width of 18" or 1.5'. The required radius is 0.37 times the face width or 0.555'. The second type of tower will use three legs only, with separate sources for each leg to simplify both the model and its viewing within software facilities (in this case, GNEC). As in past episodes, the leg diameter will be 2", that is, a radius of 0.085'. The third type of tower will show both horizontal and sloping members, except for the lowest section, which will include only horizontal members at the top of the section. Like the legs, the horizontal and sloping members will use 2"-diameter wires. Each vertical tower section will be 3' high, and we may use the GM command to replicate the necessary upper sections beyond the second one, which is the first to use a complete structure.

The three tower types will provide a sufficient basis for comparing the results with those we obtained in the preceding notes for similar tower structures.

## **A 273' 18"-Face Tower**

At 1 MHz, a 90-degree tower is 273' high. This tower is nearly 40' taller than the resonant 24"-face tower that we used as our sample earlier. We expect to derive at least two easily predictable results. First, the source impedance will be inductively reactive. Second, the tower gain and field-strength values will be a bit higher than the

5.15-dBi and 275 mV/m values that we obtained at a nearly resonant length.

The single-wire model requires no change in segmentation, since the length increase does not significantly increase the length of each of the 41 segments. With a current source, the following lines show the model file.

```
CM 90-degree monopole, perfect ground
CM NAB substitute single-wire monopole
CE
GW 1 41 0 0 0 0 0 273 0.555
GW 30901 1 9901.0000 9901.0000 9901.0000 9901.0001 9901.0001 9901.0001 .00001
GS 0 0 .3048
GE 1 0 0
GN 1
EX 0 30901 1 0 0.0 5.761
NT 30901 1 1 1 0 0 0 1 0 0
FR 0 1 0 0 1 1
RP 0 181 1 1000 -90 0 1.00000 1.00000
RP 1 1 1 0000 0 0 1.00000 1.00000 1609.344
EN
```

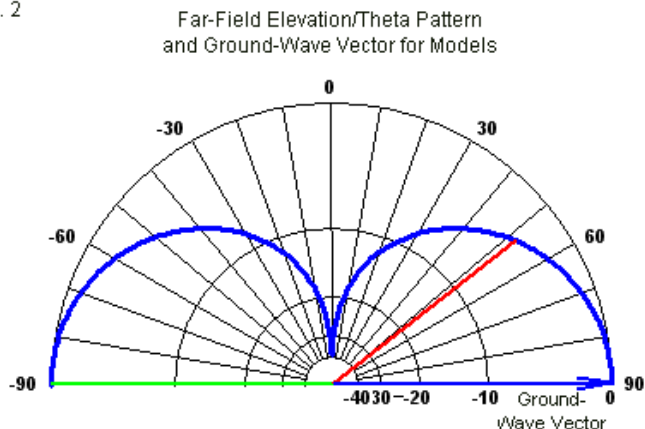
The excitation line indirectly shows the current level necessary to provide a 1-kW power level at the new tower height and source impedance. A simple table shows the critical values, at least relative to these simplified exercises.

#### 273' Single-Wire Monopole Model Data

Impedance (Ohms)	Current (Apk)	Gain (dBi)	AGT	AGT-dB	F-S @ 1 mile
60.27 + j84.91	5.761	5.30	1.999	0.00	280.0 mV/m @ -47.7 deg

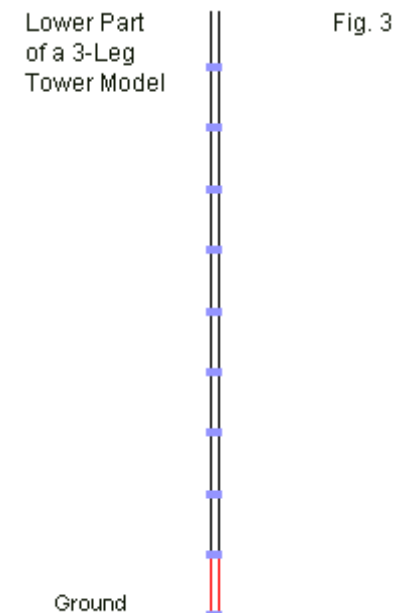
The impedance magnitude is double the value of the resonant tower, resulting in a significantly lower current (7.45 A for the resonant tower). The gain is up about 0.15 dB, while the field-strength is about 5 mV/m higher. As a reminder, the model requests the ground wave, including both surface and sky wave components at ground ( $Z=0$ ) level. **Fig. 2** outlines the pattern and the relevant vector. The distance is 1 mile. In practice, of course, the modeler can select any height and distance (in meters) as the observation point.

Fig. 2



One alternative to using the substitute single-wire tower is to model 3 independent legs, each with its own source. The method of combining sources by using a distant short, thin wire and 3 transmission-lines of near-zero length is always available for this and the next model. However, we shall use the separate-source

method, since it allows us to view tower model details more easily in the software (GNEC) facilities. In fact, **Fig. 3** shows the lower part of the alternative model, with one tower leg hidden.



Except for tripling the number of wires, sources, and networks, the model is not much more complex than the single-wire model. Since the face dimension of the triangular tower is smaller than for the models in the preceding episode, the X and Y coordinates have changed to place the coordinate center at the mid-tower position.

```

CM 90-deg 3-leg monopole, perfect ground
CM 3 sources
CE
GW 1 41 0.866 0 0 0.866 0 273 0.085
GW 2 41 -0.433 .75 0 -0.433 .75 273 0.085
GW 3 41 -0.433 -.75 0 -0.433 -.75 273 0.085
GW 30901 1 9901.0000 9901.0000 9901.0000 9901.0001 9901.0001 9901.0001 .00001
GW 30902 1 9902.0000 9902.0000 9902.0000 9902.0001 9902.0001 9902.0001 .00001
GW 30903 1 9903.0000 9903.0000 9903.0000 9903.0001 9903.0001 9903.0001 .00001
GS 0 0 .3048
GE 1
GN 1
EX 0 30901 1 0 0.0 1.9217
EX 0 30902 1 0 0.0 1.9217
EX 0 30903 1 0 0.0 1.9217
NT 30901 1 1 1 0 0 0 1 0 0
NT 30902 1 2 1 0 0 0 1 0 0
NT 30903 1 3 1 0 0 0 1 0 0
FR 0 1 0 0 1 1
RP 0 181 1 1000 -90 0 1.00000 1.00000
RP 1 1 1 0000 0 0 1.00000 1.00000 1609.344
EN

```

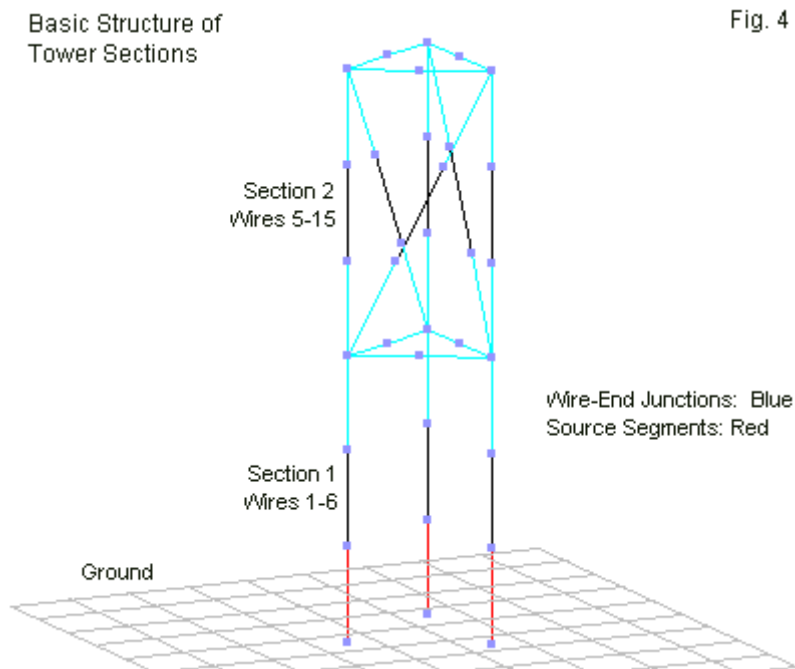
In the earlier models, 3 independent legs yielded data values that closely correlated to the single-wire values. As the data table shows, the situation does not change much when we lengthen the tower to 273'.

#### 273' 3-Leg Monopole Model Data

Impedance (Ohms)	Current (Apk)	Gain (dBi)	AGT	AGT-dB	F-S @ 1 mile
60.17 + j83.97	1.9217/leg	5.30	1.999	0.00	280.0 mV/m @ -47.8 deg

The resistive component of the impedance is within 0.1-Ohm of the single-wire model, while the reactance report differs by just under 1 Ohm. Multiplying the current-per-leg by 3 gives us 5.765 Apk at 1 kW, an increase of 4 mA. In short, the data for the two models does not diverge significantly.

The full-structure simulation in the preceding episode used 2' vertical tower sections. For the present models, 3' sections are arithmetically more convenient. Each vertical and sloping member uses 3 segments, while the horizontal cross members use 2 segments. This procedure equalizes segments length to the degree possible within the model without unnecessarily multiplying the segment count. **Fig. 4** shows the basic structure, using only the lower section and the second section of the much taller tower.



The leg and other element diameters and X-Y coordinates are the same as in the model with 3 independent legs. To complete the full 273' of the tower, we must use the GM command to replicate the second section 89 more times. Including the remote source wires, the model contains 819 wires and 2178 segments.

```

CM 90-deg 3-leg monopole, perfect ground
CM 3 sources
CM 117 sections with cross braces
CE
GW 1 3 0.866 0 0 0.866 0 3 0.085
GW 2 3 -0.433 .75 0 -0.433 .75 3 0.085
GW 3 3 -0.433 -.75 0 -0.433 -.75 3 0.085
GW 4 2 0.866 0 3 -0.433 .75 3 0.085
GW 5 2 -0.433 .75 3 -0.433 -.75 3 0.085
GW 6 2 -0.433 -.75 3 0.866 0 3 0.085
GW 7 3 0.866 0 3 0.866 0 6 0.085
GW 8 3 -0.433 .75 3 -0.433 .75 6 0.085
GW 9 3 -0.433 -.75 3 -0.433 -.75 6 0.085
GW 10 2 0.866 0 6 -0.433 .75 6 0.085
GW 11 2 -0.433 .75 6 -0.433 -.75 6 0.085
GW 12 2 -0.433 -.75 6 0.866 0 6 0.085
GW 13 3 0.866 0 3 -0.433 .75 6 0.085
GW 14 3 -0.433 .75 3 -0.433 -.75 6 0.085
GW 15 3 -0.433 -.75 3 0.866 0 6 0.085
GM 9 89 0 0 0 0 0 3 7 1 15 3
GW 30901 1 9901.0000 9901.0000 9901.0000 9901.0001 9901.0001 9901.0001 .00001
GW 30902 1 9902.0000 9902.0000 9902.0000 9902.0001 9902.0001 9902.0001 .00001
GW 30903 1 9903.0000 9903.0000 9903.0000 9903.0001 9903.0001 9903.0001 .00001
GS 0 0 .3048
GE 1
GN 1
EX 0 30901 1 0 0.0 1.8857
EX 0 30902 1 0 0.0 1.8857
EX 0 30903 1 0 0.0 1.8857
NT 30901 1 1 1 0 0 0 1 0 0
NT 30902 1 2 1 0 0 0 1 0 0
NT 30903 1 3 1 0 0 0 1 0 0
FR 0 1 0 0 1 1
RP 0 181 1 1000 -90 0 1.00000 1.00000
RP 1 1 1 0000 0 0 1.00000 1.00000 1609.344
EN

```

Like the resonant tower in the earlier exercises, the data for the full-structure model at 273' shows numerically noticeable differences relative to the simpler models.

#### 273' Full-Structure Monopole Model Data

Impedance (Ohms)	Current (Apk)	Gain (dBi)	AGT	AGT-dB	F-S @ 1 mile
62.49 + j86.20	1.8857/leg	5.40	2.043	0.09	283.2 mV/m @ -48.8 deg

The reported gain is about 0.1-dB high relative to the models with nearly ideal AGT scores. The field-strength report is also high. The AGT-dB value provides a means to correcting the gain report. It answers to a simple conversion equation:  $\text{AGT-dB} = 10 \log(10)(\text{AGT}/2)$ . (Note: when using the AGT test in free space, do not use the /2 portion of the equation.) A positive AGT-dB value shows by how much the gain report in dBi is high. The more nearly correct gain is simple the reported gain minus the AGT-dB value. To arrive at a more nearly correct field-strength value divide the reported value by  $\text{SQRT}(\text{AGT}/2)$  (again, omitting the /2 portion for AGT values taken in free space). The calculated correct value for the peak field-strength is 280.2 mV/m. This value is within 0.2 mV/m of the values shown for the simpler models.

The impedance components of the full-structure model are within about 2 Ohms of the values shown in the simpler models. For reference, a MININEC model of the substitute single-wire model showed a gain of 5.29 dBi, with a source impedance of 62.29 + 85.96 Ohms. All of the values within this collection of models are tightly grouped. Whether the differences reach the level of being



significant is driven by the specifications brought to the modeling enterprise.

## A 201' 18"-Face Tower

In most respects, modeling the tower that is shorter than resonant will be identical in procedure to modeling either a resonant or a long tower. For visual details, refer to the figures already shown in the first part of this exercise and in preceding exercises. Our interest will lie almost wholly with the models themselves and with the data that they report.

A 201' tower with an 18" triangular face width requires only one change when using the single-wire substitute with the NAB recommended radius (0.555'). Only the Z-coordinate for the upper end changes. The use of 41 segments in no way presses any NEC limits or recommendation. Therefore, we obtain a model like the following one.

```
CM 201' monopole, perfect ground
CM NAB substitute single-wire monopole
CE
GW 1 41 0 0 0 0 0 201 0.555
GW 30901 1 9901.0000 9901.0000 9901.0000 9901.0001 9901.0001 9901.0001 .00001
GS 0 0 .3048
GE 1 0 0
GN 1
EX 0 30901 1 0 0.0 9.3772
NT 30901 1 1 1 0 0 0 1 0 0
FR 0 1 0 0 1 1
RP 0 181 1 1000 -90 0 1.00000 1.00000
RP 1 1 1 0000 0 0 1.00000 1.00000 1609.344
EN
```

For this model using perfect wire and perfect ground, we obtain the following data as a starting point in our comparisons.

201' Single-Wire Monopole Model Data

Impedance (Ohms)	Current (Apk)	Gain (dBi)	AGT	AGT-dB	F-S @ 1 mile
22.75 - j70.37	9.3722	5.04	1.999	0.00	271.8 mV/m @ -44.4 deg

Although the precise numbers might not be predictable, their general range certainly meets expectations. The resistive component of the impedance is only about 2/3 of the resonant value and about 1/3 of the value for the long tower. The reactive component is capacitive and significant. The lower impedance requires a higher current (given in peak Amps) at the source for a constant power level of 1 kW. The AGT score is close enough to ideal that it does not require any correction of the gain value, which is lower than the value for a resonant tower due to the lesser height of our present tower. Since the gain is lower, the field-strength reading (given in peak mV/m) is also lower than for either resonant or the long tower. (Multiply the field strength by 0.7071 to obtain the RMS value.)

The single-wire model corresponds to the left hand sketch in **Fig. 1**. Our interest from a modeling perspective is the correlation of the data collection with alternative models, such as the center sketch of a 3-leg tower, where each leg is independent and we use 3 sources to feed the assembly. As we have done in previous sketches from the single-wire to 3-leg towers, we shall use 2"-diameter legs (0.085' radius) and retain the 41 segments for each leg. The triangle for the tower is 18" (1.5') on a side, and the model will

position the legs so that the coordinate center falls at the midpoint of the triangle of legs.

```
CM 201' 3-leg monopole, perfect ground
CM 3 sources
CE
GW 1 41 0.866 0 0 0.866 0 201 0.085
GW 2 41 -0.433 .75 0 -0.433 .75 201 0.085
GW 3 41 -0.433 -.75 0 -0.433 -.75 201 0.085
GW 30901 1 9901.0000 9901.0000 9901.0000 9901.0001 9901.0001 9901.0001 .00001
GW 30902 1 9902.0000 9902.0000 9902.0000 9902.0001 9902.0001 9902.0001 .00001
GW 30903 1 9903.0000 9903.0000 9903.0000 9903.0001 9903.0001 9903.0001 .00001
GS 0 0 .3048
GE 1
GN 1
EX 0 30901 1 0 0.0 3.1298
EX 0 30902 1 0 0.0 3.1298
EX 0 30903 1 0 0.0 3.1298
NT 30901 1 1 1 0 0 0 1 0 0
NT 30902 1 2 1 0 0 0 1 0 0
NT 30903 1 3 1 0 0 0 1 0 0
FR 0 1 0 0 1 1
RP 0 181 1 1000 -90 0 1.00000 1.00000
RP 1 1 1 0000 0 0 1.00000 1.00000 1609.344
EN
```

Once we are satisfied with the model structure, we may turn to the data.

#### 201' 3-Leg Monopole Model Data

Impedance (Ohms)	Current (Apk)	Gain (dBi)	AGT	AGT-dB	F-S @ 1 mile
22.69 - j70.20	3.1298/leg	5.04	1.999	0.00	271.8 mV/m @ -44.4 deg

The gain, field-strength, and AGT data are all identical to the values derived from the single-wire model. The total current is the sum for 3 legs or 9.389 Apk. The impedance reports for the two models are well within a quarter-Ohm of each other. Obviously, the single-wire and the 3-leg model (using independent legs) correlate extremely well no matter what standard we apply to them.

The most complex full-structure model uses the same basic sections as we used for the long tower: 3' sections using 3 segments for each vertical and sloping member and 2 segments for the horizontal members. All wires use a 2" diameter. The lowest section omits the sloping members to avoid unwanted current divisions at the point where the source segments meet the ground. We replicate the full 9-wire second section (as viewed in **Fig. 4**) the number of times necessary to reach the final tower height. 201' as a sample tower height is convenient, since it divides nicely into 3' sections. Beyond the second section, we require 65 replications at 3' intervals using the GM command on just the wires of the second section.

```
CM 201' 3-leg monopole perfect ground
CM 3 sources
CM 67 sections with cross braces
CE
GW 1 3 0.866 0 0 0.866 0 3 0.085
GW 2 3 -0.433 .75 0 -0.433 .75 3 0.085
GW 3 3 -0.433 -.75 0 -0.433 -.75 3 0.085
GW 4 2 0.866 0 3 -0.433 .75 3 0.085
GW 5 2 -0.433 .75 3 -0.433 -.75 3 0.085
GW 6 2 -0.433 -.75 3 0.866 0 3 0.085
GW 7 3 0.866 0 3 0.866 0 6 0.085
GW 8 3 -0.433 .75 3 -0.433 .75 6 0.085
GW 9 3 -0.433 -.75 3 -0.433 -.75 6 0.085
GW 10 2 0.866 0 6 -0.433 .75 6 0.085
GW 11 2 -0.433 .75 6 -0.433 -.75 6 0.085
GW 12 2 -0.433 -.75 6 0.866 0 6 0.085
GW 13 3 0.866 0 3 -0.433 .75 6 0.085
GW 14 3 -0.433 .75 3 -0.433 -.75 6 0.085
GW 15 3 -0.433 -.75 3 0.866 0 6 0.085
GM 9 65 0 0 0 0 0 3 7 1 15 3
GW 30901 1 9901.0000 9901.0000 9901.0000 9901.0001 9901.0001 9901.0001 .00001
GW 30902 1 9902.0000 9902.0000 9902.0000 9902.0001 9902.0001 9902.0001 .00001
GW 30903 1 9903.0000 9903.0000 9903.0000 9903.0001 9903.0001 9903.0001 .00001
GS 0 0 .3048
GE 1
GN 1
EX 0 30901 1 0 0.0 3.1729
EX 0 30902 1 0 0.0 3.1729
```

```

EX 0 30903 1 0 0.0 3.1729
NT 30901 1 1 1 0 0 0 1 0 0
NT 30902 1 2 1 0 0 0 1 0 0
NT 30903 1 3 1 0 0 0 1 0 0
FR 0 1 0 0 1 1
RP 0 181 1 1000 -90 0 1.00000 1.00000
RP 1 1 1 0000 0 0 1.00000 1.00000 1609.344
EN

```

From this model, we obtain an interesting data collection.

#### 201' Full-Structure Monopole Model Data

Impedance (Ohms)	Current (Apk)	Gain (dBi)	AGT	AGT-dB	F-S @ 1 mile
22.07 - j62.14	3.1729/leg	5.14	2.043	0.09	274.8 mV/m @ -44.7 deg

The AGT score--in both forms--for this model is the same as for the full-structure version of the long tower. Hence, we find a gain figure that is too great compared to the other models. If we subtract the AGT-dB value from the reported gain, the value falls into line with the other model reports. The field-strength is also too large. However, if we divide it by the square root of half the basic AGT value, we obtain 271.9 mV/m (pk), a value that again is in line with the reports from models with more nearly ideal AGT values.

The source impedance report is perhaps the most interesting item in the collection. The resistive component is within about a half-Ohm of the other reports. However, the reactive component is about 8 Ohms lower. The amount of variance from the other models is not correctable by usual techniques--at least not to a degree that brings the value into alignment with the values derived from the other two short-tower models. Whether the source impedance variations represent anything significant remains a judgment that requires reference to the overall task within which we

do modeling of this order. If the variation is significant, the models do not tell us clearly which values to use, since the model with the deviant figures also has a slightly non-ideal AGT value. If the difference is not significant, then we need not--except perhaps for curiosity--use a full structure model with its increased wire (603) and segment (1602) counts.

## **Conclusion**

Our collection of models does show some interesting trends. Using the AGT and AGT-dB values, we may correct the gain and field-strength reports of the full-structure models to coincide very tightly with the reports from the simpler models. Only the trends in the source impedance variations remain for exploration. To explore these trends, I revised the models in the last episode to reflect the structure used in the present models. The key difference is the use of an 18" triangle face width, down from the 24" value used earlier. As well, the full-structure model uses 3' sections, as described earlier in these notes. The 234' near-resonant height also divides nicely by 3. However, the thinner tower structure--at least in the simpler models, is about 0.5' shy of being a resonant length. We need not show the models involved, since we have already described the types of change required to move from one model to another of a different height. However, the data tables may prove instructive.

## Near Resonant (234') 18" Face Monopole Models: Data

Impedance (Ohms)	Current (Apk)	Gain (dBi)	AGT	AGT-dB	F-S @ 1 mile
Single-Wire Model					
35.65 - j 1.29	7.4897	5.14	1.999	0.00	275.1 mV/m @ -45.6 deg
3-Leg Model					
35.57 - j 1.61	2.4993/leg	5.14	1.999	0.00	275.1 mV/m @ -45.6 deg
Full-Structure Model					
35.47 + j 2.74	2.5029/leg	5.24	2.043	0.09	278.2 mV/m @ -46.2 deg

Within the range for the short through the long tower (201' to 273' at 1 MHz), the full-structure models show a rising deviation in the resistive impedance component from the simpler model values as we increase the tower height. The short full-structure tower is about 0.5-Ohm low. At resonance, the full-structure value is very close to equal, and at the greatest height in the collection, the resistive component is about 2 Ohms high. Three data points do not make a curve, but they may indicate a trend.

The reactive component of the source impedance of the full-structure models shows a seemingly more random set of fluctuations. The value for the tallest tower is only about 1 Ohm more inductive than the value reported by the simpler models. At a resonant height, the value is about 4 Ohms inductive compared to the counterpart models, while the shortest tower reports a reactance that is about 8 Ohms more capacitive than the other models.

As we have noted, it is not clear from the models themselves whether the trends and fluctuations are functions of the AGT deviation from the ideal or from the full structure itself. At each section start, we have a division of the current between the sloping

and the vertical members of the section, although the vertical leg shows anywhere from 2 to nearly 4 times the current magnitude that we find on the corresponding sloping member.

For some applications, the variations may be meaningful. In such cases, and within the limits of NEC recommendations for proper structuring of the model geometry, one may wish to employ models that come closer to the actual physical structure of a tower under study. The key geometry factors include the minimum segment length relative to the design frequency, the segment-length-to-radius ratio, and the angle of intersection between joining members of the structure. In all such cases, the modeler must carefully check the AGT score to ensure that the model remains within whatever limits one sets for maximum departure from an ideal score.

Although software makers provide some general guidance, the standards of acceptable deviation remain in the end a modeler responsibility based on the required degree of precision brought to the task. In all cases, where the AGT score indicates less than ideal values, the modeler should adjust the gain and the field-strength values accordingly.

In other applications, the variations among models may not be significant. In such cases, one may productively use the simpler models and bypass the tedious work of trying to capture every detail of structure that holds the tower legs together.



## Chapter 134: AM BC Modeling with NEC

### 4. Square, Sloping, and Tapered

All of the samples that we have explored in our journey through modeling AM BC towers over perfect ground have used triangular towers with a uniform face-width along the total length. These towers have served well in examining the correlations among the chief types of models: the NEC-recommended substitute single-wire version, the alternative of using 3 independent legs, and the full-structure models.

Although the triangular tower with a uniform face-width may be the most common sort of structure used, there are a number of other structures that we occasionally find. The notes in this episode work with a few of the non-standard tower shapes.

#### The Square Tower

The most notable alternative to a triangular tower is a square tower. We shall initially work with squares having a uniform face-width in order to correlate the results with past triangular towers that we have examined. Therefore, we shall use a face width of 18" (1.5') and a height of 234' at 1 MHz. As always we shall use lossless conductors and a perfect ground. As well, each model will use a current source, with its associated modeling requirement of an extra distant thin and short wire along with a network (NT) entry.

The simplest model consists of a single vertical wire with a single source. The NAB-recommend value for the wire radius is 0.56

times the face-width. For the 18" face of a square towers, the substitute wire requires a radius of 0.84' (10.08"). Except for the change of the radius, the single-wire 234' model, with 41 segments for the modeled wire, looks very much like the corresponding single-wire substitute model for a triangular tower.

```
CM near-resonant monopole, perfect ground, square (0.56)
CM NAB substitute single-wire monopole
CE
GW 1 41 0 0 0 0 0 234 0.84
GW 30901 1 9901.0000 9901.0000 9901.0000 9901.0001
9901.0001 9901.0001 .00001
GS 0 0 .3048
GE 1 0 0
GN 1
EX 0 30901 1 0 0.0 7.4329
NT 30901 1 1 1 0 0 0 1 0 0
FR 0 1 0 0 1 1
RP 0 181 1 1000 -90 0 1.00000 1.00000
RP 1 1 1 0000 0 0 1.00000 1.00000 1609.344
EN
```

For the moment, we shall by-pass the data that we may collect from this model of a square tower to move directly to the second way to handle the model. We may also model the tower as 4 independent legs, each 234' tall with 41 segments. As in past models, we shall use 2"-diameter legs (radius = 0.085'). In this tower arrangement, the legs form a square around the center of the coordinate system. Therefore, each leg has X- and Y-coordinates of 0.75', with numerical signs indicating the quadrant of each leg. Relative to triangular towers, we require one more source (with its added wire

and network) and the divisor for the net source impedance will be 4 instead of 3. If we wish to employ a common source, then we simply add a 4th transmission line to the collection that we used for triangular towers. However, we may continue to use the separate source model and perform the simple external calculation. Although the model appears to be more complex than its triangular counterpart, it actually has only 4 more lines, each of which is a near copy of its neighbor.

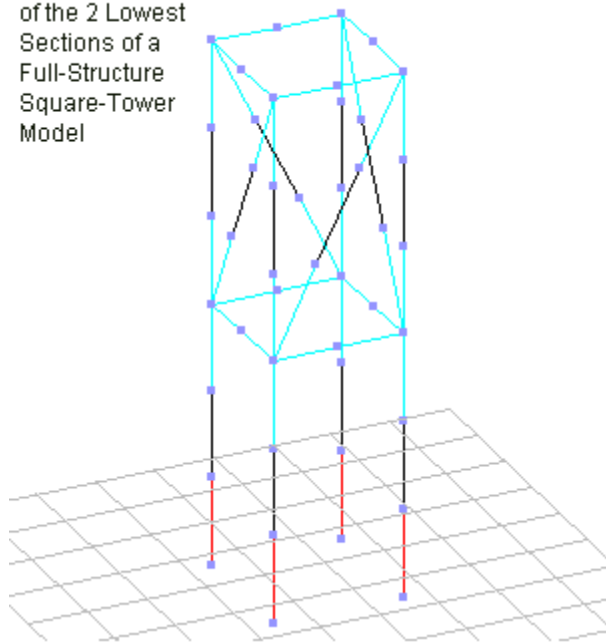
```
CM near-resonant monopole, perfect ground, square, straight
CM 4 sources, independent legs
CE
GW 1 41 .75 .75 0 .75 .75 234 0.085
GW 2 41 -.75 .75 0 -.75 .75 234 0.085
GW 3 41 -.75 -.75 0 -.75 -.75 234 0.085
GW 4 41 .75 -.75 0 .75 -.75 234 0.085
GW 30901 1 9901.0000 9901.0000 9901.0000 9901.0001 9901.0001 9901.0001 .00001
GW 30902 1 9902.0000 9902.0000 9902.0000 9902.0001 9902.0001 9902.0001 .00001
GW 30903 1 9903.0000 9903.0000 9903.0000 9903.0001 9903.0001 9903.0001 .00001
GW 30904 1 9904.0000 9904.0000 9904.0000 9904.0001 9904.0001 9904.0001 .00001
GS 0 0 .3048
GE 1
GN 1
EX 0 30901 1 0 0.0 1.8643
EX 0 30902 1 0 0.0 1.8643
EX 0 30903 1 0 0.0 1.8643
EX 0 30904 1 0 0.0 1.8643
NT 30901 1 1 1 0 0 0 1 0 0
NT 30902 1 2 1 0 0 0 1 0 0
NT 30903 1 3 1 0 0 0 1 0 0
NT 30904 1 4 1 0 0 0 1 0 0
FR 0 1 0 0 1 1
RP 0 181 1 1000 -90 0 1.00000 1.00000
RP 1 1 1 0000 0 0 1.00000 1.00000 1609.344
EN
```

Once more we shall by-pass the data and move directly to the third type of model, one using a simulated full structure. Because we may divide 234' by 3' to obtain in integer for the total number of required sections (78), we can use 3' section for the model. The

lowest section will use only a horizontal member at its upper limit, omitting the sloping sections. As we discovered with triangular towers, the use of sloping members in the lowest section results in a current division at the ground-contact end of the source segment, seriously distorting the model results. We introduce sloping model wires in the second section, as shown in **Fig. 1**. The view shows only the lowest two sections to reveal the segmentation scheme, which is the same as used for the full-structure triangular tower model in the preceding episode.

Model Structure  
of the 2 Lowest  
Sections of a  
Full-Structure  
Square-Tower  
Model

Fig. 1



To complete the tower, we need only one further geometry command. The GM entry replicates the second section 76 more times to arrive at the total height required. The final model is a bit larger than its triangular counterpart, with 708 wires and 2488 segments. Lest the model size seem forbidding, the model required a 62-second total run time on a moderately old 1.8 GHz machine.

```

CM near-resonant monopole, perfect ground, square, straight
CM 4 sources, full structure
CE
GW 1 3 .75 .75 0 .75 .75 3 0.085
GW 2 3 -.75 .75 0 -.75 .75 3 0.085
GW 3 3 -.75 -.75 0 -.75 -.75 3 0.085
GW 4 3 .75 -.75 0 .75 -.75 3 0.085
GW 5 2 .75 .75 3 -.75 .75 3 .085
GW 6 2 -.75 .75 3 -.75 -.75 3 .085
GW 7 2 -.75 -.75 3 .75 -.75 3 .085
GW 8 2 .75 -.75 3 .75 .75 3 .085
GW 9 3 .75 .75 3 .75 .75 6 0.085
GW 10 3 -.75 .75 3 -.75 .75 6 0.085
GW 11 3 -.75 -.75 3 -.75 -.75 6 0.085
GW 12 3 .75 -.75 3 .75 -.75 6 0.085
GW 13 2 .75 .75 6 -.75 .75 6 .085
GW 14 2 -.75 .75 6 -.75 -.75 6 .085
GW 15 2 -.75 -.75 6 .75 -.75 6 .085
GW 16 2 .75 -.75 6 .75 .75 6 .085
GW 17 3 .75 .75 3 -.75 .75 6 .085
GW 18 3 -.75 .75 3 -.75 -.75 6 .085
GW 19 3 -.75 -.75 3 .75 -.75 6 .085
GW 20 3 .75 -.75 3 .75 .75 6 .085
GM 9 76 0 0 0 0 0 3 9 1 20 3
GW 30901 1 9901.0000 9901.0000 9901.0000 9901.0001 9901.0001 9901.0001 .000001
GW 30902 1 9902.0000 9902.0000 9902.0000 9902.0001 9902.0001 9902.0001 .000001
GW 30903 1 9903.0000 9903.0000 9903.0000 9903.0001 9903.0001 9903.0001 .000001
GW 30904 1 9904.0000 9904.0000 9904.0000 9904.0001 9904.0001 9904.0001 .000001
GS 0 0 .3048
GE 1
GN 1
EX 0 30901 1 0 0.0 1.8623
EX 0 30902 1 0 0.0 1.8623
EX 0 30903 1 0 0.0 1.8623
EX 0 30904 1 0 0.0 1.8623
NT 30901 1 1 1 0 0 0 1 0 0
NT 30902 1 2 1 0 0 0 1 0 0
NT 30903 1 3 1 0 0 0 1 0 0

```

```

NT 30904 1 4 1 0 0 0 1 0 0
FR 0 1 0 0 1 1
RP 0 181 1 1000 -90 0 1.00000 1.00000
RP 1 1 1 0000 0 0 1.00000 1.00000 1609.344
EN

```

I have reserved the data collections to present them together, not only with each other, but with the data for the three models of 234' 18" face-width triangular towers from the preceding episode. The total data collection for the near-resonant tower models will prove instructive.

#### Near Resonant (234') 18" Face Monopole Models: Data

Impedance (Ohms)	Current (Apk)	Gain (dBi)	AGT	AGT-dB	F-S @ 1 mile
<b>Triangular</b>					
<b>Single-Wire Model</b>					
35.65 - j 1.29	7.4897	5.14	1.999	0.00	275.1 mV/m @ -45.6 deg
<b>3-Leg Model</b>					
35.57 - j 1.61	2.4993/leg	5.14	1.999	0.00	275.1 mV/m @ -45.6 deg
<b>Full-Structure Model</b>					
35.47 + j 2.74	2.5029/leg	5.24	2.043	0.09	278.2 mV/m @ -46.2 deg
<b>Square</b>					
<b>Single-Wire Model</b>					
36.20 + j 1.01	7.4329	5.15	1.999	0.00	275.2 mV/m @ -46.0 deg
<b>4-Leg Model</b>					
35.97 + j 0.08	1.8643/leg	5.15	1.999	0.00	275.2 mV/m @ -45.9 deg
<b>Full-Structure Model</b>					
36.04 + j 3.85	1.8623/leg	5.22	2.034	0.07	277.6 mV/m @ -46.6 deg

Within the data for square towers, we find a very small variation in the resistive component of the three models, about 0.25 Ohm. The reactance varies more widely among models, but less than 3 Ohms overall. Among the triangular models, we found slightly less variation in the resistive component and slightly more variation in the reactance. However, with both types of models, the full-structured version showed a less-than-ideal AGT value that

required correction of the gain report and the field-strength report. If we correct the square-model field strength raw data by dividing the report by the square root of half the basic AGT score, we obtain a reading of 275.3 mV(pk)/m, which brings into accord with the raw reports of the simpler models. Applying the AGT-dB value to correct the raw gain reports also brings it into line with the other gain values.

Between the triangular and the square models, we find very little difference in the values. The seemingly fatter square tower shows a source impedance that is about 0.5-Ohm higher resistively and about 1-Ohm more inductive with respect to reactance. For many applications, the difference would not make a difference. Effectively, for the same face width, the square tower is 1.5 times fatter than the triangular model, but a 50% change in diameter does not change modeling results by a great amount.

## A Sloping Square

One very common form for a square tower is a sloping structure that is broader at the base than at the top. To sample this configuration from a modeling perspective, we might consider a 234' tower consisting of 4 legs. The face width at the base might be 48" (4') and at the top 24" (2'). **Fig. 2** illustrates one face of such a sloping structure, but not to scale. The rate of change of face width is only 0.05"/foot of height. However, that small rate will be sufficient to show us what to expect from such structures.

Sloping-Leg  
Square-Tower  
Outline

Not to  
Scale

Face = 24"

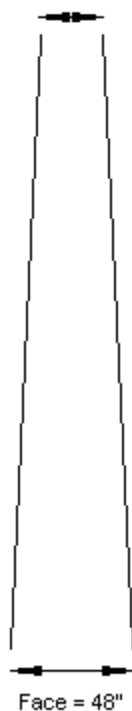


Fig. 2

234'

Face = 48"

If we accept the correlation among the three model versions that we have so far examined, then we may develop a relatively simple model for the sloping tower. Perhaps the easiest model consists of 4 independent legs, using our standard 2" diameter (0.085' radius). Each leg slopes inward by the requisite amount to arrive at the desired top face width. Except for the X- and Y-coordinates, the



model closely resembles the 4-leg version of the square tower with a uniform face width.

```

CM near-resonant monopole, perfect ground, square, sloping legs
CM 4 sources
CE
GW 1 41 2 2 0 1 1 234 0.085
GW 2 41 -2 2 0 -1 1 234 0.085
GW 3 41 -2 -2 0 -1 -1 234 0.085
GW 4 41 2 -2 0 1 -1 234 0.085
GW 30901 1 9901.0000 9901.0000 9901.0000 9901.0001 9901.0001 9901.0001 .00001
GW 30902 1 9902.0000 9902.0000 9902.0000 9902.0001 9902.0001 9902.0001 .00001
GW 30903 1 9903.0000 9903.0000 9903.0000 9903.0001 9903.0001 9903.0001 .00001
GW 30904 1 9904.0000 9904.0000 9904.0000 9904.0001 9904.0001 9904.0001 .00001
GS 0 0 .3048
GE 1
GN 1
EX 0 30901 1 0 0.0 1.9062
EX 0 30902 1 0 0.0 1.9062
EX 0 30903 1 0 0.0 1.9062
EX 0 30904 1 0 0.0 1.9062
NT 30901 1 1 1 0 0 0 1 0 0
NT 30902 1 2 1 0 0 0 1 0 0
NT 30903 1 3 1 0 0 0 1 0 0
NT 30904 1 4 1 0 0 0 1 0 0
FR 0 1 0 0 1 1
RP 0 181 1 1000 -90 0 1.00000 1.00000
RP 1 1 1 0000 0 0 1.00000 1.00000 1609.344
EN

```

Because the tower is so much fatter than its uniform-face-width counterpart, we might expect the data to show some inductive reactance at a height of 234', which was very close to resonant with the 18" uniform face width. The data collection tells a somewhat different story.

#### 234' 4-Leg Sloping Monopole Model Data

Impedance (Ohms)	Current (Apk)	Gain (dBi)	AGT	AGT-dB	F-S @ 1 mile
34.41 - j 8.81	1.9062/leg	5.14	1.999	0.00	275.0 mV/m @ -46.5 deg

In fact, the tower "plays short." That is to say, due to the tapering of the effective diameter of the tower along its length from the source outward toward the element end, the tower requires a larger value for its height to achieve resonance than a comparable uniform-diameter (or uniform-face-width) tower. The tower simply reflects one of the fundamental properties of elements that taper downward in diameter moving away from the feedpoint. (If it were practical to invert the tower so that it exhibited an increase in effective diameter as we moved away from the source at perfect ground level, it would show the properties of one-half of a biconical element and "play long." Of course, what we cannot do in reality, we often can do as a modeling exercise and thereby naturalize our expectations of element behavior.) For our very gently sloping tower to achieve resonance within  $j \pm 1$  Ohm of remnant reactance, we need to increase the height by about 5' or about 2%.

More radically sloped square towers, which might be more typical in actual installations, would show somewhat different results. The typical base face width will in practical installations generally increase faster than the rate of slope. These two tendencies tend to counteract each other, with the wider footprint shrinking the required height for resonance and the rate of slope increasing the required height. For anyone anticipating modeling a real physical square sloping tower, running a series of models for familiarization may be a useful exercise. The nearly ideal AGT score gives the 4-sloping-leg model as much validity as its uniform-face-width counterpart.

## Tapered or Stepped-Diameter Triangular Towers

Although uncommon in the AM BC industry, we do find many triangular towers that employ the rough equivalent of the square tower's sloping legs. Technically, we should refer to such models as stepped-diameter structures, although it is common practice also to refer to them as tapered-diameter elements. (That is why I specifically referred to the square tower as having a sloping face width, since the width decreased continuously rather than in steps.)

**Fig. 3** shows a simplified but representative situation.

Sample Stepped-Face-Width Tower

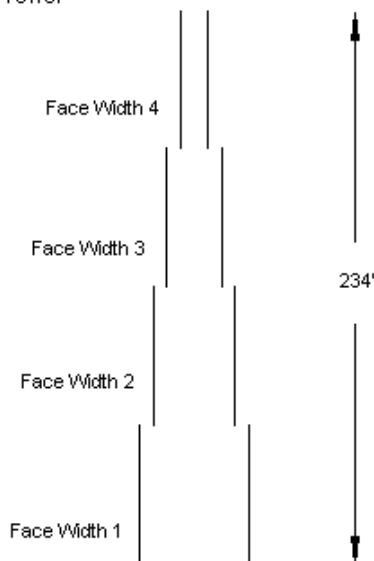


Fig. 3

We may use the not-to-scale sketch to create some interesting models. However, trying to set up a full-structure model will usually end up in frustration. The steps between sections are normally sudden and very short, resulting in a need for wire segments that fall below the recommended NEC minimum length of 0.001-wavelength (or 11.803" at 1 MHz). If we find the NAB-recommended single-wire equivalent of tower faces acceptable, we can create a simplified model.

Let's begin with our 234' total height and break it into 4 equal 58.5' sections, each with its own face width. The base will be 24" wide and the top 12" wide, with equal face width steps between. Hence, we might end up with the following chart.

Stepped-Diameter Triangular Tower Section Face Widths and Equivalent Diameters

Section	Face-Width	Equiv. Diameter	Radius in Feet
Base	24"	17.76"	0.74'
2	20	14.80	0.6167
3	16	11.84	0.4934
Top	12	8.88	0.37

We can easily create a single-wire tower using 4 modeling wires having the desired properties.

```
CM near-resonant monopole, perfect ground, stepped triangle
CM NAB substitute single-wire monopole
CE
GW 1 10 0 0 0 0 0 58.5 .74
GW 2 10 0 0 58.5 0 0 117 .6167
GW 3 10 0 0 117 0 0 175.5 .4934
GW 4 10 0 0 175.5 0 0 234 .37
GW 30901 1 9901.0000 9901.0000 9901.0000 9901.0001 9901.0001 9901.0001 .00001
GS 0 0 .3048
GE 1 0 0
```

```

GN 1
EX 0 30901 1 0 0.0 7.7772
NT 30901 1 1 1 0 0 0 1 0 0
FR 0 1 0 0 1 1
RP 0 181 1 1000 -90 0 1.00000 1.00000
RP 1 1 1 0000 0 0 1.00000 1.00000 1609.344
EN

```

Next, let's run the model, first using NEC-2 and then using NEC-4. We obtain the following data collection.

#### 234' Stepped-Diameter Triangular Monopole Model Data

Impedance (Ohms)	Current (Apk)	Gain (dBi)	AGT	AGT-dB	F-S @ 1 mile
NEC-2					
33.52 - j 7.85	7.7245	5.26	2.058	0.12	279.0 mV/m @ -45.6 deg
NEC-4					
33.07 - j15.21	7.7777	5.18	2.020	0.04	276.2 mV/m @ -45.6 deg

With the number and size of the diameter steps, neither core yields a very precise results. As we would expect, the NEC-2 results shows a much poorer AGT score than the NEC-4 run, but both are off the mark where we wish to have relatively high precision.

The most common way to achieve precision in cases like this one is to use substitute elements with a uniform diameter. The most precise method available to calculate the length of these elements derives from the work of David Leeson (see chapter 8 of his *Physical Design of Yagi Antennas*). Leeson adapts the work of Schelkunoff to the calculation of the length and diameter of a uniform-diameter element equivalent to a stepped-diameter element. The equivalence equation is useful for unloaded elements within about 15% of resonance. If we do not wish to perform the calculations manually, we can turn to programs such as NEC-Win Plus or EZNEC that contain the facility within their input interface

programming. Note that the substitute element will have a different length as well as diameter relative to the original. For the present sample, the required radius is 0.5593', while the element length is 226.292'. However, the resulting model is very simple.

```
CM near-resonant monopole, perfect ground, leeson
CM NAB substitute single-wire monopole
CE
GW 1 41 0 0 0 0 0 226.292 .5593
GW 30901 1 9901.0000 9901.0000 9901.0000 9901.0001 9901.0001 9901.0001 .00001
GS 0 0 .3048
GE 1 0 0
GN 1
EX 0 30901 1 0 0.0 7.4329
NT 30901 1 1 1 0 0 0 1 0 0
FR 0 1 0 0 1 1
RP 0 181 1 1000 -90 0 1.00000 1.00000
RP 1 1 1 0000 0 0 1.00000 1.00000 1609.344
EN
```

The substitute element provides us with the following data collection.

#### Substitute Stepped-Diameter Triangular Monopole Model Data

Impedance (Ohms)	Current (Apk)	Gain (dBi)	AGT	AGT-dB	F-S @ 1 mile
32.15 - j17.47	7.8876	5.12	1.999	0.00	274.3 mV/m @ -45.3 deg

As we might expect from the tower height using the substitute element, the stepped-diameter tower is short of resonance. The NEC-2 data might have given the impression that its values were closer to the anticipated resonant impedance. However, it turns out that the NEC-2 run produced values further from accurate data, and both uncorrected models tended to produce reactance values that were too inductive. (A MININEC (Antenna Model) model using the dimensions for the original versions with a changing diameter

yielded a gain of 5.13 dBi with a source impedance of  $32.63 - j18.85$  Ohms.)

## Conclusion

In this episode, we examined some of the variations that we might well encountered in modeling monopole towers over perfect ground for various AM BC enterprises. As always, the samples were hypothetical, but illustrative of the principles involved in modeling tower structures. We saw that uniform-face-width square towers have simplified forms that are as reliable as the simplified forms used for triangular towers. As well, the full-structure versions of those models, even when adhering as strictly as possible to all NEC guidelines, still resulted in a slight deviation from an ideal AGT score--just enough to show report values that required correction.

The sloping-leg and stepped-face-width models, although uncommon in most practice, gave us an opportunity to select the best modeling technique for a given task. In the case of square towers with sloping legs, using independent tower legs for the model proved not merely to simplify the model, but also to avoid the modeling flaws that would easily result from trying to construct a full-structure model. The stepped-face-width triangular model using the NEC-recommended single-wire model allowed us to calculate a uniform-diameter substitute element for which NEC produces more reliable data.

We have traveled a considerable distance from our first procedural steps in using NEC to model AM BC towers under standard conditions. However, we still have steps to take.



## Chapter 135: AM BC Modeling with NEC

### 5. Multiple Tower Arrays

In our journey through the netherworld of AM BC towers modeled over perfect ground, we have examined the techniques needed with NEC cores (especially NEC-4) for obtaining the type of results that modelers obtain from specialized MININEC programs. Among the items that we have explored are the correlations among models using the NAB-recommended substitute single wire tower models, independent 3- and 4-leg tower models, and full-structure models. We noted along the way steps necessary to ensure that we supply a model with a set power (in all the samples, 1 kW) and the output command necessary to obtain field-strength readings (RP1). We noted that NEC itself uses peak values of voltage and current. Hence, field-strength readings and supplied current specifications require adjustment by the usual 0.7071 multiplier to convert them into RMS values. We also looked at various cases in which one or another model version appeared to be preferable for various reasons. For example, we turned to the 4 independent leg model to handle square towers that slope from bottom to top. However, for working with stepped-diameter towers, the single-wire substitute model provides the most advantageous model.

All of our samples in the 4 preceding episodes used a single tower centered on the coordinate system center ( $X=0$ ,  $Y=0$ ). Typical of those one-tower models was the near resonant 234' tower at 1 MHz, with an 18" face of a triangular tower. The model that we used earlier looked almost like the one that we shall show here.

```

CM near-resonant monopole, perfect ground
CM NAB substitute single-wire monopole
CE
GW 1 41 0 0 0 0 0 234 0.555
GW 30901 1 9901.0000 9901.0000 9901.0000 9901.0001 9901.0001 9901.0001 .00001
GS 0 0 .3048
GE 1 0 0
GN 1
EX 0 30901 1 0 0.0 7.4897
NT 30901 1 1 1 0 0 0 1 0 0
FR 0 1 0 0 1 1
RP 0 181 1 1000 -90 0 1.00000 1.00000
RP 0 1 361 1000 90 0 1.00000 1.00000
RP 1 1 1 0000 0 0 1.00000 1.00000 1609.344
RP 1 1 1 0000 0 0 1.00000 1.00000 3218.688
EN

```

The only difference between past models and this one is that the new version adds a second RP1 command at a distance of 2 miles to the original that uses a distance of 1 mile. Both commands use ground level as the observation height for the command. The basic data collection is in the following lines.

Near Resonant (234') 18" Face Triangular Single-Wire Monopole Model Data

Impedance (Ohms)	Current (Apk)	Gain (dBi)	AGT	AGT-dB	F-S @ 1 mile	F-S @ 2 miles
35.65 - j 1.29	7.4897	5.14	1.999	0.00	275.1 mV/m @ -45.6 deg	137.5 mV/m @ -178.1 deg

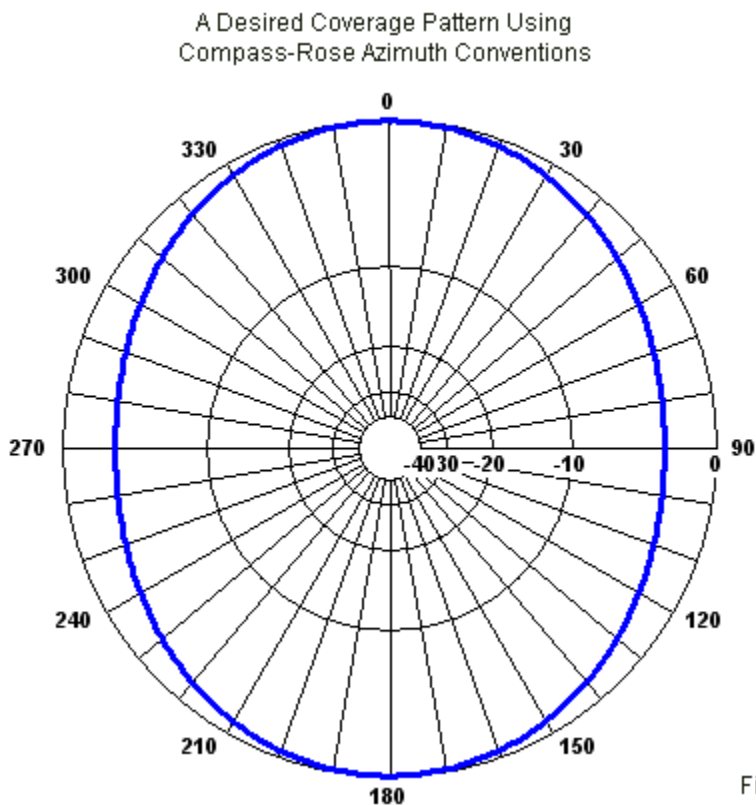
If the only field-strength value in which we have any interest is the magnitude (in peak mv/m as shown or adjusted to RMS), then we need not add the second RP1 request. For perfect ground, field-strength magnitude values decrease linearly with distance from the antenna. However, if we have any interest in the phase angle, the second request is necessary to obtain the additional figures.

In this episode, the tower that we have just modeled will play a significant role, but not solo. In this episode, we shall look at some very basic cases that employ two towers with considerations of the

current magnitude and phase angle at each source--remembering that we are using the standard method in NEC to provide current sources. The task will sometimes involve more than simply adding a second tower to the GW portion of the list.

## Two Towers Fed In-Phase for a Broadside Pattern

Suppose that we need a pattern like the one shown in **Fig. 1** to fulfill broadcast needs and restrictions. The simplest way to obtain it is with two towers, in this case, using broadside array techniques. In the present sample, we shall use only simple arrays to illustrate the modeling aspects. Actual arrays may be considerably more complex, and the resultant patterns may be equally complex. The pattern is laid out according to the compass-rose azimuth conventions favored by some agencies and many field engineers.



The desired coverage calls for a moderate increase in gain along the N-S axis with lesser gain in the E-W directions. One way to obtain such coverage is to arrange two towers about  $1/4$ -wavelength apart in the E-W plane (+Y and -Y) and to feed them in phase. Initially, this feed requirement will use two sources, each

supplied with the same current magnitude and phase angle, with the magnitude determined by our standard 1-kW power level. We shall use our single-wire substitute for a 234' tower in each case. A wavelength at 1 MHz is 983.571 feet, so the separation between towers is 245.893'.

```
CM 2 near-resonant monopoles, perfect ground
CM NAB substitute single-wire monopole
CM in-phase feeding--l/-wl spacing
CE
GW 1 41 0 122.946 0 0 122.946 234 0.555
GW 2 41 0 -122.946 0 0 -122.946 234 0.555
GW 30901 1 9901.0000 9901.0000 9901.0000 9901.0001 9901.0001 9901.0001 .00001
GW 30902 1 9902.0000 9902.0000 9902.0000 9902.0001 9902.0001 9902.0001 .00001
GS 0 0 .3048
GE 1 0 0
GN 1
EX 0 30901 1 0 0.0 4.3339
EX 0 30902 1 0 0.0 4.3339
NT 30901 1 1 1 0 0 0 1 0 0 0
NT 30902 1 2 1 0 0 0 1 0 0 0
FR 0 1 0 0 1 1
RP 0 181 1 1000 -90 0 1.00000 1.00000
RP 0 1 361 1000 90 0 1.00000 1.00000
RP 1 1 37 0000 0 0 1.00000 10.00000 1609.344
EN
```

The simple data collection, as we can see from the following lines, does not tell the full story, as it did for the single tower models. The collection also omits the 2-mile field-strength report.

#### Two-Tower Broadside Array 18" Face Triangular Single-Wire Monopole Model Data

Impedance (Ohms)	Current (Apk)	Gain (dBi)	AGT	AGT-dB	F-S @ 1 mile
53.24 - j17.40 x2	4.3339/tower	6.23 max.	1.999	0.00	311.5 mV/m @ -47.2 deg

The impedance reports are for each tower, as is the current magnitude. The gain and the field-strength values are maximum values, taken in the northern direction (0 degrees, which

corresponds to the +X direction on the geometry coordinate system). However, we shall be interested in both the gain and the field strength in various directions around the pattern. Because the field strength is likely to be the more important figure, we may wish to examine a table of figures taken at suitable intervals. The following sample from the model traces 1/4 of the pattern (because it is symmetrical) at 10-degree intervals.

```
**** Electric Field: Phi Pattern ****
Z=0, Freq=1, File=fcc51.NOI
```

---E (Theta)---			--- E (Phi) ---	
Phi	Magnitude	Phase	Magnitude	Phase
Degrees	Volts/m	Degrees	Volts/m	Degrees
0.00	3.1157E-001	-47.23	5.3620E-022	-108.51
10.00	3.0868E-001	-47.23	4.3494E-022	105.73
20.00	3.0040E-001	-47.23	3.2047E-022	-167.59
30.00	2.8786E-001	-47.23	1.9626E-022	137.96
40.00	2.7271E-001	-47.23	6.6090E-023	-66.91
50.00	2.5687E-001	-47.23	6.6090E-023	113.09
60.00	2.4224E-001	-47.23	1.9626E-022	-42.04
70.00	2.3051E-001	-47.23	3.2047E-022	12.41
80.00	2.2293E-001	-47.23	4.3494E-022	-74.27
90.00	2.2032E-001	-47.23	5.3620E-022	71.49

The E(theta) columns represent the vertical component of the field-strength calculations. The horizontal component (E(phi)) is too small to be significant. To better visualize the changes in field strength as we move around the overall pattern, we may also graph the values, as shown in **Fig. 2**.

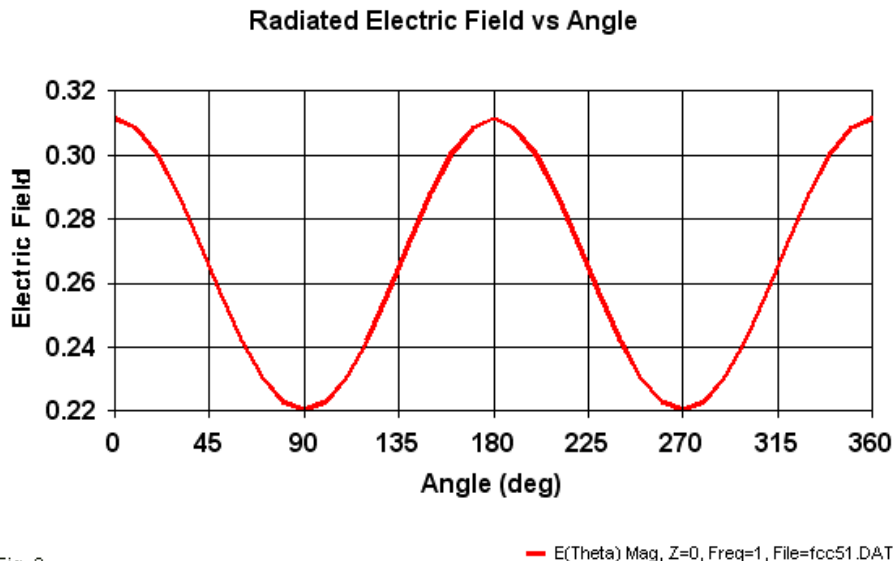


Fig. 2

The combination of data allows significant evaluation of the likely performance of the 2-tower broadside array. Of course, the sample selects a spacing between towers that yields less than the full broadside bi-directional gain of such towers. Wider spacing will yield more gain in the N-S direction with less gain in the E-W direction. As a certain point as we increase spacing, the oval pattern will gradually evolve into a figure-8.

Our interest does not lie in what we can do with towers so much as it lies in what we can include in and show by appropriate modeling. For example, we may wish to include in the model a composite

feed system so that we have only a single source. The normal form of feeding the system would be to bring transmission lines from each tower to a central point so that each line is equal in length (and characteristic impedance) to the other. We may set up such lines by selecting the junction point and placing a short, thin wire to serve as the source as well as the junction between lines. Let's arbitrarily set up two 600-Ohm transmission lines, one from each tower. The terminal points for the lines and the source will be a position exactly centered between the towers ( $Y=0$ ) and 245' (1/4-wavelength) away from the towers. The general outline of the model will have the appearance of the set-up in **Fig. 3**.

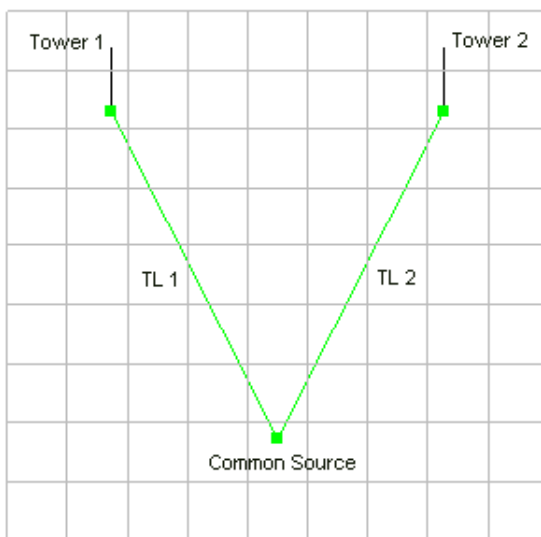


Fig. 3



To model this situation, without altering the tower positions or other attributes, we need a model that resembles the following lines.

```
CM 2 near-resonant monopoles perfect ground
CM NAB substitute single-wire monopole
CM in-phase common feeding--1/4-wl spacing
CE
GW 1 41 0 122.946 0 0 122.946 234 0.555
GW 2 41 0 -122.946 0 0 -122.946 234 0.555
GW 3 1 -245 0 1 -245 0 2 0.0001
GW 30901 1 9901.0000 9901.0000 9901.0000 9901.0001 9901.0001 9901.0001 .000001
GS 0 0 .3048
GE 1
GN 1
EX 0 30901 1 0 0.0 1.5138
NT 30901 1 3 1 0 0 0 1 0 0
TL 1 1 3 1 600 0 ! User Defined VF
TL 2 1 3 1 600 0 ! User Defined VF
FR 0 1 0 0 1 1
RP 0 181 1 1000 -90 0 1 1
RP 0 1 361 1000 90 0 1 1
RP 1 1 37 0000 0 0 1.00000 10.00000 1609.344
EN
```

Form this model we may obtain the usual data collection.

Two-Tower Broadside Array, Common Source, 18" Face Triangular Single-Wire Monopole  
Model Data

Impedance (Ohms)	Current (Apk)	Gain (dBi)	AGT	AGT-dB	F-S @ 1 mile
872.8 - j1457.8	1.5138	6.23 max.	1.999	0.00	311.5 mV/m @ -47.2 deg

Only the impedance and the required current for 1kW differ from the dual-source model. To confirm the high source impedance, we may independently calculate the current transformation down each 600-Ohm line, with a length of 274.12' based on the separate source impedance values of 53.24 - j17.40 Ohms. The result will be separate impedances of about 1754 - j2920 Ohms, which combine in parallel to 877 - j1460 Ohms, very close to the modeled values,

considering the rapid change in value for each small increment of length.

If the impedance is inconvenient due to the 100.3-degree lines required, we may always change the position of the junction. The shortest lines occur when we place the junction in line with the towers at  $Y=0$ , as suggested by **Fig. 4**. The lines have shrunk to 45 degrees.

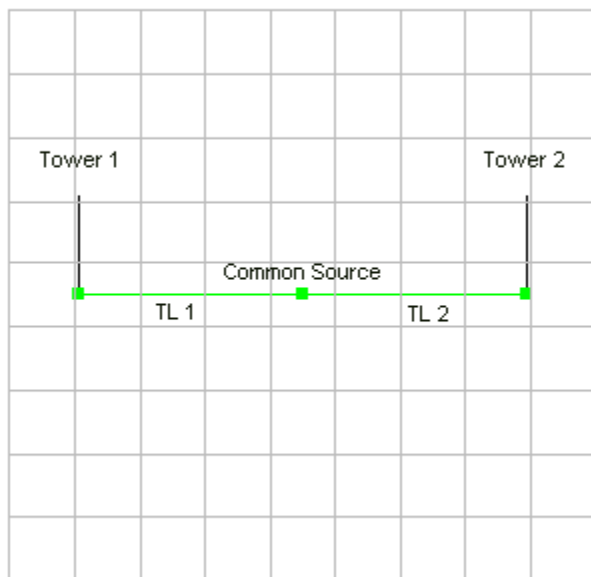


Fig. 4

The only change to the model is in the placement of GW3, as the following partial model file shows.

```
GW 1 41 0 122.946 0 0 122.946 234 0.555
GW 2 41 0 -122.946 0 0 -122.946 234 0.555
GW 3 1 0 0 1 0 0 2 0.0001
```

We do not required changes in the TL command entries because we have used zeros (after the characteristic impedance entry of 600) to specify that the line length is the actual distance between the terminal points as defined by the wire entries.

```
TL 1 1 3 1 600 0 ! User Defined VF
TL 2 1 3 1 600 0 ! User Defined VF
```

In the data collection, we find that the only resultant differences occur in the entries for the composite source impedance and the required peak current level needed at this impedance to achieve a 1-kW power level.

Two-Tower Broadside Array, Common Source, 18" Face Triangular Single-Wire Monopole  
Model Data

Impedance (Ohms)	Current (Apk)	Gain (dBi)	AGT	AGT-dB	F-S @ 1 mile
49.96 + j 278.9	6.3272	6.23 max.	1.999	0.00	311.5 mV/m @ -47.2 deg

NEC employs lossless transmission lines for its calculations. At 1 MHz for virtually any line less than 1/2-wavelength long, the values for lossless line calculations will not differ significantly from calculations including line losses. The model set-ups also presume a velocity factor of 1.0. If the velocity factor of a line departs significantly from that value, one may always insert the electrical

line length in place of our use of zero to force the program to use the actual distance between terminal points on the line.

Not all arrays require patterns with maximum field-strength values going north and south. Suppose that we require that the pattern have its gain maximum point aligned along an axis defined by compass heading of 60 and 240 degrees. In general, there are two major ways to achieve this goal. One is to set up each tower so that the broadside direction is automatically along the desired axis. The other method, shown here, is to set up the model in the simple manner shown earlier and then to turn the entire array around the Z-axis by the required 60 degrees. Note in the following model lines, that to turn the axis clockwise--as the present situation requires, we specify -60 degrees in the GM line. (+60 degrees turns the pattern counterclockwise.)

```
CM 2 near-resonant monopoles perfect ground
CM NAB substitute single-wire monopole
CM in-phase common feeding--1.4-wl spacing
CM rotated for 60/240-deg AZ axis
CE
GW 1 41 0 122.946 0 0 122.946 234 0.555
GW 2 41 0 -122.946 0 0 -122.946 234 0.555
GW 3 1 -245 0 1 -245 0 2 0.0001
GM 0 0 0 0 -60 0 0 0
GW 30901 1 9901.0000 9901.0000 9901.0000 9901.0001 9901.0001 9901.0001 .000001
GS 0 0 .3048
GE 1
GN 1
EX 0 30901 1 0 0.0 1.5138
NT 30901 1 3 1 0 0 0 1 0 0
TL 1 1 3 1 600 0 ! User Defined VF
TL 2 1 3 1 600 0 ! User Defined VF
FR 0 1 0 0 1 1
RP 0 181 1 1000 -90 0 1 1
RP 0 1 361 1000 90 0 1 1
RP 1 1 37 0000 0 0 1.00000 10.00000 1609.344
EN
```

The model shown uses the long transmission lines. However, that fact only allows the GM rotation to show with clarity in **Fig. 5**.

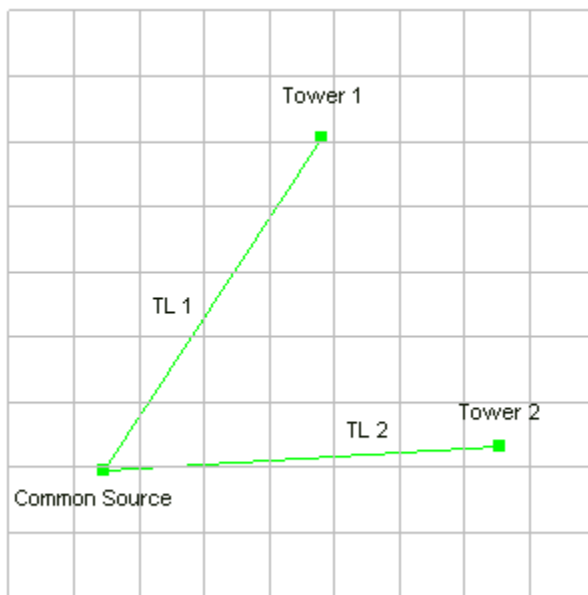


Fig. 5

We need not show the data collection, since it has not changed. What has changed is the field-strength table. The magnitudes will be the same as the earlier sample shown, but the headings on which they occur will differ. Remember that for tabular information, NEC uses the phi or counterclockwise convention. Therefore, the 60-degree compass-rose azimuth bearing coincides with the phi 300-degree bearing in the following table.

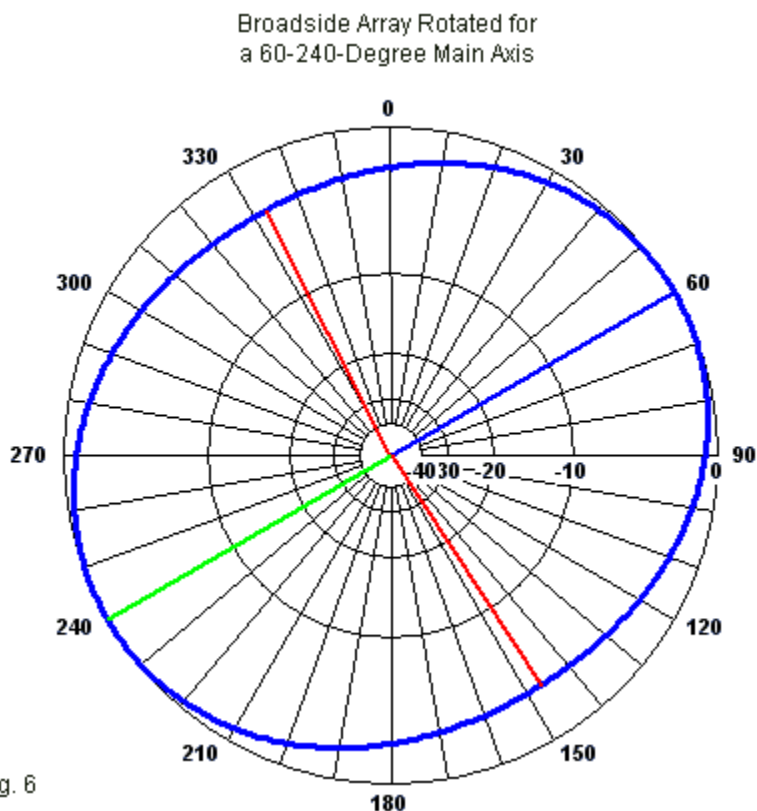
\*\*\*\* Electric Field: Phi Pattern \*\*\*\*

Z=0, Freq=1, File=fcc53.NOI

---E (Theta)---			--- E (Phi) ---	
Phi	Magnitude	Phase	Magnitude	Phase
Degrees	Volts/m	Degrees	Volts/m	Degrees
0.00	2.4224E-001	162.75	9.3641E-023	-108.70
10.00	2.3051E-001	162.75	7.5958E-023	105.52
20.00	2.2294E-001	162.75	5.5967E-023	-167.82
30.00	2.2032E-001	162.75	3.4275E-023	137.71
40.00	2.2294E-001	162.75	1.1542E-023	-67.17
50.00	2.3051E-001	162.75	1.1542E-023	112.83
60.00	2.4224E-001	162.75	3.4275E-023	-42.29
70.00	2.5687E-001	162.75	5.5967E-023	12.18
80.00	2.7271E-001	162.75	7.5958E-023	-74.48
90.00	2.8786E-001	162.75	9.3641E-023	71.30
100.00	3.0041E-001	162.75	1.0848E-022	106.98
110.00	3.0869E-001	162.75	1.2002E-022	53.35
120.00	3.1158E-001	162.75	1.2792E-022	-66.10
130.00	3.0869E-001	162.75	1.3192E-022	134.16
140.00	3.0041E-001	162.75	1.3192E-022	-39.16
150.00	2.8786E-001	162.75	1.2792E-022	161.09
160.00	2.7271E-001	162.75	1.2002E-022	41.65
170.00	2.5687E-001	162.75	1.0848E-022	-11.99
180.00	2.4224E-001	162.75	9.3641E-023	23.69
190.00	2.3051E-001	162.75	7.5958E-023	169.48
200.00	2.2294E-001	162.75	5.5967E-023	82.82
210.00	2.2032E-001	162.75	3.4275E-023	137.29
220.00	2.2294E-001	162.75	1.1542E-023	-17.83
230.00	2.3051E-001	162.75	1.1542E-023	162.17
240.00	2.4224E-001	162.75	3.4275E-023	-42.71
250.00	2.5687E-001	162.75	5.5967E-023	-97.18
260.00	2.7271E-001	162.75	7.5958E-023	-10.52
270.00	2.8786E-001	162.75	9.3641E-023	-156.31
280.00	3.0041E-001	162.75	1.0848E-022	168.01

290.00	3.0869E-001	162.75	1.2002E-022	-138.35
300.00	3.1158E-001	162.75	1.2792E-022	-18.91
310.00	3.0869E-001	162.75	1.3192E-022	140.84
320.00	3.0041E-001	162.75	1.3192E-022	-45.84
330.00	2.8786E-001	162.75	1.2792E-022	113.90
340.00	2.7271E-001	162.75	1.2002E-022	-126.65
350.00	2.5687E-001	162.75	1.0848E-022	-73.02
360.00	2.4224E-001	162.75	9.3641E-023	-108.70

**Fig. 6** re-confirms the successful rotation by showing the far-field pattern for the revised model. The lines on either side of the main axis lines indicate the half-power beamwidth, suggesting that the gain is about 3 dB weaker at right angles to the main axis. You may correlate this to the ratio of the relevant field-strength reports by the usual equation in which  $P_{dB} = 20 \log_{(10)}(E1/E2)$ .



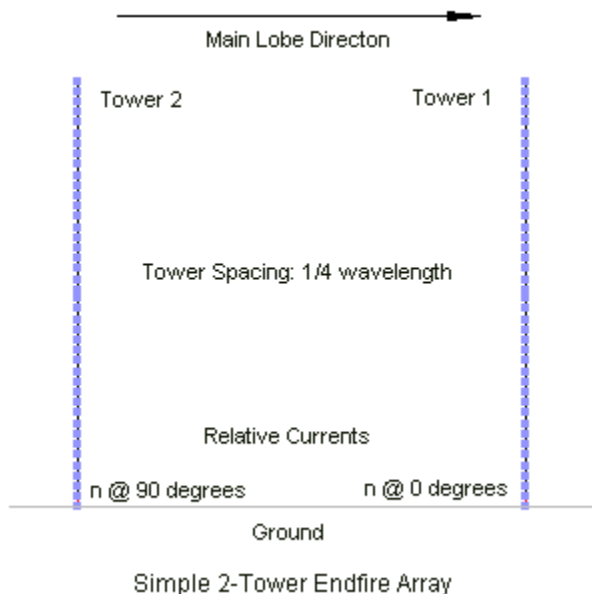
The notes so far have dealt with the simple case in which the sources for each broadside element are identical with respect to current magnitude and phase angle. Not all arrays of towers have such an easy requirement.



## An Endfire Array of Two Towers

For directional patterns, that is, patterns with a dominant lobe in only one direction, array designers generally use end-fire techniques so that the pattern is in line with the towers rather than broadside to them. We shall employ only a very basic two-tower array to note the key modeling points of interest. However, some installations have used up to 4 towers to obtain specific pattern shapes. As well, in some instances, designs have combined broadside with end-fire techniques for truly large arrays. Since there are texts devoted to the design of such arrays, we may focus on translating endfire arrays into models over perfect ground. We shall retain our 234' tower with the single-wire equivalent of an 18" face on a triangular structure. As was clear in the broadside array, mutual coupling between towers in relatively close proximity alters the source impedance so that each tower in the array is no longer self-resonant. (Compare the source impedance values for the initial 2-source broadside model with the source impedance of the reference single-tower model at the beginning of these notes.) Our present exercise will require even closer attention to the impedances reported for each tower.

Fig. 7



Our sample will use two towers separated by 1/4-wavelength. To set the main-lobe direction at north (0-degrees azimuth), we align the towers along the X-axis. To ensure that we place the array center at the coordinate center, each tower is 1/8-wavelength from  $X=0$ . The resulting geometry is simply our broadside array turned 90 degrees. In fact, if we were to feed the two sources in phase, we would obtain the earlier broadside pattern with the stronger field-strength reading east and west.

```

CM 2 near-resonant monopoles, perfect ground
CM NAB substitute single-wire monopole
CM end-fire two-tower array
CM 90-degree feeding--1/4wl spacing
CE
GW 1 41 122.946 0 0 122.946 0 234 0.555
GW 2 41 -122.946 0 0 -122.946 0 234 0.555
GW 30901 1 9901.0000 9901.0000 9901.0000 9901.0001 9901.0001 9901.0001 .00001
GW 30902 1 9902.0000 9902.0000 9902.0000 9902.0001 9902.0001 9902.0001 .00001
GS 0 0 .3048
GE 1 0 0
GN 1
EX 0 30901 1 0 5.3579 0
EX 0 30902 1 0 0.0 5.3579
NT 30901 1 1 1 0 0 0 1 0 0 0
NT 30902 1 2 1 0 0 0 1 0 0 0
FR 0 1 0 0 1 1
RP 0 181 1 1000 -90 0 1.00000 1.00000
RP 0 1 361 1000 90 0 1.00000 1.00000
RP 1 1 37 0000 0 0 1.00000 10.00000 1609.344
EN

```

In the model, GW 1 is the forward tower, that is, the tower in the direction of the main lobe, with GW 2 to the rear. Basic array theory tells us that we shall obtain a highly directional pattern if we feed the towers so that the rear tower has the same current magnitude as the forward tower. However, the phase angle of the rear tower current should be +90-degree relative to the forward tower (or the forward tower phase angle should be -90 degrees relative to the rearward tower). Some software allows the modeler to enter the desired values directly into the input interface screens. However, we shall do it the "old-fashioned" way by manipulating the currents on the remote EX entries for our current-fed array.

The problem at hand is simplified by the use of equal current magnitudes. However, the EX entry in NEC lists the excitation voltage in terms of real and imaginary components of the voltage that we shall transform into a current via the NT entries. **Fig. 8** shows the help screens (a composite of 2 screens, one for each source) to assist us in sorting out the entries. The screens list both the components and the magnitude and phase angle, and we may set up the line by placing the values in either format. As the screen shows, the forward tower (1) is 90 degrees behind the rearward tower (2) with respect to the phase angle. Compare these entries to the EX commands in the model.

**Excitation - NEC4**

Source Type  
☒ Voltage (applied E-field)

Voltage

Tag Number: 30901 Segment Number: 1

Magnitude: 5.35790 Real: 5.3579  
Phase: 0.00 Imaginary: 0

Tower 1 Units: Peak

Voltage

Tag Number: 30902 Segment Number: 1

Magnitude: 5.35790 Real: 0.0  
Phase: 90.00 Imaginary: 5.3579

Tower 2 Units: Peak

☐ Print Impedance Table for Frequency Sweep

Fig. 8

Now let's perform one more comparison: the EX entries with the currents that appear on the source segments of the two towers. We may glean this information from the NEC output file.

\*\*\*\* Segment Current versus Frequency \*\*\*\*

FREQUENCY (MHz)	SEG. NO.	TAG NO.	COORD. OF X	SEG. CENTER Y	Z	SEG. LENGTH	- - - CURRENT (AMPS) - - -	REAL	IMAG.	MAG.	PHASE
1.000000	1	1	0.1250	0.0000	0.0029	0.00580	-9.6451E-16	-4.3339E+00	4.3339E+00	-90.000	
1.000000	42	2	-0.1250	0.0000	0.0029	0.00580	4.3339E+00	-1.4008E-16	4.3339E+00	0.000	

Although we entered the source voltages with phase angles of 0 and 90 degrees for towers 1 and 2, respectively, the currents on the sources have phase angles of -90 and 0 degrees, respectively. We now understand two things. First, the voltage entries for the EX line have preserved their phase difference in the conversion to current values on the source segments. Second, the NT command responsible for the conversion shifts the entered phase angle by -90 degrees relative to the final current reports on the affected segments. If we forget this second fact, it shows up quite rapidly, since the pattern for entering the phase angles backwards will also be backwards.

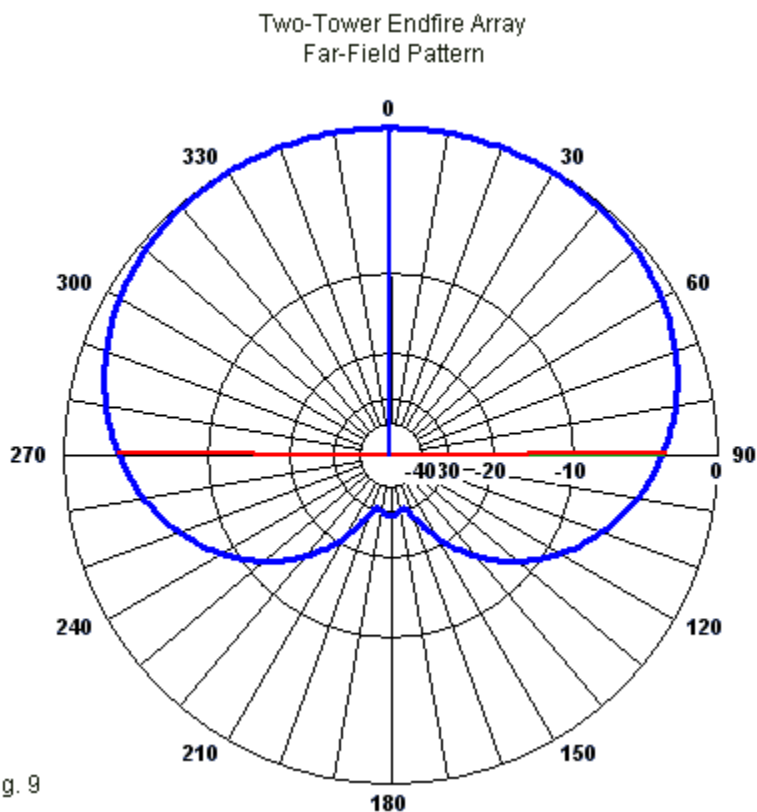


**Fig. 9** shows the resulting far-field patterns that merges from the model that we have constructed. If we truly needed to reduce the rearward radiation further, we may juggle both the magnitude and the phase angle of the EX entries until satisfied. However, once we have established the desired pattern, we would need to re-adjust

the current magnitudes with respect to the total power supplied to the array as indicated by the power budget portion of the NEC output report, using the technique shown in the first of these episodes. The values shown are for our pre-set power level of 1 kW.

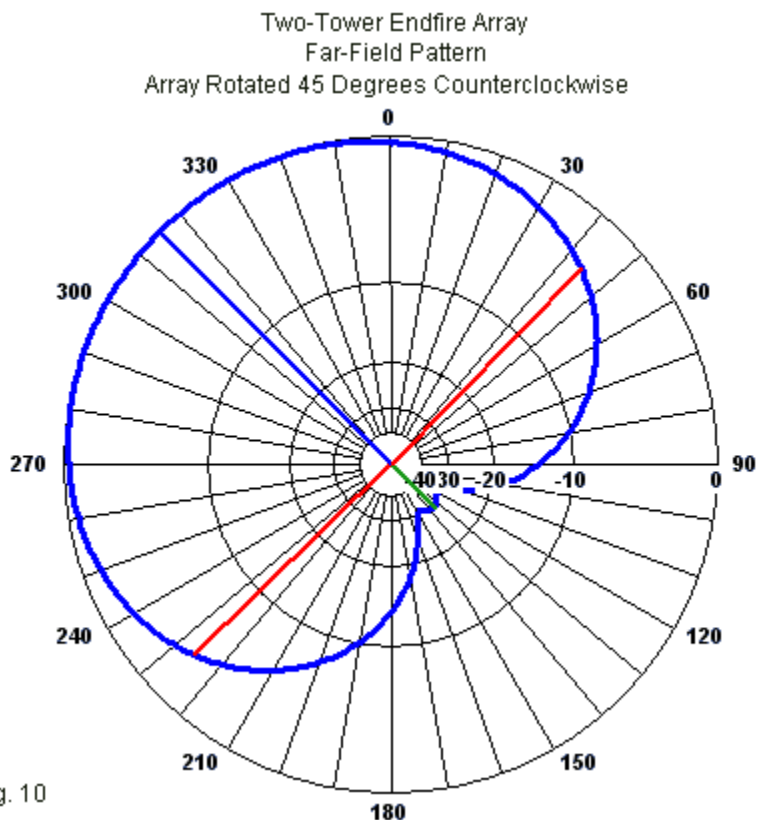
The methods for obtaining a main-lobe direction other than north are the same as for the broadside array. We may perform pre-modeling calculations so as to place the towers in the correct positions to yield a pattern with the desired heading, or we may construct the tower using the X-axis as the main line and then rotate the tower wires using the GM command. Let's rotate the array so that the main lobe has a heading of 315 degrees on the compass-rose azimuth scale. We need to inform the GM command to rotate the structure +45 degrees to effect the counterclockwise rotation, as shown in the following model.

```
CM 2 near-resonant monopoles, perfect ground
CM NAB substitute single-wire monopole
CM end-fire two-tower array
CM 90-degree feeding--1/4wl spacing
CM 315-deg AZ heading via GM
CE
GW 1 41 122.946 0 0 122.946 0 234 0.555
GW 2 41 -122.946 0 0 -122.946 0 234 0.555
GM 0 0 0 0 45 0 0 0
GW 30901 1 9901.0000 9901.0000 9901.0000 9901.0001 9901.0001 9901.0001 .00001
GW 30902 1 9902.0000 9902.0000 9902.0000 9902.0001 9902.0001 9902.0001 .00001
GS 0 0 .3048
GE 1 0 0
GN 1
EX 0 30901 1 0 5.3579 0
EX 0 30902 1 0 0.0 5.3579
NT 30901 1 1 1 0 0 0 1 0 0 0
NT 30902 1 2 1 0 0 0 1 0 0 0
FR 0 1 0 0 1 1
RP 0 181 1 1000 -90 0 1.00000 1.00000
RP 0 1 361 1000 90 0 1.00000 1.00000
```



```
RP 1 1 37 0000 0 0 1.00000 10.00000 1609.344  
EN
```

**Fig. 10** shows the resulting pattern.



The data collection for both of our sample endfire arrays is the same.

Two-Tower Endfire Array, Source at 90-Degree Phasing, 18" Face Triangular Single-Wire Monopole Model Data

Tower	Impedance( Ohms)	Current (Apk)	Gain (dBi)	AGT	AGT-dB	F-S @ 1 mile
1	50.74 + j16.91	5.3579 @ -90	8.25 max.	1.999	0.00	393.5 mV/m @ -90.7 deg
2	18.93 - j19.90	5.3579 @ 0 deg				

Obtaining the desired phase shift and power division with a single ultimate source is subject to many techniques that we shall leave to external calculations. However, it is possible to construct a fairly complex model with a combination of TL and NT entries to incorporate the desired technique into the model. However, for most purposes, obtaining the individual source impedance values and the source-segment current magnitudes and ratios allow these calculations to proceed most efficiently externally to the model.

The data collection shows the maximum values for gain and field-strength (the latter still in peak form and needing conversion to RMS). Since most installations will need values in many directions to correlate with field measurements, the modeler should attend to the RP1 tabular output. The sample that follows shows the values for the rotated example. Once more, remember that NEC output reports employ the phi or counterclockwise convention for listing azimuth angles. Therefore, the value applicable to a compass-rose heading of 315 degrees occurs between the phi entries for 40 and 50 degrees.

\*\*\*\* Electric Field: Phi Pattern \*\*\*\*

Z=0, Freq=1, File=fcc55.NOU

---E (Theta)---			--- E (Phi) ---	
Phi	Magnitude	Phase	Magnitude	Phase
Degrees	Volts/m	Degrees	Volts/m	Degrees
0.00	3.8121E-001	-90.93	4.6724E-022	-153.51
10.00	3.8834E-001	-90.77	3.7881E-022	60.73
20.00	3.9181E-001	-90.66	2.7900E-022	147.41
30.00	3.9313E-001	-90.58	1.7082E-022	92.96
40.00	3.9347E-001	-90.54	5.7515E-023	-111.91
50.00	3.9347E-001	-90.54	5.7515E-023	68.09
60.00	3.9313E-001	-90.58	1.7082E-022	-87.04
70.00	3.9181E-001	-90.66	2.7900E-022	-32.59
80.00	3.8834E-001	-90.77	3.7881E-022	-119.27
90.00	3.8121E-001	-90.93	4.6724E-022	26.49
100.00	3.6887E-001	-91.12	5.4160E-022	62.13
110.00	3.5005E-001	-91.35	5.9964E-022	8.46
120.00	3.2409E-001	-91.64	6.3956E-022	-111.03
130.00	2.9115E-001	-92.01	6.6011E-022	89.18
140.00	2.5232E-001	-92.49	6.6063E-022	-84.18
150.00	2.0949E-001	-93.14	6.4106E-022	116.03
160.00	1.6509E-001	-94.10	6.0193E-022	-3.46
170.00	1.2182E-001	-95.61	5.4442E-022	-57.13
180.00	8.2234E-002	-98.30	4.7023E-022	-21.49
190.00	4.8653E-002	-103.96	3.8163E-022	124.27
200.00	2.3437E-002	-119.59	2.8130E-022	37.59
210.00	1.1594E-002	-170.26	1.7232E-022	92.04
220.00	1.3540E-002	146.90	5.8035E-023	-63.09
230.00	1.3540E-002	146.90	5.8035E-023	116.91
240.00	1.1594E-002	-170.26	1.7232E-022	-87.96
250.00	2.3437E-002	-119.59	2.8130E-022	-142.41
260.00	4.8653E-002	-103.96	3.8163E-022	-55.73
270.00	8.2234E-002	-98.30	4.7023E-022	158.51
280.00	1.2182E-001	-95.61	5.4442E-022	122.87

290.00	1.6509E-001	-94.10	6.0193E-022	176.54
300.00	2.0949E-001	-93.14	6.4106E-022	-63.97
310.00	2.5232E-001	-92.49	6.6063E-022	95.82
320.00	2.9115E-001	-92.01	6.6011E-022	-90.82
330.00	3.2409E-001	-91.64	6.3956E-022	68.97
340.00	3.5005E-001	-91.35	5.9964E-022	-171.54
350.00	3.6887E-001	-91.12	5.4160E-022	-117.87
360.00	3.8121E-001	-90.93	4.6724E-022	-153.51

## Conclusion

The notes in this episode have focused on the modeling convention, methods, and cautions applicable to multi-tower installations. I have used very simple arrays in order to set the modeling aspects of the situation in bold relief. Far more complex arrays are possible--and with them come far more complex models.

Some implementations of NEC are set up to ease the process of modeling arrays. For example, EZNEC provides RMS input and output values of voltages and currents. As well, the use of current sources is completely hidden, allowing the user simply to set in place the desired source values for current magnitude and phase. Our use of a more generic form of NEC has had the goal of showing some of what may go on "behind the scenes" in such interfaces.

A five-episode run of notes on a single topic--however broad--might seem to answer most of the beginning level questions one might have about tower modeling. Unfortunately, there is at least one

major category of question left over at the interface between AM BC tower modeling and tower modeling in general.

## Chapter 136: AM BC Modeling with NEC

### 6. Grounds

**W**e have essentially completed our journey through modeling broadcast towers with respect to the basic dimensions of modeling them. In many of the later episodes, we used NAB-recommended single-wire substitutes for full tower structures to maintain the clarity of the modeling suggestions in question. Of course, one may choose to model a full structure or a multi-leg alternative to the single-wire monopole. These notes only represent the barest of starts along the AM BC tower modeling task using NEC.

Nevertheless, as we look back over our work, we may harbor questions based on one facet of the modeling work: the use of a perfect ground for all models. Actual AM BC antennas use extensive radial fields, normally with each of 120 radials about 1/4-wavelength long at the assigned frequency. (Many actual fields include intervening shorter radials, but we shall not work with them here.) The radials are buried within the earth's surface in soils of highly variable quality as we move from one site to another. Hence, some folks may question the ability of a perfect ground to replicate accurately the conditions. In one sense, the questions are otiose, since standard practice is to refer such towers to perfect ground. However, there remain for some a few nagging questions about correlating site measured values of feedpoint current magnitude and phase and field-strength measures as well to modeled values using perfect ground.

NEC-4 allows us to explore these questions to a limited degree. Like NEC-2, it uses the Sommerfeld-Norton (SN) ground calculating system, which many refer to as the "high accuracy" ground compared to the reflection coefficient approximation (RCA) system. To use the SN ground calculation system accurately requires that we create a buried radial field of actual wires (GW entries), a task only available in NEC-4. As we saw in an early episode, we may assign a radial field to the RCA ground calculating system, but that system does not create actual wires. Instead, it adjusts the ground losses in the ground calculations. If we add enough radials to the specification, the RCA ground calculating system will return source impedance values that are identical to those we obtain with a perfect ground. An open question here is what values of source impedance we might obtain with true buried radials. Allied to this question is whether we can expect differences in either the far-field gain or the field-strength between models using the RCA system and models using the SN system with buried radials.

## Ground and Buried Radial Models

All NEC modeling systems share some common traits. First, we specify ground quality in terms of two basic properties: conductivity (in S/m) and relative permittivity (no unit). From these entries, NEC calculates a complex permittivity value used in ground calculations. Conductivity values--as measured or taken from tables--generally range from 0.001 S/m up to about 0.05 S/m for land locations. One accepted value for salt water's conductivity is 5.0 S/m. Permittivity usually tracks conductivity in the sense that soils with high conductivity tend to have high values of permittivity. The range of

permittivity values ranges roughly from 3 to 25 for land locations. Water locations may show values as high as 80. The direct parallel between conductivity and permittivity increases is not universal, and there are odd locations with respect to the general progression.

For our sampling purposes, we may resort to 3 values taken from very old (1939) tables.

#### Sample Ground Qualities

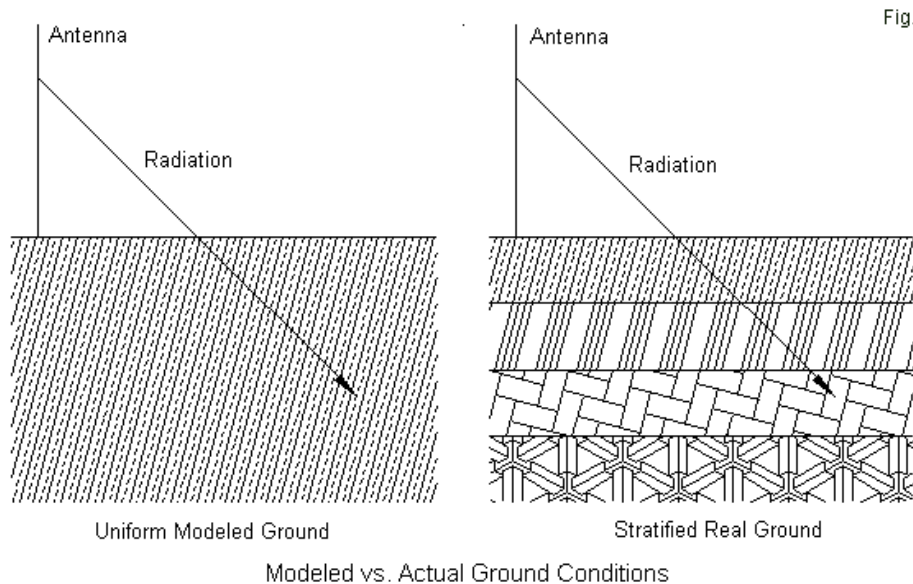
Label	Conductivity (S/m)	Permittivity
Very Good	0.0303	20
Average	0.005	13
Very Poor	0.001	5

For many kinds of modeling studies, very good soil yields data results about as distant from those emerging from average soil as very poor soil data depart from average soil values, although the directions are opposite.

NEC, however, regardless of the ground calculating system selected (except for perfect ground) has a limitation suggested by **Fig. 1**. The ground medium is homogenous and unlimited below the  $Z=0$  level. As we increase the operating frequency of an antenna or as we make use of horizontal antennas, this feature becomes insignificant. However, using a relatively low frequency (1 MHz in all examples) and vertical monopoles, the NEC ground medium is subject to some degree of error based on two facts. First, real soils tend to be stratified, as suggested on the right in **Fig. 1**. Second, the lower the operating frequency, the deeper will be the penetration of RF energy into the ground. With a radial system, the



penetration in the immediate vicinity of the antenna is limited, presumably controlled by the extensive radial field. However, in the region beyond the radial field, outside the control of antenna site builders, stratified soil may have an effect on the far field of an antenna that even SN models cannot fully calculate.



Within this limitation, we may still look at models using buried radials for the general purpose of comparing them with other kind of models. For this enterprise, we shall use 120 radials, each about 1/4-wavelength long at 1 MHz (245'), as shown in **Fig. 2**. We shall use a wire diameter of about 0.1", roughly corresponding to AWG

#10 wire. Since our dimensions are in feet, we shall round the radius to 0.004'.

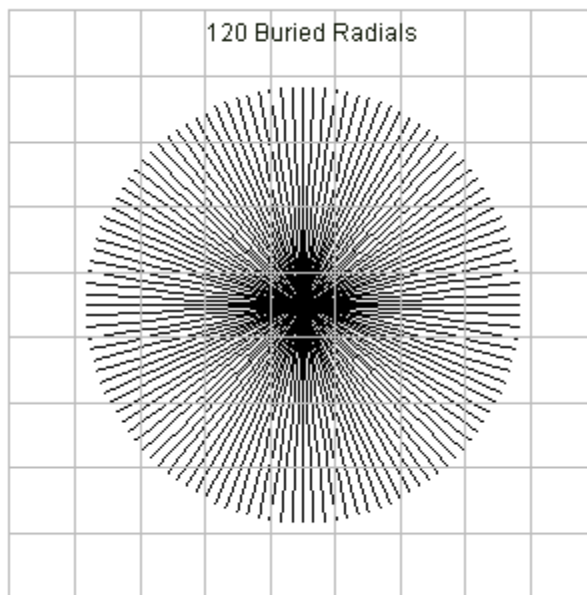


Fig. 2

If we assign each radial 10 segments, we shall end up with 1200 segments in the radial field alone. (The 10-segment per radial assignment is not critical in this application, since the radials will be symmetrically arranged around the monopole that extends through the surface to make contact with the ultimate junction. As well, as we change the soil quality and hence the complex permittivity

generated by NEC, the program will change the length of each segment in the current calculations based upon calculated affects of a medium that is not a vacuum or dry air.) We shall also wish to use the same set of 3 radial fields, each with a different soil quality, one more than one antenna. Under these conditions, we may wish to simplify the modeling by using Numerical Greens Files. For 1200 segments a Green's file may be exceedingly large. However, if we confine ourselves to entering only the radials in the Green's file models, we may shorten both calculating time and file size by the use of rotational symmetry. The GR command permits us to specify a single radial and to replicate it rotationally as many times as necessary while invoking symmetry. The resulting file for a 120-radial field in average soil appears in the following lines.

```
CM 120 radials, average ground
CE
GW 1 10 0 0 -1.5 245 0 -1.5 .004
GR 1 120
GS 1 0 0
GE -1 -1 0
FR 0 1 0 0 1 1
GN 2 0 0 0 13 .005
LD 5 0 0 0 5.8E7 1
WG ave120r5.wgf
```

The WG command writes the results of initial calculations to a file. Different implementations of NEC may allow only some file-name extensions. The model itself must contain the features shown in the sample. The GW entry lists one radial although the geometry to be replicated may be more complex. The GR command produces a

total of 120 versions of the radial with equal angular spacing between them. The GR command will always produce the wires and segments specified. However, the model run will not invoke symmetry if the GR command is followed by a succeeding geometry command, such as another wire (GW). The GS command uses NEC-4 shorthand for converting feet to meters, while the GE command is set up for buried wires.

In addition to the geometry elements, the Green's file model must also contain the overall specifications for the frequency and the ground quality. In these files, we must specify a single frequency. With respect to ground (GN), the only difference between this model and its counterparts for very good and very poor soils are the values for conductivity and relative permittivity. I have added an LD 5 command to construct the radials from copper wire. Any LD command within the model will apply only to the wires in the structure shown. It will not apply to wires that we later add to complete the modeling task. Finally, the WG command adds the file name for storing the results that we shall later call upon. The file name must begin with an alphabetic character, and a number at the start of the file name will generally produce an error message.

We shall produce three files, one for each type of ground. Each requires about 6 second to run and produces a file that is less than 600KB long. Unlike the NEC output file, the Green's file is not itself meaningfully readable by a user. Notable in these files is the depth of the buried radials: 1.5'. We shall discuss this aspect of the modeling as we complete our buried radial system monopole modeling work.

## Completing the Model

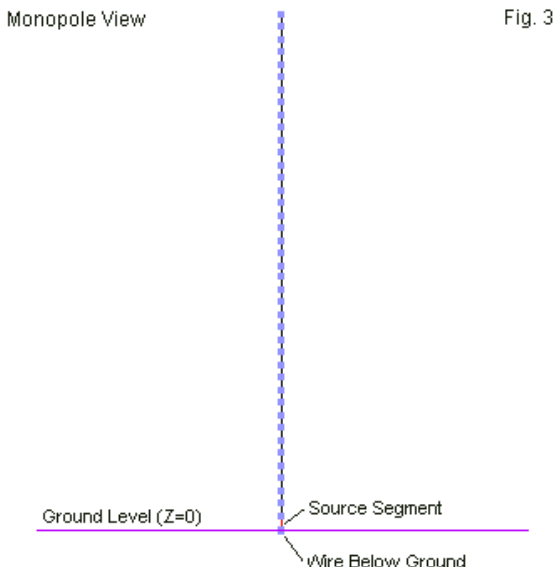
The monopole that we use for these calculations is simplest and most reliable if a single-wire is brought to ground and then extended to meet the junction of the radials. To achieve this goal, we need to write a simple new model that first calls up the Green's file and then adds further model refinements, such as a source (EX) and output requests (RP). The following lines sample the model for a near resonant NAB-recommended single-wire monopole substituting for a triangular tower with an 18" (1.5') face.

```
CM near-resonant monopole, perfect ground
CM NAB substitute single-wire monopole
CM buried 120 radials
CE
GF 0 avel20r5.wgf
GW 301 41 0 0 0 0 0 234 0.555
GW 302 1 0 0 -1.5 0 0 0 .555
GW 30901 1 9901.0000 9901.0000 9901.0000 9901.0001 9901.0001 9901.0001 .00001
GS 0 0 .3048
GE -1 0 0
EX 0 30901 1 0 0.0 7.3971
NT 30901 1 301 1 0 0 0 1 0 0
RP 0 181 1 1000 -90 0 1.00000 1.00000
RP 1 1 1 0000 0 0 1.00000 1.00000 1609.344
EN
```

Following the comment lines, the first geometry command (GF) calls the Green's file. Then we add our monopole, at least the portion that is above ground. NEC-4 requires that an element that passes through  $Z=0$  must do so at either a wire junction or a segment junction. In most cases, we may best avoid errors later on by making  $Z=0$  a position for a wire junction. Therefore, we place a second wire that runs from the junction with the radials to the ground end of the monopole. We assign the wires arbitrarily large

tag numbers, large enough to assure us that the tag numbers of the radials do not overrun the monopole tag numbers. (NEC will not normally mind the overlap, but reading the NEC output file becomes much more difficult.)

Although in reality, we might make such connections with one or more wires that are considerably thinner than the tower legs or the single-wire substitute for the tower, NEC shows various degrees of inaccuracy when joining wires of different diameters. Therefore, the wire radius for the extension should be the same as for the aboveground portion of the assembly.



How long we should make this wire and therefore how deeply the model should bury the wires presents us with a bit of a problem. As shown in **Fig. 3**, the new model view shows only the new wires of the extended monopole. Since we cannot bring the wires together and replicate the dual medium in the AGT test, it cannot help us to determine the model adequacy. However, if we recall some basic NEC guidelines, we can perform a substitute test. The radius of the monopole and its extension is 0.555'. As the segment length (here the extension-wire length) approaches a ratio of 2:1 or less, the results of NEC calculations become less certain. The goal then becomes arriving at a balance between the ideal segment length (equal to the segments in the upper part of the monopole) and the shortest segment length that will not yield readily detectable drifts in the output reports.

To test the situation, I created radial fields at depths of 1' and 1.5'. Next I created a series of 234' monopole, beginning with a radius of 0.5" (0.04') and gradually increasing the radius to 4.5" (0.375'). With the radials at 1' below ground, the trend in the progression of impedance reports reversed direction in the final step between 0.375' and 0.555'. However, by increasing the depth of the radials (and the monopole extension) to 1.5', I obtained a normal progression of impedance values. Since the effects of different radial depths with the thinnest monopoles in the series were minimal, I chose the 1.5' radial depth for this exercise.

The model that calls the Green's file contains a set of control commands that do not replicate those of the Green's file model. Hence, we find no ground or frequency specification. Had we

added an LD command for the monopole, it would appear in this file and apply only to the wires shown in this model. It would not apply to the wires in the Green's file. Of course, our completion model contains source information, including the added wire and network to invoke a current source and the adjustment to the current level to effect a power of 1 kW. Finally, we find output requests for an elevation/theta pattern and for a field-strength report at 1 mile at ground level.

We are now ready to look at the results of our models and compare them to models over perfect ground and over the RCA ground.

## Near-Resonant and Long Monopoles over Various Grounds

The model format for all of the near-resonant monopoles over buried radials is identical except for the file name of the Green's file. The root or reference model over perfect ground uses the same monopole, but a different and simpler format.

```
CM near-resonant monopole, perfect ground
CM NAB substitute single-wire monopole
CE
GW 1 41 0 0 0 0 0 234 0.555
GW 30901 1 9901.0000 9901.0000 9901.0000 9901.0001 9901.0001 9901.0001 .00001
GS 0 0 .3048
GE 1 0 0
GN 1
EX 0 30901 1 0 0.0 7.4897
NT 30901 1 1 1 0 0 0 1 0 0
FR 0 1 0 0 1 1
RP 0 181 1 1000 -90 0 1.00000 1.00000
RP 0 1 361 1000 90 0 1.00000 1.00000
RP 1 1 1 0000 0 0 1.00000 1.00000 1609.344
EN
```



Over the RCA ground, the NEC-4 model looks very much like the model over perfect ground, except for the entries in the GN command line. (Note: a NEC-2 model--as described in an earlier episode--will require an RP4 entry for the far-field pattern.) The entry not only specifies the ground quality, but as well the radial system (expressed in meters). Hence, we have 120 radials with a wire radius of 0.00127 m (which is the metric equivalent to the 0.1" diameter wires used with the SN system) and 75 meters (246') long each. We may use fatter radials in the RCA model since we do not construct them of individual wires and therefore need not be concerned about wire interpenetrations at angular junctions.

```
CM resonant monopole, RCA ave ground
CM NEC-4 procedures
CE
GW 1 41 0 0 234 0 0 0 0.555
GW 30901 1 9901.0000 9901.0000 9901.0000 9901.0001 9901.0001 9901.0001 .00001
GS 0 0 .3048
GE 1
GN 0 120 0 0 13.0000 0.0050 75 .00127
EX 0 30901 1 0 0.0 7.4897
NT 30901 1 1 41 0 0 0 1 0 0
FR 0 1 0 0 1 1
RP 0 181 1 1000 -90 0 1.00000 1.00000
RP 1 1 1 0000 0 0 1.00000 1.00000 1609.344
EN
```

We may tabulate the results of the modeling as follows.

Model Reports for a Near Resonant (234') 1-MHz Monopole with Varying Ground Situations							
System	Ground Quality	Impedance Ohms)	Current A(pk)	Max. Gain (dBi)	TO Angle (Deg)	F-S @ 1 mile	
Perfect	Perfect	35.65 - j 1.29	7.4897	5.14	0	275.1 mV/m @	-45.6 deg
	Very Good	37.29 + j 2.30	7.3235	3.37	16	263.3	-64.1
	Average	36.55 + j 2.10	7.3971	2.00	21	234.8	-85.8
	Very Poor	33.09 + j 1.82	7.7742	0.16	26	153.6	-121.3
RCA	Very Good	35.65 - j 1.29	7.4897	3.89	15	268.8	115.5
	Average	35.65 - j 1.29	7.4897	3.22	21	238.4	92.2
	Very Poor	35.65 - j 1.29	7.4897	2.62	27	150.1	52.8

The table is revelatory in several respects. Over the SN ground, the impedance of the antenna system decreases as the soil quality decreases. For some people, this result is counter-intuitive, especially if we over-stress the idea that ground losses increase with a decrease in soil quality. To a large but incomplete degree, the size of the radial system overcomes this fact. However, the radials do not counteract all ground effects. As we lower the conductivity toward zero and decrease the relative permittivity toward 1, the ground increasingly acts like free space. In free space, a monopole with ground radials having the same dimensions as the system in the models will show lower feedpoint impedance values than we obtain over perfect ground using the image assumption that underlies the calculations. Even over very poor ground, the lower impedance appears. Of course, the radial system does not counteract the RF losses in the region beyond the radials that is responsible for the bulk of the reflected energy that combines with the incident energy.

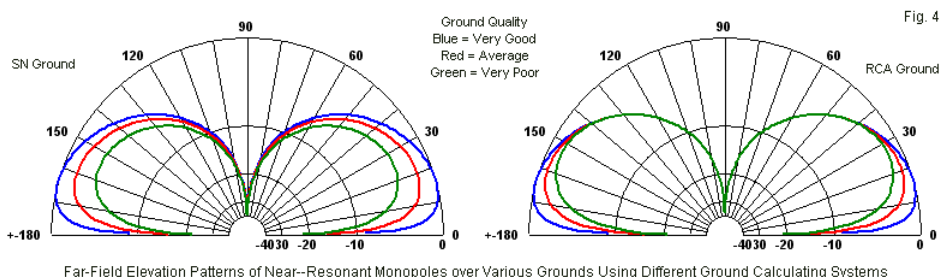


**Fig. 4** overlays the elevation patterns for the three ground qualities for each of the ground calculating systems. We may correlate the

patterns to the maximum gain values in the table. The RCA system overestimates the maximum far-field gain with increasing calculational optimism as the ground quality decreases. Moreover, the figure shows that the RCA ground calculating system result in stronger high-angle radiation (in the 60-degree elevation angle region) than the SN system. In fact, the patterns for the 3 ground qualities in the RCA system are identical for elevation angles of 40 degrees or more. The SN system shows weaker radiation at every angle (except perhaps at 90-degrees elevation) as we decrease the ground quality.

For most AM BC applications, we are less interested in the higher angle radiation, except perhaps when calculating the consequences for skip in periods of darkness. More interesting are the field-strength reports. Here we find only small differences (3 to 5 mV/m) as we move from one ground system to the other.

To confirm that the results of the initial modeling sequence are not anomalous, I repeated the exercise using the 273' or 90-degree monopole. Since all of the models are identical to those already shown, the model over perfect ground may serve as a stand-in for the entire collection. The only differences will appear in the GW line specifying the monopole and in the EX line specifying the current necessary for a 1-kW power level. These models should show sufficient off-resonance qualities to detect anomalies, if present.

```
CM 273' monopole, perfect ground
CM NAB substitute single-wire monopole
CE
GW 1 41 0 0 0 0 0 273 0.555
GW 30901 1 9901.0000 9901.0000 9901.0000 9901.0001 9901.0001 9901.0001 .00001
```

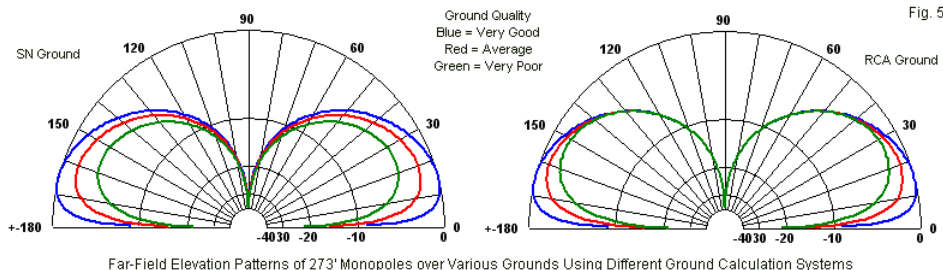
```

GS 0 0 .3048
GE 1 0 0
GN 1
EX 0 30901 1 0 0.0 5.7606
NT 30901 1 1 1 0 0 0 1 0 0
FR 0 1 0 0 1 1
RP 0 181 1 1000 -90 0 1.00000 1.00000
RP 0 1 361 1000 90 0 1.00000 1.00000
RP 1 1 1 0000 0 0 1.00000 1.00000 1609.344
RP 1 1 1 0000 0 0 1.00000 1.00000 3218.688
EN

```

The result can be tabulated in parallel to those shown for the shorter monopole.

Model Reports for a 273' 1-MHz Monopole with Varying Ground Situations								
System	Ground Quality	Impedance Ohms	Current A(pk)	Max. Gain (dBi)	TO Angle (Deg)	F-S @ 1 mile		
Perfect	Perfect	60.27 + j84.91	5.7606	5.30	0	280.0 mV/m @	-47.7 deg	
SN	Very Good	62.30 + j88.31	5.6657	3.49	15	268.7	-66.2	
	Average	60.98 + j87.85	5.7268	2.04	20	239.1	-87.8	
	Very Poor	55.10 + j87.63	6.0246	0.13	25	156.2	-122.8	
RCA	Very Good	60.27 + j84.91	5.7606	3.89	16	272.8	113.4	
	Average	60.27 + j84.91	5.7606	3.01	22	241.2	90.4	
	Very Poor	60.27 + j84.91	5.7606	2.22	28	151.3	52.0	



Far-Field Elevation Patterns of 273' Monopoles over Various Grounds Using Different Ground Calculation Systems

**Fig. 5** shows no aberrations relative to the patterns in **Fig. 4**. However, the table has some oddities relative to the maximum far field strength of the signals as modeled over the different ground calculating systems. The SN ground gives the taller monopole slightly more gain over very good ground than its 234' counterpart.

However, the gain increase grows smaller over decreasing ground quality so that the gain over very poor ground is a tiny amount less for the 273' tower. We find a similar trend, but with quite different numbers, over the RCA ground. With very good soil, the two monopoles report the same far-field gain. For all lesser quality soils, the taller tower actually reports a smaller value for maximum gain. Whatever the values for maximum far-field gain, the field-strength reports for any level of soil quality show a much smaller difference between systems--about 2-5 mV/m. However, in both tables, we find very different phase-angle reports between the two systems, with the SN reports more in accord with the value for perfect ground.

The source impedance reports replicate the results for the near-resonant monopole very closely. With 120 radials, the RCA system returns the same impedance as the model over perfect ground. The SN system shows a resistive component that decreases as the ground quality decreases. By the time we reach very poor ground, the source resistance is lower than the value reported for perfect ground.

The consistency of the source impedance reports between the two tables for system using monopoles of different length only confirms that the reports are true to the system of modeling employed.

## Conclusion

With this episode, we can bring the series of notes on modeling AM BC monopoles to a close. Our focus has been on the modeling that

goes into such systems, not on theory and practice within the design and engineering of AM BC towers. Hence, all of the models are very much simplified to allow us to see certain aspects of the process more clearly.

Even in this final section, it is not possible to suggest that one or another modeling system is superior. Such a conclusion is only possible if we bring to such a discussion the task-specific specifications in which modeling plays a role, but not the only role.

Nevertheless, the various episodes have shown that we may derive from NEC models the entire data set that AM BC modelers have traditionally derived from MININEC software--and some other things as well.

## Chapter 137: NEC Implementations Cores, Limitations, and Work-Arounds

In this series of columns, we have examined the NEC-2 and NEC-4 programs, with some attention to MININEC, in order to master to some degree the geometry and control commands and to assure that our models are as adequate to various modeling tasks as we can make them. We have not used various programs to recommend the particular implementations of NEC, but only to illustrate how we may reach or approximate (in some cases) a point where the core will calculate usable results. However, we have not undertaken in any systematic way an account of some of the differences among implementations of the cores. We shall turn our attention to this subject from time to time. Our goal is not to review programs. Nor is it to make recommendations. Instead, the aim is to note the various ways by which we may achieve the same goals in modeling using different means.

When working with implementations of NEC and MININEC, all notes carry a time-stamp. They are--assuming that I make no major blunders along the way--limited to program capabilities at the time of writing, which is always well in advance of publication. Therefore, if I assign a task method or a limitation to a program, the program may have changed by the time you read these notes. Hence, you have the final responsibility of investigating implementations of NEC or MININEC to determine current techniques and limitations before committing to one of them.

## 1. Core Concerns

Our first step is to note that both available versions of NEC (-2 and -4) and all versions of MININEC begin by assuming that the antenna is composed of thin round wires. Both use the Method of Moments to calculate the mutual impedance among the segments in a wire and in all of the wires that make up the antenna's geometry. From that point, the programs calculate the current in each segment relative to an assigned source, and from there the programs go on to calculate a wide variety of useful antenna performance data. The most commonly used data is the far-field radiation pattern, although some NEC entry-level programs also allow calculation of near-field, ground wave, and other data, depending upon the implementation.

NEC-2 is in the public domain. Therefore, programmers may modify the core as necessary to create a unified software package. For example, EZNEC, when using the NEC-2 core, does not transfer data to the core using the standard input file, illustrated in **Fig. 1**. In contrast, NEC-Win Plus creates a special input file in the standard format so that the core remains a separable module.



```

CM OWA 6-el Yagi
CE
GW 1,15,0.,-.25,0.,0.,-.25,0.,.00125
GW 2,15,.125,.247,0.,.125,-.247,0.,.00125
GW 3,15,.177,.231,0.,.177,-.231,0.,.00125
GW 4,15,.321,.225,0.,.321,-.225,0.,.00125
GW 5,15,.461,.225,0.,.461,-.225,0.,.00125
GW 6,15,.671,.216,0.,.671,-.216,0.,.00125
GE 0
FR 0,1,0,0,299.7925
GN -1
EX 0,2,8,0,0.,1.0
RP 0,1,361,1000,90.,0.,0.,1.,0.
EN

```

Fig. 1

Typical ASCII .NEC-Format Model File

Licensing agreements with LLNL/UCal, which holds proprietary rights on NEC-4, require programmers to use the core as given or only with authorized correctives that emerge from time to time. There are, at present, only two programming sources for NEC-4 programs: EZNEC (Pro/4) and Nittany-Scientific (GNEC). [Ed: *We do not recommend Nittany-Scientific for lack of program upgrades and technical support*]. Both create standard ASCII format input files for core runs. Since the use of NEC-4 requires a separate license from LLNL/UCal--in addition to any costs associated with commercial implementations--the licensee may use the supplied core with any other I/O system available and compatible. For example, both Multi-NEC and 4NEC2 permit (with greater or lesser difficulty) access to any NEC core using their input and output facilities. A good number of NEC-4 licensees have developed their

own interface systems, either because it is a challenge or because there may be special individual or company needs.

NEC-4 from the 1990s is an advance over NEC-2. The 1980s core had some significant limitations, many centered on the current algorithm used. Two of those limitations prompted extensive further developments. NEC-2 could not handle buried wires, that is, wires placed with  $Z$  less than zero when using a real ground. As well, NEC-2 introduced significant errors in the performance calculations associated with antenna elements using a diameter taper schedule. The most common taper schedule is the gradual reduction in the wire (or tubing) diameter from the center of a dipole-type element to its tips. However, the limitation also applies to biconical elements constructed in the same manner. NEC-4 uses a more complex current algorithm that overcomes much--but not all--of the tapered element difficulty. It also permits the placement of wires below the surface of a ground medium, but with geometry rules for handling wires that pass through the surface.

The most accurate way to handle element taper schedules amounts to a program add-on by those who develop modeling software. The method involves the use of the Leeson correctives, which create uniform-diameter substitute elements equivalent to the tapered-diameter element. Programs perform calculations using the substitute elements, which have proven to be highly accurate for HF antenna design work when rightly used. One common modeler flaw involves allowing the segments in the substitute sections to have radically different lengths, especially in the high-current regions of the element. As well, the Leeson corrections are only

applicable to linear elements without loads (except at the very center) within about  $\pm 15\%$  of self-resonance. (The substitute elements are also applicable to tapered diameter monopoles fed at the base with loads only at the base.) **Fig. 2** illustrates a tapered element wire table and the substitute uniform-diameter element.

Wires											
Wire Create Edit Other <span style="float: right;">Fig. 2</span>											
<input type="checkbox"/> Coord Entry Mode <input type="checkbox"/> Preserve Connections <span style="float: right;"><input type="checkbox"/> Show Wire Insulation</span>											
Wires											
No.	End 1				End 2				Diameter (in)	Segs	
	X (in)	Y (in)	Z (in)	Conn	X (in)	Y (in)	Z (in)	Conn			
1	-203.5	72	0		-138	72	0	W2E1	0.5	8	
2	-138	72	0	W1E2	-96	72	0	W3E1	0.625	6	
3	-96	72	0	W2E2	-48	72	0	W4E1	0.75	6	
4	-48	72	0	W3E2	-4	72	0	W5E1	0.875	5	
5	-4	72	0	W4E2	4	72	0	W6E1	3.419	1	
6	4	72	0	W5E2	48	72	0	W7E1	0.875	5	
7	48	72	0	W6E2	96	72	0	W8E1	0.75	6	
8	96	72	0	W7E2	138	72	0	W9E1	0.625	6	
9	138	72	0	W8E2	203.5	72	0		0.5	8	
*											

Stepped Diameter Correction											
Edit Other											
Wires											
No.	End 1				End 2				Diameter (in)	Segs	
	X (in)	Y (in)	Z (in)	Conn	X (in)	Y (in)	Z (in)	Conn			
1	-197.15	72	0		-133.694	72	0	W2E1	0.676784	8	
2	-133.694	72	0	W1E2	-93.0043	72	0	W3E1	0.676784	6	
3	-93.0043	72	0	W2E2	-46.5021	72	0	W4E1	0.676784	6	
4	-46.5021	72	0	W3E2	-3.87518	72	0	W5E1	0.676784	5	
5	-3.87518	72	0	W4E2	3.87518	72	0	W6E1	0.676784	1	
6	3.87518	72	0	W5E2	46.5021	72	0	W7E1	0.676784	5	
7	46.5021	72	0	W6E2	93.0043	72	0	W8E1	0.676784	6	
8	93.0043	72	0	W7E2	133.694	72	0	W9E1	0.676784	6	
9	133.694	72	0	W8E2	197.15	72	0		0.676784	8	

Both NEC-2 and NEC-4 originated as Fortran code for use on mainframe computers. As PCs developed faster speeds and much larger memory capacities, compiled Fortran that would run in the DOS/Windows environments became common and is at the heart of almost all present implementations of NEC. However, in the 1980s, those developments were yet to come. Rockway and Logan developed an alternative modeling program with reduced features that would run on mini-computers: MININEC. The current public domain version is 3.13, although without extensive modification, the program has many inadequacies when taken above the mid-HF region or into complex antenna geometries. The early MININEC resulted in a number of commercial DOS implementations, most notably EZNEC by W7EL and AO (MN) by K6STI. Although both programmers introduced some correctives to overcome MININEC limitations, the emergence of NEC-2 supplanted those efforts. Rockway and Logan re-developed the fundamental MININEC algorithms and have marketed various levels of Expert MININEC. Teri Software has extensively modified the calculation routines to produce perhaps the most accurate version of MININEC, and in the process added features only available previously in NEC, for example, the high accuracy Sommerfeld-Norton ground calculation system. There are freeware versions of MININEC available, such as MMANA. However attractive interface and auxiliary function provisions may make the program, the basic core accuracy remains the key to acceptability. For work that is to have widespread acceptance, only Antenna Model (AM) has overcome MININEC limitations so that, in regions where NEC-4 has known accuracy, benchmark models have matched the performance of the current standard in round-wire antenna modeling.

Both NEC-4 and AM's MININEC have limitations, and the use of the "other" core may be necessary for reasonable results. For example, MININEC cannot handle buried wires. Hence, for good results with buried radial fields of various sizes, NEC-4 remains necessary. On the other hand, NEC-4 tends to go astray with angular junctions of wires having different diameters, a common occurrence in many antennas using a folded geometry. MININEC does not suffer this limitation and may be necessary for these types of problems.

Unfortunately, I do not know of an implementation of the modeling cores that allows one to shift from one type of core (NEC or MININEC) to the other within the same program. One exception exists, although it is an Excel application: Multi-NEC by AC6LA. We might classify Multi-NEC as a spreadsheet shell containing both input and output facilities, but without a core of its own (other than a public-domain NEC-2 core). Rather, it will access certain cores that it recognizes and (for commercial implementations) for which it has prior agreements. Currently, Multi-NEC can access stand-alone NEC cores as well as the cores within NEC-Win/GNEC (Nittany-Scientific), EZNEC, 4NEC2, and Antenna Model. For crosschecking the results of a model in NEC and MININEC, Multi-NEC may be the easiest route.

## 2. File Keeping and Swapping

The alternative to using Multi-NEC to move among cores is to swap files from one program to another. This is not always as easy a process as it may seem on the surface, since many implementations of NEC and MININEC use unique formats or

proprietary file coding to meet the needs of the individual implementation.

1. *Formats*: The model file may be stored as an ASCII file or in a proprietary format created by the programmer. In general, the use of an ASCII file becomes evident if you can open the file using Notepad. The file shown in **Fig. 1** is perhaps the most rudimentary and universal type of file, and the file name would normally be followed by the extension .NEC. For reasons that will become clear as we go along, it is readable as given by almost any of the programs that we have mentioned.

EZNEC, NEC-Win Plus, and Antenna Model use non-ASCII file formats. There are many reasons for using such formats. For example, NEC-Win Plus uses a spreadsheet format that is capable of including equations in spreadsheet form. However, the program can also import and save files in .NEC format (of the most basic form). That does not mean, however, that the program can handle any .NEC model, since it recognizes only the commands that it uses in normal operation.

Not all ASCII-readable model files are readable by other programs as model input files. For example, as suggested by the sample in **Fig. 3**, NEC2GO files are in ASCII format, but under the extension .ANT. The format of the file derives from but is not limited to the MININEC program MN (part of AO) by K6STI, and the later NEC-Wires program. The format allows the modeler to include in the model file a collection of symbolic definitions and equations, which then enter the wire lines as symbols rather than numbers.

```
80 meter delta loop,corner feed      Typical ASCII NEC2GO Model File
Sommerfeld Norton ground
Freq:3.6 MHz, Type=copper wire Units=feet

ang = 45                ; angle
len = 85                ; side length
top = 90                ; top hgt

bot = top-sin(ang)*len   ; base hgt
y = cos(ang)*len        ; side y

sz = #16                ; #16 wire

source: endl ;
1  0, -y, bot          0,  y, bot          sz ; base wire

2  0,  y, bot          0,  0, top          sz ; side 1
3  0,  0, top          0, -y, bot          sz ; side 2

comments: A delta loop using variables. Try sweeping the angle
and length parameters.
```

Fig. 3

*Compatibility:* NEC2GO illustrates another limitation in swapping files. In its FAQ, the programmer notes that this version of NEC-2 is a flexible program for certain modeling purposes, but it does not offer full support of all NEC-2 input and output possibilities.

Nec2Go does not have provision for the following NEC2  
Geometry/Control statements: GA - Wire Arc  
GF - Read Greens Function file  
GH - Helix/Spiral specification

GR - Generate Cylinder  
GX - Reflection in coordinate planes  
SP - Surface Patch  
SM - Multiple Surface Patch  
CP - Maximum Coupling calculation  
NE/NH - Near Fields  
PQ - Print control for charge on wires  
WG - Write Greens Function

Other entry-level programs are similarly but not identically limited. For example, both EZNEC and NEC-Win Plus construct all model geometries using only the GW command (with an implicit GE command separating the geometry from the control commands that follow). To replicate the functions of some NEC commands, programs use different techniques. EZNEC employs a collection of structural facilities to develop various shapes. In contrast, NEC-Win Plus offers a spreadsheet with full variable and equation facilities by which one can create similar structures. In NEC2GO, the symbols and equations become part of the ASCII model file, while NEC-Win Plus uses a non-ASCII file format. When saving a file in .NEC form, NEC-Win Plus strips the file of the variables and equations and uses only the current set of numerical values derived from those variables and equations.

The control commands are equally limited in many entry-level programs. Virtually all entry-level NEC-2 programs allow access only to the standard voltage source in NEC. Programmers have developed a means of using a remote source wire and a network command--invisible to the user--to provide a virtual current source.

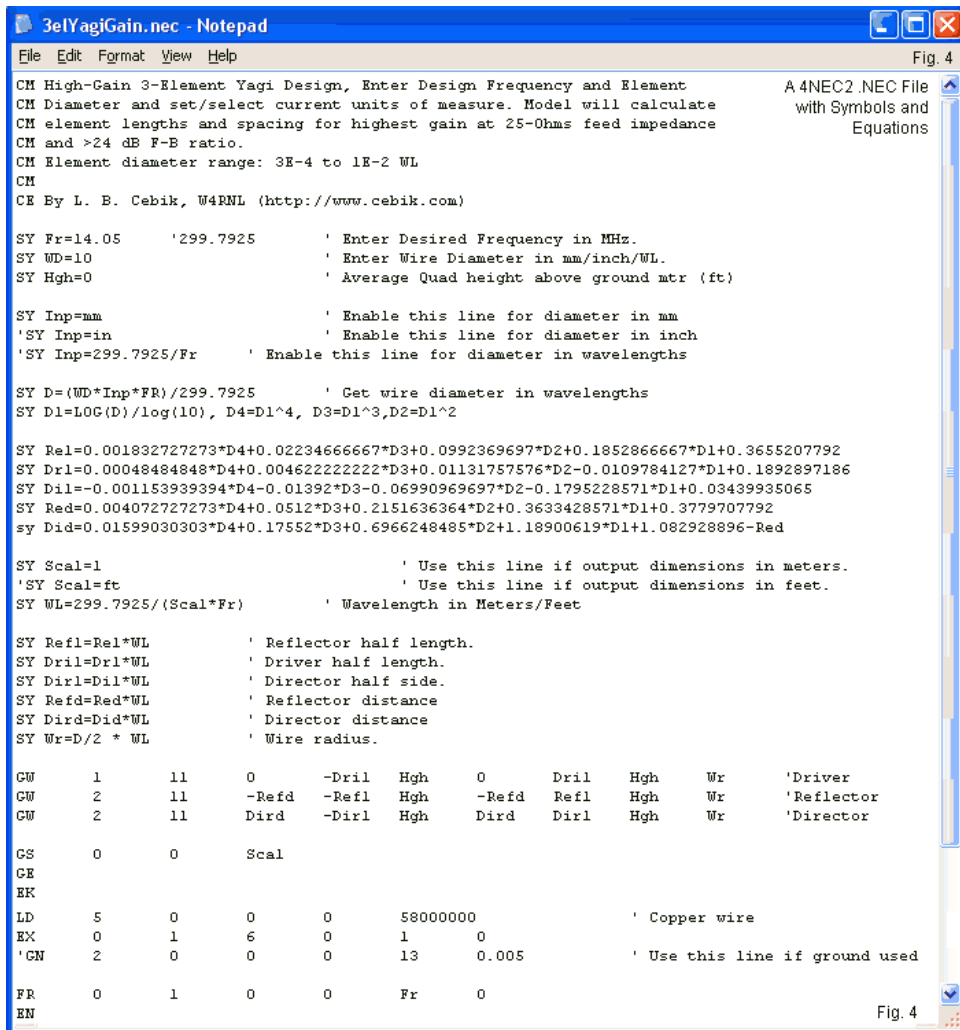


(In contrast, MININEC, as in Antenna Model, employs a true current source.) In either type of system, the user does not have access to options for plane-wave excitation and some of the current-printing facilities that are useful in connection with this command. In contrast, full versions of NEC programs allow access to the entire command structure that the core can accept. In many cases, the use of these commands requires the modeler to understand the command entry requirements. One typical error that can infect even the work of an experienced modeler is to construct a wire geometry in a unit of measure other than meters and then forget that all control commands calling for dimensions must have them only in terms of meters.

The output calculations are similarly limited in entry-level programs to the RP0 or far-field radiation patterns. In some cases, there is also no provision for the modeler to vary XNDA. However, such programs may have special functions to provide an Average Gain Test--which involves several set-up steps to be accurate. One of those steps is a change in the so-called "normal" XNDA setting. Programs may overcome some of the limitations by post-core-run calculations. One feature that is growing in popularity is the calculation of left-hand and right-hand circular polarization components.

Only some entry-level programs allow access to the near-field commands, and then usually only in tabular form. Although the development of polar 2-D and 3-D plots has reached a high level, developing graphical displays for near-field calculation results has so far defied most NEC programs.

Not all model files that end with the extension .NEC and that are ASCII-readable are fully compatible with each other. For example, the 4NEC2 file shown in **Fig. 4** derives from a set of algorithms from which one may develop models of a 3-element Yagi having certain properties over a very wide range of frequencies and element diameters. The original model used the spreadsheet function within NEC-Win Plus and has subsequently been transferred to an independent spreadsheet. Arie Voors, the developer of 4NEC2 has converted the required calculations to the file format that applies to his program, resulting in a model file with much more space devoted to the calculations than to the actual model structure.



```

3elYagiGain.nec - Notepad
File Edit Format View Help
CM High-Gain 3-Element Yagi Design, Enter Design Frequency and Element
CM Diameter and set/select current units of measure. Model will calculate
CM element lengths and spacing for highest gain at 25-Ohms feed impedance
CM and >24 dB F-B ratio.
CM Element diameter range: 3E-4 to 1E-2 WL
CM
CE By L. B. Cebik, W4RNL (http://www.cebik.com)

SY Fr=14.05      '299.7925      ' Enter Desired Frequency in MHz.
SY WD=10         '              ' Enter Wire Diameter in mm/inch/WL.
SY Hgh=0         '              ' Average Quad height above ground mtr (ft)

SY Inp=mm        ' Enable this line for diameter in mm
'SY Inp=in       ' Enable this line for diameter in inch
'SY Inp=299.7925/Fr ' Enable this line for diameter in wavelengths

SY D=(WD*Inp*Fr)/299.7925 ' Get wire diameter in wavelengths
SY D1=LOG(D)/log(10), D4=D1^4, D3=D1^3,D2=D1^2

SY Rel=0.001832727273*D4+0.02234666667*D3+0.0992369697*D2+0.1852866667*D1+0.3655207792
SY Drl=0.00048484848*D4+0.00462222222*D3+0.01131757576*D2+0.0109784127*D1+0.1892897186
SY Drl=-0.001153939394*D4-0.01392*D3-0.06990969697*D2-0.1795228571*D1+0.03439935065
SY Red=0.004072727273*D4+0.0512*D3+0.2151636364*D2+0.3633428571*D1+0.3779707792
sy Dld=0.01599030303*D4+0.17552*D3+0.6966248485*D2+1.18900619*D1+1.082928896-Red

SY Scal=1        ' Use this line if output dimensions in meters.
'SY Scal=ft      ' Use this line if output dimensions in feet.
SY WL=299.7925/(Scal*Fr) ' Wavelength in Meters/Feet

SY Refl=Rel*WL   ' Reflector half length.
SY Drl=Drl*WL    ' Driver half length.
SY Dirl=Dil*WL   ' Director half side.
SY Refd=Red*WL   ' Reflector distance
SY Dird=Did*WL   ' Director distance
SY Wr=D/2 * WL   ' Wire radius.

GW 1 11 0 -Drl Hgh 0 Drl Hgh Wr 'Driver
GW 2 11 -Refd -Refl Hgh -Refd Refl Hgh Wr 'Reflector
GW 2 11 Dird -Dirl Hgh Dird Dirl Hgh Wr 'Director

GS 0 0 Scal
GE
EK
LD 5 0 0 0 58000000 ' Copper wire
EX 0 1 6 0 1 0
'GN 2 0 0 0 13 0.005 ' Use this line if ground used

FR 0 1 0 0 Fr 0
EN
  
```

Fig. 4

In 4NEC2, symbolic expressions have a special code: SY. Otherwise, the progression of the NEC file follows the usual form for a .NEC file. Compare this file with the one in **Fig. 3**. Although both files do similar work, they are not fully compatible with each other.

*NEC-4:* Compatibility of files does not solely concern the storage format. It also involves cores. For example, NEC-4 has introduced new commands relative to NEC-2. For example, IS and UM do not exist in NEC-2. It has also eliminated others, such as EK. More easily overlooked in attempts to swap files is the fact that numerous NEC-4 commands differ in whole or part from their NEC-2 counterparts. The inter-relationships among the RP (radiation pattern), GE (geometry end), and the ground commands differ for the two programs. The GH (helix formation) command is wholly different between the two cores. As well, a few commands have added new floating decimal entries into which the NEC-4 user can place significant values. Therefore, not all NEC-2 .NEC files will run correctly with a NEC-4 core, and NEC-4 files may run incorrectly or not at all with NEC-2. There are enough perfectly compatible files relative to the two cores that it is easy to overlook the critical differences.

*File Swapping:* Setting aside the cautions that we have covered, the most-used way to move files from one program to another is by using the basic numerical entry .NEC file as the medium. Advanced versions of EZNEC can input and output files in .NEC format. In general, it informs the user when a command is not translatable, and as development time passes, fewer commands become

unacceptable. NEC-Win Plus has always had the ability to input and output files in .NEC format, although always within the boundaries of its entry-level command structure. It will abort conversions that involve unrecognized commands. NEC2GO has added .NEC file compatibility.

Even the MININEC program Antenna Model will now read and convert .NEC files to its format. The process is not just a matter of file-format conversion, but also involves modifying the file to fit the MININEC requirements. Whereas NEC places all sources and loads within segments of wires, MININEC places sources and loads on pulses, which are located at the junction of wire segments. AM will move sources and loads to the nearest pulse. Since a centered feedpoint or source is such a common antenna feature, AM will also add a segment to the source wire to ensure that the NEC-centered source is also a MININEC-centered source position.

One of the most flexible vehicles for file-format swapping is Multi-NEC. Because this spreadsheet shell works so closely with the cores of existing programs, it also has the ability to accept files and to save files in a variety of formats. Besides the native Excel spreadsheet format (.WEG), the program handles files in EZNEC (.EZ), Antenna Model (.DEF), and standard (.NEC) formats. Within the limitations of recognized commands and numerical formats, one may use Multi-NEC as a means of transferring antenna geometries based on the wires (GW) commands from almost any program to almost any other--at least among the group that we have been considering. (Of course, Multi-NEC has numerous other features that recommend it, but those are for future episodes.)

## Conclusion

Our initial entry into looking at divergent implementations of NEC and MININEC has focused primarily on differences among programs and cores. Nothing here represents a review of the implementations and even less a grading or ranking of the various programs available for round-wire antenna modeling. The focus on differences has aimed to alert the modeler who may move among programs to potential pitfalls and frustrations in order to avoid them to the degree possible. Various implementations have relatively exclusive features and auxiliary functions that we may wish to use from time to time. Understanding how the program facilities differ can ease the process--and even tell us whether we can do what we want to do.

In the end, the modeler must take final responsibility for the compatibility of his models with the program he wishes to apply to them. Knowing the differences among the cores and what is available and excluded by various implementations can change that task from guesswork into informed decision-making.

## Chapter 138: Types of Substitute Models

**W**e cannot model every possible antenna structure in NEC. Some structures are best suited for other types of software, for example, strip elements with a substrate on one side that has a definite dielectric constant. In fact, strip elements in free space may alone prove problematical unless we first perform some external equivalency tests to determine what size round wire best approximates the performance of a strip element. Very often, creating a series of simple dipoles at a design frequency will suffice, although there may be more critical situations in which we find a difference in the mutual coupling between strips relative to round wires.

In some cases, the limitations of NEC-2 and NEC-4 may limit our modeling abilities. NEC-2 provides various degrees of error in the output report for linear elements with stepped diameters. NEC-4 largely, but not completely, corrects this error. For small diameter changes between steps, NEC-4 is highly accurate, but becomes less accurate as the diameter steps grow larger, especially in high-current regions of a structure. Both cores tend to show errors with changes in wire diameter at angular junctions. Many software packages have modules to create substitute elements using the Leeson corrections to form uniform-diameter elements out of stepped-diameter elements. However, an angular junction will normally prevent the functioning of these modules or facilities. In addition, NEC cannot directly model coaxial wire structures. Hence, we cannot capture the physical aspects of an antenna element composed of coaxially arranged wires.

We have not listed all of the limitations of the NEC cores, but we have enough to give us sufficient reason to develop substitute models where NEC may not directly go. In a broad way, we may divide the types of substitute models into three groups.

Type 1. Substituting one geometry for another

Type 2. Substituting the electrical equivalent for the original structure where we may check our work with the original structure

Type 3. Substituting the electrical equivalent for the original structure where we may not check our work by modeling the full structure

Each type of substitute has different consequences for our trust in the models and different cautions for creating the substitute model. Therefore, let's examine a sample of each type to see what we might learn.

## **Substituting on Geometry for Another**

Perhaps the most common form of geometry substitution consists of replacing a highly complex multi-legged tower with a uniform-diameter round wire with the same height. As earlier episodes in the series established, the BC industry has developed some very reliable guidelines for the substitution. Extensive cross checks between the substitutes and full models of multi-legged towers have yielded the following equivalencies.



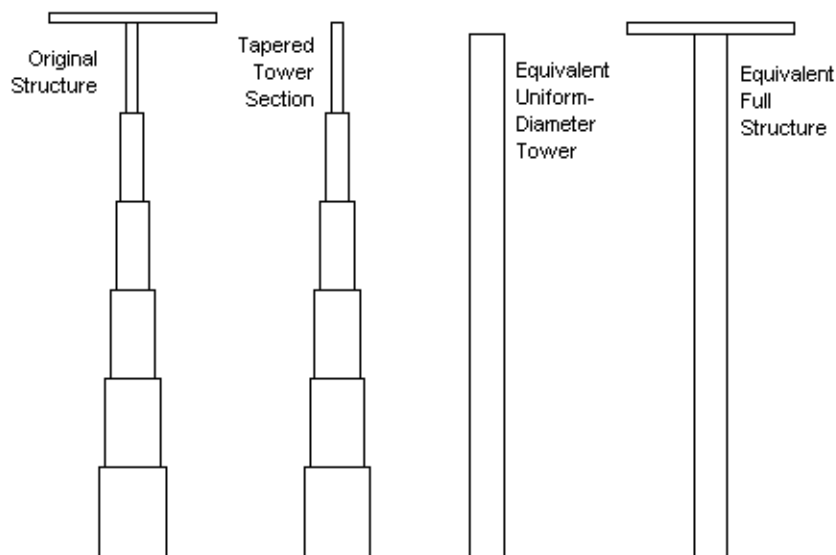
## Recommended Substitute Single-Wire Dimensions for Multi-Face Towers

Tower Type	Diameter	Radius
Triangular	$D = 0.74 * \text{Face Width}$	$R = 0.37 * \text{Face Width}$
Square	$D = 1.12 * \text{Face Width}$	$R = 0.56 * \text{Face Width}$

Note: D and R are in the same units as the Face Width

Modelers also face another problem--especially when using NEC-2--even for round tower sections when the tower steps the diameters of the sections. Let's consider a 60' tall tower over perfect ground (for simplicity of modeling) at 3.5 MHz. The tower consists of 6 10' sections, each 1/2" smaller in diameter than the next lower one. Let's use 3.5" for the base section diameter and taper it to 1" for the top section. The total tower is still short to achieve resonance at 3.5 MHz, so we shall add two short section of 1" diameter material to form a T at the tower top. We shall select lengths of tubing that just bring the tower to resonance over the prescribed ground. We shall place the source on the lowest segment of the lowest tower section.

We cannot simply invoke the Leeson corrections for the tower in this case, since the presence of the T-top will normally block the calculations, since the corrections only apply to linear section under certain conditions. Therefore, we shall have to proceed in steps, as indicated in **Fig. 1**.



Steps in Developing a Substitute Geometry Model

Fig. 1

First, we remove the T-top tubes from the tower. Now we may perform the Leeson correction calculations on the tower sections alone. Once we have derived the correct length and diameter of a uniform-diameter element that is equivalent to the original tower, we can replace the T-top and proceed to the final output reports that we might need. **Fig. 2** shows the process as it might proceed using EZNEC's version of the correctives.

Chapter 138

Some less-practiced modelers might object to the lower section of the wire table, since it includes angular junctions between very different wire diameters. Therefore, let's tabulate the results and see what we obtain. Raw Gain indicates the direct NEC output report. AGT is the average gain test score, and converts to the gain adjustment value in the AGT-dB column. The adjusted gain appears in Adj Gain. The Feed Z column reports the source impedance.

Results of substituting one geometry for another: sample 60' tower with a T-top

Model jX Ohms)	Raw Gain dBi	AGT	AGT-dB	Adj Gain dBi	Feed Z (R +/-
NEC-2 Original	5.41	1.062	0.26	5.15	35.8 + j4.4
NEC-2 Substitute	5.10	1.000	0.00	5.10	32.7 - j9.1
Substitute with 7.7' T elements	5.11	1.000	0.00	5.11	34.2 + j0.9
NEC-4 Original	5.22	1.018	0.08	5.14	35.4 - j0.3

The sample problem shows several things, not the least of which is that nothing critical is at stake except perhaps for the correct array gain value. We easily bring this into line by adjusting it with the AGT score. As well, the model shows that the symmetrically placed T-top elements at 90 degrees to the tower do not create serious errors. Unlike a single bend, as we might find in an inverted-L configuration, symmetrical elements (from two to many) result in virtually complete field cancellations from these low-current additions and do not adversely affect the AGT score or the general reliability of the results.

The original model, as shown by the last line of the table, emerged from a NEC-4 exercise using no correctives. This model is the

origin of the 6.8' T elements. However, even NEC-4 shows a small but not insignificant departure from the ideal AGT score, enough to require an adjustment to its gain report. Therefore, it also has a degree of unreliability that--while smaller than for the uncorrected NEC-2 model--casts some doubt on the accuracy of the 6.8' length for the T-top elements. Increasing their length to 7.7' each brings the corrected model to resonance. In fact, the only difference between the 2 cores with respect to the substitute model is a minuscule difference in the report source impedance. NEC-4 reports 34.0 - j0.3 Ohms.

The sample also informs us that geometric substitutions are not perfect solutions if we plan to build the modeled structure. Assuming that we could simulate perfect ground and construct the tower as originally specified, the exercise would alert us to allow for considerable adjustment range in the lengths of the T-top elements if our goal happened to be to bring the antenna to resonance at 3.5 MHz. Of course, we may increase the level of modeling complexity by adding an appropriate real ground and bury some radials (in NEC-4) according to the number we plan to place at the tower base. Nevertheless, in all of its simplicity and final indefiniteness, the sample illustrates one of the typical processes of using substitute geometry to arrive at a more adequate, if not quite perfect, model of the tapered tower and T-top situation.

## Substituting the Electrical Equivalent for the Original Structure Where We May Check Our Work with the Original Structure

We may sometimes simplify the modeling process by replacing complex wire structures with simplified electronic equivalents. The process is especially applicable if we can first establish the equivalence between the substitution technique and an all-wire structure. Once confirmed, we may apply the technique with confidence in situations where we might not be able to accurately produce an all-wire model.

One such situation is the placements of  $1/4$ -wavelength phasing stubs composed of parallel transmission line between successive  $1/2$ -wavelength sections in a collinear array. The use of stubs keeps all sections of the array in phase. Because the stubs occur at high-impedance points along the wire, where voltage and current are changing very rapidly, the use of the NEC TL facility is not recommended. Therefore, modelers normally create all-wire models of the collinear array, as suggested by the top sketch in **Fig. 3**. We shall explain the lower half shortly.

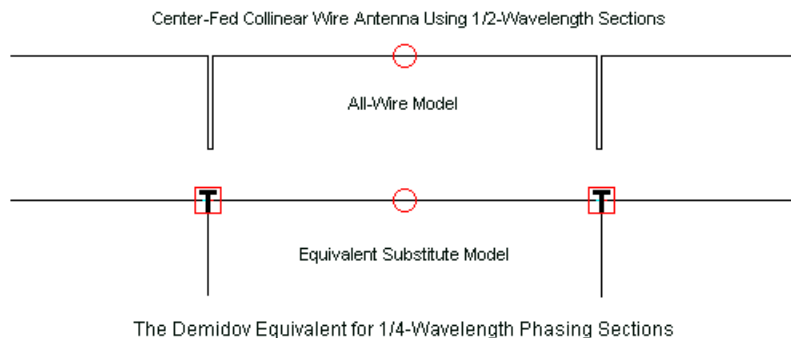


Fig. 3

The accuracy of such models often is restricted to cases in which the phase-line wires and the main element wires have the same diameter. For example, suppose that we wished the 2-wavelength array to use AWG #12 wire. We might construct the phase lines from the same wire, perhaps using a spacing of 6". Such an arrangements for a 15-meter (21.225-MHz) antenna might be quite practical. However, if we were to apply the same principles to a vertical array for the VHF or UHF range, it is more likely that the main vertical element and the phasing line would have very different diameters.

Vadim Demidov recently sent me a note outlining an alternative procedure that does not require the very high segmentation often required of all-wire (sometimes called "brute-force") models. As Vadim explained his reasoning, "After splitting TEM and common-mode phenomena in the stub I suggested considering it as an ideal auto-transformer with its midpoint "grounded" by means of a quarter wavelength wire. In this type of model, a stub is

represented by its common-mode equivalent, which is a single wire (without need for too fine segmentation), while the phasing transformer is made by a short transmission line linking two segments joining it." The result is the model in the lower sketch in **Fig. 4**, where the EZNEC designator "T" marks the location of the ideal transformer, and the vertical wire is the common-mode element.

To confirm the exercise, I converted the collinear 21.225-MHz array into a Demidov model. **Fig. 4** shows what is involved. However, understand that this is a proof-of-principle exercise. Therefore, both models use the same level of segmentation on all wires in order to minimize modeling differences. My goal was to discover to what degree we can trust the Demidov electrical substitute as an accurate representation of the all-wire model of presumed accuracy.



Wires

Wire Create Edit Other

A Sample of Electrically Equivalent Models

Fig. 4

☐ Coord Entry Mode
 ☐ Preserve Connections
 All-Wire Model
 ☐ Show Wire Insulation

Wires

No.	End 1				End 2				Diameter (in)	Segs
	X (in)	Y (in)	Z (in)	Conn	X (in)	Y (in)	Z (in)	Conn		
1	-552	0	552		-276	0	552	W2E1	#12	21
2	-276	0	552	W1E2	-276	0	420	W3E1	#12	11
3	-276	0	420	W2E2	-270	0	420	W4E1	#12	1
4	-270	0	420	W3E2	-270	0	552	W5E1	#12	11
5	-270	0	552	W4E2	270	0	552	W6E1	#12	41
6	270	0	552	W5E2	270	0	420	W7E1	#12	11
7	270	0	420	W6E2	276	0	420	W8E1	#12	1
8	276	0	420	W7E2	276	0	552	W9E1	#12	11
9	276	0	552	W8E2	552	0	552		#12	21
*										

Wires

Wire Create Edit Other

Demidov Equivalent: Wire Section

☐ Show Wire Insulation

☐ Coord Entry Mode
 ☐ Preserve Connections

Wires

No.	End 1				End 2				Diameter (in)	Segs
	X (in)	Y (in)	Z (in)	Conn	X (in)	Y (in)	Z (in)	Conn		
1	-552	0	552		-276	0	552	W2E1	#12	21
2	-276	0	552	W3E1	-276	0	417.062		#12	11
3	-276	0	552	W1E2	276	0	552	W4E2	#12	41
4	276	0	417.062		276	0	552	W5E1	#12	11
5	276	0	552	W3E2	552	0	552		#12	21
*										

Transmission Lines

Trans Line Edit

Demidov Equivalent: Transmission-Line Section

☐ Coord Entry Mode
 ☐ Preserve Connections

Transmission Lines

No.	End 1 Specified Pos.		End 1 Act	End 2 Specified Pos.		End 2 Act	Length	Z0	VF	Rev/Norm	Loss
	Wire #	% From E1	% From E1	Wire #	% From E1	% From E1	(in)	(ohms)			(dB/100 ft)
1	1	100	97.6191	3	0	1.21951	5.56083E-4	300	1	N	0
2	3	100	98.7805	5	0	2.38095	5.56083E-4	300	1	N	0
*											

The upper section of the model shows the original all wire structure, with the 6" spacing between the wires of the phasing lines. The lines are each 132" long. The middle section shows the simplified wire table of the Demidov substitute. The junctions between the main element wire and the common-mode wires appear at points exactly half way between the feedpoint and the wire outer ends. The bottom section of the figure shows the two ideal transformers. Each uses as close to an infinitesimal length as one's modeling program will permit. Anything from 1e-5 wavelength and shorter will do. The idea is to use a length of transmission line that is so short that no significant impedance transformation can occur along its length. The 300-Ohm characteristic impedance is largely arbitrary, as values between 50 and 600 Ohms work as well.

Comparative results using NEC-4, single precision, on all-wire and a Demidov models of a 2-wavelength 21,225-MHz collinear array

Model	Gain dBi	Beamwidth	Feed X (R +/- jX Ohms)	AGT
All-wire (AWG #12)	11.97	26.2 deg	2189 + j29	1.001
Demidov substitute	12.05	26.2 deg	2133 - j57	1.001

The differences between the results are insignificant, especially in view of the fact that the critical junctions and the source position occur at very high impedance positions on the model. In fact, the models shown in **Fig. 4** contain an illusion. The length of the common-mode stub in the sample is just about 3" longer than the parallel line stubs in the original model. The illusion is that the common-mode stub accounts for the original stub length plus 1/2 the spacing between stubs. In fact, if we change cores and run the same substitute model in each, variously using single and double precision versions of each core, we obtain different values for the

source impedance. They are all very high resistively and fall on the very steep curve that marks the ordinary reversal of reactance. Hence, the differences do not make a difference. In a real construction situation, a builder would need to adjust the length of the stub for best performance, taking into account the velocity factor of the actual phase line used. A quarter wavelength at 21.225 MHz is 139", the length of the Demidov common-mode line shown. However, with real wires having a small copper loss plus any dielectric shortening required, the physical length in most cases will be shorter, as it is in the original model.

The exercise does show an example of a substitute modeling technique that can be verified against an all-wire model. Once confirmed, we may use the technique in other comparable situations, even those where a direct comparison may not be feasible due to the large size of the all-wire model or the inability to handle velocity factors easily.

### **Substituting the Electrical Equivalent for the Original Structure Where We May Not Check Our Work by Modeling the Full Structure**

There are some types of antennas that we cannot directly model within NEC (or MININEC). By directly model, I mean to replicate the physical structure within the confines of the NEC wire facilities. One type of structure that we cannot effectively model physically is a coaxial element, where the physical antenna may use a coaxial cable as part or all of the structure. In some cases, especially with fairly simple structures, we may be able to construct reasonable

replicas using a series of wires surrounding a central wire. However, in most cases, we must resort to various techniques to ensure that the surrounding wires form a single relevantly continuous conductor around the central wire.

One antenna type that has recently seen renewed popularity is the coaxial collinear array, especially in vertical form for VHF and UHF use. The antenna has a very long history, but came into prominence in the 1950s as a potential VHF mobile array and also in radar uses due to the potential for developing a very narrow bi-directional beamwidth in a horizontal orientation. In the 21st century, the amateur search for an ideal omni-directional vertical array with very high gain for line-of-sight paths has brought on a surge of interest. With the interest has come an urge to model the antenna.

Fig. 5

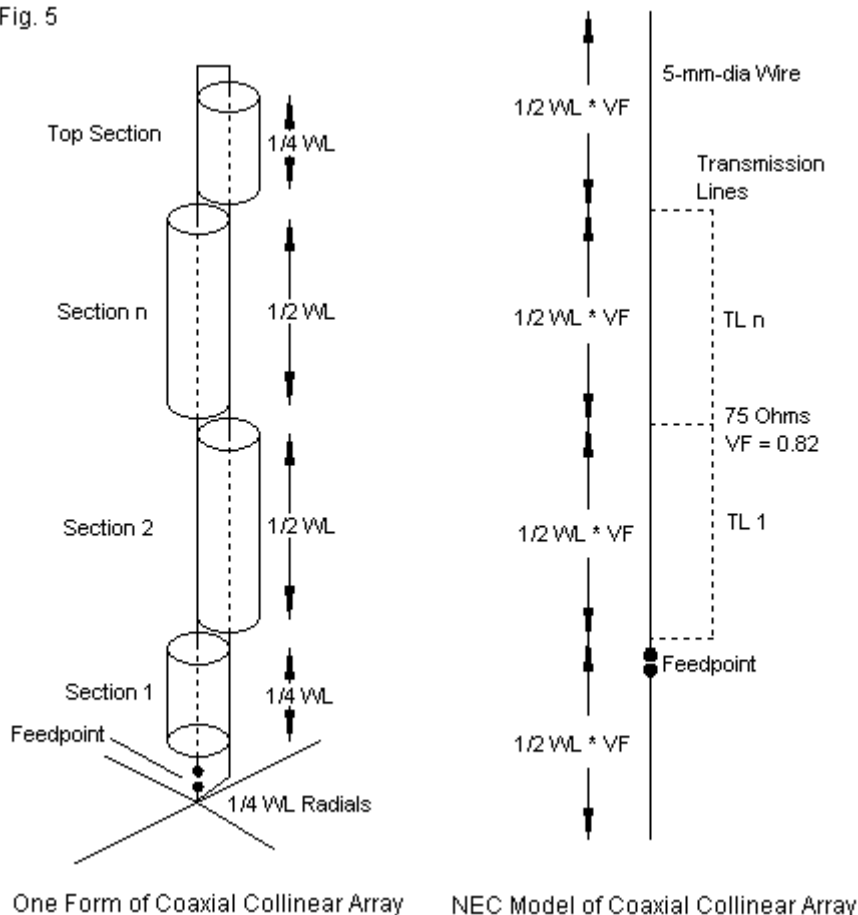


**Fig. 5**, on the left, shows the outline of the form most amateur envision using. A shorted stub  $1/4$ -wavelength top section completes the array. At the base, the lowest section consists of a  $1/4$ -wavelength section with 4 radials to form the feed portion. Between the top and bottom section, we may place any number of  $1/2$ -wavelength sections, 1 through  $n$ . Although the sketch shows only 2, the number is limited only by the physical space available to hang the somewhat floppy coaxial array.

The sections of the array consist of length of coaxial-cable transmission line. Hence, each section, whether  $1/2$ -wavelength or  $1/4$ -wavelength is electrically only that long. The physical length is shorter, since we multiply each electrical length by the velocity factor of the line used. At each junction, we reverse the connections of the lines so that we end up with the equivalent of a  $1/4$ -wavelength phasing stub without the need to install one. The required phase reversal (that actually produces a phase continuation) results from the line connection reversals at each junction.

On the right of **Fig. 5** we find a modeling work-around that has been proposed to capture the antenna's performance. We separate the TEM or transmission line currents from the radiating currents by using two separate sets of connections between sections. The physically modeled wire that is solid in the sketch does the radiating. The dotted line represents transmission-line section connected from one end to the other end of each section wire. Note that in this idealized model, the top and bottom sections are bare wire without transmission lines. As well, the feedpoint comes

between sections rather than at the base of the antenna. Hence, the model will not simulate directly the conception of a coaxial collinear antenna sketched on the left. But it may give us some idea of what happens if we successfully manage to phase successive  $1/2$ -wavelength sections of wire (with the length adjusted for the line velocity factor of the proposed cable).

**Wires**

Wire Create Edit Other
Wire and Transmission-Line Tables for a Coaxial Collinear Model
Fig. 6

☐ Coord Entry Mode
 ☐ Preserve Connections
 

☐ Show Wire Insulation

Wires											
No.	End 1				End 2				Diameter (mm)	Segs	
	X (wl)	Y (wl)	Z (wl)	Conn	X (wl)	Y (wl)	Z (wl)	Conn			
1	0	0	0.5		0	0	0.897	W2E1	5	30	
2	0	0	0.897	W1E2	0	0	0.91	W3E1	5	1	
3	0	0	0.91	W2E2	0	0	1.307	W4E1	5	30	
4	0	0	1.307	W3E2	0	0	1.32	W5E1	5	1	
5	0	0	1.32	W4E2	0	0	1.717	W6E1	5	30	
6	0	0	1.717	W5E2	0	0	1.73	W7E1	5	1	
7	0	0	1.73	W6E2	0	0	2.127	W8E1	5	30	
8	0	0	2.127	W7E2	0	0	2.14	W9E1	5	1	
9	0	0	2.14	W8E2	0	0	2.537	W10E1	5	30	
10	0	0	2.537	W9E2	0	0	2.55	W11E1	5	1	
11	0	0	2.55	W10E2	0	0	2.947	W12E1	5	30	
12	0	0	2.947	W11E2	0	0	2.96	W13E1	5	1	
13	0	0	2.96	W12E2	0	0	3.357	W14E1	5	30	
14	0	0	3.357	W13E2	0	0	3.37	W15E1	5	1	
15	0	0	3.37	W14E2	0	0	3.767	W16E1	5	30	
16	0	0	3.767	W15E2	0	0	3.78	W17E1	5	1	
17	0	0	3.78	W16E2	0	0	4.177	W18E1	5	30	
18	0	0	4.177	W17E2	0	0	4.19	W19E1	5	1	
19	0	0	4.19	W18E2	0	0	4.6		5	30	

**Transmission Lines**

Trans Line Edit

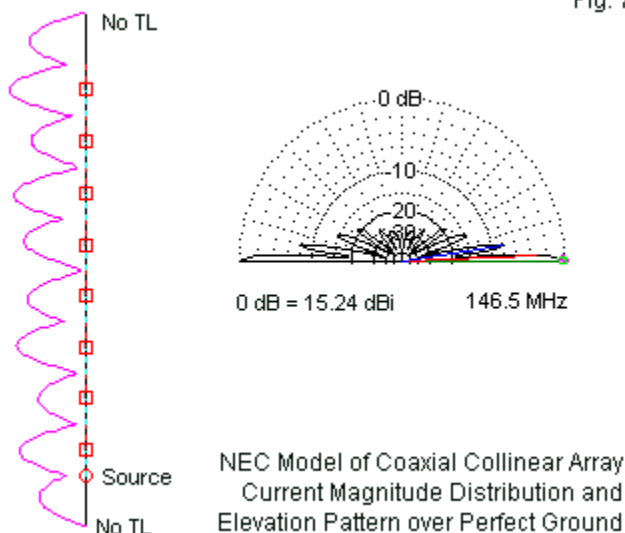
Transmission Lines											
No.	End 1 Specified Pos.		End 1 Act	End 2 Specified Pos.		End 2 Act	Length	Z0	VF	Rev/Norm	Loss
	Wire #	% From E1	% From E1	Wire #	% From E1	% From E1	(wl)	(ohms)			(dB/100 m)
1	2	50	50	4	50	50	Actual dist	75	0.82	R	0
2	4	50	50	6	50	50	Actual dist	75	0.82	R	0
3	6	50	50	8	50	50	Actual dist	75	0.82	R	0
4	8	50	50	10	50	50	Actual dist	75	0.82	R	0
5	10	50	50	12	50	50	Actual dist	75	0.82	R	0
6	12	50	50	14	50	50	Actual dist	75	0.82	R	0
7	14	50	50	16	50	50	Actual dist	75	0.82	R	0
8	16	50	50	18	50	50	Actual dist	75	0.82	R	0



**Fig. 6** shows the wire and transmission-line tables from an EZNEC version of the antenna. For convenience, the original modeler has used a separate 1-segment wire between sections on which to make the connections for both the source and the transmission lines. However, the total length of each section consisting of a longer wire and the connecting section is 0.41-wavelement, the result of multiply  $1/2$  by the line velocity factor of 0.82. The antenna begins 0.5-wavelength above a perfect ground in the ideal model.

The model provides us with two important outputs. As shown in **Fig. 7**, the current distribution is in phase and quite even along the length of the antenna. Hence, the array attenuates high angle radiation very well, as shown in the elevation pattern to the right. (Over average ground, the gain drops to 10.35 dBi, nearly 4-dB lower than over perfect ground. The elevation angle is about 4 degrees, equivalent to a single dipole at a height of over 3 wavelengths, but with a gain advantage to the coaxial collinear array.)

Fig. 7



Unlike the horizontal phased array that we previously discussed, we cannot compare the idealized coaxial collinear model with a physical version of the same antenna. Therefore, we must approach the substitute model with all due caution. For example, the reported impedance at the source is  $269 + j54$  Ohms. However, the model is exceptionally sensitive to changes in the velocity factor. Decreasing the value by only 0.01 drops the reported impedance to just above 100 Ohms, with a sizable remnant reactance. Variations in the velocity factor of cables between lots may vary by several percent. What the model cannot tell us is whether the physical implementation of the antenna will be equally

sensitive to variations in the line velocity factor. Moreover, the model does not reveal what effect a revised lower section might have, should one wish to replicate the more use practical of using a base section that is  $1/4$ -wavelength long with a set of radials. We may model such an arrangement, but casual modeling in this direction shows reduced gain, stronger high-angle lobes, and a departure from the smooth current magnitude curves of the ideal model. I shall not show any models taken in this direction because they leave us with the same difficulties in correlating the model with a real antenna.

It is possible in the abstract to create models that seemingly are the electrical equivalents of physical structures that fall outside the boundaries of direct capture in a wire structure. Many of these models may prove useful in seeing some basic properties of antenna types. However, they remain limited in their reliability as models--despite nearly perfect AGT scores--due to the fact that we have no way to compare the models with physically accurate versions. In most cases, we also lack detailed information on performance from rated test ranges. In the present case, just such information would be necessary to determine if the sensitivity to small changes in the cable velocity factor is a physical feature of the coaxial collinear antenna or an artifact of the idealized model.

## **Conclusion**

We have examined several different types of substitute models ranging from simple geometry substitutions to replacing physical structures with their electrical equivalents. The goal is not to

discourage the use of substitute models. Rather, the aim has been to alert modelers to the level of caution necessary to bring to the models. Especially in cases where we cannot model the antenna as a physical set of wires, we should exert the highest levels of caution.

## Chapter 139: Antenna Matching with EZNEC Version 5

### Part 1. Transformers and Shunt Loads

One of the most popular implementations of NEC, EZNEC, introduced in May, 2007, a new version (5) with a number of facilities that may be new to NEC users. The features include the ability to place loads in parallel to wire segments, the creation of ideal transformers, and the implementation of L-networks that use values of inductance and capacitance (or resistance and reactance). From the last item, we can create more complex networks by joining L-networks in series. A number of other implementations have facilities for calculating some of these items, but normally as adjuncts to the program. In EZNEC, the facilities are part of the input interface and therefore enter the core calculations. Moreover, the facilities are frequency nimble. For example, entering a shunt capacitor or inductor across the source wire of a model will produce correct results over a wide frequency span as an integral part of the model. In contrast, resistance-reactance loads or of Y-parameter networks insert constant values that apply only to a given frequency. As a consequence of pre-calculations in the interface, EZNEC output facilities, such as the total model sweep or the more limited SWR sweep will provide (within limits) accurate data for each frequency within the sweep.

Newer modelers may be unaccustomed to using such facilities. Therefore, in this episode and the next, we shall look at some examples of modeling with these facilities. This session will examine ideal transformers and shunt component loads. The next

will look at the use of L-networks in 2-element configurations and in combination to produce 3-element networks.

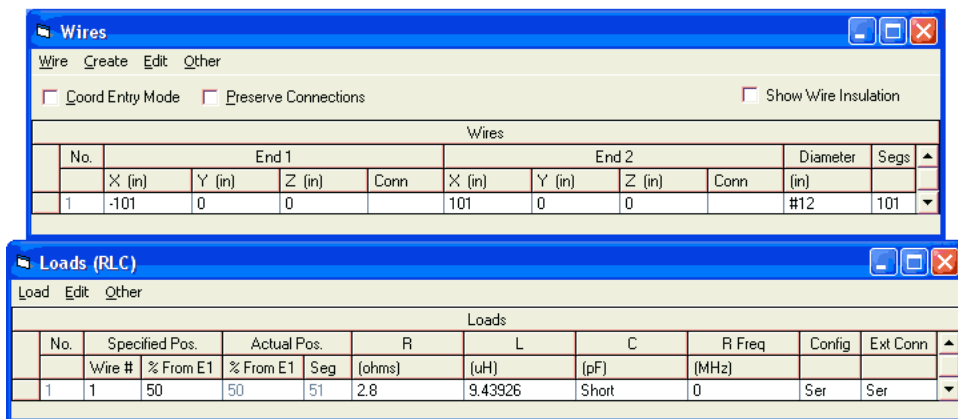
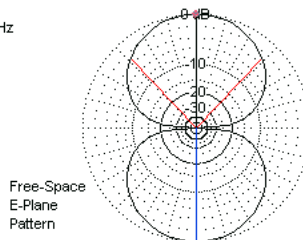
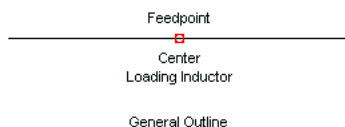
## A Simple Short Loaded Dipole and an Ideal Transformer

The process of using simple series-connected loads--the norm for the NEC cores--is familiar to virtually all modelers. Suppose that we begin with a center-fed dipole that is only 1/4-wavelength (and composed of AWG #12 copper wire for this sample). The feedpoint impedance will produce a free-space impedance of about  $15 - j840$  Ohms at a test frequency of 14.175 MHz. One way to bring the antenna to resonance is to insert a center-loading inductor. For this and ensuing examples, we shall assume a realistic Q of 200 for inductors. An inductor in series with the source, that is, a center-loading coil) will need about 9.44  $\mu\text{H}$ . **Fig. 1** shows the outline of the simple antenna, along with wire and load tables for the model. Because we wish the model to provide accurate performance reports across the entire amateur 20-meter band, we have used an RLC network rather than a frequency-specific R-X network.

1/4-Wavelength Center-Loaded  
Dipole Model with Wire and  
Load Tables

14.175 MHz

Fig. 1



The 2.8-Ohm series resistance in the center-loading coil reduces antenna gain (without changing the basic shape of the free-space pattern). Of course, the shorter wire length (relative to a full 1/2-wavelength dipole) also contributes to showing a gain of 0.88 dBi rather than the 2+ dBi value that we expect of dipoles. However, as shown in **Table 1**, the antenna is now self-resonant within about  $\pm j1$  Ohm. For reference, the table shows the 15-Ohm SWR values at the lower and upper ends of the operating passband, along with the power efficiency of the antenna, taking into account both the

material loss of the copper wire (very small) and the losses in the center inductor (sizable).

1/4- $\lambda$  Dipole with Center-Load Inductor

Table 1

Gain dBi	Feed Impedance R +/- jX $\Omega$	SWR @ 14 MHz	SWR @ 14.35 MHz	Efficiency %
A. Without Transformer (SWR Reference = 15 $\Omega$ )				
0.88	15.4 - j0.0	4.99	4.77	80.4
B. With Matching Ideal Transformer (SWR Reference = 50 $\Omega$ )				
0.87	51.3 - j0.2	4.99	4.76	80.3

The remaining operational difficulty with the antenna is the very low impedance. One way to bring the impedance closer to the standard coaxial cable and amateur equipment value of 50 Ohms is to insert a transformer of some sort between the existing feedpoint (ostensibly at the center of a split loading coil) and the feedline. In practice, we might wind a conventional transformer (with either an air or a powdered iron core) or a transmission-line transformer. We can simulate an ideal transformer within the program by entering the line shown in **Fig. 2**.



Center-Loaded 1/4-Wavelength Dipole  
with a 15-50-Ohm Matching Transformer

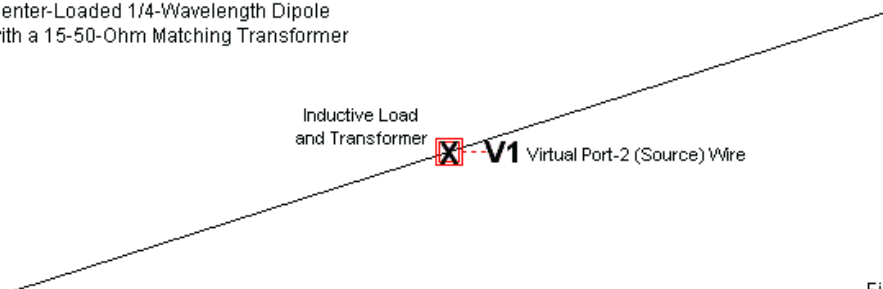


Fig. 2

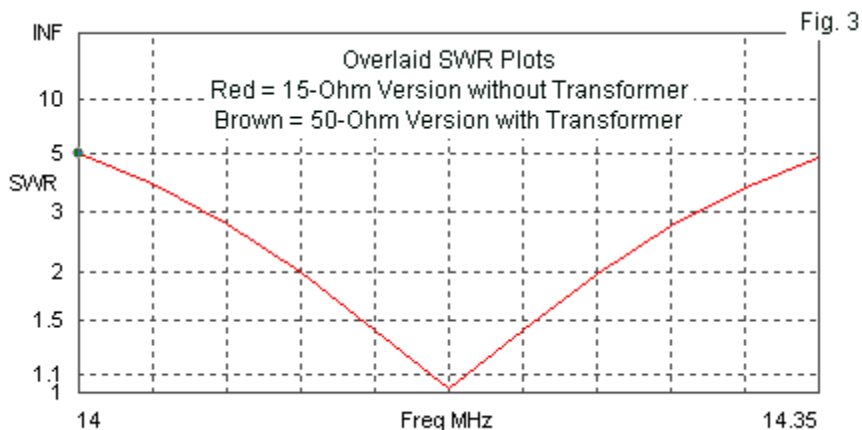
Transformers										
Xfmr Edit Matching Transformer Table										
Transformers										
	No.	Port 1 Specified		Port 1 Act	Port 2 Specified		Port 2 Act	Port 1	Port 2	Rev/Norm
		Wire #	% From E1	% From E1	Wire #	% From E1	% From E1	Rel Z	Rel Z	
1	1	50	50	V1				15	50	N

The view of the antenna shows two squares at the feedpoint. One represents the normal series inductive load. The second, with an X at its center, represents the ideal transformer that appears in parallel with the source (with the load inductor in series with both the source and the transformer port). The second port of the transformer would normally go to a remote wire to serve as the new source wire. Ordinarily, we construct such wires at very large distances from the main antenna geometry, and we make them very short and thin. The goal is to avoid interactions with the main antenna element (or elements) that might change the performance reports. In version 5 of EZNEC, the program can create these remote wires as virtual wires that need not show up in either the wire table or the view of the antenna. Instead, the view indicates

the existence of the virtual wire, but does not shrink the size of the antenna element in an effort to show both the source wire and the main element.

Note that the specification of the transformer requires that we attend to both the port connections and the values. For highest accuracy, the relative impedance values should be close to the desired values (and not be simply arbitrary values that yield the same ratio of impedances). For the sample, I have used the approximate raw element impedance (15 Ohms) at Port 1, which connects to the element wire segment that used to be the source. Port 2 lists the desired impedance value and connects to the virtual wire to which the model has also assigned the source. In the sample, I have used the desired values, even though the impedance ratio is 1 to 3.33. In practice, one might have used 60 Ohms for Port 2 in order to simulate a 1:4 transmission-line transformer.

One reason for referring to the transformer input and output terminals as ports is that the program creates for the core a network (or its equivalent) that follows the general rules described in episode 127 of this series. The program therefore follows Y-parameter port designations, even though the input values are impedance values rather than admittance values. It does not matter which port serves as the source and which as the load so long as the modeler associates the correct impedance value with the correct connection to the model's geometry.



We can see the ideality of the transformer in **Fig. 3**, a dual SWR sweep of the model before and after the addition of the transformer. One line is the 50-Ohm SWR at the source with the transformer in place; the other line is the 15-Ohm SWR before the addition of the transformer. One of the lines is invisible, because the other lines overlays it with graphical perfection. Similar data appears in the SWR values at the band edges in **Table 1**. The line tracking of the sweeps provides evidence that the transformer is (within limits) frequency nimble and yields correct results for what is essentially a lossless component. As constituted at present, there is no practical way to introduce losses into the transformer facility. Its existence in the model yields only a 0.1% change in the model's reported power efficiency.

## Matching a Resonant 3-Element Yagi

Let's change examples and review a broader spectrum of matching possibilities. As shown in **Fig. 4**, we shall now use a 3-element Yagi for 28.5 MHz, with the elements consisting of 1/2"-diameter aluminum. The antenna is full size and the driver is set to resonance, about 25.7 Ohms. Once more, the environment is free space, and the E-plane pattern shows the generally high performance potential of the design.

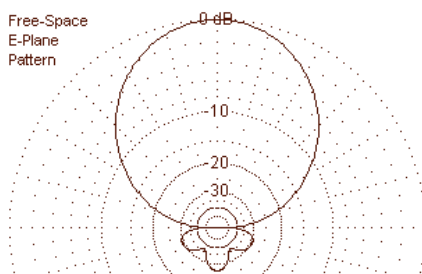
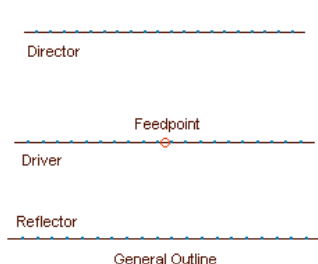
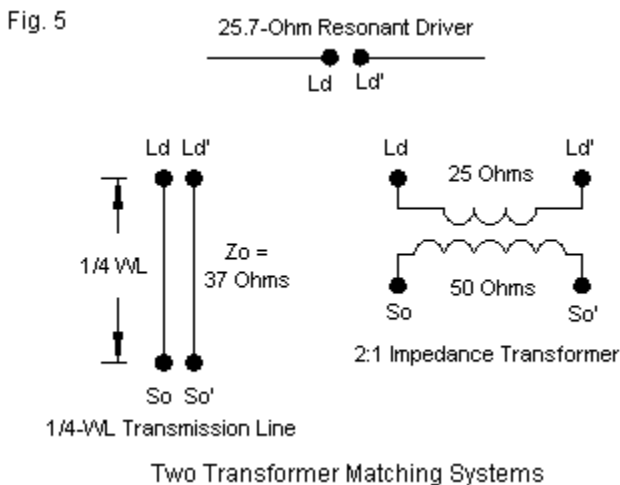


Fig. 4

Wires											
Resonant Feedpoint Version      Basic Antenna for Match-Loss Exercises											
<input type="checkbox"/> Coord Entry Mode <input type="checkbox"/> Preserve Connections    Model Dimensions <input type="checkbox"/> Show Wire Insulation											
No.	End 1				End 2				Diameter	Segs	
	X (ft)	Y (ft)	Z (ft)	Conn	X (ft)	Y (ft)	Z (ft)	Conn			
1	-8.595	0	0		8.595	0	0		0.5	21	
2	-8.207	5.2	0		8.207	5.2	0		0.5	21	
3	-7.722	11.212	0		7.722	11.212	0		0.5	21	
*											

With the listed feedpoint impedance of the parasitic array, we generally have two major avenues of conveniently matching the

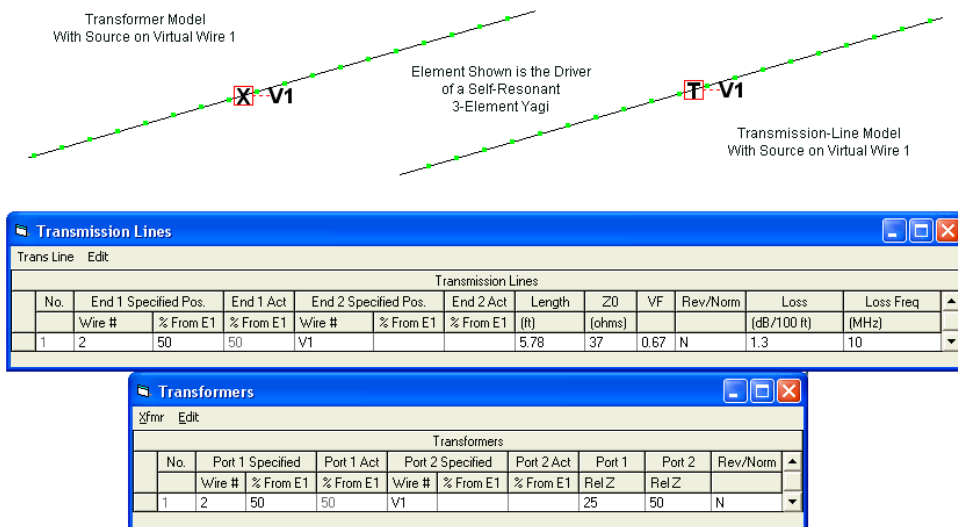
source to a 50-Ohm feedline. One method is to create a 37-Ohm  $1/4$ -wavelength section of transmission line from the present source segment to a remote model wire that becomes the new source segment. Although 35-Ohm coaxial cables do exist, the more common amateur practice is to place two length of 70-75-Ohm line in parallel to create the desired line. A second method is to employ a 1:2 impedance transformer between old source segment and the new one. **Fig. 5** outlines the options in schematic form.



We may implement either matching system within the modeling facilities of EZNEC, V5, using in one case the transmission-line facility and in the other case the ideal transformer facility. In both cases, the source segment moves to the new virtual wire that is part of each model. **Fig. 6** shows a close-up view of the driver

element to record the designations for the transformer (X) and the transmission line (T) in the views of the antenna.

Fig. 6



The transformer version of the model follows the exact pattern that we selected for the dipole, with changes in segment numbers and impedance values to reflect the new situation. The transmission-line entry may seem a bit odd to those who are only used to working with the lossless lines of NEC itself. The program has instituted a method of accounting for approximate transmission-line losses by allowing the user to enter a loss value and a frequency. Such values are readily available from charts, such as the one on page 24-19 of *The ARRL Antenna Book*. The values in the sample

entry are for a version of RG-59, a 70-Ohm cable that most amateur might use in a parallel arrangement to effect the 1/4-wavelength line. The listed physical length divided by the listed velocity factor would yield an electrical quarter wavelength.

Matching a Self-Resonant 3-Element Yagi

Table 2

Basic antenna performance: 3-element Yagi with a resonant driver

Design Frequency = 28.5 MHz

Gain dBi	F-B Ratio dB	Feed Impedance R +/- jX $\Omega$	SWR @ 28 MHz	SWR @ 29 MHz	Efficiency %
8.11	27.11	25.7 - j0.8	1.96	2.30	99.2

Note: SWR relative to 25.7- $\Omega$  reference

Performance with  $\frac{1}{4}$ - $\lambda$  37- $\Omega$  matching section (5.78' @ 0.67 VF)

Gain dBi	F-B Ratio dB	Feed Impedance R +/- jX $\Omega$	SWR @ 28 MHz	SWR @ 29 MHz	Efficiency %
1. 0-loss transmission line					
8.11	27.11	53.2 + j1.5	1.95	2.32	99.2
2. Parallel RG-11 (loss = 0.7 dB/100' @ 10 MHz)					
8.03	27.12	52.9 + j1.0	1.91	2.32	97.5
3. Parallel RG-59 (loss = 1.3 dB/100' @ 10 MHz)					
7.97	27.12	52.7 + j0.5	1.87	2.32	96.1

Note: SWR relative to 50 reference

Performance with a 25-50- $\Omega$  low-loss transformer

Gain dBi	F-B Ratio dB	Feed Impedance R +/- jX $\Omega$	SWR @ 28 MHz	SWR @ 29 MHz	Efficiency %
8.10	27.12	51.5 - j1.6	1.98	2.31	99.0

**Table 2** shows the reported results of our variations in the methods of matching the 25-Ohm element impedance to a coaxial feedline. The table begins with data for the model with no matching systems.

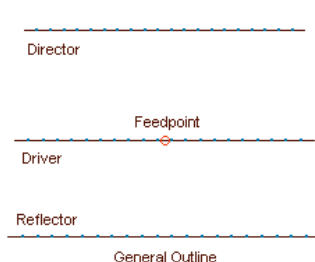
The second section uses three versions of the 1/4-wavelength matching section composed of transmission line. If we do not assign losses to the transmission line, the gain and front-to-back values remain the same as in the pre-matched model. The following two entries note the loss values that we may glean from tables for RG-11 (a half-inch cable) and RG-59 (a thinner cable). Note that the matching line losses do make a difference to the reported gain value (without altering the front-to-back value). However, losses are below the level of being operationally detectable, and the SWR limiting values have not changed by any amount that we could detect in normal testing. Since the 1/4-wavelength transformer is also part of the linear run of feedline cable, the net loss is simply the difference between the matching section loss and an equivalent length of main feedline cable.

The bottom of the table shows the results from inserting an ideal transformer into the model. As both the gain and the efficiency values show, the ideal transformer leaves the basic values virtually unchanged. A real transformer of conventional design might introduce perhaps 2-3% losses. Such losses would bring the efficiency down to the level of the 1/4-wavelength transmission-line transformation system, with gain values that are likely to reflect those values. However, our goal is not to weigh the merits of specific implementations of a matching system. Rather, the goal has been to show the modeling facilities involved in both methods of matching.



## Matching a Non-Resonant 3-Element Yagi

To advance our progression through the matching options offered as frequency-nimble facilities in EZNEC, V5, let's make a small alteration in the 3-element 28.5-MHz Yagi composed on 1/2"-diameter aluminum elements. Element spacing will be unchanged, as will the lengths of the director and reflector. However, we shall shorten the driver so that it shows an impedance of about  $24 - j24$  Ohms. **Fig. 7** shows the general outline of the array, along with the free-space E-plane pattern. These graphics would not reveal the model changes. Hence, the figure also includes the wire table for comparison with the table in **Fig. 4**. The total driver length change is just about 0.4' or 4.75". The change makes virtually no difference to the beam's performance with respect to gain or the front-to-back ratio.



Free-Space  
E-Plane  
Pattern

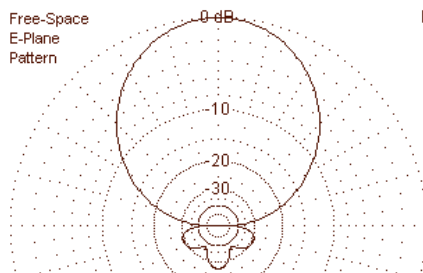


Fig. 7

Wires

Wire Create Edit Other

Non-Resonant Feedpoint Version

Basic Antenna for Match-Loss Exercises

Coord Entry Mode

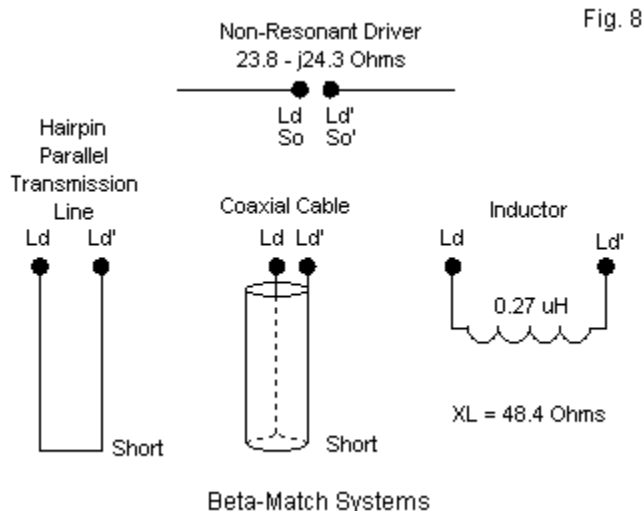
Preserve Connections

Show Wire Insulation

Wires

	No.	End 1				End 2				Diameter	Segs
		X (ft)	Y (ft)	Z (ft)	Conn	X (ft)	Y (ft)	Z (ft)	Conn	(in)	
	1	-8.595	0	0		8.595	0	0		0.5	21
	2	-8.00833	5.2	0		8.00833	5.2	0		0.5	21
	3	-7.722	11.212	0		7.722	11.212	0		0.5	21
*											

The driver impedance conditions ripen the array for matching to a 50-Ohm cable via a beta or hairpin matching system. A beta match is simply an L-network in which the series load-side reactance is contained in the element impedance. Since the element series reactance is capacitive, the source-side shunt reactance must be inductive. We connect the shunt component directly across the feedpoint terminals, essentially in parallel with the source. In practice, we usually find one of three types of shunt components to create the required reactance. **Fig. 8** shows the general options for our beam.



Essentially, two of the three options boil down to one: a shorted transmission-line stub. The stub length depends on the required reactance, about  $j48$  Ohms in the present case. It also depends upon the characteristic impedance ( $Z_0$ ) of the transmission line used to create the reactance: the higher the value of  $Z_0$ , the shorter the line to achieve the reactance.

The transmission-line facility of NEC is ideal for implementing a shunt inductive reactance across the feedpoint, since transmission-lines (as special forms of networks) appear in parallel with sources. EZNEC has long used a remote, invisible wire to effect transmission line opens and shorts, so the modeler need not create a special terminating wire for such lines. The latest version of the

program adds the ability to calculate the losses of such lines when used as stubs (or in any other application). **Fig. 9** shows two different stubs. One uses a 600-Ohm line, which would normally employ parallel transmission line--often homemade. From such lines, the label "hairpin" match emerged. The sample version uses the 10-MHz loss factor for 600-Ohm ladder line to estimate losses that the stub might introduce into the model.

Transmission Lines

Trans Line

Edit

600-Ohm Beta Stub

Fig. 9

Transmission Lines

No.	End 1 Specified Pos.	End 1 Act	End 2 Specified Pos.	End 2 Act	Length	Z0	VF	Rev/Norm	Loss	Loss Freq		
	Wire #	% From E1	% From E1	Wire #	% From E1	% From E1	(in)	(ohms)		(dB/100 ft)	(MHz)	
1	2	50	50	Short ckt			5.2	600	1	N	0.06	10

Transmission Lines

Transmission Lines

Trans Line

Edit

50-Ohm Beta Stub

Transmission Lines

No.	End 1 Specified Pos.	End 1 Act	End 2 Specified Pos.	End 2 Act	Length	Z0	VF	Rev/Norm	Loss	Loss Freq		
	Wire #	% From E1	% From E1	Wire #	% From E1	% From E1	(in)	(ohms)		(dB/100 ft)	(MHz)	
1	2	50	50	Short ckt			50	50	1	N	1.3	10

As an alternative to the 600-Ohm hairpin stub, we might also employ a length of common 50-Ohm cable to create the shorted stub. The impedance is less than 1/10 the impedance of the hairpin line, but the length is a little under 10 times longer. The difference appears because the reactance of a shorted stub is not a linear function of length, but a tangent function of the line length in electrical degrees (or radians). Despite the differences of appearance, both versions of the beta stub perform the same function with equal success.

The third option is a shunt inductor, which by some convoluted logic received a bygone label of "hairpin inductor." Our problem with the shunt inductor (where an inductance of about 0.27  $\mu\text{H}$  provides the required  $j48\ \Omega$  at 28.5 MHz) lies in trying to create a model that includes it. In the past, we have needed to develop a physical structure composed of very short wires around an equally short source segment. Then we could add the inductive load to one of the wires in the box as a standard series connected load. To create a structure that provides the least effect on beam performance, we then had to use very short segments throughout the model, resulting in a sizable model (in terms of segment count) for a fairly simple beam. **Fig. 10** shows such a model that uses 2" segments, which is approaching the limit for wires having a radius of 0.25". Indeed, the outline does not show entire elements due to space restrictions. However, the wire table shows the degree to which the initial model has grown. Despite its limitations, the work-around has been useful.

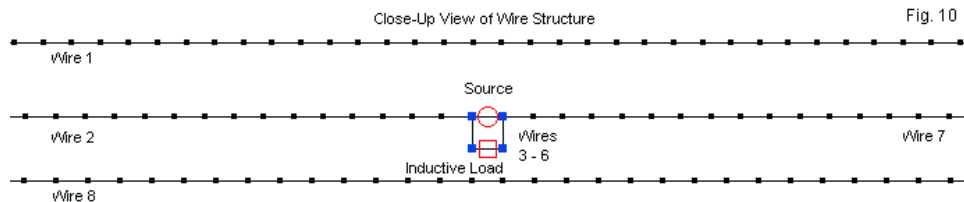


Fig. 10

Wires											
All-Wire Beta Shunt Inductor Model											
<input type="checkbox"/> Coord Entry Mode <input type="checkbox"/> Preserve Connections <input type="checkbox"/> Show Wire Insulation											
Wires											
No.	End 1				End 2				Diameter	Segs	
	X (in)	Y (in)	Z (in)	Conn	X (in)	Y (in)	Z (in)	Conn	(in)		
1	-103.14	0	0		103.14	0	0		0.5	101	
2	-96.1	62.4	0		-1	62.4	0	W3E1	0.5	50	
3	-1	62.4	0	W4E1	1	62.4	0	W6E2	0.5	1	
4	-1	62.4	0	W2E2	-1	62.4	-2	W5E1	0.5	1	
5	-1	62.4	-2	W4E2	1	62.4	-2	W6E1	0.5	1	
6	1	62.4	-2	W5E2	1	62.4	0	W7E1	0.5	1	
7	1	62.4	0	W3E2	96.1	62.4	0		0.5	50	
8	-92.664	134.544	0		92.664	134.544	0		0.5	101	

The latest version of EZNEC puts the work-around out to pasture by allowing the user to create any of the standard loads (plus the EZNEC trap load) and to then place them either in series with or in parallel to sources or transmission lines on the same segment. **Fig. 11** shows the simple 1-line Load entry that uses an inductor with a Q of 200. The load configuration (that is, the relationship of the load R-L-C or R-X elements) is a series arrangement, as is appropriate to the resistance and inductance in a coil. However, rather than the default series connection with the wire segment, the entry specifies a parallel connection. The antenna viewing feature differentiates load boxes by using squares for series-connected loads and

diamonds for shunt or parallel-connected loads, as indicated in the upper right corner of the graphic.

The first question is whether the arrangement works. **Table 3** provides the results for the series of models illustrated in these notes, beginning with the pre-match model of the antenna. The pre-match SWR values emerge from a sweep that used a series inductor to allow the resistive portion of the feedpoint impedance to serve as the SWR reference.

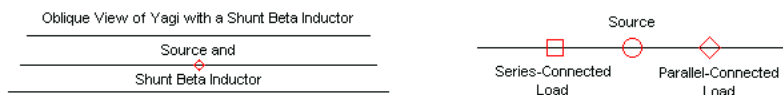


Fig. 11

Loads (RLC)											
Parallel (Shunt) Connected Load Table											
Loads											
No.	Specified Pos.		Actual Pos.		R	L	C	R Freq	Config	Ext Conn	
	Wire #	% From E1	% From E1	Seg	(ohms)	(uH)	(pF)	(MHz)			
1	2	50	50	11	0.24	0.27	Short	0	Ser	Par	

The second portion of the table shows the results of using models of shorted transmission-line stubs as the beta shunt component. For both hairpin and coaxial components, the table lists no-loss versions of the line as well as versions with loss factors derived from various tables. In principle, RG-58 results in a numerically noticeable loss that is greater than any other beta shunt. However, the total gain reduction is about 0.15-dB relative to a lossless situation, a level that one would be hard-pressed to measure under the best of circumstances.

The final part of the table begins with the reported values from the all-wire bridge construction, which happen to extend so that its broadside is in the plane of the elements. The gain value seems to be numerically high, and it is. The AGT for the model is 1.011, indicating an overestimate of gain of about 0.05 dB. The remaining 0.4-dB is a function of the bridge wires themselves. Of course, once we add in the inductor losses from having a finite  $Q$  (200), the gain value comes down and disguises the result.

We obtain a clearer picture of the effects of inductor losses by using the parallel connected inductive load. With no losses, the gain returns to the value shown by the pre-match version of the mode. Adding in the loss reduces the gain by only 0.02 dB, a reduction that is less than the better of the two coaxial cable shorted stubs. Once upon a time, some amateur texts claimed a wider operating bandwidth for beta inductors over hairpins due to the inductor's lower  $Q$  and higher losses. The small exercise shows that the losses, even with a  $Q$  as low as 200, rival those of the 600-Ohm hairpin. The difference in band-edge SWR values is largely a function of the different rates of reactance change for transmission-line stubs and inductors across a span of frequencies.



Table 3

## Beta Match

Basic antenna performance: 3-element Yagi with a non-resonant driver

Design Frequency = 28.5 MHz

Gain dBi	F-B Ratio dB	Feed Impedance R +/- jX $\Omega$	SWR @ 28 MHz	SWR @ 29 MHz	Efficiency %
8.11	27.13	23.8 - j24.3	1.99	2.49	99.2

Note: SWR relative to 23.8- $\Omega$  reference

## Transmission line inductive reactances

Gain dBi	F-B Ratio dB	Feed Impedance R +/- jX $\Omega$	SWR @ 28 MHz	SWR @ 29 MHz	Efficiency %
-------------	-----------------	-------------------------------------	-----------------	-----------------	-----------------

A. 600- $\Omega$ , VF 1, 5.2"

1. 0-loss

8.11	27.13	48.6 + j0.1	1.94	2.53	99.2
------	-------	-------------	------	------	------

2.. 0.06-dB/100' @ 10 MHz

8.11	27.13	48.5 + j0.1	1.94	2.53	99.0
------	-------	-------------	------	------	------

B. 50- $\Omega$ , VF 0.67, 50.0"

1. 0-loss

8.11	27.13	48.6 + j0.1	1.95	2.52	99.2
------	-------	-------------	------	------	------

2.. 0.6-dB/100' @ 10 MHz (RG-213)

8.04	27.13	47.8 + j0.1	1.89	2.54	97.6
------	-------	-------------	------	------	------

2.. 1.3-dB/100' @ 10 MHz (RG-58)

7.96	27.13	46.9 + j0.1	1.83	2.56	95.7
------	-------	-------------	------	------	------

Shunt inductor (0.27  $\mu$ H)

Gain dBi	F-B Ratio dB	Feed Impedance R +/- jX $\Omega$	SWR @ 28 MHz	SWR @ 29 MHz	Efficiency %
-------------	-----------------	-------------------------------------	-----------------	-----------------	-----------------

A. Wire bridge and series inductor

1. 0-loss

8.19	25.61	53.1 - j2.9	2.10	2.35	98.9
------	-------	-------------	------	------	------

2.. Inductor Q = 200

8.16	25.61	52.9 - j2.7	2.08	2.35	98.7
------	-------	-------------	------	------	------

B. Parallel inductor load

1. 0-loss

8.11	27.13	48.5 - j0.9	1.92	2.52	99.2
------	-------	-------------	------	------	------

2.. Inductor Q = 200

8.09	27.13	48.3 - j0.8	1.91	2.52	98.7
------	-------	-------------	------	------	------

We might briefly glimpse at part of the means by which EZNEC, V5, achieves frequency-nimble parallel-connected loads. The interface calculates a Y-parameter network at each frequency before supplying the data to the core for its run at each frequency within a sweep. EZNEC Pro/4 allows us to save .NEC format model files for each frequency. The models are identical except for the NT command that is unique to each frequency. **Table 4** shows the NT lines for the parallel inductor in the sample model. After the two port location entry pairs, we find the Y-parameter equivalents of the inductive load for the specified frequency. The EZNEC interface calculates these values and supplies them to the core in the form applicable to its implementation of the NEC-2 and NEC-4 cores. (Data transfer to the core for its run may differ between core types.) The table suffices to show that by moving the calculation to the input interface portion of the program, it can achieve frequency-nimble and accurate results within the limits of each type of facility that it offers.

Table 4. Unique NTs created for each frequency for a parallel-connected inductive load

28 MHz:	NT 2 11 4 1 1.0636E-4 -.0210517 0. 0. 0. 0.
28.5 MHz	NT 2 11 4 1 1.0267E-4 -.2068E-2 0. 0. 0. 0.
29 MHz	NT 2 11 4 1 9.9156E-5 -.2033E-2 0. 0. 0. 0.

## **To Be Continued**

We have examined only some of the facilities offered by the new version of EZNEC. The program also offers at all levels access to L-networks, from which we can construct networks with from 2 to N components. We shall see how to model a few of the options in our next episode.

## Chapter 140: Antenna Matching with EZNEC Version 5

### Part 2. L-Networks

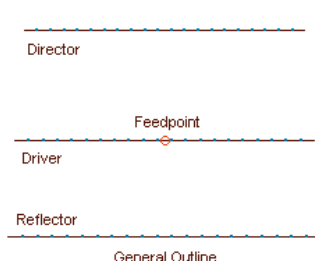
**T**he overall goal of this pair of episodes is to show how, fundamentally, to model with some of the new frequency-nimble facilities in EZNEC Version 5. In Part 1, we examined such functions as ideal transformers, parallel or shunt-connected loads, and transmission-line losses. In this session, we shall look at the use of the L-Network facility in creating networks from common components rather than from Y-parameters of complex structures. We shall begin with a single L-network to create a 2-element or 2-component network. Then we shall proceed to creating 3-component networks, such as Ts and Pis, by connecting together more than one L-Network in the program.

Like parallel or shunt-connected loads, EZNEC L-Networks are frequency-nimble and use the same basic technique that was applied to parallel-connected loads. NEC contains an NT command for creating Y-parameter networks. Like  $R \pm jX$  loads, Y-parameter networks are frequency specific, and the user must change the command for each new frequency. Hence, a single set of NT values normally will not provide accurate results across a broad frequency sweep. EZNEC calculates a new NT command or its equivalent for each L-Network at each new frequency in a sweep. Therefore, for a given set of values for inductance and capacitance, the core has the correct data to provide accurate results at each frequency in a sweep.

Our sample networks will apply to matching a self-resonant Yagi to a 50-Ohm coaxial feedline. The root problem is only one of many possible applications for L-networks. However, by focusing in on a single exercise, we can master the steps required to use the L-network facility effectively. Once you take this step, you can easily proceed on your own to other applications.

## 2-Element/Component L-Networks

Let's begin with the self-resonant 28.5-MHz 3-element Yagi using 1.2"-diameter aluminum elements, the same one that we used for part of the preceding episode. **Fig. 1** shows the outline and the free-space E-plane pattern of the antenna, along with the wire table needed to create the model. All of the matching sections that we shall explore will be designed to convert the 27.5-Ohm feedpoint impedance to 50 Ohms.



Free-Space  
E-Plane  
Pattern

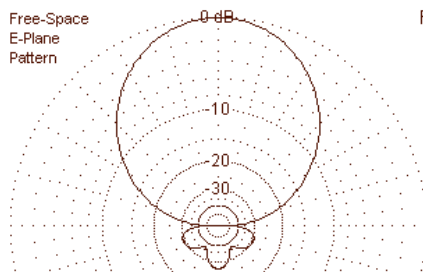


Fig. 1

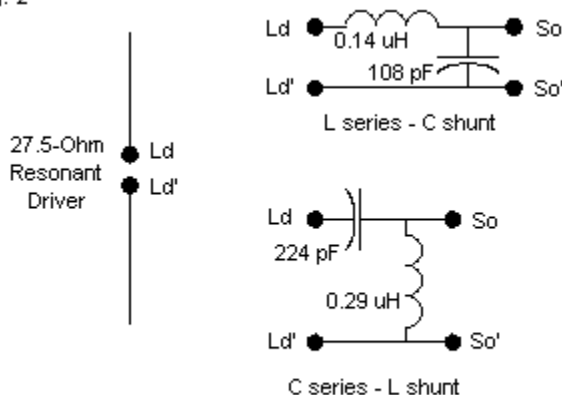
Wires											
Resonant Feedpoint Version      Basic Antenna for Match-Loss Exercises											
<input type="checkbox"/> Coord Entry Mode <input type="checkbox"/> Preserve Connections    Model Dimensions <input type="checkbox"/> Show Wire Insulation											
Wires											
No.	End 1				End 2				Diameter	Segs	
	X (ft)	Y (ft)	Z (ft)	Conn	X (ft)	Y (ft)	Z (ft)	Conn	(in)		
1	-8.595	0	0		8.595	0	0		0.5	21	
2	-8.207	5.2	0		8.207	5.2	0		0.5	21	
3	-7.722	11.212	0		7.722	11.212	0		0.5	21	
*											

One way to effect the impedance conversion is to place an L-network between the antenna terminals and the feedline. L-networks are 2-component networks consisting of one series component and one shunt or parallel component. Let's call the cable impedance the source impedance, and the antenna terminal impedance will be the load impedance. If the source impedance is higher than the load impedance--as it is in our case--then the series component goes on the load side of the network, with the shunt component on the source side. If the load impedance is higher than the source impedance, then the shunt component goes on the load side with the series component on the source side. The L-network

serves as the foundation for many more complex networks, which we can treat as collections of L-networks.

Since our goal is to model with EZNEC L-Networks, we shall not cover the calculation of L-network components for given impedance transformation situations. Instead, we shall rely on one of many utility programs and spreadsheets to arrive at the required values for the series and the shunt components. **Fig. 2** shows the values of capacitance and inductance needed for two forms of the L-network that will convert our terminal or load impedance to the 50-Ohm source or cable impedance.

Fig. 2



Two-Element L-Network Matching Systems

Although the two forms use very different components, both circuits have some things in common. First, the reactive series component

is the opposite types from the reactive shunt component. (There are special cases of load impedances that may call for components of the same type, but they involve load or antenna terminal impedances with high reactance. Our loads are almost purely resistive.) Second, the absolute value of the series and the shunt reactances are the same. In both cases, the series reactance is 26 Ohms (with a sign appropriate to the type of reactance) and the shunt reactance is 51.5 Ohms (again with a sign appropriate to the type of reactance).

To implement a model of the L-network in EZNEC, V5, we must get used to the conventions used by the program. **Fig. 3** provides some guidance. A network consists of two ports. Port 1 always goes with the series branch or component. Port 2 always goes with the shunt branch or component. Labeling the ends of the network as Port 1 and Port 2 is simply a way to differentiate them. Depending on the application, either port may be the source and either may be the load. Our sample case shall call for Port 1 to connect to the antenna terminals, that is, to the source segment of the driver-element wire. Port 2 will use a virtual wire (described in the preceding episode), which will become the new source segment for the model. Other applications may reverse the ports for converting low source impedances to high load impedances.



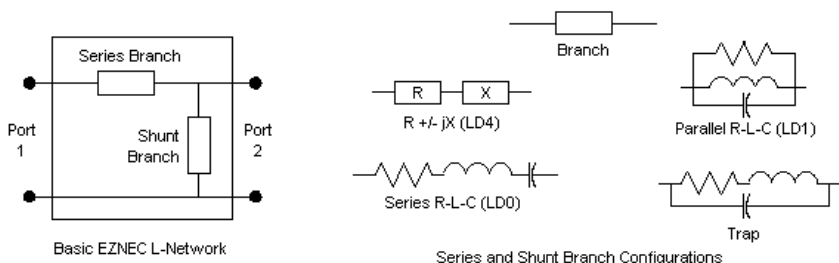


Fig. 3

Fundamental Ideas of the EZNEC L-Network

The sketch also shows us our options in assigning component values to the branches of an L-network. For a single-frequency application, we may use  $R + jX$  loads. For applications that may need to cover a range of frequencies, we can use several different forms of R-L-C configurations. The most common will be the series configuration. It will apply to our sample, since the most complex entry that we shall make is to have both resistance and inductance in series. As in Part 1, we shall assign a Q of 200 to all inductors. When we choose not to have one of the R-L-C components as part of the branch, we shall enter a zero. In this case, zero is not the component value, but instead is a NEC convention for indicating a missing element in a load. The EZNEC tables will use the word "short" to indicate the missing component.

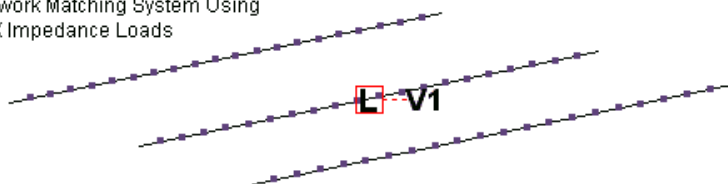
In addition to series R-L-C loads, we may also use a parallel configuration. EZNEC also makes available a trap configuration consisting of a series resistance and inductance that together are in parallel with a capacitance. Whichever configuration we select for an application, both branches of the L-network must use the same




type of configuration. However, other loads that might be present in the antenna assembly can use any of the possible configurations and do not need to match the configuration used in the L-network.




We can orient ourselves to the process of modeling an L-network by starting with a frequency-specific  $R \pm jX$  load in each branch of the L-network. **Fig. 4** shows the model with the designation for the network (the L in the box) plus a designation that shows we are using a virtual wire, namely, V1 as the source wire. The first table shows the source entry that applies to both models. The two L-Network tables show the two versions of the network.




L-Network Matching System Using  
R+/-jX Impedance Loads

Fig. 4



Sources								  	
Source Edit Other						Source Placement			
Sources									
	No.	Specified Pos.		Actual Pos.		Amplitude	Phase	Type	▲
		Wire #	% From E1	% From E1	Seg	(V, A)	(deg.)		▼
	1	V1				1	0	V	

L Networks (R + j X)										
L Ntwk    Edit    Other								Version 1		
L Networks										
	No.	Specified Pos.		Actual Pos.		R (ohms)	X (ohms)			
		Port 1 Wire #	Port 1 % From E1	% From E1	Seg	Series Branch	Series Branch			
		Port 2 Wire #	Port 2 % From E1	% From E1	Seg	Shunt Branch	Shunt Branch			
	1	2	50	50	11	0	26			
		V1				0	-51.4			

L Networks (R + j X)								  		
L Ntwk   Edit   Other								Version 2		
L Networks										
	No.	Specified Pos.		Actual Pos.		R (ohms)		X (ohms)		▲
		Port 1 Wire #	Port 1 % From E1	% From E1	Seg	Series Branch	Series Branch			
		Port 2 Wire #	Port 2 % From E1	% From E1	Seg	Shunt Branch	Shunt Branch			
	1	2	50	50	11	0	-26			
		V1				0	51.4			▼

Because the actual source impedance has several decimal places, as do the calculated components, the rounded numbers in the tables do not return identical source impedance values. The first version reports an impedance of  $50.5 - j0.0$  Ohms, while the second reports  $53.6 - j0.0$  Ohms. In practice, the difference does not make a difference, since every model will depart slightly from physical reality that includes small variations from the model.

If we wish to employ series R-L-C branches in the L-network--the more normal case--the L-Network table becomes more complex. **Fig. 5** shows the tables for the two varieties of L-networks pictured in **Fig. 1**. The first version provides a series inductor with a Q of 200 and a shunt branch holding the capacitor. (In a series R-L-C load, you may ignore the Frequency entry. It applies to trap-type loads. Traps are very often designed to be self-resonant at the bottom or just below the bottom of an operating passband.)

L Networks (RLC)										
L Series - C Shunt										
L Networks										
No.	Specified Pos.		Actual Pos.		R (ohms)	L (uH)	C (pF)	R Freq (MHz)	Config	
	Port 1 Wire #	Port 1 % From E1	% From E1	Seg	Series Branch	Series Branch	Series Branch	Series Branch	Ser Br	
	Port 2 Wire #	Port 2 % From E1	% From E1	Seg	Shunt Branch	Shunt Branch	Shunt Branch	Shunt Branch	Sh Br	
1	2	50	50	11	0.125	0.14	Short	0	Ser	
	V1				Short	Short	108.7	0	Ser	

L Networks (RLC)										
C Series - L Shunt										
L Networks										
No.	Specified Pos.		Actual Pos.		R (ohms)	L (uH)	C (pF)	R Freq (MHz)	Config	
	Port 1 Wire #	Port 1 % From E1	% From E1	Seg	Series Branch	Series Branch	Series Branch	Series Branch	Ser Br	
	Port 2 Wire #	Port 2 % From E1	% From E1	Seg	Shunt Branch	Shunt Branch	Shunt Branch	Shunt Branch	Sh Br	
1	2	50	50	11	Short	Short	223.5	0	Ser	
	V1				0.257	0.287	Short	0	Ser	

The second version of the L-network uses a series capacitor with a shunt inductor--again with a Q of 200. Both versions connect Port 1 to the load wire, in this case, segment 11 of wire 2, the Yagi driver. Port 2 for both networks goes to wire V1, the remote short virtual wire, which also serves as the source segment.

**Table 1** lists the results of the modeling with each L-network. Each version lists a variant of the model that omits the series resistance in the inductor branch, this providing a lossless model, except for the aluminum element material, of course. These entries also supply the performance data (excluding the feedpoint impedance) for the basic or pre-match model.

With a normal or lossy coil, both version of the L-network result in the same gain value and the same efficiency. Version 1 shows an

impedance about as much below 50 Ohms as the impedance of version 2 is above 50 Ohms. The variance results from rounding the values, beginning with the original source impedance applied to the external L-network calculator.

## 3-Element Self-Resonant Yagi

Table 1

Performance with 2-element L-networks

A. Series L (0.14  $\mu$ H), parallel (shunt) C (109 pF)

Gain dBi	F-B Ratio dB	Feed Impedance R +/- jX $\Omega$	SWR @ 28 MHz	SWR @ 29 MHz	Efficiency %
1. 0-loss inductor					
8.11	27.11	48.7 - j0.1	1.97	2.36	99.2
2. Inductor Q = 200					
8.09	27.12	48.7 - j0.4	1.97	2.35	98.7

B. Series C (224 pF), parallel (shunt) L (0.29  $\mu$ H)

Gain dBi	F-B Ratio dB	Feed Impedance R +/- jX $\Omega$	SWR @ 28 MHz	SWR @ 29 MHz	Efficiency %
1. 0-loss inductor					
8.11	27.11	51.5 - j0.1	2.00	2.33	99.2
2. Inductor Q = 200					
8.09	27.12	51.2 - j0.1	1.99	2.34	98.7

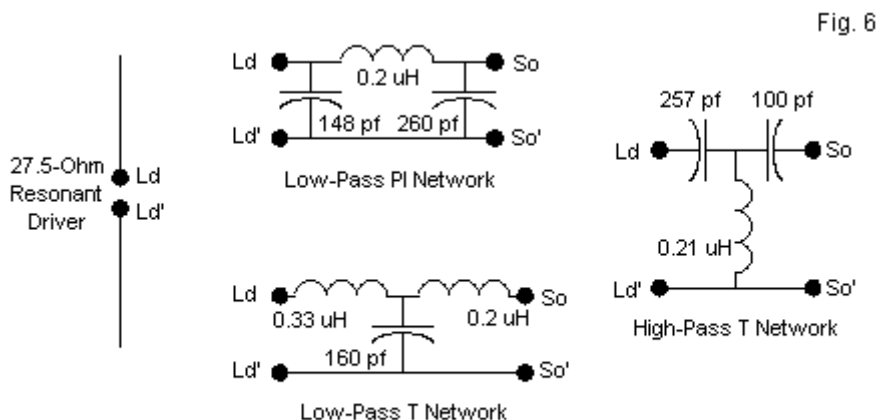
The modeler can be as creative as he or she wishes in the development of models that use a single L-network. For example, one might model a multi-band center-fed doublet, perhaps about 125' long overall. From the center segment of the doublet, one may insert a transmission line of choice, including the loss factor, and set its length to approximate the length of a practical line. Initially, one can place the source on the virtual wire that terminates the transmission line. From a record of source impedance values for

the various bands, one can derive from an external L-network calculator the type of network and the component values needed to transform the impedance to 50 Ohms. (The type of network refers to whether the shunt or the series branch connects to the load.) Then one may go back and insert the prescribed L-network for each band into a separate model to confirm the results. If the modeler is dissatisfied with the results, perhaps due to the need for extreme component values in one or the other leg of the network, one might try different doublet lengths, different transmission-line characteristic impedances (with adjustments to the velocity factor and the loss factor), and even different line lengths. Since the line length is not a part of the overall antenna geometry, the procedure cannot account for disruptive influences on the line that a casual physical installation might encounter. Nevertheless, the exercise can give the modeler with an L-network tuner a good idea--well in advance of purchasing materials--what approximate setting an L-network tuner may need--not to mention the best line to use for a given installation.

### 3-Element/Component Networks

We can connect the individual ports of an L-Network in EZNEC to any wire, real or virtual. Therefore, we might place two (or more) L-Networks back-to-back to form a 3-component network, such as a PI or a T. Although rarely used at the terminals of an antenna, they are often the network forms used in antenna tuners. For our samples, we can dispense with the transmission line and connect our new networks directly to the terminals of our self-resonant 3-element Yagi. For the impedance of the driver (about 27.6 Ohms)

and the cable or source impedance (50 Ohms), we might use any of the networks shown in **Fig. 6**. Indeed, there is a remaining option, the high-pass PI, but I have never seen it used in this type of application.

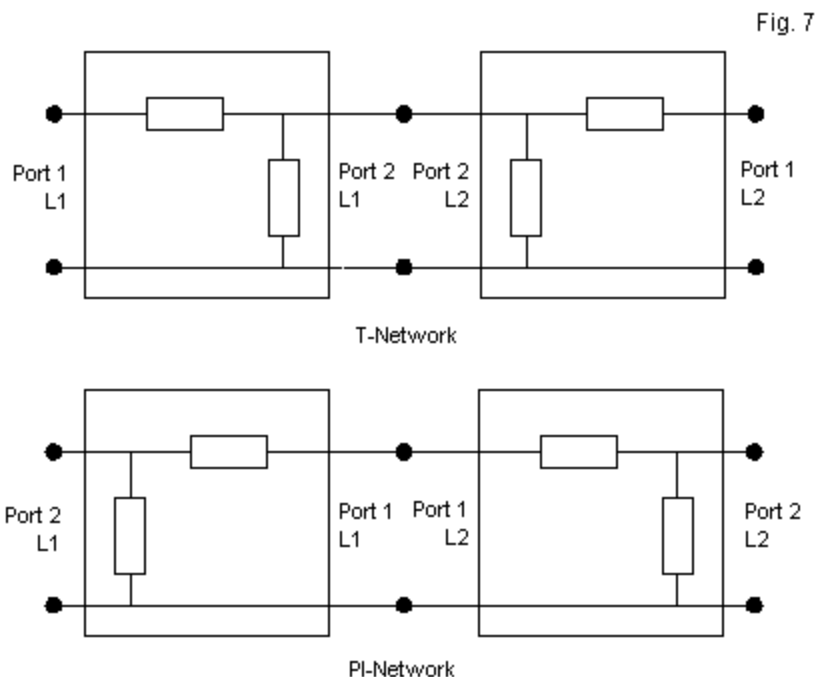


Three-Element Network Matching Systems

Creating such networks will require that we use 2 L-Networks. In each case, the center component is shared by both networks, so we shall have to connect together either a pair of Port 1s or a pair of Port 2s, as shown in **Fig. 7**. For a PI network, the Port 1s go together (on a suitable virtual wire) so that we have two series branches connected in series. A T network requires that we bond the two Port 2s together on a wire. The result is two shunt branches connected in parallel. We also need to keep track of the ultimate ends of the system. For convenience, I shall adopt the convention



of treating the first L-Network as connected to the load, that is, the antenna terminals (or, in the model, the proper driver segment). A new virtual wire, V2, which also receives the model source, terminates the far end of the second L-Network. Some convention of this sort is necessary to ensure model-to-model consistency and to thereby minimize the chances for misconnection errors.

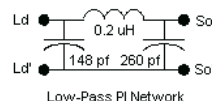
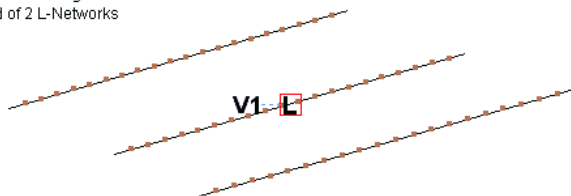


Constructing N-Element Networks from L-Networks

Let's begin by forming the low-pass PI network. **Fig. 8** shows the model, but lists only one network and one virtual wire. On the right, we have the network to compare with the L-Network table that follows. In the table, we can readily identify the shunt capacitors at the extreme ends of the assembly.

Low-Pass PI Matching Network  
Composed of 2 L-Networks

Fig. 8



Low-Pass PI Network

L Networks (RLC)										
L Ntwk Edit Other										
L Networks										
No.	Specified Pos.		Actual Pos.		R (ohms)	L (uH)	C (pF)	R Freq (MHz)	Config	
	Port 1 Wire #	Port 1 % From E1	% From E1	Seg	Series Branch	Series Branch	Series Branch	Series Branch	Series Branch	Series Branch
	Port 2 Wire #	Port 2 % From E1	% From E1	Seg	Shunt Branch	Shunt Branch	Shunt Branch	Shunt Branch	Shunt Branch	Shunt Branch
1	V1				0.09	0.1	Short	0	Ser	
	2	50	50	11	Short	Short	148	0	Ser	
2	V1				0.09	0.1	Short	0	Ser	
	V2				Short	Short	260	0	Ser	

The series branches divide the inductor. In this case, the inductance and its series resistance for a Q of 200 form two equal parts. Since inductances and resistances simply add when in series, the sum of the resistive and the inductive values represent the total that forms the PI network. It is not necessary to divide the values in half. Other partitions will result in accurate results. However, for greatest accuracy, the smaller of the two parts should

be above about 1% of the total. If you place all of the inductance in one L-Network and simply set the other network's series branch to zero, you will end up with a missing component, and the results may not be accurate. For reasons that will become clear as we proceed, the division in half is a convenient convention to adopt.

Let's next form a low-pass T network from 2 L-Networks. **Fig. 9** shows the ultimate network and the formation tables within EZNEC. The series components are clear. The two shunt capacitors each carry half the value of the total capacitance required by the T-network, since capacitances in parallel simply add. (Note: these exercises have presumed perfect capacitors with an indefinitely high Q. However, you may find occasion to assign a series-equivalent resistor to a capacitance to simulate a Q.) Once more, other splits in the total capacitance will work equally well so long as the lower value is at least 1% of the total. Do not place the entire capacitance within one L-network and treat the other shunt value as zero or a short.

Low-Pass T Matching Network  
Composed of 2 L-Networks

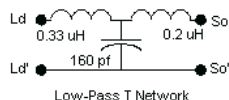


Fig. 9

L Networks (RLC)										
L Ntwk Edit Other										
L Networks										
No.	Specified Pos.		Actual Pos.		R [ohms]	L [uH]	C [pF]	R Freq [MHz]	Config	
	Port 1 Wire #	Port 1 % From E1	% From E1	Seg	Series Branch	Series Branch	Series Branch	Series Branch	Series Branch	Ser Br
	Port 2 Wire #	Port 2 % From E1	% From E1	Seg	Shunt Branch	Shunt Branch	Shunt Branch	Shunt Branch	Shunt Branch	Sh Br
1	2	50	50	11	0.3	0.33	Short	0		Ser
	V1				Short	Short	80	0		Ser
2	V2				0.18	0.2	Short	0		Ser
	V1				Short	Short	80	0		Ser

Our final sample uses a high-pass T network. As shown in **Fig. 10**, this situation produces two capacitors as the series elements. The inductance falls into the shunt branches of the 2 L-Networks. Here, equal parts for each shunt simplifies the arithmetic to an easy mental exercise. If we assign to each shunt branch twice the inductance and twice the resistance relative to the externally calculated total, the parallel combination will be correct. There are other combinations that will do the job, but they might require a calculator.

High-Pass T Matching Network  
Composed of 2 L-Networks

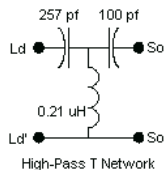


Fig. 10

L Networks (RLC)										
L Ntwk Edit Other										
L Networks										
No.	Specified Pos.			Actual Pos.		R [ohms]	L [uH]	C [pF]	R Freq (MHz)	Config
	Port 1 Wire #	Port 1 % From E1		% From E1	Seg	Series Branch	Series Branch	Series Branch	Series Branch	Sh Br
	Port 2 Wire #	Port 2 % From E1		% From E1	Seg	Shunt Branch	Shunt Branch	Shunt Branch	Shunt Branch	Sh Br
1	2	50		50	11	Short	Short	257	0	Ser
	V1					0.37	0.412	Short	0	Ser
2	V2					Short	Short	100	0	Ser
	V1					0.37	0.412	Short	0	Ser

The question that follows from these formation drills is whether results are accurate. The schematics reflect (with rounding) the network values derived from an external program, which we shall presume to be correct. Ideally, the source impedance for each model should be 50 Ohms. The data in **Table 2** provides the reports from running the NEC models. Each entry in the table provides reports for perfect or lossless inductors and for inductors with a Q of 200.

## 3-Element Self-Resonant Yagi

Table 2

## Performance with 3-element networks

A. Low-pass PI: Cld (148 pF) L (0.2  $\mu$ H) Cso (260 pF)

Gain dBi	F-B Ratio dB	Feed Impedance R +/- jX $\Omega$	SWR @ 28 MHz	SWR @ 29 MHz	Efficiency %
1. 0-loss inductor					
8.11	27.13	50.4 + j0.6	2.24	2.64	99.2
2. Inductor Q = 200					
8.01	27.13	49.6 - j0.2	2.19	2.65	96.9

B. Low-pass T: Lld (0.33  $\mu$ H) C (160 pF) Lso (0.2  $\mu$ H)

Gain dBi	F-B Ratio dB	Feed Impedance R +/- jX $\Omega$	SWR @ 28 MHz	SWR @ 29 MHz	Efficiency %
1. 0-loss inductor					
8.11	27.13	51.2 + j0.9	2.05	2.54	99.2
2. Inductor Q = 200					
8.04	27.13	50.7 + j0.9	2.03	2.50	97.6

C. High-pass T: Cld (257 pF) L (0.21  $\mu$ H) Cso (100)

Gain dBi	F-B Ratio dB	Feed Impedance R +/- jX $\Omega$	SWR @ 28 MHz	SWR @ 29 MHz	Efficiency %
1. 0-loss inductor					
8.11	27.13	50.1 + j0.1	2.09	2.51	99.2
2. Inductor Q = 200					
8.04	27.13	50.2 - j0.6	2.04	2.52	97.7

The low-pass PI network is interesting because it exhibits the lowest efficiency of the group with an inductor Q of 200. The high-pass and low-pass T networks are about equal with respect to efficiency. However, as the gain values suggest, none of the matching network types yields performance reductions that one could notice in operation. As well, the efficiencies of the 3-

component networks is only 1% to 2% lower than the values associated with 2-component L-networks.

A more direct measure of the EZNEC L-Network system is the source impedance reports. Using components calculated externally, the network systems produce the results expected within very close tolerances. Like the parallel-connected components examined in the preceding episode, the L-networks convert--at each frequency within a sweep range--into Y-parameter networks or their equivalents. Hence, the L-network system used in EZNEC provides accurate results across a significant span of frequencies.

Nothing prevents us from using sequential L-Networks rather than back-to-back configurations. Although we would gain nothing from the process in many circumstances, let's create the situation to establish that they work. In the preceding episode, we examined a 1/4-wavelength shortened dipole for 14.175 MHz composed of AWG #12 copper wire. It used a 9.44-uH center-loading coil to bring it to resonance with an impedance of about 15.4 Ohms. Normally, we might use a single L-network with a series inductor on the load or antenna side of 0.26 uH, with a shunt capacitor on the source side of 337 pF. This arrangement would yield a source impedance of 49.7 - j0.3 Ohms.

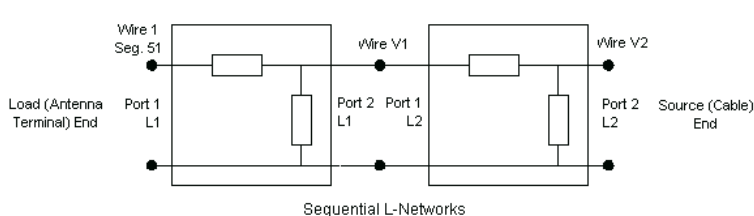


Fig. 11

Wires										
Wire Create Edit Other 14.175-MHz 1/4-Wavelength Dipole with Center Loading Inductor										
<input type="checkbox"/> Coord Entry Mode <input type="checkbox"/> Preserve Connections <input type="checkbox"/> Show Wire Insulation										
Wires										
No.	End 1				End 2				Diameter (in)	Segs
	X (in)	Y (in)	Z (in)	Conn	X (in)	Y (in)	Z (in)	Conn		
1	-101	0	0		101	0	0		#12	101

L Networks (RLC)										
L Ntwk Edit Other Sequential L-Networks										
L Networks										
No.	Specified Pos.		Actual Pos.		R (ohms)	L (uH)	C (pF)	R Freq (MHz)	Config	
	Port 1 Wire #	Port 1 % From E1	% From E1	Seg					Ser Br	Sh Br
1	Port 2 Wire #	Port 2 % From E1	% From E1	Seg	Series Branch	Series Branch	Series Branch	Series Branch	Ser	Ser
	V1	50	50	51	0.067	0.15	Short	0	Ser	Ser
2	Port 2 Wire #	Port 2 % From E1	% From E1	Seg	Shunt Branch	Shunt Branch	Shunt Branch	Shunt Branch	Ser	Ser
	V2				0.12	0.28	Short	0	Ser	Ser
					Short	Short	207.3	0	Ser	Ser

For our sequential system, let's install two L-networks arranged as shown in **Fig. 11**. The first network will convert the 15.5-Ohm load impedance to 27 Ohms. The second will convert the 27-Ohm impedance to 50 Ohms. The tables show the basic dipole, although I have omitted the inductive load. The network tables show the series and shunt branch values necessary to effect the 2-stage impedance transformation. As always, the inductors have a Q of 200.



The 2-stage L-network system produces a source impedance on wire V2 of  $49.8 - j0.2$  Ohms. The dipole gain is 0.84, indicating a small network loss. The efficiency is 79.3%, considering the effects of both the network and the loading coil. A single-stage L-network shows an efficiency of 79.4%. Even though the 2-stage L-network system shows no advantage over a single-stage network--and indeed requires unnecessary component complexity--it does illustrate well enough the accuracy of EZNEC L-networks in the sequential mode. The SWR graph is identical to the one shown for the dipole in Part 1 of this episode pair.

## Conclusion

The goal of these episodes has been to show the steps needed to model effectively using new facilities within the latest version of EZNEC. These facilities include transmission-line losses, parallel-connected loads, ideal transformers, and L-networks. As applicable, each facility shares the frequency-nimble properties of R-L-C loads in NEC. The program achieves this ability by recalculating an NT command or its equivalent for each frequency step within a defined sweep. Hence, the new facilities are highly useful in evaluating potential antenna performance across a band of frequencies.

Although the examples have focused on antenna impedance matching, this application is but one of many possible uses to which we might put the facilities. For example, L-networks--and more complex networks that we might construct from them--are useful not only for impedance transformation, but as well for phase-

shifting a signal. Learning the required modeling steps and developing personal conventions that make them consistent from one model to the next is crucial to error-free and confident modeling with the new facilities in this program.

## Chapter 141: Circular R-X Graphs

**T**he NEC calculation cores produce only a tabular output. Any graphical outputs that we may wish represent post-core-run manipulations of the output data. Most of the work involves finding and parsing the data into a form that a graphing module may use to present the information in a more useful visual manner. Various implementations of NEC provide some of these graphs, namely, the ones most often required or desired by antenna modelers.

Graphs that accompany an implementation of NEC generally come in two forms: polar and rectangular. Polar graphs generally apply to the radiation pattern outputs, since the data values appear in terms of angles and magnitudes. In past episodes, we have examined some of the considerations that go into the forms and plot ring arrangements for such graphs. It is also possible to present these graphs in rectangular form, using the X-axis of the graph for the angular information and the Y-axis for the magnitude. Rectangular graphs are also very useful to present other information, such as the current magnitude and/or phase angle along one or more wires in the model or the resistance, reactance, and SWR information over a specified frequency range.

Some graphical outputs from NEC implementations involve post-core-run calculations. The most common calculation is the SWR relative to a user-selected (or a default) resistive impedance. In addition, some implementations have created polar plots of the left-hand and the right-hand circular components of radiations patterns

using calculations based on the radiation pattern data. We have also examined some of these calculations in past episodes.

There is one type of graph that is both very useful and very absent from implementations of NEC. In fact, the only NEC-related program that makes the graph available--to the best of my knowledge at the time of writing--is AC6LA's Multi-NEC. This Excel application does not use a core, but taps into the cores of a number of popular programs for the core run itself. However, Multi-NEC does provide a large collection of facilities unavailable in most NEC implementations.

The graph to which I am referring is the X-Y graph. It is available in many graphing and in most spreadsheet programs. Instead of plotting the magnitude of Y against a progression of set values for the X-axis, the graph plots both X and Y as points on a field. The graphing facility normally calculates the field area needed to contain the points and then creates X- and Y-axes to accommodate the values. Some graphing programs allow the user to modify the axes limits and subdivisions. In addition, most X-Y graphing facilities add a line connecting the successive data points in the series.

X-Y graphs have numerous uses. With respect to antennas, one of the most useful versions is a plot of resistance and reactance across a large frequency span. There is much that we can glean from a close examination of X-Y graphs of  $R \pm jX$ . So let's probe a bit further. Once we catch on to how we can create our own X-Y graphs of NEC output data and look at a few comparative

situations, we may transform such graphs from mere interesting oddities into genuinely useful data presentations that we are likely to use often in the future.

## The Exercise

To see what we might learn from X-Y graphs, we shall need a few antennas. **Fig. 1** shows the four that we shall use. The first three are linear dipoles, but with very different length-to-diameter ratios (1000:1, 100:1, and 20:1). The last of the sequence is a biconical dipole composed of 4 wires simulating the element cones. To simplify graphing, I have resonated all four antennas at 300 MHz as 1/2-wavelength elements. We shall be interested in the impedance behavior of each antenna over an 8:1 frequency range (3 octaves).

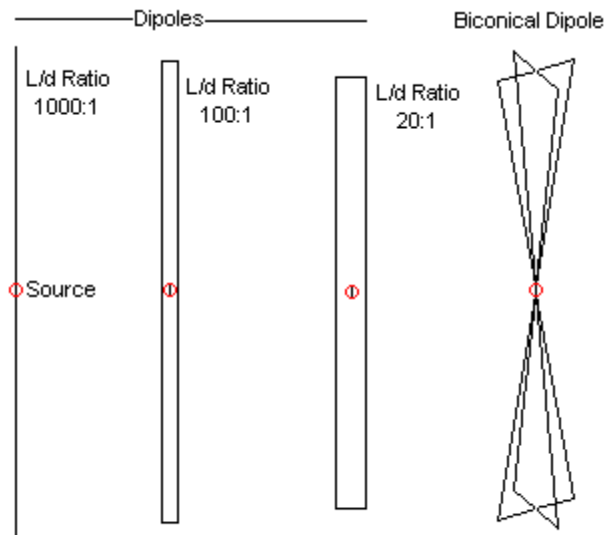


Fig. 1 Sample Antenna Shapes for This Exercise

To obtain the requisite data, we need to conduct frequency sweeps across the prescribed range. I have selected a 30-MHz increment to yield 71 sweep steps as defined for the FR command, beginning at 300 MHz. We have enough steps to produce some interesting graphs, but not so many as to tax our patience while the core generates the necessary data. Some programs have tabular facilities to collect the impedance data from each run for each frequency into a single table. The partial table in **Fig. 2** samples the information as presented by software. The entire table would be unnecessarily long, since we may view it more compactly for each of our subject antennas in graphical form.

Input Impedance and VSWR Fig. 2

Frequency	Tag	Seg.	Real(Z)	Imag(Z)	Mag(Z)	Phase(Z)	Zo	VSWR
300.000000	1	2	52.870	-3.221	52.968	-3.486	52.000	1.07
330.000000	1	2	70.766	43.482	83.057	31.569	52.000	2.14
360.000000	1	2	94.123	88.213	128.999	43.144	52.000	3.68
390.000000	1	2	124.640	131.004	180.824	46.426	52.000	5.27
420.000000	1	2	164.403	170.861	237.111	46.104	52.000	6.74
450.000000	1	2	215.657	205.282	297.739	43.588	52.000	8.02
480.000000	1	2	280.114	229.604	362.190	39.341	52.000	9.08
510.000000	1	2	357.323	236.575	428.541	33.508	52.000	9.93
540.000000	1	2	442.016	217.252	492.521	26.174	52.000	10.58
570.000000	1	2	521.724	164.892	547.161	17.539	52.000	11.04
600.000000	1	2	578.537	81.614	584.265	8.030	52.000	11.35
630.000000	1	2	597.745	-17.817	598.010	-1.707	52.000	11.51
660.000000	1	2	577.473	-112.011	588.236	-10.977	52.000	11.53
690.000000	1	2	528.803	-184.729	560.141	-19.256	52.000	11.42
720.000000	1	2	467.056	-230.716	520.933	-26.288	52.000	11.20
750.000000	1	2	404.175	-252.935	476.795	-32.039	52.000	10.85
780.000000	1	2	346.717	-257.341	431.784	-36.584	52.000	10.39
810.000000	1	2	297.186	-249.593	388.093	-40.025	52.000	9.82
840.000000	1	2	255.887	-233.943	346.710	-42.435	52.000	9.13
870.000000	1	2	222.206	-213.244	307.975	-43.821	52.000	8.32
900.000000	1	2	195.296	-189.288	271.975	-44.105	52.000	7.42

We shall be interested in the Z(real) and Z(imag) columns, since we wish to plot R and X. However, we might have as easily selected Z(mag) and Z(phase)--or any other pair of data items--for our work. R and X simply give us some focus to develop a sense of what we might eventually learn from the graphing exercise.

Unless we are using Multi-NEC, we shall have to create graphs for ourselves externally to the NEC implementation. The first step is to perform whatever re-shaping we might need to do to enable us to import the data from the table into a spreadsheet. Many spreadsheets create separate columns only when the separator between data values in a table is of a certain sort. TAB is perhaps

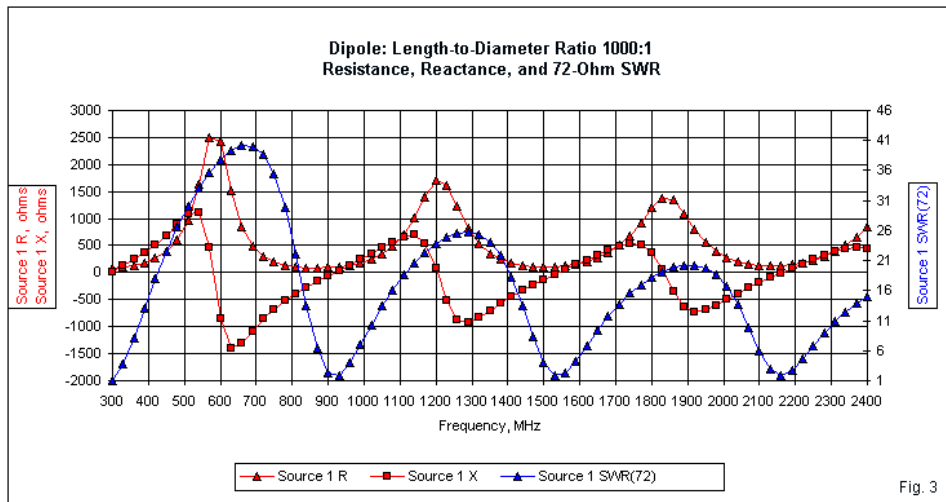
the most universal separator for easy spreadsheet entry. If we save the data table and open it in a word processing program, then we can find and replace a uniform series of spaces with a TAB code. From that point, we can copy and paste the revised table into a spreadsheet.

The rest of the job is simply creating a graphic using the X-Y format, along with axis labels, titles, and any marker notations that we might find useful. For example, the X- and Y-axes of our graph will note only the range of values for R and X. They will not locate specific frequencies. Therefore, we may wish to add a few marker notations to facilitate comparing graphs.

### The 1000:1 L/d Dipole

The very thin-wire dipole provides a useful starting point. At 300 MHz, its length is 0.4810 wavelength (or meters), with a diameter of 0.000481 wavelength (or meters). Both dimensions translate directly into meters at this frequency. Let's begin with a very conventional graph of the feedpoint or source resistance, reactance, and 72-Ohm SWR values. **Fig. 3** provides the data as developed via EZPlots, another AC6LA program for analyzing frequency sweeps taken with EZNEC.

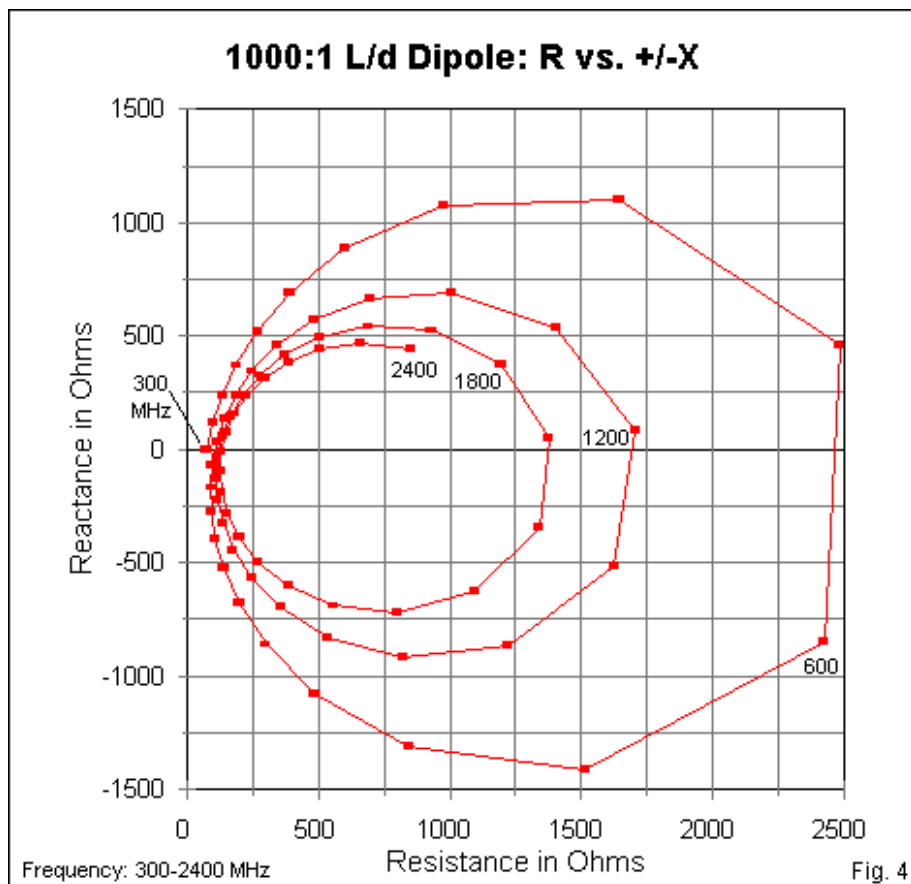




The chart seems clear enough, despite the three data curves. Between the points of minimum SWR, which also generally mark the low values of  $R$ , we can see the peaking of the values of  $X$  as we increase frequency. As we increase the frequency, we can also see that the peak values of SWR systematically decrease, along with the peak values of  $R$  and  $X$ . The SWR peaks seem to correspond roughly to frequencies at which the antenna element is an integral multiple of 1 wavelength--but not exactly.

If we take an X-Y graph of the resistance and the reactance, we obtain a chart with the appearance of **Fig. 4**. I have purposely shrunk the width of the chart so that the X- and the Y-divisions are about equal in space, even if not in numerical values. Since most such charts that appear in texts have a relatively square form,

producing nearly circular patterns of data values, this shape gives the sample an air of familiarity. Unfortunately, my spreadsheet does not have a spline function to round the curves, and we do not have enough data points to yield a good round outer curve to the spiral.



The spiral itself captures some of the essential features of the linear graph and sets them into fairly bold relief. As we increase the operating frequency, the resistance at the low-impedance resonances increases with each passage. In addition, with each increase in frequency, the peak values of resistance and reactance decline. The data points for resistance and reactance are the same ones that appeared in **Fig. 3**. However, the presentation in **Fig. 4** allows us to see some of the interesting relationships more clearly.

Note that I have added a few frequency markers. One points to the beginning of the curve at 300 MHz. The others mark the frequencies at which we might have expected the antenna to show a resonance as the reactance makes its sudden transition from a very high inductive value to a very high capacitive value. However, due to end effect and other factors, these frequencies do not mark resonant points on the curve.

Rather than probe this single graph for various further details, let's turn to a second dipole. Some of the utility of X-Y graphs lies in comparing one with another--so long as the antennas involved are indeed comparable.

### The 100:1 L/d Dipole

A fit comparator for the dipole with a length-to-diameter ratio of 1000:1 is another dipole with a 100:1 ratio. At 300 MHz, the length is 0.4676 wavelength (or meters) with a diameter of 0.004676 wavelength (or meters). Like the first antenna, it will be resonant at 300 MHz as a 1/2-wavelength dipole. The question that we may

pose to our resistance vs. reactance X-Y graphs is how the two antennas behave similarly and differently between 300 and 2400 MHz.

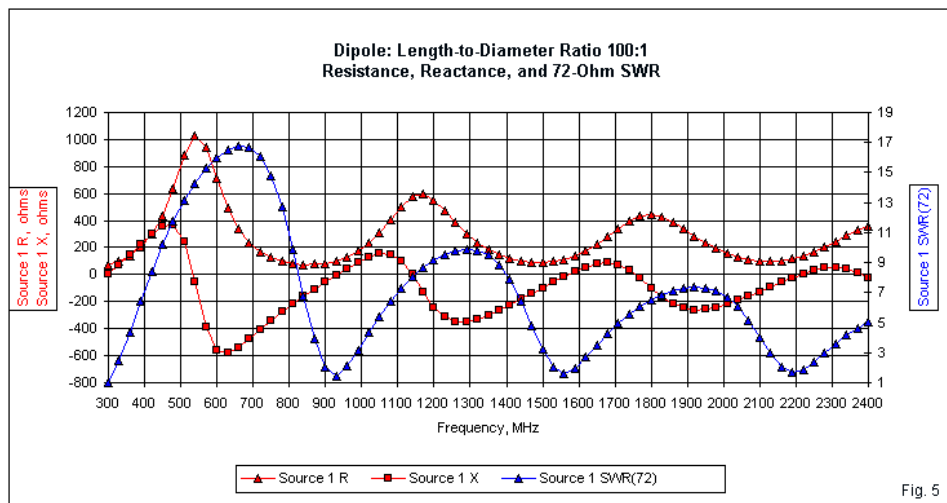
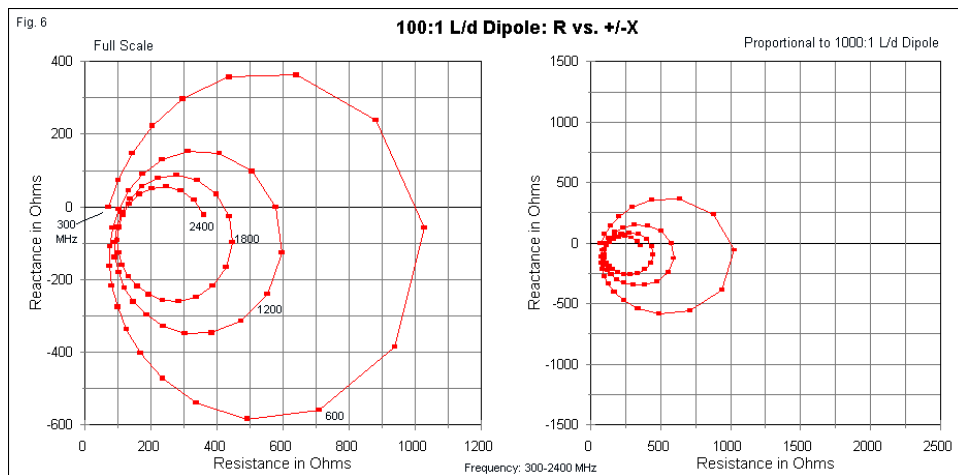


**Fig. 5** shows the conventional graph of resistance, reactance, and 72-Ohm SWR for the fatter dipole, using a frequency-based X-axis. In many respects, the curves for the two dipoles are very similar in shape. However, if we compare the values on the left and the right Y-axes, we shall see that the peak values are far lower in every category.



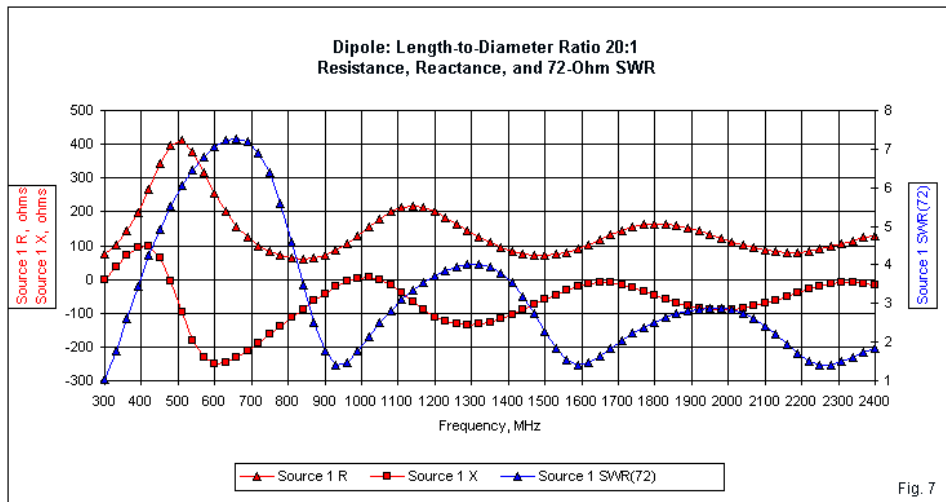
The left part of **Fig. 6** shows the X-Y graph of resistance vs. reactance for the 100:1 dipole. The spiral resembles the one in **Fig. 4**, but with a few exceptions. For example, the peak values are rather vividly lower. The version of the graph on the right uses the same axis range as **Fig. 4**, and the smaller range of values in the new antenna's spiral becomes very clear.

In addition, note the positions of the frequency markers on the graphs in **Fig. 4** and **Fig. 6**. The fatter version of the antenna places the markers further along the spiral than does the thinner dipole. In addition, we may note that in both of the resistance vs. reactance graphs, we see a more extreme value of capacitive reactance than of inductive reactance.

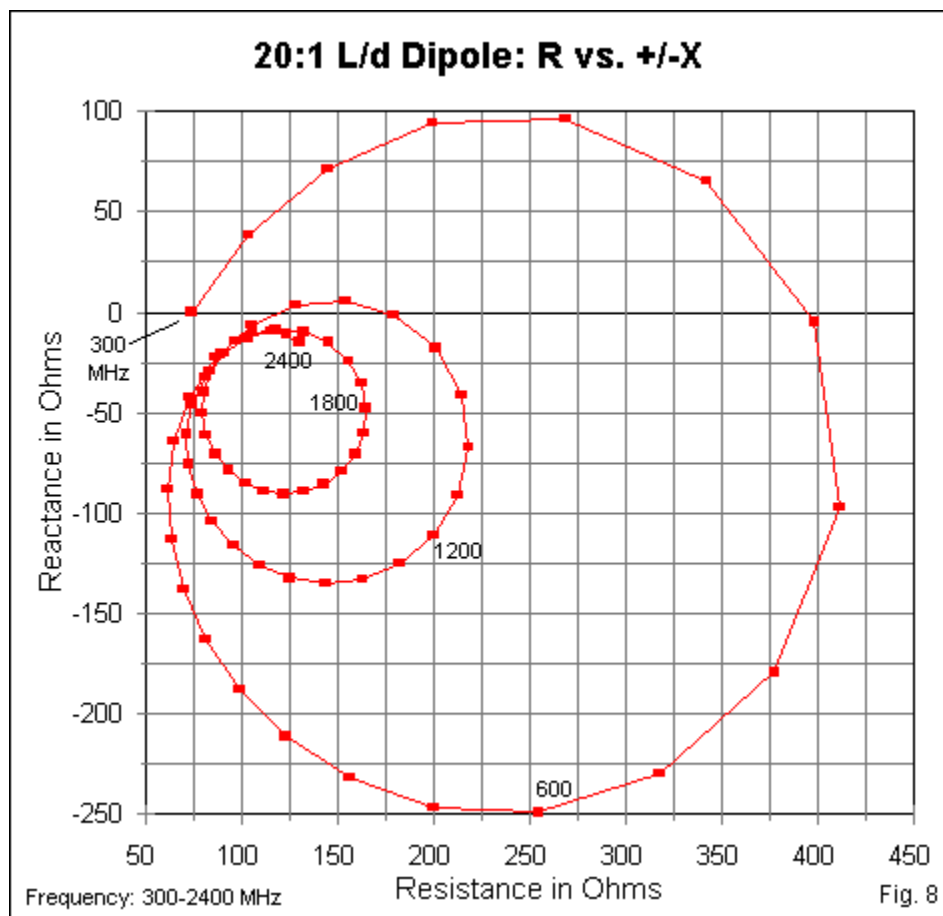
These are by no means new discoveries about dipoles of varying length-to-diameter ratios. Basic college texts will contain a number of equations by which to calculate the impedance behavior. The function of the X-Y graph is to present the data in a manner that naturalizes it so that it becomes part of our expectations of dipole behavior.

### The 20:1 L/d Dipole

Two instances do not themselves establish a trend. Therefore, let's add one more dipole to our collection, this time with a length-to-diameter ratio of 20:1. The length at 300 MHz is 0.45 wavelength (or meters), with a diameter of 0.0225 wavelength (or meters). This dipole is about as fat as we dare let the model go while still expecting reliable data. **Fig. 7** provides the resistance, reactance, and SWR data in the conventional format.



Once more, the curves have their by-now familiar shapes, but the peak values have declined even further. Above about 1200 MHz, the resistance begins to flatten so that a value of about 100 Ohms becomes the median value. Indeed, a center-fed element with a 20:1 length-to-diameter ratio becomes a candidate for being a broadband antenna, were it not for the fluctuations in the reactance. For example, the antenna exhibits a 400-Ohm SWR of under 2:1 from about 400 through 575 MHz.



The X-Y graph in **Fig. 8** provides the spiral perspective on the fattest of our dipoles. The smaller range of both resistance and reactance values removes much of the distortion from the actual



smooth curves of the transition between values. In fact, the 20:1 dipole shows total ranges of both resistance and reactance that are about 1/3 of the range shown by the 100:1 element and well under 20% of the ranges displayed in the spiral for the 1000:1 center-fed antenna. Nonetheless, all three spirals share the common trait of shrinking ranges of both resistance and reactance with rising frequencies. If we keep the 3:1 range difference in mind between the fatter two dipoles, we can also see that the frequency markers are farther along the spirals for the thicker of the two, continuing the potential trend that we saw when comparing the first two antennas in our exercise.

We also raised the question as to whether the apparent domination of the spirals by capacitive rather than inductive reactance was a real phenomenon or an artifact of the increment selected for creating the curves. In fact, the phenomenon is real. From 400 to 600 MHz, the capacitive reactance peaks at about  $-j250$  Ohms. However, the inductive reactance never quite reaches  $j100$  Ohms. One might leave the explanation for this condition--reflected to lesser degrees in the thinner dipoles--as "an exercise for the reader," but we should not forget the capacitance between the element halves at the feedpoint gap created in the model and in real antennas. Most cage elements (assuming periodic rings around the wire collection to ensure even current distribution) bring the wires forming the fat dipole together in a sloping point, a structure that reduces the capacitance. Some wide-band elements may create a biconical structure for up to half the length of each side of the center feedpoint.

And that last note brings us to the final element of our collection.

## The Biconical Dipole

As a contrast to the uniform-diameter dipoles with which we have been working in order to develop an appreciation of resistance vs. reactance X-Y graphs, we may examine a sample biconical dipole having the structure shown in **Fig. 1**. We shall use 4 wires to simulate the cone, brining the ends of each wire together at the center of each end. The nominal slope of reach cone is 10 degrees relative to the dipole's centerline. The value is nominal, since the feedpoint region consists of a short 3-segment wire, with the middle segment serving as the source segment. Hence, there is about a 0.2-degree difference between the angle of each wire relative to where it joins the source wire and the virtual angle taken from the exact center to the outer tip of the cone wires. The differential is not sufficient to invalidate the very general outline of impedance behavior for the biconical antenna between 300 and 2400 MHz.

Each of wires has a diameter at 300 MHz of 0.002 wavelength (meters). The overall length is 0.3522 wavelength (meters). The maximum distance across the extreme end of the element is 0.061 wavelength (meters). Whether we can call this dimension the diameter of the cone at its widest opening depends upon the degree to which 4 wires simulates a solid-surface cone, a consideration requiring a different context and discussion from the present topic. As well, because the biconical element changes its diameter along its length, we cannot readily assign to it a length-to-diameter ratio. However, see Kraus, *Antennas*, 2nd Ed., Section 9-

11 for a discussion of and equations for calculating the impedance of thin cylinder and biconical elements. Imperfect as the simulated biconical structure may be, it does provide a good indication of biconical properties. Note, for example, the overall length, resonant at 300 MHz (with an impedance of 52 Ohms), in comparison to the lengths of the uniform-diameter dipoles, the shortest of which is 0.45-wavelength (meters)

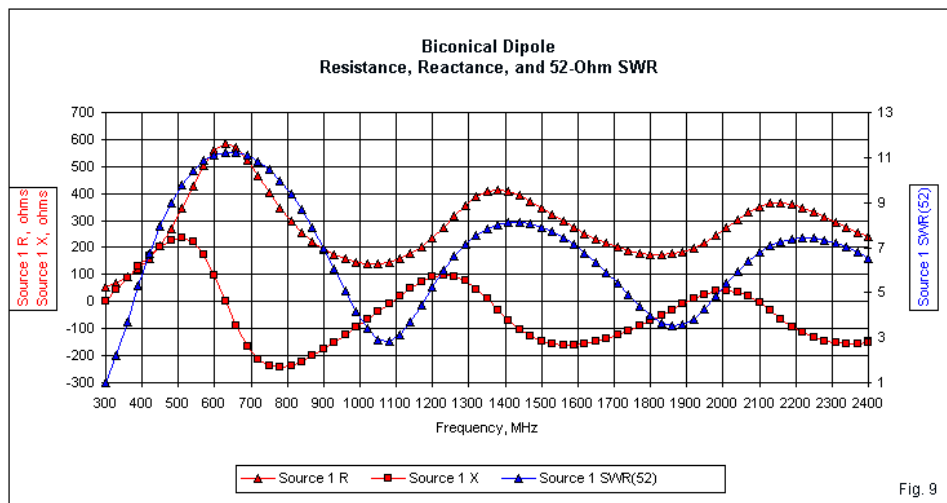
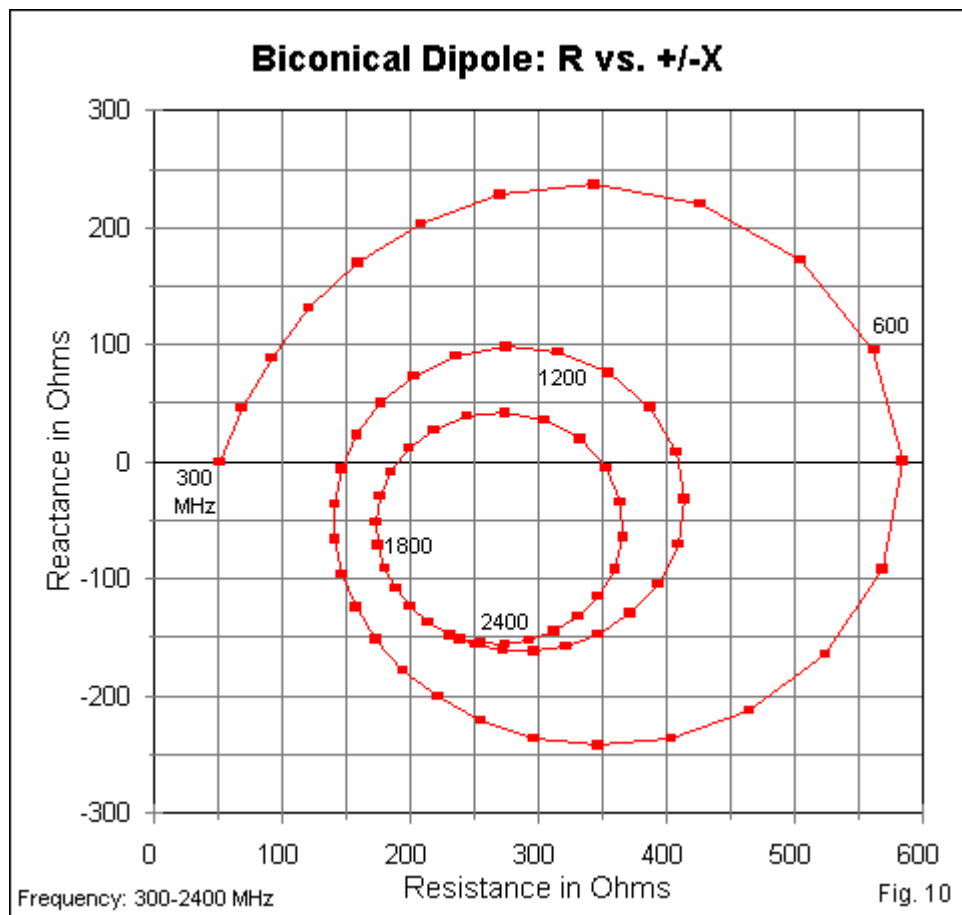


Fig. 9

The conventional graph of resistance, reactance, and (52-Ohm) SWR in **Fig. 9** displays much of what we expect in any dipole. The undulations of all three properties recorded in the graph resemble those of the 20:1 L/d dipole, although the biconical element shows slightly higher peak values in the first SWR cycle. For example, the

fat dipole shows a peak resistance of about 400 Ohms, while the biconical antenna has a peak resistance of about 600 Ohms.

Perhaps the most notable difference between the uniform-diameter dipoles and the biconical element becomes evident when we count SWR cycles. All of the cylindrical dipoles show an average of about 3-1/4 SWR cycles between 300 and 2400 MHz. In the same span, the biconical antenna exhibits about half a cycle less. Although we see a progressive broadening of the bandwidth as we increase the diameter of the dipoles, the biconical simulation outstrips the dipole progression by a significant margin.



The X-Y graph of resistance and reactance in **Fig. 10** reveals some additional properties that may, under certain circumstances, be useful to know. Unlike the uniform-diameter dipoles, the biconical

antenna shows nearly equal inductive and capacitive reactance peaks in the first cycle of the spiral. However, as we raise the operating frequency, capacitive reactance begins to dominate each cycle. An average reactance line drawn across the face of the graph would fall in the vicinity of the  $-j50\text{-}\Omega$  marker. We must moderate this average by noting that the dominance of the capacitive reactance in the source impedance appears to become stronger with each successive cycle. In contrast, the uniform-diameter models seem to present a near symmetry of reactance in each cycle once we establish an average value line on the graph. To what degree modeling limitations may enter the values for the higher frequencies would become a necessary consideration for an actual antenna that might be under analysis.

One of the important external additions to the graph is annotating the curves with frequency markers at critical points. In the case of the biconical dipole, these notes allow us to see clearly to what degree the antenna geometry has spread the undulations of resistance and reactance across a wider range than we found for the cylindrical dipoles.

## Conclusion

Our excursion into the sample dipoles has not tried to establish anything new about these fundamental antennas. The exercise examples have simply served as a convenient way to illustrate the benefits of adding to what modeling programs provide by creating an external graphing functions. In this case, we have extracted the source information from NEC core runs over a wide frequency

sweep to produce X-Y graphs of resistance and reactance. The result is a spiral graph of the values that served to reveal some properties more clearly than standard linear graphs. Although we have used an external spreadsheet to produce the sample graphs, Multi-NEC provides this facility as part of its spreadsheet shell for using a variety of NEC cores. **Fig. 11** shows a resistance-reactance plot for a sample antenna in the Multi-NEC application.

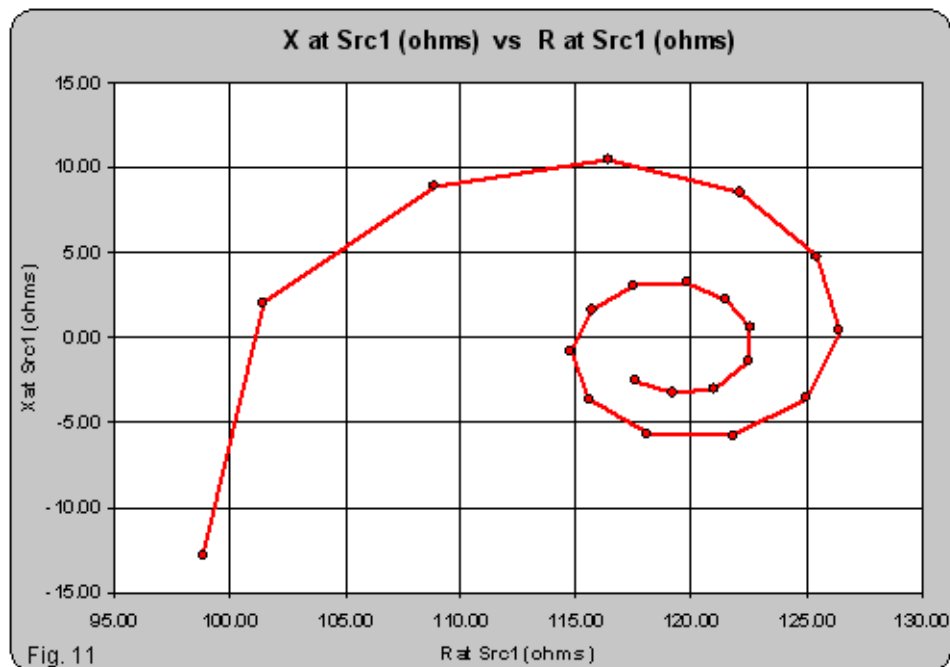


Fig. 11

Although the resistance-reactance X-Y graph is the most common form in antenna work, other pairs of values may prove relevant for X-Y graphing in many contexts. Even at a fundamental level, the R-X plot has significant use. For example, amateurs often install single-wire antennas design to serve all frequencies from about 3.5 MHz through 30 MHz. A series of X-Y plots of resistance and reactance can assist the average ham in finding a wire length at the proposed height and ground conditions that best avoids radically high and radically low antenna impedance values in each amateur band so as to minimize losses in the selected parallel transmission-line to the station's antenna tuner. Since some current programs allow the entry of transmission lines with their listed velocity factors and loss factors, one might model the entire system using various trial element lengths to arrive at the best combinations that is usable within the antenna construction site.

In short, additional post-core and post-program manipulation of data can serve useful purposes, and the X-Y graph is only one of them.



## Chapter 142: VOACAP Type 13 Files

**B**etween antenna modeling via NEC or MININEC and ionospheric propagation prediction software, we find a nexus that goes under a deceptively simple title: the type-13 file. In these notes, we shall look at three questions. What is a type-13 file? Why is it important for at least some modelers to develop such files? How can we make a type-13 file within NEC that is compatible with the most common propagation programs? Our account will be very general relative to the first two questions, since our focus will be on the modeling aspects of the Type 13 file.

### What is a type-13 file?

Like modeling cores, such as NEC and MININEC, propagation software has one or two primary calculation cores with embellished implementing software. The older core is IONCAP, although the most commonly used package is VOACAP. In 1985, the Voice of America (VOA) adopted the Ionospheric Communications Analysis and Prediction Program (IONCAP) as the approved engineering model to be used for broadcast relay station design and antenna specification. As the program was modified for these purposes, the name was changed to the Voice of America Coverage Analysis Program (VOACAP) to distinguish it from the official National Telecommunications and Information Administration (NTIA) IONCAP program. The Fortran code for VOACAP is readily available, allowing a number of implementations, such as ACE-HF, available from *antenneX*.

Although developed for shortwave broadcast interests, the VOACAP program is equally useful for predictions of ionospheric propagation conditions governing long-range two-way communications in the HF range. Hence, we find the program widely used in government, military, commercial, and amateur installations designed for such communications. Within these installations, there are almost innumerable different antennas in use, too many for any program to contain as samples. Within VOACAP, we define an antenna not solely by its geometry, but as well by its height above ground (including ground mounted monopoles with various types of radial systems) and the quality of ground beneath the antenna at a specific frequency. In fact, VOACAP is not interested specifically in the antenna geometry, but in the far-field radiation pattern produced by the antenna at the selected frequency. Geometry (including electrical features that affect the far-field), height, frequency, and ground quality together determine the far-field pattern for a station interested in propagation predictions.

To make the most accurate predictions of propagation potentials for a given station, VOACAP requires a frequency-specific radiation pattern file for any subject antenna. The file must meet certain standards. It must provide a 360-degree azimuth pattern in 1-degree increments. The azimuth pattern must proceed in compass-rose order, that is clockwise from the starting point--ordinarily North or 0-degrees. For each azimuth increment, the file must list the signal gain in dBi for each elevation angle from the horizon to the zenith in 91 entries. The result will be an ASCII file that is over 250 kB long. Moreover, virtually all implementations of VOACAP require

the older file-name entry of no more than 8 characters, with a file extension of no more than 3 characters. In most cases, the extension will be .13.

The file has several other requirements, illustrated by the partial file in **Fig. 1**. The figure shows only the first 3 azimuth headings of the 360 required by the file, but the remaining entry groups follow the same pattern as those shown. The filename is TF50280C.13, indicating a terminated folded dipole antenna that is 50 m long over average ground. The file is one of a large series of type-13 files for this antenna, one for every MHz of the anticipated operating range. Since terminated folded dipoles come in a considerable variety of lengths (and other details), the file name should use a code that allows ready identification of the antenna, the frequency, and the ground quality (where C indicates average ground with a conductivity of 0.002 S/m and a permittivity of 13 on the scale used in this particular coding system).

L.B.Cebik Wideband terminated folded dipole at 28.0 MHz, level, 15m high, 50m long, avg ground

```

4      4 parameters
0.00   [ 1] Max Gain dBi...
13     [ 2] Antenna Type... 360 x 91 gain values follow
0.0    [ 3] Efficiency (for IONCAP)
28.0   [ 4] Frequency
      0
      -99.99 -12.10 -6.229 -2.927 -0.722  0.847  1.983  2.792  3.333  3.643
        3.742  3.637  3.328  2.805  2.046  1.010 -0.368 -2.206 -4.729 -8.433
      -14.50 -17.49 -10.55 -6.270 -3.501 -1.551 -0.118  0.950  1.740  2.305
        2.677  2.880  2.927  2.826  2.579  2.186  1.641  0.930  0.036 -1.072
      -2.438 -4.130 -6.243 -8.880 -11.87 -13.52 -11.82 -9.028 -6.635 -4.748
      -3.256 -2.063 -1.099 -0.316  0.320  0.834  1.244  1.566  1.810  1.985
        2.100  2.160  2.172  2.140  2.068  1.961  1.821  1.652  1.458  1.240
        1.003  0.749  0.481  0.202 -0.086 -0.378 -0.672 -0.965 -1.254 -1.535
      -1.805 -2.061 -2.300 -2.519 -2.715 -2.885 -3.028 -3.141 -3.222 -3.272
      -3.288
    1
      -99.99 -12.26 -6.390 -3.088 -0.883  0.686  1.823  2.632  3.175  3.485
        3.585  3.481  3.173  2.652  1.893  0.859 -0.517 -2.353 -4.874 -8.575
      -14.64 -17.63 -10.70 -6.409 -3.638 -1.686 -0.251  0.820  1.612  2.179
        2.555  2.760  2.809  2.711  2.467  2.077  1.534  0.827 -0.065 -1.170
      -2.534 -4.222 -6.333 -8.968 -11.96 -13.62 -11.91 -9.111 -6.713 -4.821
      -3.326 -2.130 -1.163 -0.376  0.263  0.779  1.193  1.517  1.763  1.941
        2.059  2.122  2.136  2.106  2.037  1.931  1.794  1.627  1.435  1.219
        0.984  0.732  0.465  0.188 -0.098 -0.389 -0.682 -0.974 -1.261 -1.541
      -1.810 -2.065 -2.303 -2.521 -2.717 -2.886 -3.028 -3.141 -3.223 -3.272
      -3.288
    2
      -99.99 -12.75 -6.881 -3.579 -1.373  0.197  1.335  2.146  2.691  3.004
        3.106  3.006  2.701  2.184  1.430  0.400 -0.971 -2.801 -5.315 -9.005
      -15.04 -18.05 -11.13 -6.834 -4.056 -2.096 -0.654  0.424  1.225  1.799
        2.182  2.396  2.453  2.363  2.128  1.746  1.212  0.513 -0.370 -1.467
      -2.822 -4.502 -6.605 -9.236 -12.23 -13.90 -12.18 -9.363 -6.948 -5.044
      -3.538 -2.331 -1.354 -0.559  0.089  0.615  1.036  1.369  1.623  1.810
        1.935  2.005  2.027  2.004  1.942  1.843  1.712  1.552  1.365  1.156
        0.926  0.679  0.418  0.145 -0.136 -0.422 -0.711 -0.999 -1.283 -1.559
      -1.825 -2.078 -2.313 -2.529 -2.722 -2.890 -3.031 -3.142 -3.223 -3.272
      -3.288
    3
      -99.99 -13.59 -7.726 -4.424 -2.216 -0.644  0.496  1.311  1.859  2.176
        2.283  2.188  1.891  1.380  0.633 -0.387 -1.749 -3.568 -6.069 -9.739
      -15.73 -18.75 -11.87 -7.563 -4.771 -2.799 -1.343 -0.252  0.562  1.150
        1.547  1.774  1.846  1.770  1.549  1.182  0.663 -0.021 -0.889 -1.971
      -3.311 -4.976 -7.067 -9.690 -12.69 -14.39 -12.64 -9.789 -7.347 -5.420
      -3.895 -2.671 -1.677 -0.866 -0.203  0.337  0.774  1.120  1.388  1.588
        1.726  1.810  1.844  1.833  1.783  1.695  1.575  1.426  1.250  1.050
        0.830  0.592  0.340  0.075 -0.198 -0.477 -0.759 -1.040 -1.318 -1.589
      -1.850 -2.098 -2.329 -2.541 -2.731 -2.896 -3.035 -3.145 -3.224 -3.272
      -3.288
  
```

Fig. 1

For any group, the initial entry is -99.99 dBi, indicating an elevation angle of 0 degrees. The final entry in each group is the same, since

every 90-degree elevation or zenith angle records the same far-field direction and hence the same gain. Note the internal grouping limits and the spacing required to have a file that is readable within VOACAP.

Equally important are the initial entries. The first entry is a limited space for recording antenna details. The next 4 entries are standard except for the frequency entry, which should indicate the frequency for this particular file. Note again the spacing of the entries from the left edge to ensure that VOACAP can read the data correctly.

Although this antenna creates a series of files at 1-MHz intervals (from 2 through 30 MHz), a developer of type-13 files should use the specific operating frequencies of operation. In general, a single frequency within each amateur or similarly narrow band will suffice for accurate propagation forecasts. Consult the applicable directions within specific implementations of VOACAP for recommendations on how to correlate type-13 files with the actual use of the propagation prediction software.

### **Why is it important for at least some modelers to develop type-13 files?**

Accurate propagation forecasting depends upon using a reasonably accurate far-field projection of the actual antenna used at the site that is interested in such forecasts. The term "reasonably accurate" is subject to all manner of external considerations. For some very generalized applications, one of the sample models usually

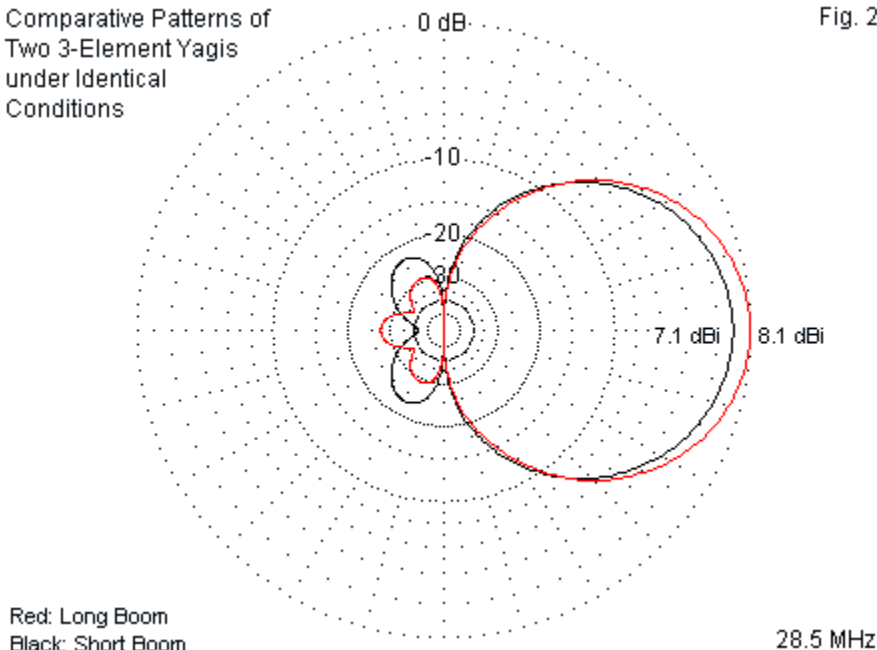
included in the VOACAP package may be sufficient. However, the variety of antennas available and in use precludes replication of all of them at all heights and over all types of ground. Hence, a customized collection of type-13 files may be necessary.

Ideally, one should develop a model of the entire antenna installation so as to show all potential interactions among the antennas and relevant non-antenna objects. This extensive modeling is practical under two conditions. First, all antennas should be fixed (that is, not rotatable). Second, the modeling program must have a very large maximum segment count in order to include all antennas and relevant objects. In most cases, practical models will include only the subject antenna.

However, subject antennas should be modeled accurately. A generalized label, such as "3-element Yagi," may not be specific enough for critical applications. **Fig. 2** shows the azimuth patterns in free space of 2 3-element Yagis at the same frequency. The difference between the two is the boom length (and its consequences for element placement and length). The result is a full dB difference in forward gain.

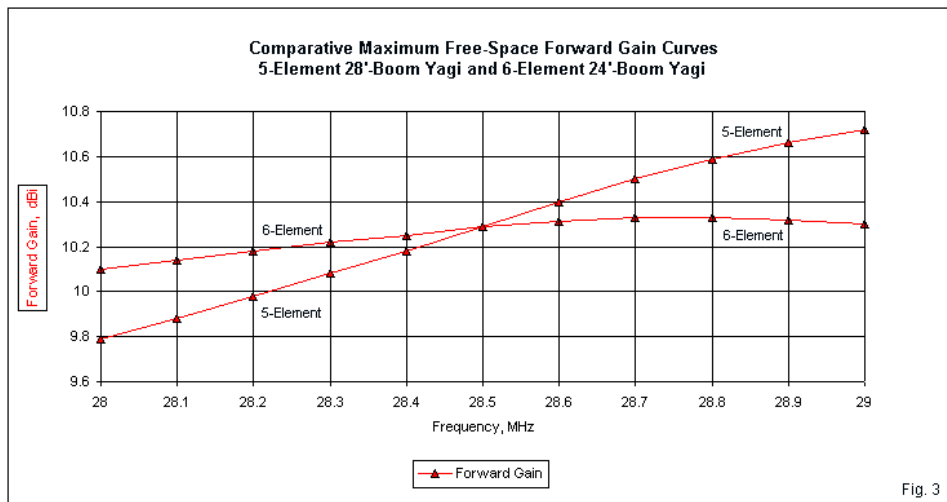
Comparative Patterns of  
Two 3-Element Yagis  
under Identical  
Conditions

Fig. 2



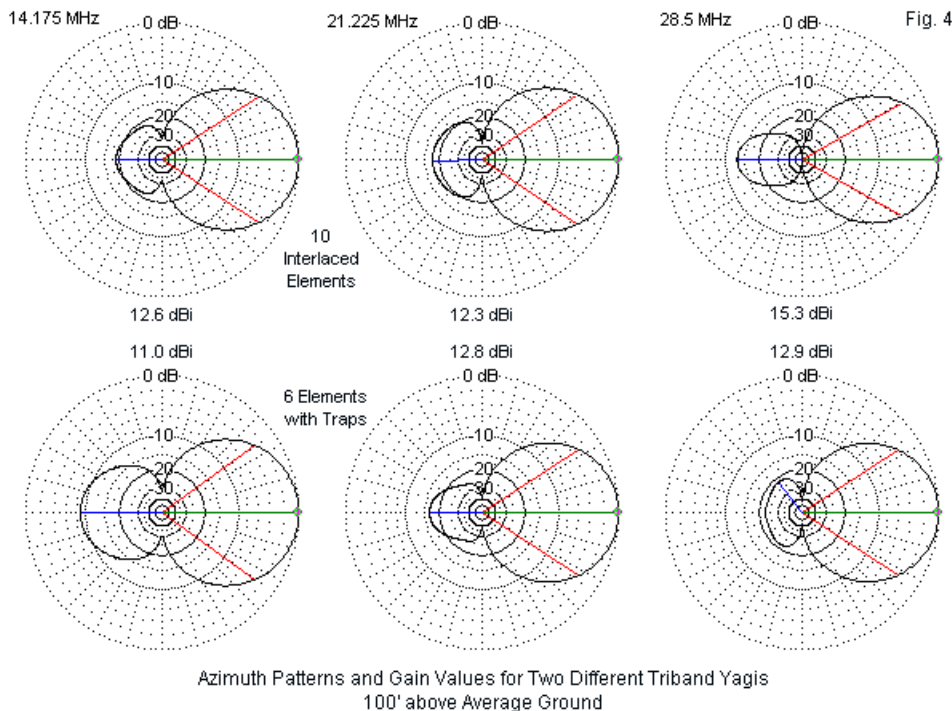
Under some conditions, the use of a single frequency within an amateur band may not suffice. Some antennas show relatively equal gain across an amateur band, while others may show considerable differences between the low end (CW and digital) and the high end (SSB). Compare the gain curves for the two Yagis of similar boom length in **Fig. 3**. The gain values are identical at mid-band. However, the 6-element version varies only slightly from one band edge to the other. In contrast, the 5-element version varies in gain by nearly a full dB from one band edge to the other. For

maximum accuracy, if needed, one might wish to create separate type-13 files for the 5-element Yagi, one for the lower end of the band and one for the upper end.



One questionable presumption used by many amateur operators is to treat tri-band Yagis of similar boom lengths as having similar characteristics. **Fig. 4** shows the azimuth patterns of two different designs at 100' above average ground. The figure lists the modeled maximum gain values for each design at the TO angle (10, 7, and 5 degrees for 20, 15, and 10 meters, respectively). Although both designs use 24' booms, the band-to-band performance is quite different. The differences include not only the maximum gain on each band, but also the rearward lobe performance.





The illustrations make a case for developing type-13 files for the specific antenna in use at an amateur station at the height and over the ground that applies to the site. The modeled performance may differ considerably from the values used in antenna specification sheets. These considerations also apply to non-amateur antenna installations. Commercial and governmental installations often assume that vendor specifications sheets are precise or that calculations by internal engineering staff are transferable without

checking to propagation programs. In most cases, a better procedure would be to model each antenna, using the actual values for height and ground conditions, with a single modeling core. For non-amateur use, NEC-4 may be the most generally usable package, since it allows the modeling of buried ground radials for any monopoles at the site. We cannot assume that propagation predictions are "accurate enough" using program samples until or unless we compare the results with those obtained from more precisely modeled versions of the site antennas. Of course, once we have more precisely modeled antenna far fields, we need not make the comparison, since the resulting type-13 files will take precedence.

### **How can we make a type-13 file within NEC that is compatible with the most common propagation programs?**

1. The first step in developing a VOACAP type-13 file is to orient the antenna properly. Using ACE-HF as an example of a VOACAP propagation forecasting and analysis program, we may heed the following guidelines.

1. The software assumes that all antenna patterns (or mathematical antenna models) have their main beam energy pointed at zero degrees azimuth (north).

2. For a rotatable beam, like a Yagi or log-periodic, the user simply sets an azimuth angle after choosing the directional antenna model. The angle is on a spinner that can be set from 1 to 360 degrees. This action points the antenna toward a distant target along a great

circle line, just as a real operator would point the antenna at his station.

3. To simplify the setting, there is a "Point At" control, which when checked, automatically points the antenna toward the distant station along a predetermined path. There are independent controls to do this with antennas at both ends of a circuit.

4. For the case where a station uses a directional antenna but leaves it at a fixed setting, then the user sets the azimuth to his preferred direction and does not use the "Point At" control. This means that stations not on his predetermined great circle path will receive radiation off the side of the antenna's main beam, and will be so simulated.

5. For fixed directional antennas, like a horizontal rhombic or a sloping V, the user must know the physical direction in which his antenna's main beam is facing. He then merely sets the azimuth control to that fixed angle and avoids the "Point At" control.

6. For fixed high-gain directional antennas like the curtain dipole arrays used in International Broadcasting, the azimuth-angle control may be used to simulate the use of phased feeds to create slew angles. In that case, the slew angles are usually expressed with respect to the main beam's nominal angle, so they must be added (or subtracted) from that nominal angle. (It is, of course, an approximation to "slew" such models by varying the azimuth setting in this manner. For more accuracy, use separate models for each

slew angle, since patterns for each slew angle may vary slightly from the broadside pattern.)

The obvious consequence of these guidelines is that initial type-13 files should point North to 0-degrees azimuth if the antenna is directional. For bi-directional arrays, such as a lazy-H or a W8JK flattop, one of the two main lobes, which are symmetrical on each side of the antenna-wire plane, should point North. There are a number of nearly symmetrical arrays, such as unterminated long wires, Veess, or rhombics having several wavelengths of wire per side. In these cases, the end with the higher gain, normally away from the feedpoint, should face north. Vertical arrays with more than one (omni-directional) element should also be set into type-13 files with the main-beam lobe facing north, with one possible exception. A number of broadcast arrays undergo development using compass-rose azimuth bearings and directions--often figured from one of the elements. Hence, they already have fixed geometric characteristics that correspond to world map standard. One might create a type-13 model directly from the developmental (and licensing) model, with the understanding that the subject antenna should make use of no azimuth-changing controls available within the VOACAP program. There are a number of vertical arrays with switchable main lobes, such as the 4-square and similar phased arrays. The modeler faces some alternatives in this type of case. One is to create a single model with the main lobe pointed North and then to use program controls to point the lobe in one of the four main directions corresponding to the switching arrangement. A second alternative is to create 4 separate

immovable models, one for each of the main lobe directions referenced to a compass rose.

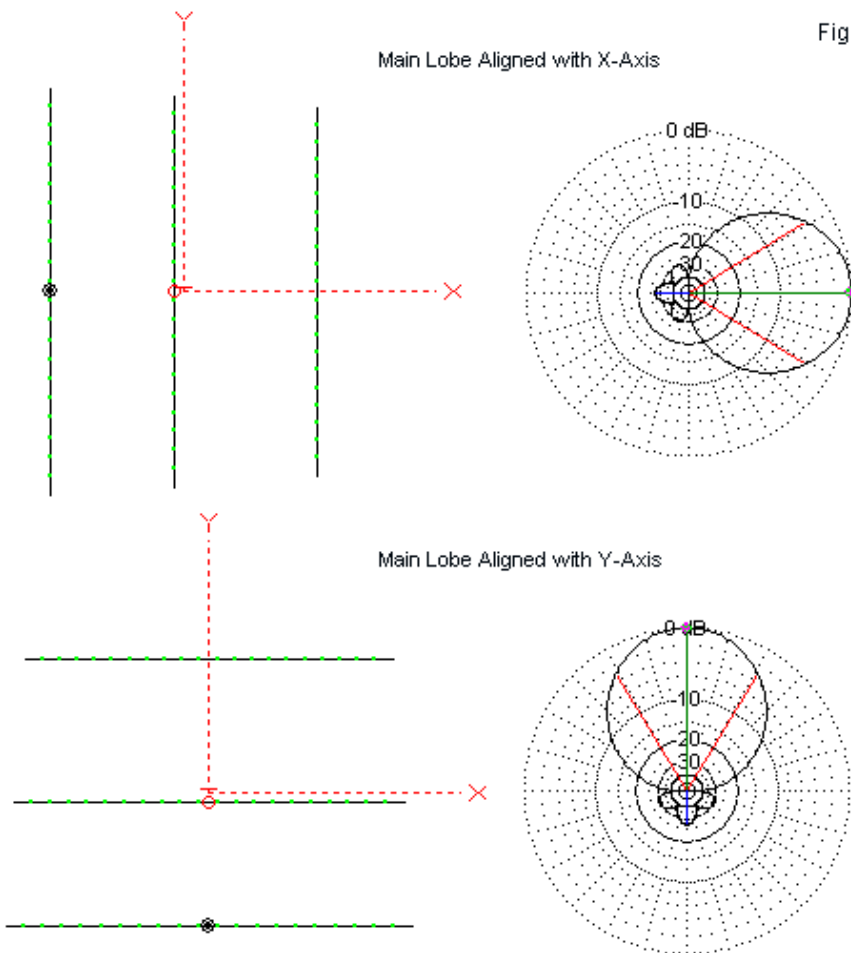
The final class of cases does not readily admit to any primary direction. A center-fed doublet and a terminated folded dipole represent one subclass of this group. In this kind of case, one may create a single model and set the antenna wire lengthwise along one of the compass axes. Then, one would use the azimuth-changing control to orient the wire to reflect its position on the actual site. This procedure would be necessary if one uses a pre-set collection of files, such as the set of terminated folded dipoles included with the ACE-HF package. Alternatively, one may create a fixed antenna model with the wire length having the actual compass directions used at the site. This model would require that the propagation software user make no changes to the azimuth. A second subclass emerges when we use off-center feeding. When such a wire antenna is  $1/2$ -wavelength long, its pattern is virtually identical to the pattern of a center-fed antenna of the same length. However, as the operating frequency increases, the patterns of an off-center-fed antenna depart from the center-fed pattern, but are not identical to the patterns of an end-fed unterminated wire (the so-called end-fed Zepp). Since the patterns at many operating frequencies will be asymmetrical, the modeler and the propagation software user must be very careful that the final orientation of the antenna corresponds to the physical layout. Otherwise, the stronger lobes of the model may not reflect the stronger lobes of the real antenna.

If an antenna site has multiple antennas of different types, such as some that are rotatable, some that are fixed, and some that are switched, all propagation software users should be alerted to the rules that apply to each antenna at each frequency within the collection of type-13 files for which propagation analysis may be relevant.

2. The second step is to coordinate the compass-rose bearing for the antenna, even if simply pointed North to 0-degrees compass azimuth, to the modeling software to be used. NEC operates by using phi angles that count counterclockwise from a 0-degree point that corresponds to the X-axis of the wire layout in the model. (NEC also uses the theta convention, but the simple conversion to elevation angles is normally an automated feature in NEC implementations.) To create a type-13 file correctly--taking into account any asymmetries in the pattern--the software must be able to convert to a compass-rose or clockwise azimuth pattern.

The required conversion may occur in one of two general ways. Programs like NEC-Win Plus employ a polar plot graphic that places the X-axis in a vertical position and labels the top point as zero degrees. Hence, for a directional antenna such as a Yagi, the modeler simply lays out the elements that are broadside to the main directional lobe along the +/-Y-axis. When creating a type-13 file, the program "merely" interrogates the NEC output data for the radiation pattern in reverse order.

Fig. 5

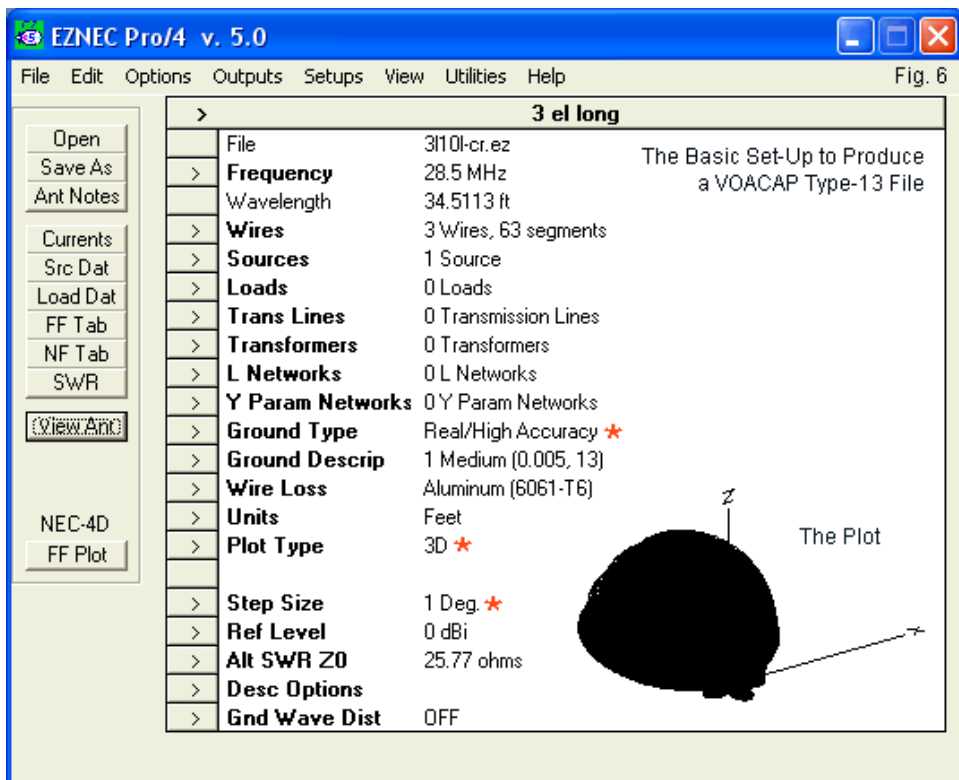


Model and Plot Correlations within EZNEC

EZNEC allows the creation of type-13 files at its Plus and Pro levels (beginning with Version 5.0 of the program). However, EZNEC creates polar plots using a different convention, with the X-axis aligned horizontally in the plot, so 0-degrees is to the right. This convention places 90 degrees, which corresponds to the +Y-axis, at the top. The program offers within the polar plot function a compass-rose alternative with 0-degrees at the top, but the direction still corresponds to the +Y-axis. Therefore, to use this option and to create a pattern with the main lobe pointing North, the modeler must set the Yagi elements along the +/-X-axis. **Fig. 5** contrasts the two conventions by showing the same antenna oriented each way and the resulting polar plot using the compass-rose pattern option. There is a shortcut relative to type-13 files and we shall discuss this mode of model creation as we proceed in step 3.

3. Creating an EZNEC VOACAP type 13 file is the final step in the process. EZNEC's latest version provides perhaps the easiest means of creating type-13 files that are compatible with virtually all versions of IONCAP and VOACAP. The process begins by setting the antenna at the desired height above a real ground that best approximates conditions at the antenna site. The sample antenna will be a 3-element Yagi at 100' above average ground.





As indicated by the starred items in **Fig. 6**, the next requirement is to select a 3-D pattern and to set the increment to 1-degree, as required by the VOACAP file. The resulting plot, shown as an inset on the EZNEC main screen, is not usable in determining lobe structures. A more normal step for that work would be a 5-degree increment. However, our goal is not to analyze the lobe structure, but instead to produce the type-13 file. The plot is clear enough to

reveal that the model has its main lobe directed along the Y-axis for direct use with the compass-rose set-up.

After the calculation is finished, there are three places where you can initiate the file writing action. If you chose the 3-D plot option, open the File menu in the 3D Plot Window, and select Write IONCAP/VOACAP File. If you chose the far-field table option, you can click the Write IONCAP/VOACAP File button at the lower left of the formatting dialog box which opens when the calculation is complete, or you can choose a format and use the option to write the IONCAP/VOACAP file in the File menu of the tabular data display. We have chosen the Plot rather than the Table option to verify that we have everything in the model correctly oriented. Therefore, we shall open the File option within the 3-D Plot window.

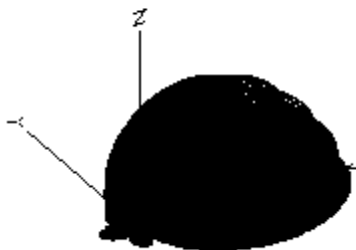
The program will offer an option to "Write IONCAP/VOACAP File." Had we chosen to create a table rather than a plot, we would have received the same option. When we select this option, the program offers a default directory for storing such files, although the user may select a different directory. Use the earlier notes to give the file a distinctive name, perhaps identifying the operating frequency and the antenna type, with possibly a ground code, if relevant. EZNEC will add the extension .13. The program will write the file, virtually instantly on most modern computers. **Fig. 7** shows the first 3 degrees of azimuth for our sample model with the main lobe oriented toward North as defined by the +Y-axis, corresponding to the EZNEC convention for compass-rose patterns. The antenna description line is seriously deficient for use in any serious context.

3 el long		Standard Option with Main Bearing North										Fig. 7	
4		4 parameters											
0.00	[ 1]	Max Gain dBi...											
13	[ 2]	Antenna Type... 360 x 91 gain values follow											
0.0	[ 3]	Efficiency (for IONCAP)											
28.5	[ 4]	Frequency											
0		-99.99	4.	9.52	12.23	13.55	13.89	13.34	11.79	8.81	2.83		
		-11.52	4.09	9.16	11.7	12.95	13.28	12.77	11.35	8.7	3.81		
		-6.65	1.43	7.23	10.16	11.73	12.38	12.29	11.48	9.84	7.06		
		2.29	-4.8	0.7	5.76	8.58	10.2	11.02	11.22	10.87	9.96		
		8.41	6.05	2.48	-2.48	-2.89	1.68	4.93	6.99	8.29	9.04		
		9.36	9.31	8.92	8.2	7.14	5.7	3.82	1.39	-1.58	-4.27		
		-4.19	-1.87	0.4	2.14	3.41	4.33	4.96	5.37	5.6	5.68		
		5.64	5.48	5.23	4.91	4.51	4.06	3.55	3.01	2.43	1.84		
		1.23	0.61	0.	-0.61	-1.19	-1.74	-2.26	-2.75	-3.18	-3.57		
		-3.91											
1		-99.99	4.	9.52	12.23	13.55	13.89	13.34	11.79	8.81	2.82		
		-11.52	4.08	9.16	11.7	12.95	13.27	12.76	11.35	8.7	3.81		
		-6.65	1.43	7.23	10.16	11.72	12.38	12.29	11.48	9.84	7.05		
		2.29	-4.8	0.7	5.76	8.58	10.2	11.02	11.22	10.87	9.95		
		8.41	6.04	2.48	-2.48	-2.89	1.68	4.92	6.99	8.29	9.04		
		9.36	9.3	8.92	8.2	7.14	5.7	3.81	1.39	-1.58	-4.27		
		-4.19	-1.88	0.4	2.14	3.41	4.33	4.96	5.37	5.6	5.68		
		5.64	5.48	5.23	4.91	4.51	4.06	3.55	3.01	2.43	1.84		
		1.22	0.61	0.	-0.61	-1.19	-1.74	-2.26	-2.75	-3.18	-3.57		
		-3.91											
2		-99.99	3.99	9.51	12.22	13.54	13.88	13.33	11.78	8.8	2.81		
		-11.51	4.08	9.15	11.69	12.94	13.26	12.76	11.34	8.69	3.8		
		-6.65	1.42	7.22	10.15	11.71	12.37	12.28	11.47	9.83	7.05		
		2.28	-4.8	0.7	5.75	8.57	10.19	11.01	11.21	10.86	9.95		
		8.4	6.04	2.48	-2.49	-2.9	1.67	4.92	6.98	8.28	9.03		
		9.35	9.3	8.91	8.2	7.14	5.7	3.81	1.38	-1.59	-4.27		
		-4.19	-1.88	0.39	2.14	3.41	4.32	4.96	5.37	5.6	5.68		
		5.63	5.48	5.23	4.9	4.51	4.05	3.55	3.01	2.43	1.83		
		1.22	0.61	-0.01	-0.61	-1.19	-1.74	-2.27	-2.75	-3.18	-3.57		
		-3.91											
3		-99.99	3.97	9.5	12.2	13.52	13.86	13.31	11.76	8.79	2.8		
		-11.5	4.06	9.13	11.68	12.93	13.25	12.74	11.32	8.68	3.79		
		-6.65	1.41	7.21	10.14	11.7	12.36	12.27	11.45	9.81	7.03		
		2.27	-4.8	0.69	5.74	8.56	10.18	11.	11.2	10.85	9.94		
		8.39	6.03	2.47	-2.49	-2.9	1.66	4.91	6.98	8.27	9.02		
		9.34	9.29	8.9	8.19	7.13	5.69	3.8	1.37	-1.59	-4.27		
		-4.19	-1.88	0.39	2.13	3.4	4.32	4.95	5.36	5.59	5.67		
		5.63	5.47	5.23	4.9	4.5	4.05	3.55	3.	2.43	1.83		
		1.22	0.61	-0.01	-0.61	-1.19	-1.75	-2.27	-2.75	-3.18	-3.57		
		-3.91											

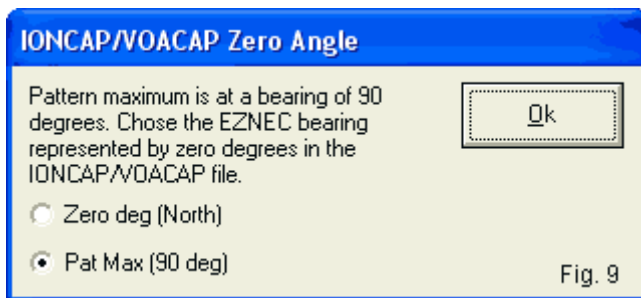
The same process can be used with the pattern that we obtained when we oriented the main lobe along the X-axis. We assign a ground, select a 3-D pattern with an increment of 1-degree and obtain the 3-D pattern shown in **Fig. 8**. Again, the pattern itself has only one main use: to keep us informed about where the main lobe lies.

3-D Plot along X-Axis

Fig. 8



When we select the option to write the type-13 file and choose a directory and filename, EZNEC will flash a new screen that only appears when the main lobe bearing does not coincide with the compass-rose North bearing. **Fig. 9** shows this screen, which gives us the option of letting the plot value of 0-degrees be North or of setting the main lobe's maximum gain bearing to be North. Since we are dealing with a rotatable beam, we select the pattern maximum as the file's 0-degree bearing.



If we had set in place an antenna having a fixed position and had already used coordinates that correspond with the real antenna, we likely would have received the same set of options. However, we would have chosen to let the plot North be the file's 0-degree bearing. Likewise, we might have set up a fixed antenna for multi-band use with the prospect of rotating it to its fixed position within the propagation program. For such an antenna, we might have files at many frequencies, reflecting a wide range of use. The patterns for each frequency would differ. In such a case, each frequency's type-13 file would again opt to let North = 0-degrees. Using the option of allowing the pattern maximum to be north applies only to rotatable and other directional antennas whose azimuth we may set within the propagation program.

3 el long		Option with Main Bearing Set to Maximum Gain										Fig. 10
4	4 parameters											
0.00	[ 1] Max Gain dBi...											
13	[ 2] Antenna Type...: 360 x 91	gain values follow										
0.0	[ 3] Efficiency (for IONCAP)											
28.5	[ 4] Frequency											
0	-99.99	4.	9.52	12.23	13.55	13.89	13.34	11.79	8.81	2.83		
	-11.52	4.09	9.16	11.7	12.95	13.28	12.77	11.35	8.7	3.81		
	-6.65	1.43	7.23	10.16	11.73	12.38	12.29	11.48	9.84	7.06		
	2.29	-4.8	0.7	5.76	8.58	10.2	11.02	11.22	10.87	9.96		
	8.41	6.05	2.48	-2.48	-2.89	1.68	4.93	6.99	8.29	9.04		
	9.36	9.31	8.92	8.2	7.14	5.7	3.82	1.39	-1.58	-4.27		
	-4.19	-1.87	0.4	2.14	3.41	4.33	4.96	5.37	5.6	5.68		
	5.64	5.48	5.23	4.91	4.51	4.06	3.55	3.01	2.43	1.84		
	1.23	0.61	0.	-0.61	-1.19	-1.74	-2.26	-2.75	-3.18	-3.57		
	-3.91											
1	-99.99	4.	9.52	12.23	13.55	13.89	13.34	11.79	8.81	2.82		
	-11.52	4.08	9.16	11.7	12.95	13.27	12.76	11.35	8.7	3.81		
	-6.65	1.43	7.23	10.16	11.72	12.38	12.29	11.48	9.84	7.05		
	2.29	-4.8	0.7	5.76	8.58	10.2	11.02	11.22	10.87	9.95		
	8.41	6.04	2.48	-2.48	-2.89	1.68	4.92	6.99	8.29	9.04		
	9.36	9.3	8.92	8.2	7.14	5.7	3.81	1.39	-1.58	-4.27		
	-4.19	-1.88	0.4	2.14	3.41	4.33	4.96	5.37	5.6	5.68		
	5.64	5.48	5.23	4.91	4.51	4.06	3.55	3.01	2.43	1.84		
	1.22	0.61	0.	-0.61	-1.19	-1.74	-2.26	-2.75	-3.18	-3.57		
	-3.91											
2	-99.99	3.99	9.51	12.22	13.54	13.88	13.33	11.78	8.8	2.81		
	-11.51	4.08	9.15	11.69	12.94	13.26	12.76	11.34	8.69	3.8		
	-6.65	1.42	7.22	10.15	11.71	12.37	12.28	11.47	9.83	7.05		
	2.28	-4.8	0.7	5.75	8.57	10.19	11.01	11.21	10.86	9.95		
	8.4	6.04	2.48	-2.49	-2.9	1.67	4.92	6.98	8.28	9.03		
	9.35	9.3	8.91	8.2	7.14	5.7	3.81	1.38	-1.59	-4.27		
	-4.19	-1.88	0.39	2.14	3.41	4.32	4.96	5.37	5.6	5.68		
	5.63	5.48	5.23	4.9	4.51	4.05	3.55	3.01	2.43	1.83		
	1.22	0.61	-0.01	-0.61	-1.19	-1.74	-2.27	-2.75	-3.18	-3.57		
	-3.91											
3	-99.99	3.97	9.5	12.2	13.52	13.86	13.31	11.76	8.79	2.8		
	-11.5	4.06	9.13	11.68	12.93	13.25	12.74	11.32	8.68	3.79		
	-6.65	1.41	7.21	10.14	11.7	12.36	12.27	11.45	9.81	7.03		
	2.27	-4.8	0.69	5.74	8.56	10.18	11.	11.2	10.85	9.94		
	8.39	6.03	2.47	-2.49	-2.9	1.66	4.91	6.98	8.27	9.02		
	9.34	9.29	8.9	8.19	7.13	5.69	3.8	1.37	-1.59	-4.27		
	-4.19	-1.88	0.39	2.13	3.4	4.32	4.95	5.36	5.59	5.67		
	5.63	5.47	5.23	4.9	4.5	4.05	3.55	3.	2.43	1.83		
	1.22	0.61	-0.01	-0.61	-1.19	-1.75	-2.27	-2.75	-3.18	-3.57		
	-3.91											

**Fig. 10** shows the first three azimuth entries for the Yagi's pattern maximum = 0-degrees selection. Compare this partial file to the corresponding entries in **Fig. 7**. The values are identical, since the antenna has not changed other than turning 90 degrees. (In fact, I created the earlier compass rose version of the Yagi by rotating the present version by 90 degrees. The type-13 file creation function performed the same action, but at a different stage, namely, by operating on the NEC output radiation pattern data.)

## Conclusion

The Yagi samples with which we have experimented are, of course, simplistic, since their main function was to show a procedure and process, not to produce a type-13 file for an actual antenna. That fact is clear from the incomplete file descriptions in the first line of each type-13 file. A more complete model would have used the stepped diameter structure for the actual antenna structure. As well, it might have included relevant surrounding objects, including inert antennas for other frequencies that we might have stacked above or below the subject antenna. In all cases, a serious type-13 file would have used the antenna's actual height above ground and would have included the most accurate ground specification one might be able to derive from local sources or measurements. (Ground quality precision is less important for horizontal antennas than for vertical antennas.) The degree of model complexity will always be a user judgment.

Nevertheless, the addition of VOACAP type-13 file capabilities to NEC software provides a means for both amateurs and

professionals to make better use of propagation software, such as ACE-HF, in the pursuit of more reliable communications.



## Chapter 143: Modeling Radiating Surfaces

The notes in this exercise derive from my attempts to determine if it is possible to model with reasonable accuracy the results obtain by an experimental exercise conducted in 1952 by two RCA researchers, George H. Brown and O. M. Woodward, Jr. Among their numerous contributions to the development of VHF and UHF antennas, including the emergent television antenna industry, was an experimental characterization of conical and triangular antennas. (See "Experimentally Determined Radiation Characteristics of Conical and Triangular Antennas," *RCA Review*, Dec., 1952, pp, 425-452.) The work eventuated in the widespread use of solid-surface fan dipoles in TV antennas, especially for the new UHF channels from about 480 to 920 MHz. It even resulted in the bent bow-tie dipole used in corner-reflector TV antennas. I had some limited success in capturing in NEC models some, but by no means all, of the capabilities of the corner reflector with a bent bow-tie in *Planar and Corner Reflectors*.

Brown and Woodward wanted to experimentally characterize the properties of bi-conical dipoles and fan dipoles, antennas that had undergone extensive theoretic analysis, but with what Brown and Woodward saw as "simplifying assumptions and approximations in order to satisfy the required boundary conditions and to reduce the mathematical difficulties." (p.425) As shown in simplified form in **Fig. 1**, they reduced the dipoles to UHF solid-surface monopoles with a very large highly conductive ground-plane surface to simulate a perfect ground (PEC).

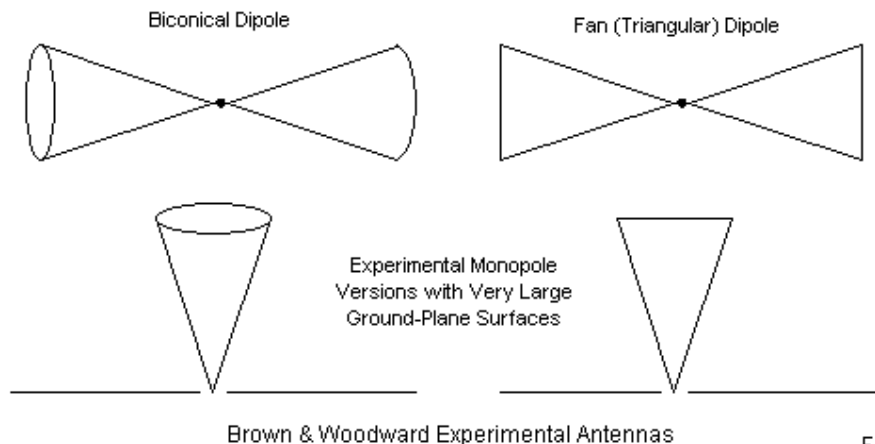


Fig. 1

The practical interest in these antenna types does not involve their  $1/2$ -wavelength impedance. Instead, it involves the impedance and radiation properties of these antenna shapes as they approach and surpass a 1-wavelength electrical length at a given operating frequency. A linear dipole shows a very high impedance at 1-wavelength, with regular repetitions of the impedance peak at integral multiples of that length. However, the biconical shape shows a regular decrease in the peak impedance as the angle formed by opposite sides of the cone gradually increases. At very large angles--about 60 degrees apex angle--the reactance swing associated with a linear dipole decreases to a level that is manageable for wide-band antenna service. In addition, the difference between the impedance at odd multiples of  $1/2$ -wavelength and integral multiples of 1 wavelength also decreases. As a result, the biconical shape--with a sufficiently large apex

angle--results in the potential for an antenna with a 300-Ohm SWR of less than 2:1 over a very broad frequency range. For reasons of pattern shape that we shall see along the way, VHF and UHF use of the phenomenon is limited to about a 2:1 frequency range. This characteristic is eminently convenient for TV antennas that typically use a 300-Ohm feedpoint impedance.

Since the biconical dipole is somewhat complex as a manufactured item, Brown and Woodward also explored the easier-to-make flat triangular dipole, again with a solid surface. For equivalent apex angles, it showed similar characteristics, but not quite as flat a bandwidth impedance as the biconical antenna. However, the result was good enough to allow Brown and Woodward to report on a successful flat, solid, fan dipole using a 60-degree apex angle to cover 480 to 920 MHz with a 300-Ohm SWR level of less than 2:1.

## **The Modeling Interest**

A number of questions arise from the Brown and Woodward work for the antenna modeler. First, one may ask whether it is possible to replicate in models the core of the Brown and Woodward experimental effort. Given the use of solid surface cones and triangles in the original experiments, this question does not have as easy an answer as we might like to give. NEC employs round wires to model the geometry of radiating elements. Its surface-patch facilities were intended to simplify the construction of surround bodies and objects--such as the hulls of ships--that might affect the antenna's radiation characteristics. Their function was not intended to serve as radiating elements with direct voltage sources. Hence,

the NEC surface patches use considerably simplified equations to speed core runs. If we are to simulate the Brown and Woodward antennas, we must use round wires to form the surfaces.

The second question that we shall explore is whether we may extrapolate the VHF/UHF results using solid-surface antenna elements down to the HF range. Wide-band center-fed elements have proven to be highly desirable over the decades since the Brown and Woodward paper, for example in curtain arrays for both SW broadcasting and over-the-horizon HF radar systems. However, the ability to extrapolate the experimental results will depend upon our ability to translate solid surface structures into structures using individual wire elements components. Hence, from the perspective of modeling, the first question is the key to the second. Although we may easily model wire-based extended-range elements at HF, relating their properties via models to the Brown and Woodward experiments requires that we be able to successfully (within reasonable limits) model the solid surfaces with round wires.

## The Biconical Dipole

One advantage of modeling in NEC is that we may proceed directly to the biconical dipole and not pass through the monopole stage. Modelers have long known that we may model a solid-surface biconical dipole with reasonable success by using a collection of longitudinal wires, so long as we use enough of them. **Fig. 2** shows the outline of a bi-conical dipole with a 40-degree apex angle. Each cone uses 12 wires. Experience has shown that there is very little

difference in the output of models using 12, 25, and 45 wires per cone. To achieve a usable average gain test score (AGT), the more wires that we use, the thinner must be each wire, since all cone wires meet at a junction. As we increase the number of wires, the angle between wires at the junction becomes narrower, increasing the length along the first segment of each wire in which we have surface interpenetration for a given wire size. As we add more wires, the interpenetration increases unless we use thinner wires. In addition, the length and segmentation of the center or source wire connecting the two cones may require custom treatment to achieve the AGT score nearest to the ideal.

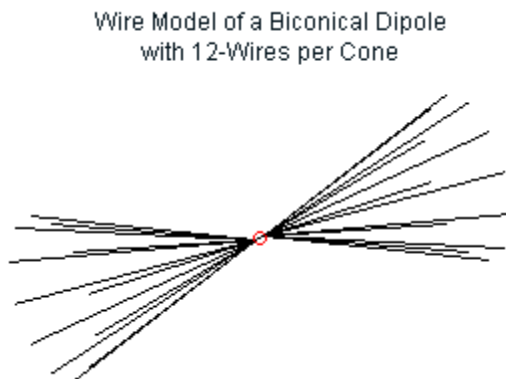


Fig. 2

The simulated biconical dipole in the figure is 16.8" long, with an end diameter of 5.2". The wire diameter is 0.002". The intended useful frequency range for the antenna is from 480 MHz to at least 920 MHz, to coincide with the Brown and Woodward TV fan dipole.

To achieve this range, the 1/2-wavelength self-resonant frequency of the antenna is about 231 MHz in this free-space model. However, we are not interested in the first self-resonant point. Rather, we are interested in the antenna's behavior as it approaches and passes 1 wavelength.

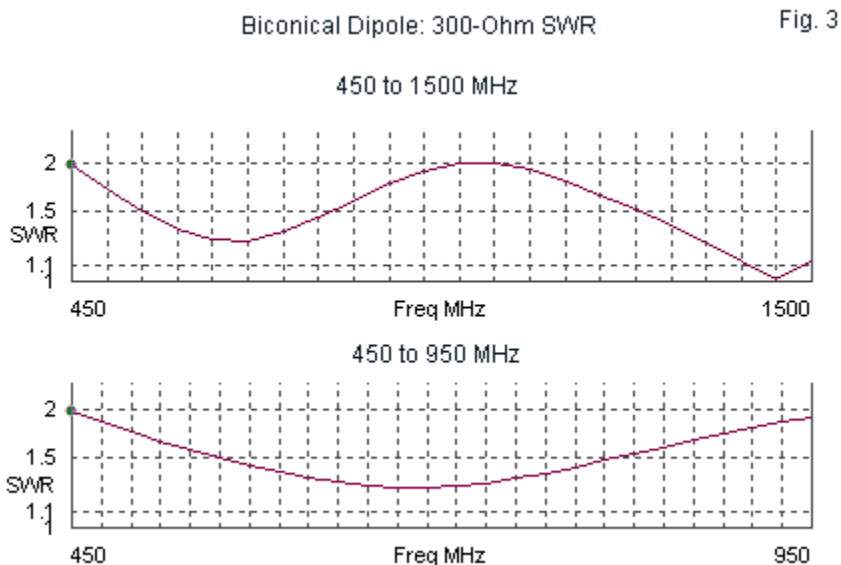
The biconical dipole meets the Brown and Woodward requirements for a UHF TV dipole. Those requirements include having a bi-directional pattern and a 300-Ohm SWR that is less than 2:1 across the passband. **Table 1** shows the key antenna characteristics and the AGT value (with adjusted gain values) at the passband ends and at the approximate geometric mean frequency.

Table 1. Biconical dipole performance

Frequency Gain MHz	Source Impedance R +/- jX Ohms	300-Ohm SWR	Raw Gain dBi	AGT	AGT-dB	Adj. dBi
480	346 + j187	1.80	2.59	1.012	0.05	2.54
665	345 - j 58	1.26	3.32	1.012	0.05	3.27
920	167 + j 33	1.83	3.30	1.012	0.05	3.25

With respect to the desired SWR values, the tabular entries seem to describe a curve. The bottom half of **Fig. 3** confirms the impression. The top half of the figure extends the SWR curve to 1500 MHz to establish the general pattern of biconical behavior. As we increase the electrical length of the antenna by increasing the operating frequency, the resistive and reactive components--as indicated indirectly by the SWR values--continue to decrease the difference between the values at odd multiples of a half-wavelength and integral multiples of a full wavelength. In short, the higher the frequency of operation or the longer the antenna length for the 40-

degree apex angle biconical antenna, the flatter the SWR curve grows.

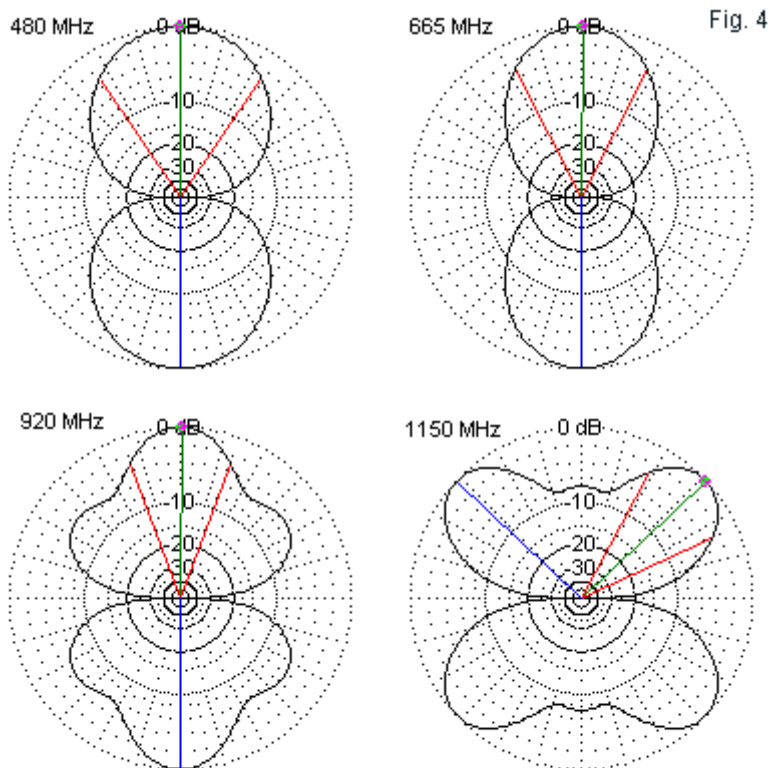


Our interest in this behavior is not to establish it. That has long been done via theoretical analysis and physical experimentation. Our interest lies in seeing whether the 12-wire biconical model can effectively and reasonably capture that behavior. The model does that job. There are variations on the model that will affect its dimensions, but with no great change in the results. For example, we may connect the outer ends of the cone wires to form a circle. Essentially, the end wires add length to each individual wire, a

length that is roughly but not exactly half the distance between the wire tips. Hence, for the same performance curve, we would have to reduce the physical length of the cone. As well, adding or subtracting wires from the assembly will slightly change the required length for the same performance curve, although each such change should be accompanied by a change in the wire diameter within the limits of NEC's ability to handle angled junctions of wires at the center.

Applications for the biconical antenna in TV antennas that might make use of a planar or a corner reflector rarely make use of the extended impedance stability of the antenna shape. All such arrays depend upon using a fed element with a bi-directional pattern. **Fig. 4** shows sample free-space E-plane patterns for the biconical dipole within the passband of intended use with one extra pattern a bit beyond the upper limit.





Biconical Dipole: Free-Space E-Plane Patterns  
at Selected Frequencies

A linear dipole would show multiple lobes with stronger angular lobes than broadside lobes by the point at which the antenna is about 1.5 wavelengths long. The biconical dipole extends the range

of bi-directional patterns to nearly the 2-wavelength point, although the 920-MHz pattern shows significant but non-fatal sidelobe development. By 1150 MHz, the pattern has become completely useless for a directional beam with a planar or corner reflector. (We shall be interested in comparing these patterns with a corresponding set for a flat-face fan dipole.)

For some applications, the change in pattern is less important. For example, scaled by a factor of 100, the antenna would provide a very wide-band antenna for general purposes. The lowest frequency would be about 4.8 MHz, with an undetermined upper limit for a 300-Ohm feedpoint impedance that would not require a tunable matching network. A single transformation of 300 Ohms to 50 Ohms (by way of a balun) would satisfy the impedance requirements for most common transceiving equipment.

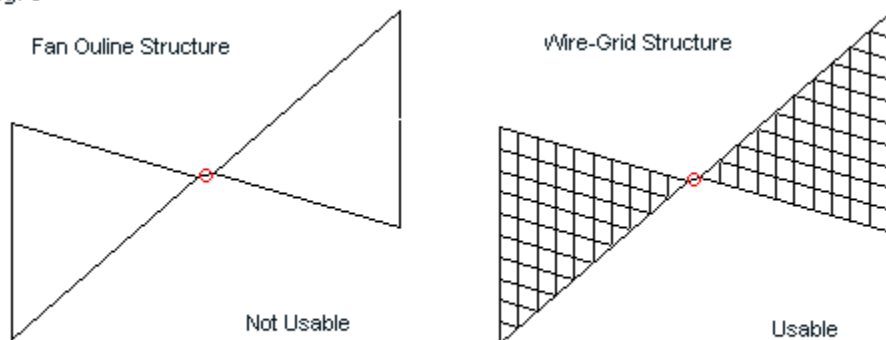
The limitation for this antenna is that it would require a length of 140' with end diameters of 43.3'. As well, it likely would require considerable mounting height to overcome the effects of ground proximity on the feedpoint impedance across the operating span. The scaled wire size would be 0.2", equivalent to AWG #4 wire. However, one might easily use thinner wire by increasing the number of wires in each cone. With an additional scaling factor of 2, the antenna would cover 80 through 10 meters. If we increase the added scaling factor to 2.7, we might add 160 meters, but the chances of having a support system that would handle 115' diameter ends at a sufficient height to avoid deleterious ground effects on the source impedance would dwindle to the day-dream level.

Our notes on modeling a biconical dipole have not sought to establish a number-by-number correlation to the Brown and Woodward experiments using a mono-conical element with a perfectly conducting ground-plane surface. Rather, our goal has been only to establish that we can simulate a biconical dipole with NEC's round wires. The successful result is not surprising, since there are many examples of physical antennas that employ the same technique. In fact, there are HF discones, a first cousin to the biconical dipole and a more immediate kin to the Brown and Woodward test antennas that employ wire structures for successful operation.

### **A Model of a Solid-Surface Fan (Triangular) Dipole**

Brown and Woodward also reported on their experiments with a triangular monopole using the same large highly conductive ground plane surface. The antenna was equivalent to one-half of a fan dipole. However, as suggested by **Fig. 5**, their element used a solid sheet rather than a simple outline of a fan. To see something of the performance difference, **Table 2** provides performance figures for an outline fan dipole that is 14" from one end to the other and 7.8" tall at the ends. The apex angle is 60 degrees so that the element half, exclusive of the short center source wire, forms an equilateral triangle. This shape is very close to the UHF fan dipole created by Brown and Woodward for use from 480 to 920 MHz.

Fig. 5



### Simulating a Solid-Surface Fan (Triangular) Dipole

Table 2. Fan outline dipole performance

Frequency	Source Impedance	300-Ohm	Raw Gain	AGT	AGT-dB	Adj.
Gain						
MHz	R +/- jX Ohms	SWR	dBi			dBi
480	718 + j190	2.59	3.32	1.010	0.04	3.28
665	93 - j276	6.13	6.42	1.018	0.08	6.34
920	337 - j212	1.95	0.37	1.012	0.05	0.32
(multiple lobes)						

In effect, the fan outline operates more like a linear dipole than a biconical dipole. With a half-wavelength resonance at 250 MHz, the 4-lobe structure at 920 MHz is an approach to an electrical 2-wavelength equivalent. To obtain performance that more closely approaches the Brown and Woodward results, we must fill the outline to simulate a solid surface. The right side of **Fig. 5** shows the pattern used in the test model. One triangle results from an exercise using NEC-Win Synth (program may not be compatible with OS newer than Win2k) and saved as a .NEC file. The 60-

degree triangle was then re-opened in EZNEC Pro/4 v.5 as an incomplete model. EZNEC prefers to create models by using a single wire between junctions, but does accept without an error report a set of wires where wire crossings occur at segment junctions. I moved the triangle to one correct position for a dipole half and then replicated the structure and rotated it by 180 degrees to form the other dipole half. A short connecting wire between triangle apex points for the source completed the model.

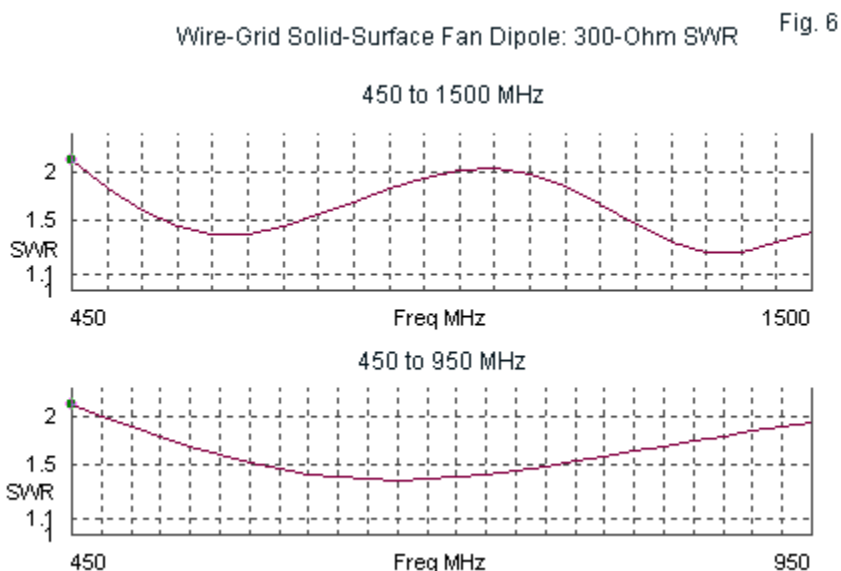
To simulate a solid surface requires that we use a sufficient wire diameter. Selecting the diameter is a compromise between true electrical solidity at all operating frequencies and an acceptable AGT score. A 0.1" diameter wire yielded AGT values that averaged about 1.06, not quite ideal but usable on the premise that we are seeking the operating trends and not construction guidance from the model. **Table 3** provides the reported data from the model at the three sample frequencies. The half-wavelength self-resonant frequency for the model is 252 MHz.

Table 3. Wire-grid fan dipole performance

Frequency Gain MHz	Source Impedance R +/- jX Ohms	300-Ohm SWR	Raw Gain dBi	AGT	AGT-dB	Adj. dBi
480	278 + j194	1.94	2.91	1.057	0.24	2.67
665	392 - j 56	1.37	3.89	1.059	0.25	3.64
920	171 - j 61	1.86	5.42	1.067	0.28	5.14

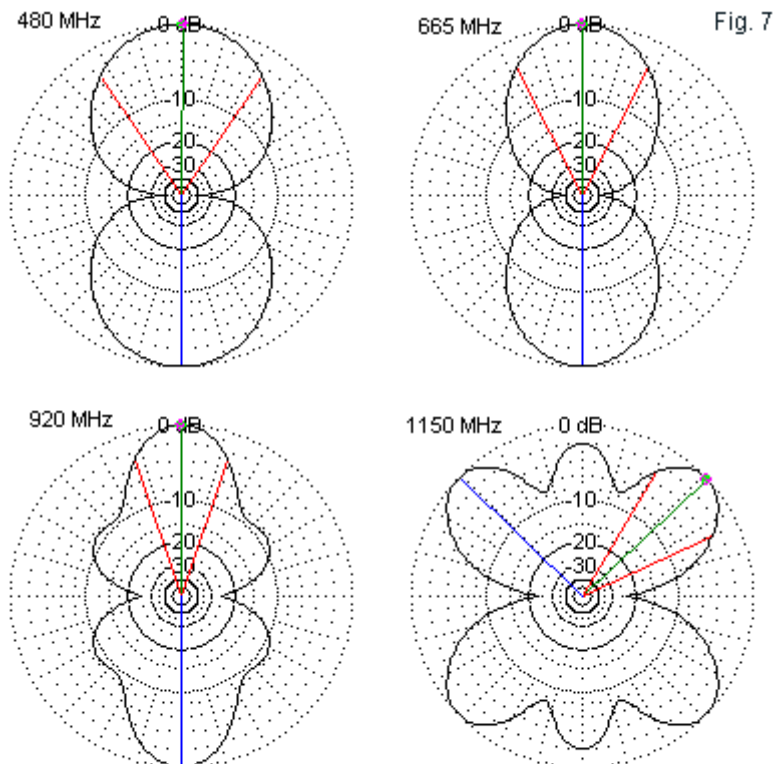
The SWR values are much closer to the biconical of **Table 1** than they are to the fan outline values of **Table 2**. In fact, the SWR curve at the bottom of **Fig. 6** is very close to the curve obtained by the Brown and Woodward fan dipole (Fig. 42 on p. 452 of the

referenced article). The upper portion of the SWR charts shows the extended SWR curve to 1500 MHz. It almost replicates the smoothness of the corresponding biconical curve but shows a slight compression of values relative to frequency, suggesting that the wire-grid simulation of the flat fan dipole does not achieve the broad-banding effect to the same degree as the biconical element.



The gain data for the wire-grid simulation of the fan does not quite match the performance reported by the Brown and Woodward experimental solid-surface fan. If we subtract the gain of a linear dipole (about 2 dB) from the values on the Brown and Woodward

curve, the gain curves correspond. However, the pattern shapes reported by Brown and Woodward do not coincide with the curves in **Fig. 7**. The Brown and Woodward pattern for 920 MHz shows no sidelobe development, although the wire-grid fan pattern for the same frequency shows moderate sidelobe strength. By increasing the wire diameter of the wire-grid simulation of the solid surface, it is possible to reduce the sidelobe development in the 920-MHz pattern, but the model becomes wholly unreliable before the sidelobes diminish completely. Hence, the model fails to capture the pattern shapes reported by Brown and Woodward for the upper end of the operating spectrum.



Wire-Grid Solid-Surface Fan Dipole: Free-Space  
E-Plane Patterns at Selected Frequencies

Although outside the operating passband of the antenna, the additional pattern for 1150 MHz allows some initial comparison with the performance of the biconical dipole at the same frequency. With



respect to gain and pattern formation, the flat 60-degree fan shows a broader bandwidth than the 40-degree biconical antenna. The 1150-MHz pattern still shows the broadside lobes that are characteristic of a linear dipole just slightly longer than 1.5-wavelengths. In contrast, the biconical pattern at the same frequency displayed a pattern closer to a 2-wavelength linear dipole. The difference is largely due to the difference in the self-resonant half-wavelength frequencies needed to obtain the desired SWR curves in the defined operating passband.

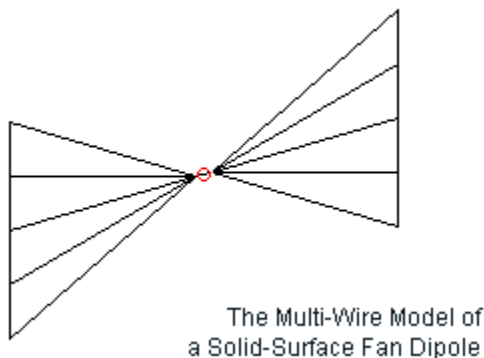
The wire-grid fan dipole does manage to capture most of the data reported by Brown and Woodward for their UHD TV dipole, even if imperfectly. It also shows its relationship to the biconical shaped element and to the fan outline element. However, there are alternative structures used historically to simulate a solid flat fan shape. We now have enough modeling data that we are positioned to evaluate them as potential methods of capturing the Brown and Woodward solid-surface fan dipole.

## The Multi-Wire Fan Dipole Model

One popular way sometimes used in the HF range to simulate a solid surface in a fan dipole is the use of a series of wires in each fan triangle, with each wire extending from the apex to the opposite side. **Fig. 8** shows such a structure using 5 wires. In all dimensions, the fan dipole is identical to the wire-grid simulation of a solid surface. It is 14" from end to end and 7.8" high at the outer ends, with a 60-degree apex angle. The wire diameter for this model is also 0.1". The question for modeling is whether this model, much

simpler to form, is an adequate simulation of the solid surface antenna upon which Brown and Woodward developed their data.

Fig. 8

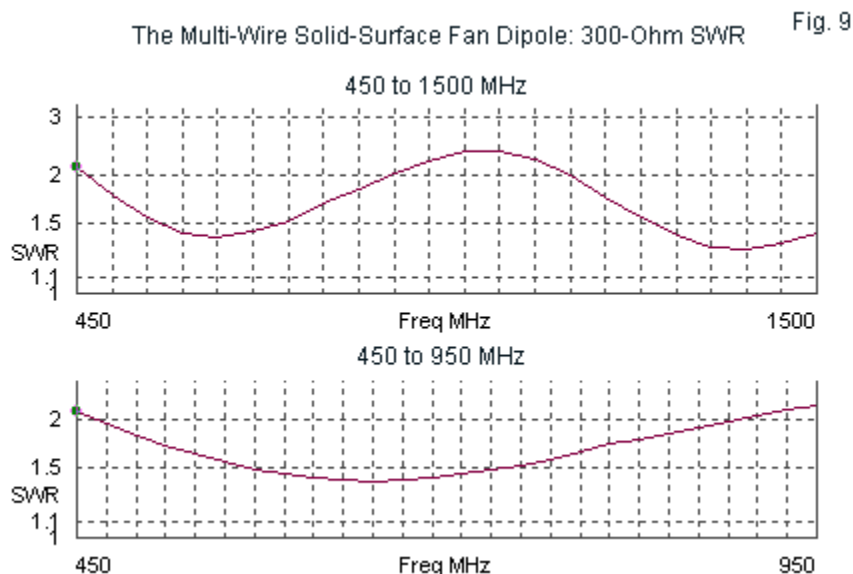


If we were concerned about the half-wavelength self-resonant performance of the antenna, the simplified model might serve. The self-resonant frequency is 260 MHz, which is not far from the 252-MHz self-resonant frequency of the wire-grid version. In both versions, the highest current occurs relatively close to the apex of each triangle, where the wire density in the multi-wire version is highest. However, the stable impedance performance of the solid-surface fan antenna depends upon using the antenna at a length that approaches and passes 1 wavelength. Current maximums occur at positions well away from the center source wire. In the multi-wire version of the fan dipole, the wire density diminishes steadily as we move away from the center source wire. **Table 4** shows some of the consequences of the decreasing wire density toward the fan ends.

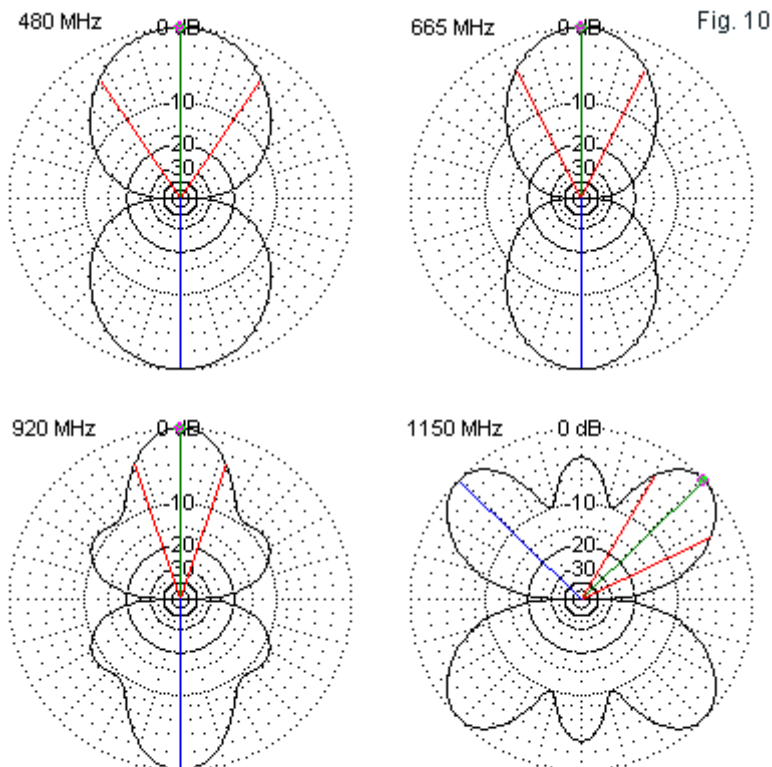
Table 4. Multi-wire fan dipole performance

Frequency Gain MHz	Source Impedance R +/- jX Ohms	300-Ohm SWR	Raw Gain dBi	AGT	AGT-dB	Adj. dBi
480	285 + j188	1.87	2.79	1.027	0.12	2.67
665	382 - j 76	1.39	3.86	1.048	0.20	3.66
920	149 - j 58	2.10	5.68	1.077	0.32	5.36

The results are both promising and disappointing. In some respects, the impedance data appears to be comparable to the data in **Table 3** for the wire-grid model. However, the resistive component of the multi-wire model's impedance has a wider range of variation across the operating passband than we find in the wire-grid model's data. The consequences for the 300-Ohm SWR curve, in the lower half of **Fig. 9**, are a reduction in the 2:1 SWR bandwidth. The extended SWR curve at the top of the same figure shows essentially the same general pattern that we found in the wire-grid curve (**Fig. 6**), but with a much wider variation in value.



With respect to gain and pattern shape, the multi-wire model using relatively fat (0.1" diameter) wires shows less variation from the wire-grid model than the SWR curves. The adjusted gain values are similar for the two models. As revealed by **Fig. 10** (when compared to **Fig. 7**), the pattern shapes are very nearly twins, even at 1150 MHz. For some purposes, the simpler multi-wire model may be a suitable substitute for the more complex wire-grid model. However, the multi-wire version alone does not disclose its shortcomings with respect to capturing the solid-surface SWR curve.



Multi-Wire Solid-Surface Fan Dipole: Free-Space  
E-Plane Patterns at Selected Frequencies

The 60-degree fan dipole might form a wide-band antenna in the HF range with suitable scaling. Roughly speaking, scaling the dimensions by a factor of 100 would yield an antenna theoretically

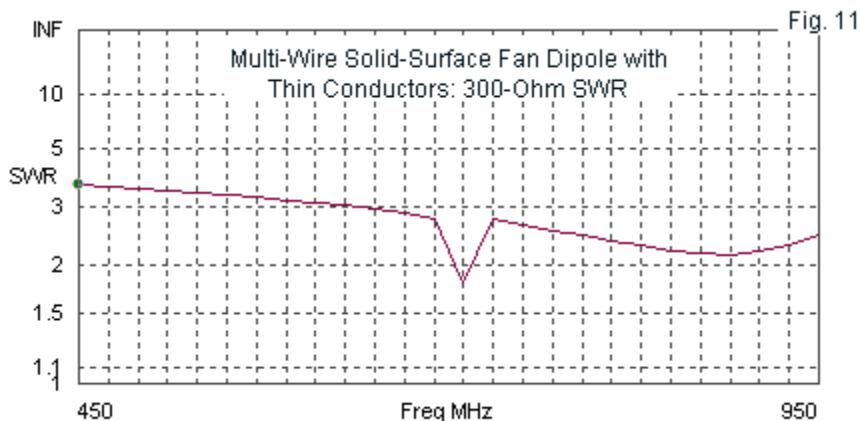
covering 4.8 through 9.2 MHz--and beyond, if the pattern shape is not a matter of concern. The resulting antenna would be a bit under 117' long with an end spread of 65'. However, the limiting factor in the scaling is the requirement to multiply the wire diameter by 100 to maintain the wire density. 10" diameter conductors generally fall outside the realm of feasibility for most (but by no means all) installations.

The temptation is to use common wire sizes. The original UHF model wire is 0.1", corresponding closely to AWG #10 wire. If we retain this practical wire size, the multi-wire model loses its ability to capture the properties of a solid surface. In the UHF model, the wire size would scale to 0.001". **Table 5** provides the kind of data that we obtain for such a model (and for an HF antenna using 0.1" wire).

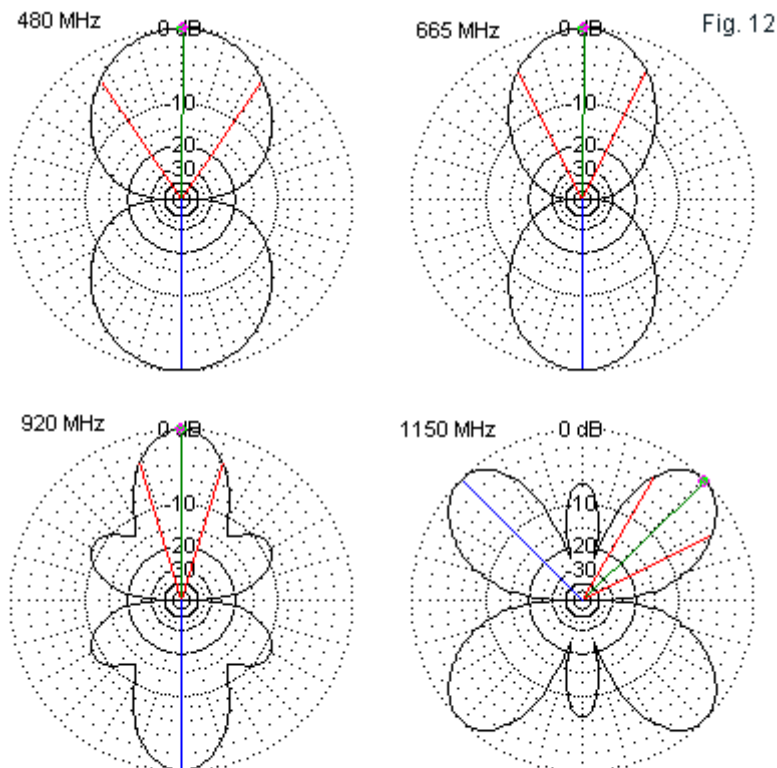
Table 5. Multi-thin-wire fan dipole performance

Frequency MHz	Source Impedance R +/- jX Ohms	300-Ohm SWR	Raw Gain dBi	AGT	AGT-dB	Adj. Gain dBi
480	289 + j391	3.48	2.50	0.965	-0.15	2.65
665	864 - j 29	2.89	3.71	0.967	-0.15	3.86
920	155 - j102	2.23	6.01	0.975	-0.11	6.12

The impedance information from the thin-wire version of the 60-degree fan dipole shows very large excursions of both resistance and reactance. The 300-Ohm SWR curve for the operating range in **Fig. 11** shows only one sudden dip below the 2:1 level, behavior that we might normally associate with a linear dipole/doublet at the self-resonant 3/2-wavelength mark. The frequency of the SWR minimum is 710 MHz in the model.



The association of the thin-wire model with the behavior of a linear doublet also shows up in the sample free-space E-plane patterns, shown in **Fig. 12**. The 920-MHz pattern is especially interesting for the crisp sidelobes, similar to those we might find in the pattern for a 1.25-wavelength center-fed wire. All of the broadband patterns for both the biconical element and the fat-wire fans show far less of a null between the sidelobes and the main bi-directional lobes. The crispness of the lobe structure in the thin-wire model carries over into the pattern for 1150 MHz. Compare the null depth values to those in **Fig. 10** for the fat-multi-wire version of the same antenna.



Multi-Thin-Wire Solid surface Fan Dipole  
Free-Space E-Plane Patterns at Selected Frequencies

In models and in physical antennas using multiple wires to simulate the performance of a solid surface, wire diameter and wire density both make a difference to the performance. As a fan element



decreases the wire diameter without increasing the number of wires, the antenna gradually creases to perform like a solid surface. It becomes a version of a linear wire antenna with a somewhat wider bandwidth at the  $1/2$ -wavelength resonant frequency region. However, using the necessary wire diameter and increasing the wire density are strategies that have undesirable consequences in physical antennas.

## **Conclusion**

This exercise has explored the modeling of solid surface antennas, so easily fabricated for UHF frequencies, through the use of various round-wire modeling techniques. The Brown and Woodward experimental data from 1952 provided a standard against which we could measure to some degree the success of the modeling techniques. Biconical properties, with a few reservations, prove amenable to using a multiple-wire simulation, a method reflected in the construction of practical biconical antennas.

The flat solid-surface fan elements explored by Brown and Woodward required that we use some form of wire-grid structure to simulate the surface adequately. Even fat-wire models composed of multiple linear elements showed some departure from the performance curves in the original experiments. As we discovered in the final exercise, the use of wires that are too thin degraded the performance from its desired levels completely with respect to broadband coverage.

Even the wire-grid model failed to capture every nuance of solid-surface performance. Nevertheless, it proved productive to capturing most of the data experimentally derived by Brown and Woodward. Within the range of what the model successfully simulated and in what ways it fell short lie some lessons for effective modeling.

## Chapter 144: Receiving Directivity

A number of years ago, a Ham suggested a somewhat different way of looking at the directivity, one especially applicable to receiving antennas, and--more specifically--receiving antennas designed for the lower HF and upper MF portions of the spectrum. In these regions, amateurs (and others) often use separate receiving antennas, many with very low gain. The goal is not forward gain, but an acceptable signal-to-noise ratio. Many receiving concepts, dating back to the original Beverage antenna, place antennas relatively low to the ground to reduce noise levels. In the process, they sacrifice one of the seemingly holy grails of antenna work, gain. However, these antennas, including the K9AY, the EWE, and others, provide very low-level signals, but even lower noise levels. Since modern receivers tend to have surplus gain, whether inherently or with pre-amplification, the resulting received signal improves its strength over the noise with resulting improvements in readability.

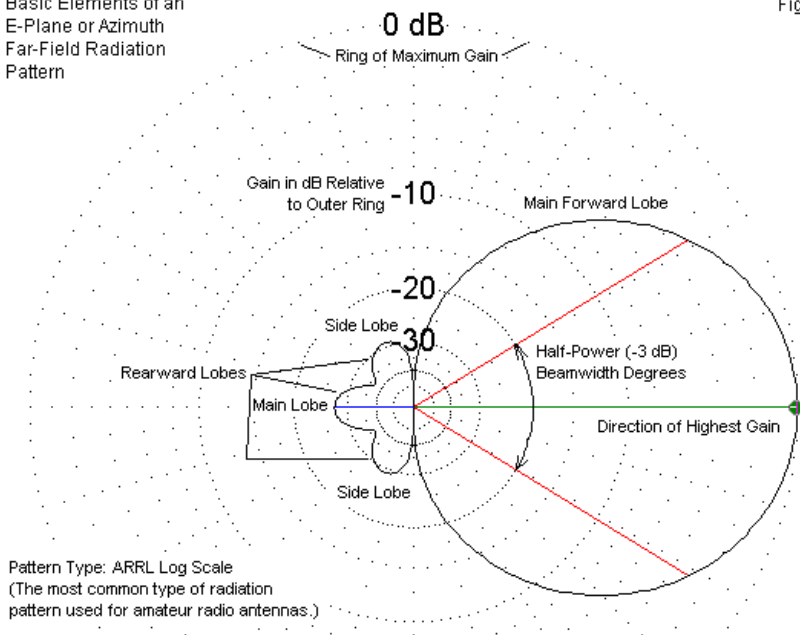
Despite their low gain, many of the low-band receiving antennas exhibit strikingly good directivity. Conventionally, we might think that one of the available versions of a front-to-back ratio might suffice to characterize the directivity adequately. However, if we review the various front-to-back ideas, we may soon learn why they may not be suitable to the special needs of low-band receiving antennas.

## Conventional Front-to-Back Ratios

The language of upper HF directional antennas has grown very conventionalized over the decades. It rests on a 2-dimensional graphic portrayal of the far-field pattern of a directional beam, such as a Yagi-Uda array. **Fig. 1** provides some of the key elements in the usual pattern description that we find in much literature. We find variations in some of the terms and in the style of the graphics used to present the pattern, but the terms shown in the sketch are very usual ones.

Basic Elements of an  
E-Plane or Azimuth  
Far-Field Radiation  
Pattern

Fig. 1

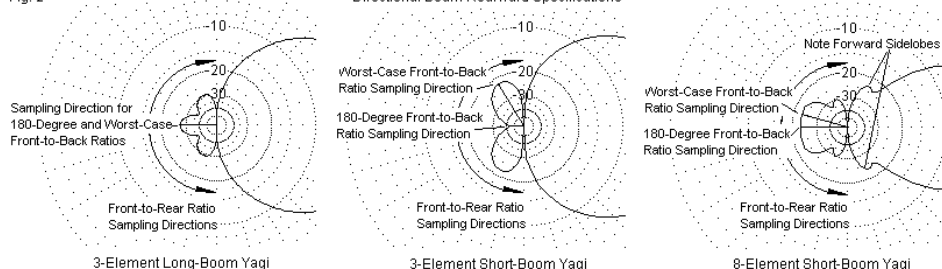


One key to our discussion is the clear directivity of the pattern that allows us to distinguish forward and rearward lobes that represent gain maximums in the various directions. The pattern appears in normalized form, that is, with the maximum antenna gain just reaching the outer ring of the background scale. Other presentations either with a different level of gain for the outer ring or with a different scale for inner rings are possible and often useful. The key property of the pattern and its parts is the fact that it is a 2-dimensional portrayal. In free-space, the pattern represents the E-plane of the antenna, in this case a 3-element Yagi array. Over ground, the pattern would use a constant elevation angle. We normally select either the take-off angle, that is, the elevation angle of maximum gain, or some other elevation angle of special interest, such as the elevation angle dictated by a propagation forecast for strongest signals into or out of a target communications area.

Sample Forward-Rearward Power Gain Ratios							Table 1	
Antenna	Max Fwd Gain dBi	180 Rear Gain dBi	180-D F-B Ratio dB	Max Rear Gain dBi	Wst-Case F-B dBi	Ave Rear Gain dBi	Front-Rear Ratio dB	
3 El Long-Bm Yagi	8.11	-19.01	<b>27.12</b>	-19.01	<b>27.12</b>	-23.20	<b>31.31</b>	
3 El Short-Bm Yagi	7.12	-34.72	<b>41.84</b>	-14.80	<b>21.92</b>	-21.39	<b>28.51</b>	
8 El Short-Bm Yagi	12.29	-10.71	<b>23.00</b>	-10.31	<b>22.60</b>	-16.12	<b>28.41</b>	
Any Front-Rear Ratio in dB = Max Fwd Gain in dBi - Rear Gain (180, Max Rear, or Ave Rear) in dBi								

Fig. 2

Directional Beam Rearward Specifications



The 2-dimensional nature of the pattern has yielded the concept of the front-to-back ratio as a measure of directivity. First, not everyone uses the basic term in the same way. So we shall find some refinements in the terminology. Second, not everyone who uses the refined terminology uses it in the same way. **Table 1** and **Fig. 2** will be our guides, but only for part of the journey. Both the table and the graphic present information on the rearward performance of 3 sample antennas. Numbers and pictures do not always determine how people use words. Our first step will be to present some initial definitions (with modifications to come). These definitions will coincide with the labels in **Table 1**. The  $180^\circ$  front-to-back ratio is the main lobe forward gain (or the maximum antenna gain) minus the gain of the lobe (however big or small) that is  $180^\circ$  away from the heading of the maximum forward gain. This value of front-to-back ratio is most commonly used in general antenna literature and is the one shown in most NEC antenna software. If the main forward lobe is split or does not align with the graph heading, the  $180^\circ$  front-to-back ratio is  $180^\circ$  away from the direction of maximum pattern strength. Hence, the value may not be for a heading directly to the rear of the antenna structure. Since a Yagi is usually symmetrical, the maximum gain will normally be directly forward, and the  $180^\circ$  front-to-back ratio will indicate the relative strength to the direct rear. Note that if we use a normalized scale, we can read the front-to-back ratio directly from the plot--between 25 and 30 dB relative to the maximum gain of the antenna in the leftmost pattern.

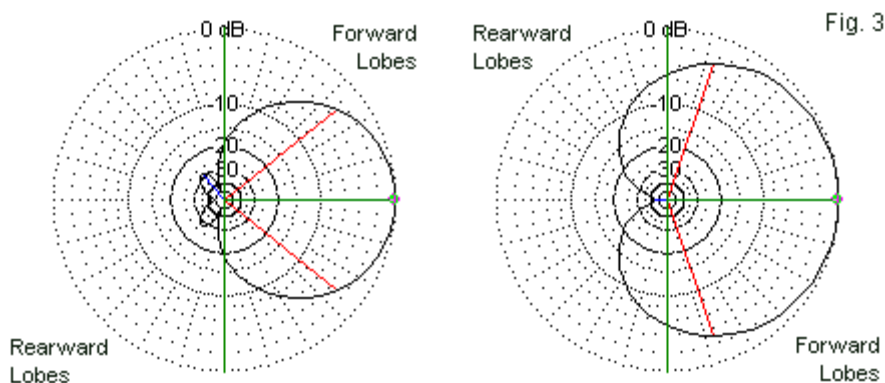
In **Fig. 2**, the leftmost pattern comes from **Fig. 1**. The strongest rearward lobe is  $180^\circ$  from the main lobe. However, the center

pattern shows a 180-degree gain of very tiny proportions. Hence, the 180° front-to-back ratio is very large (over 40 dB compared to a "mere" 27 dB for the leftmost pattern). Yet, we find rearward lobes that have considerable strength. The line through one of those lobes indicates the direction of maximum strength. It is only about 22 dB weaker than the maximum gain. Some sources call this the worst-case front-to-back ratio, and its value is the maximum forward gain minus the highest value of gain in either rearward quadrant. For this antenna, the 180° front-to-back ratio does not give a true picture of the QRM levels from the rear, so some folks prefer to use this figure as a better indicator. The worst-case front-to-back ratio provides the most conservative value for rearward suppression of QRM. The rightmost graphic in **Fig. 2** shows that the 180° and the worst-case front-to-back values do not require separate lobes, even though the values differ. (We may debate elsewhere whether the 8-element Yagi main rearward radiation is a single main lobe or a junction of 3 overlapping lobes.) When we find the two ratios related to the same rearward lobe, we usually do not find much difference in their value.

We are not done with front-to-back ratios. Each sketch in **Fig. 2** contains an arc going from 90° on one side of the line of maximum gain around the rear to the other point that is 90° from the maximum gain line. Suppose that we add up all of the gain values at the headings that pass through the arc. Next take their average value. Subtract the average gain value to the rear from the maximum forward gain and you arrive at what some call the front-to-rear ratio. Others call this the averaged front-to-back ratio. **Table 1** performs this task at 5° intervals, which is sufficient for this

sampling. If you compare the front-to-rear ratio with the other front-to-back ratios, you can see why an antenna maker might use it. The value is higher than all of the other values (with the exception of the  $180^\circ$  front-to-back ratio for the 3-element short-boom Yagi). The rationale behind using the front-to-rear ratio is that it provides an averaged total picture of the rearward QRM suppression.

The 2-dimensional scheme works reasonably well in characterizing the directivity of antennas used from the middle of the HF region through the UHF portion of the radio spectrum. In most cases, we are concerned with the rearward quadrants at angles equal or close to the elevation angle that we select for the forward lobe. However, even within this region, the scheme has limitations, especially the versions of the front-to-back ratio intended to overcome limitations of the  $180^\circ$  version. **Fig. 3** offers just two samples.



Two Cases of Imprecision for Worst-Case and Averaged Front-to-Back Ratios



The conventions of front-to-back ratios arose largely with the Yagi array in mind. One feature of these antennas is that in the E-plane, the array exhibits a very deep null  $90^\circ$  away from the main forward direction. Therefore, the use of a  $90^\circ$  convention to set the limits between forward and rearward lobes seemed quite natural. The far-field pattern on the left in **Fig. 3** is for a Moxon rectangle in a horizontal orientation. The deep side nulls do not occur at  $90^\circ$  from the main forward bearing, but somewhere between  $110^\circ$  and  $120^\circ$  from that bearing. An automated system for determining the worst-case front-to-back ratio, such as found in NSI software, would identify the worst-case rearward lobe bearing at  $91^\circ$  from the main forward heading. Whether or not this bearing deserves such an identification falls outside of our discussion, but the quandary is clear.

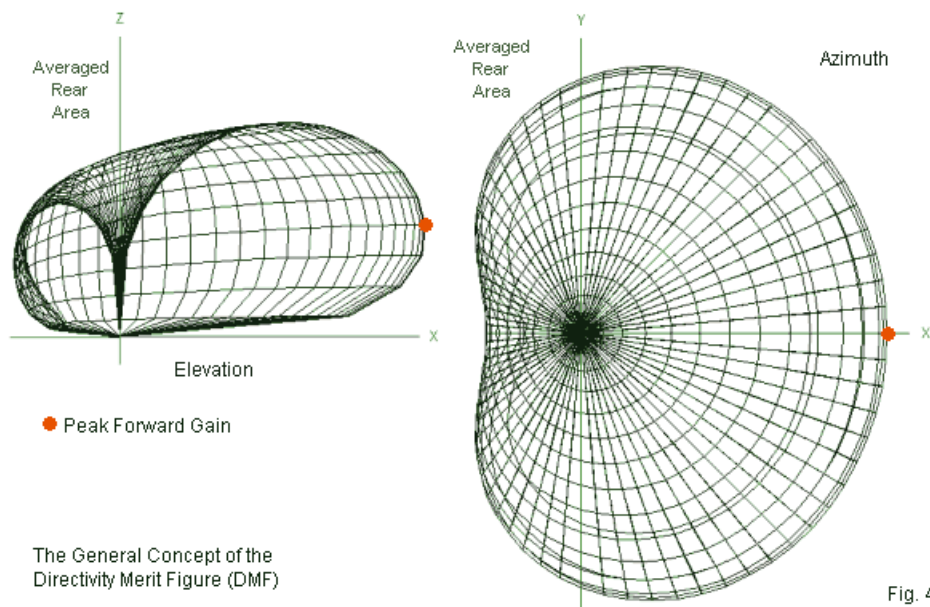
The right side of **Fig. 3** shows a pattern that is typical of many phased vertical arrays. In one sense, there are no rearward lobes, but only a single deep null  $180^\circ$  opposite the direction of maximum gain. From the pattern alone, it is not clear whether any of the front-to-back ratio conventions except the  $180^\circ$  version has appropriate application to such patterns.

## Re-Thinking Directivity

In the lower HF and the MF portions of the spectrum, noise is a much more important and fundamental factor for receiving antennas than it is at higher frequencies. Noise may come from any direction, ranging from ground-wave paths to very high-angle propagation routes. As well, many more of the antennas used at

lower frequencies have cardioid and similar patterns such as the one on the right in **Fig. 3**. Together, these facts showed some of the shortcomings of the conventional front-to-back ratio ideas as a measure of receiving antenna directivity. Over the years, two efforts emerged to overcome these failings of the 2-dimensional system.

*DMF*: The first of these systems of finding a replacement for the front-to-back ratio emerged from the work of John Devoldere, ON4UN, whose book *Low-Band DXing* has acquired just fame. John calls his concept the Directivity Merit Figure (DMF). ON4UN calculates the average gain in the entire back azimuth half of the antenna, from  $90^\circ$  to  $270^\circ$  (where the bearing of maximum forward gain is presumed to be  $0^\circ$ ), and over the entire elevation range from  $2.5^\circ$  to  $87.5^\circ$ . Doing all of this at  $5^\circ$  increments means that he considers 666 gain values. The average rearward gain now is the average of 666 values. **Fig. 4** shows the rearward areas evaluated as elevation and azimuth slices of a 3-dimensional pattern (for a phased 2-element vertical array). He then defines a figure of merit for the directivity (front response to back half-hemisphere) as being the difference between the forward gain at an optimum wave angle (for example,  $20^\circ$ ) and the average rearward gain. (See Chapter 7 of the most recent edition, section 1.8, page 7-8.)



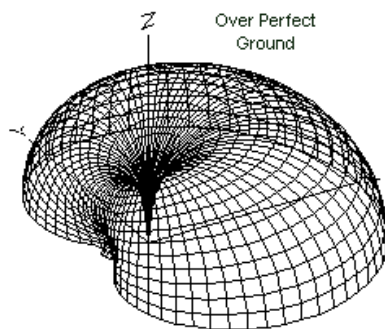
The process requires a separate utility program, since John compensates for the changing equivalent physical distance between angular points on the azimuth rings for different elevation angles. The elevation angles extend from  $2.5^\circ$  to  $87.5^\circ$  because NEC does not calculate a far field at  $0^\circ$ , that is, at ground-wave level using the RP0 command for real lossy, ground. (NEC does allow RP1 ground-wave analysis as a separate command, although this command may not be available on entry-level implementations of NEC.)

DMF has the advantage of allowing a comparison of any bearing with a specific azimuth and elevation setting against the full rear half-hemisphere of the pattern. Hence, it takes into account the sensitivity of the pattern to noises from virtually all angles, as well as the various vertical as well as horizontal lobes and nulls in the rearward pattern. However, the advantage may also be a disadvantage insofar as noise may come from any direction. Hence, DMF provides a rough directivity figure that extends the concept of the averaged front-to-rear idea, but it does not directly provide an indicator of the overall directivity of an antenna with respect to sorting noise from signals in the desired direction.

*RDF:* Several years ago, one Ham suggested an alternative analysis with several simplifying steps for antenna modelers and some inherent advantages over the DMF measure. This Ham's Receiving Directivity Factor (RDF) compares forward gain at a desired direction and elevation angle to average gain over the entire hemisphere. RDF includes all areas around and above the antenna, considering noise to be evenly distributed and aligned with the element polarization. (See Chapter 7 of the most recent edition of *Low-Band DXing*, section 1.9, page 7-9.)

The RDF measure rests in part on the same calculations used to determine the value for the Average Gain Test (AGT). To obtain the average gain test value for a given antenna, the modeler removes all resistive loads, including the material conductivity of the model wires. The one sets up an RP0 command with an even spread of both azimuth and elevation (phi and theta) points. For most purposes, a 5° increment will suffice, but some complex patterns

may require a small increment. In free space, the request will include a complete sphere, while over perfect ground, the request will create a hemisphere of sampling points. **Fig. 5** shows the difference in the 3-dimensional pattern produced, in one case a phased 2-element vertical array and in the other a simple vertical dipole.



3-Dimensional Patterns Used  
to Determine Average Gain

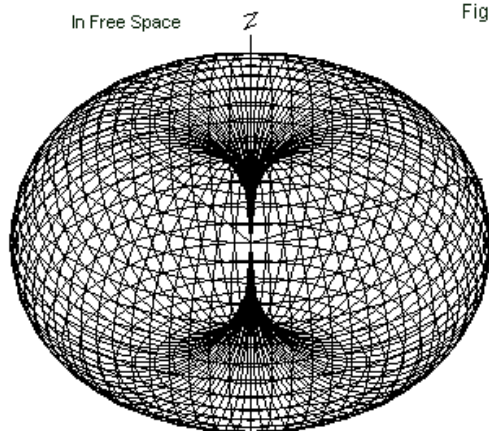


Fig. 5

To obtain the average gain, the RP0 XNDA entry should be either 1001 or 1002. The former prints the radiation pattern values plus the average gain data, while the latter prints only the average gain information. The following line is the NEC output report of the average power value for a simple monopole over perfect ground.

```
AVERAGE POWER GAIN= 1.99891E+00
SOLID ANGLE USED IN AVERAGING=( 2.0000)*PI STERADIANS.
```

A free-space pattern would have shown a value of  $4 * \text{PI}$  steradians, and the value--assuming a very good model, would have been very close to  $1.00000\text{E}+00$ . However, over perfect ground, the solid angle value is  $2 * \text{PI}$  steradians, and the value of the very good model is close to  $2.00000\text{E}+00$ . To remove any ambiguity, programs like EZNEC perform the necessary division to arrive at an AGT score over perfect ground that is consistent with the free-space value, in this case,  $0.99945\text{E}+00$ .

All AGT values are convertible to gain correction values in dB. 10 times the log of the AGT score (relative to  $1.00000$ ) yields the correction factor, which the modeler should subtract from the raw gain reported by NEC. In the sample case, no correction is necessary because the value is so close to the ideal. In fact, there is no universal standard of how close the AGT value should be to  $1.00000$  to be truly adequate. The allowable range of variation depends upon the specific modeling task. However, as we progress toward a hopefully reliable RDF measure, the initial AGT should be as close to  $1.00000$  as the modeler can make it. The AGT value is a measure of model adequacy and stands as a necessary but not a sufficient condition of true model adequacy.

When we place an antenna over real lossy ground, we may still request the average gain via the RP0 XNDA values of 1001 or 1002. However, the value that we obtain will be significantly lower than the AGT value used to evaluate model adequacy. Consider a vertical monopole with 4 radials only a few feet above average ground (conductivity  $0.005 \text{ S/m}$ , permittivity 13). A sample model

that includes material losses under these conditions returns the following report.

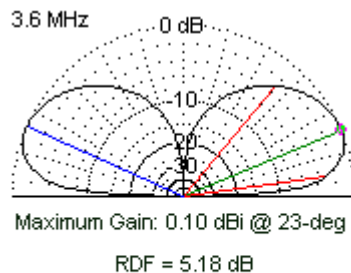
```
AVERAGE POWER GAIN= 5.72269E-01  
SOLID ANGLE USED IN AVERAGING=( 2.0000)*PI STERADIANS.
```

The average power gain for this example over ground is 1/2 the value shown or 2.86135E-01 relative to a standardized gain of 1.00000E00. One useful interpretation of this value is as a measure of radiation efficiency (in contrast to the power efficiency value provided by the NEC power budget section of the output report). Essentially, the antenna is almost 29% efficient relative to radiation in the far field. Like the AGT value, the average gain report is convertible to a gain value in dB by the same calculation used earlier. In this case, the calculation returns -5.43 dB.

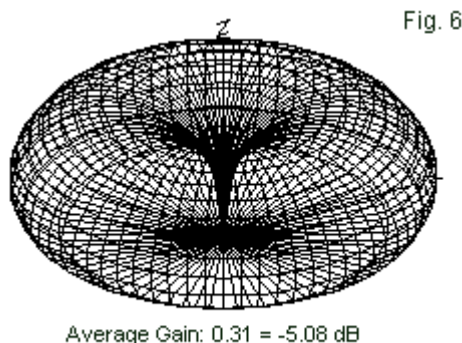
To calculate the RDF, we need one more modeled value: the gain at the elevation angle and azimuth angle selected by the user. The selected heading for the gain value need not necessarily be the elevation and azimuth angle of maximum gain, although we may often find it convenient for a general evaluation to use these values. The antenna model that produced the listed average power gain happens to show an omni-directional pattern with maximum gain at an elevation angle of 19°. The gain is 0.72 dBi. The difference between the overall average gain and gain at the desired direction and elevation angle is the RDF. Hence, the RDF for this antenna is 6.15 dB.

Although we may easily calculate the RDF for an antenna in EZNEC as a 2 step process, some implementations of NEC, such as 4NEC2, have automated the process of obtaining an average gain value and then obtaining the gain at the desired azimuth and elevation angle in order to calculate the RDF.

Unless used wisely, the RDF can mislead us, just as can any of the other measures of directivity that compare forward gain vs. rearward or overall gain. **Fig. 6** provides the elevation pattern and the 3-dimensional pattern of an omni-directional vertical monopole for 3.6 MHz. At the TO angle, the gain is 0.1 dBi, while the average gain is 0.310 or -5.08 dB. Therefore, the RDF is 5.18 dB. As ON4UN points out in his book, omni-directionality in an antenna does not necessarily result in a low or non-existent RDF (or DMF), since the pattern shows relatively low gain at high elevation angles, all of which go into the calculation of average gain.

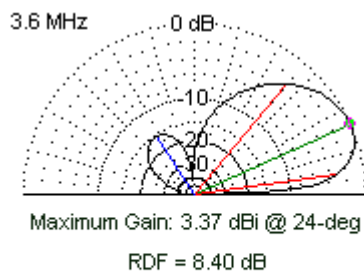


RDF for a Vertical Monopole  
with 4 Radials over Average Ground

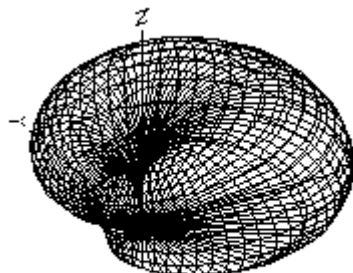




If we create a simple pair of phased monopoles, we can obtain the pair of patterns shown in **Fig. 7**. These patterns show an average gain close to that of the single monopole (0.314 or -5.03 dB). This result is natural since the array elements use the same height, radial system, and material as the single monopole. However, phasing gives the array a gain of 3.37 dBi at the TO angle. The resulting RDF is 8.40 dB. The difference between the two antennas is 3.22 dB, roughly corresponding to the difference in their maximum gain (3.27 dB).



RDF for 2 Phased Vertical Monopoles  
with 4 Radials over Average Ground



Average Gain: 0.314 = -5.03 dB

Fig. 7

The close relationship between the gain differential and the RDF differential occurs with these two antennas due to the similarities in the type of antenna and their elevation pattern properties. Had we selected very disparate antenna types for the examples, the two differentials might not have correlated well.

In addition, when noise abatement is a key issue, the RDF measure will not always tell a complete story. As our Ham reports, for best noise attenuation, a narrow half-power beamwidth may be as important as a very high front-to-rear ratio. Moreover, the factor does not itself account for the bandwidth of an antenna. Many noise sources are very broad band. Receiving antennas vary in their bandwidth in terms of signal strength across a span of frequencies corresponding to the input bandwidth of a receiver. In some application, using a narrow bandwidth antenna may yield a better signal-to-noise ratio. These are factors that fall outside the single-frequency requirement for obtaining an RDF calculation.

Nevertheless, the RDF is an adjunct function to NEC that some implementations of the modeling software may offer. Where not offered, we can easily calculate the value. It adds to list of useful measures that we may derive, even from entry-level versions of antenna modeling software.

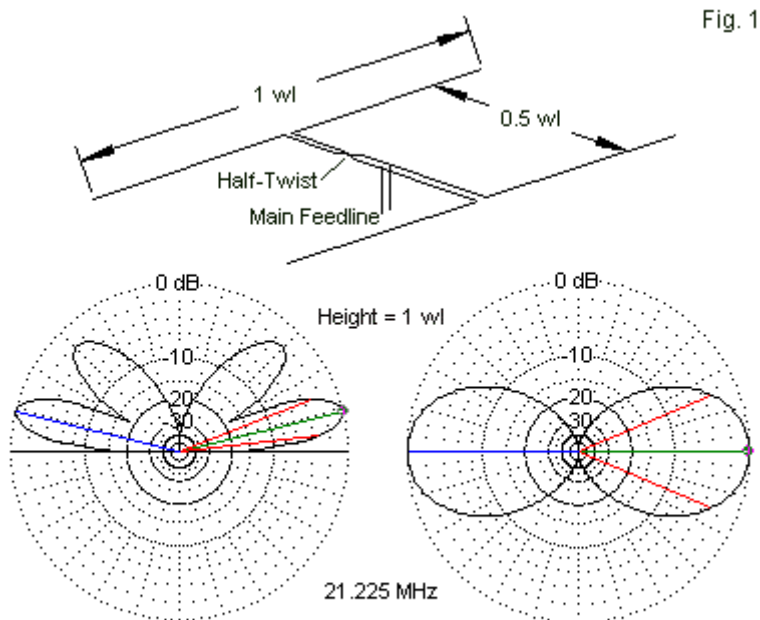
## Chapter 145: Serial Feedline Connections

**M**odeling a set of feedlines that join at a parallel connection is simple and straightforward within NEC, even if the lines join at the source segment. When transmission lines that use the NEC TL facility join on the same segment, they are automatically in parallel with each other. Moreover, they are in parallel with any source that is also placed on the same segment.

There are a few significant antenna system designs that may sometimes call for a serial connection of feedlines, as well as a further serial connection to a source. Radio amateurs especially do not think about this possibility when designing antenna systems, since the parallel connection is so ingrained into their thinking. Therefore, let's examine a few cases in which a serial connection of multiple feedlines is a plausible way to proceed and then develop some easy methods of modeling the situation within NEC.

### Junctions of 2 Identical Feedlines

There are a number of simple 2-element phased arrays that have been available to designers for about 3/4 of a century. The designs are straightforward and reliable. Interestingly, in the past, we have used a parallel connection of the identical feedlines from each element to a center point that is also the main feedpoint for the array. **Fig. 1** shows one such array, the venerable W8JK.



General Outline and Elevation and Azimuth Plots  
15-Meter W8JK "Flat-Top" End-Fire Array

The W8JK is a flattop or endfire array with its bi-directional main lobes off the end of the plane formed by the two wires. There are many version of the W8JK, with various element lengths and element spacing values. In general, the longer that we make the elements, the higher will be the gain of the array--up to an element length of about 1.25 wavelengths. As well, the closer that we space the elements, the higher will be the array gain, with the penalty that

the impedance at the junction of the two phasing feedlines tends to decrease as the spacing decreases.

Properly phasing the two elements means feeding one element 180 degrees out of phase with the other element. If we use identical lengths of identical feedlines for the phasing lines, then giving one and only one of the lines a half twist will affect the desired phasing.

Most implementations of the W8JK array employ one of the common parallel feedlines. For our sample, we shall employ 600-Ohm open ladder line, since it has lower losses than 450-Ohm window line or 300-Ohm tubular transmitting line. The latter two have vinyl casings that provide structural integrity for the line, but those casings increase losses relative to the ladder line that uses only periodic spacers to maintain the distance between the two wires forming the feedline. Note that the 300-Ohm line specified is a version designed for transmitting applications. The typical TV twinlead, especially the cheaper varieties, may have much higher losses and, indeed, may not have a 300-Ohm characteristic impedance.

In our example, let's also use the same 600-Ohm line as the main feedline. For many phased array installations, the length of feedline from the antenna system feedpoint junction to the equipment can be very long. Let's specify 100', although real installations may be much longer.

One of the dangerous sound-bite ideas that pervade amateur radio practice is that the losses in a parallel feedline are so low that its

length and the SWR mismatch between the line's characteristic impedance and the antenna terminal impedance do not matter. The line will provide a high-efficiency power transfer from the equipment to the antenna system (or vice versa on receive) regardless of the line length or the mismatch. Unfortunately, this sound bite is only correct up to a point. Like any feedline, even the 600-Ohm open ladder line has a baseline matched loss value per unit of length. A mismatch creates additional loss such that the SWR acts as a multiplier on the matched loss value. The higher the SWR value, based on the mismatch between the line characteristic impedance and the antenna terminal impedance, the greater will be the losses on the line. **Table 1** provides some approximate values of loss in 600-Ohm open ladder line for 100' of the line at two frequencies--14.175 and 28.5 MHz in the sample--to show the rising losses as the SWR increases.

Table 1. Approximate losses for 100' of 600-Ω open ladder line for two HF frequencies and with various levels of SWR

SWR	14.175 MHz	Loss dB	28.5 MHz	Loss dB
1		0.07		0.10
2		0.09		0.13
4		0.15		0.21
8		0.28		0.40
16		0.54		0.77
32		1.02		1.40

The values are approximate because we can find slightly different values in different tables of matched loss values, as well as slightly different values for the characteristic impedance of the line. In addition, we would discover different loss values depending on whether the mismatch is due to very high or very low antenna terminal impedance values. However, the values shown are useful as approximations. You may explore AC6LA's TLD program or N6BV's TLW program for more refined figures for different line lengths, different antenna terminal impedance values, and different lines. The numbers in the chart derive from using purely resistive impedances.

The baseline losses of 450-Ohm and 300-Ohm lines are considerably higher, relative to the 600-Ohm line shown. Hence, with very high SWR values, the overall loss for 100' of line will be proportionally higher. An SWR value of 32:1 is unusual, to say the least, if we think of impedances above 600 Ohms. A resistive impedance of 19,200 Ohms will yield the value. However, the much more commonly encountered value of 18.75 Ohms will also yield the same SWR value. The calculation of SWR from the antenna terminal impedance and the line characteristic impedance falls outside the scope of these notes, but the reactive component of the impedance is not a small factor in the calculation. Hence, in practical situations, SWR values above 10:1 are very common and values above 20:1 are not unusual.

Now let's add a further premise to our exercise: we wish to minimize so far as possible losses along the main 600-Ohm feedline from the antenna system terminals to the equipment. The

next question is what this might mean for our W8JK monoband flattop. Let's construct one in model form using 1-wavelength elements spaced 1/2-wavelength apart at 21.225 MHz. Further, let's place the model 1 wavelength above average ground. Initially, let's use two phase lines, each with its own source. We can give one of the phase lines a half twist by specifying that it is reversed or we can leave both lines normal and set one of the sources at a 180-degree phase angle. If we exercise either option, we obtain a pair of source impedance values that read close to  $84 + j88$  Ohms.

If we construct the W8JK using the standard parallel connection of the feedlines, then the impedance at the system terminals at the source applied to the wire forming the junction of phase lines becomes about  $42 + j44$  Ohms. Of course, we might add series capacitance to the line and employ a 50-Ohm coaxial cable as the main feedline, but that exercise belongs to a different discussion. We are committed to using 600-Ohm ladder line as our main feedline. However, as shown in **Table 2**, the 600-Ohm SWR is above 14:1.



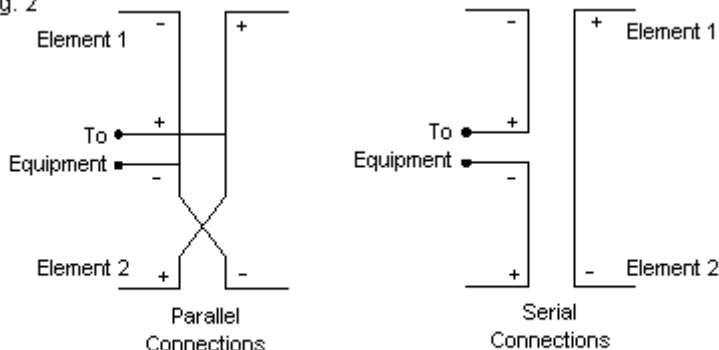
Table 2. Modeled W8JK performance at 21.225 MHz 1- $\lambda$  above average ground with separate, parallel, and serial feedline connections

Feed Mode	Gain dBi	TO angle degrees	Beamwidth degrees	Impedance R +/- jX $\Omega$	SWR 600 $\Omega$
Separate	11.31	14	46.4	84 + j89	7.27
Parallel	11.31	14	46.4	42 + j44	14.27
Serial	11.31	14	46.4	168 + j183	3.92

Note: Impedance for separate feedpoints is for each of 2 feedpoints.

One much neglected method of reducing the SWR on the main feedline is to use a series connection at the main junction of phasing and feedlines. **Fig. 2** shows the difference in the connection in schematic form. The "+" and "-" signs are simply reference points to keep the connections correct. Since most installations would use some sort of fixture--perhaps a simple plate that provides terminals and strain relief for the lines--one method is no harder to implement than the other.

Fig. 2

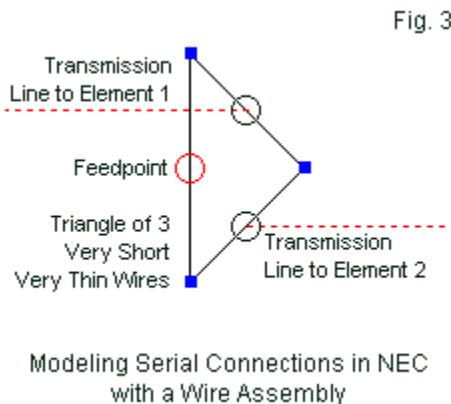


Alternative Parallel and Serial Connections  
for a W8JK (Out-of-Phase-Fed) Array

The last line in **Table 2** shows what we gain from using a serial connection. The 600-Ohm SWR is under 4:1. The voltage and current excursions along the main feedline will be much lower than with the parallel connection. A concomitant result is that the range of potential impedance values that the antenna tuner might encounter will be smaller than with the parallel connection. Let's assume that this condition is desirable and so we opt for the serial connection.

Modeling the serial connection requires us to rethink the requirements. A parallel connection only needed one very short, very thin wire at the junction of the TL-based transmission lines, and this same wire served as the source wire segment as well. However, we need a different scheme for the serial connection.

**Fig. 3** shows a usable method for two-line serial junctions with a source.



The triangle consists of three very short and very thin wires. In the HF region, I typically use AWG #20 wire (0.032" diameter). The segment lengths are between 0.0015 and 0.002 wavelengths long, to keep the segment length within NEC limits. The very small triangle can go between the elements without harm. However, you can also specify a considerable distance away from the main radiating elements, since the transmission-lines, using the TL facility, have lengths specified by the command and not by the geometric distance between the elements and the junction assembly.

In all cases, the modeler should check the average gain test (AGT) for the array plus the serial assembly to ensure an adequate value

for accuracy. The gain of the array should not change more than about 0.01 dB between the parallel and the serial models--or between either one and the model using separate sources, assuming that there is no difference in the specified transmission lines for the model set. In the figure, one dashed line is the "normal" line to one element, while the other dashed line is the "reversed" line to the second element. The source assembly is not totally invisible to the model, since the impedance values among the three models in the set will not show mathematical perfection to the last decimal place. Nonetheless, the models are good indicators of the anticipated performance, and construction variables will in most cases outweigh the slight differences in the calculated impedance values.

Serial feeding is not a solution to all conditions associated with W8JK feedline junction values. Let's briefly consider a flattop array consisting of two 44' elements with a 22' spacing between them. The element length is about 1.25-wavelengths at 10 meters. As we reduce the operating frequency, the elements grow shorter when measured in wavelengths, but so too does the element spacing. As a consequence, the array provides relatively consistent gain performance from 10 meters down to 30 meters. **Table 3** shows the free-space performance modeled for such an array using AWG #12 copper wire. As in the initial model, the phase lines are 600-Ohm open ladder line, as is the presumed main feedline.

Table 3. Free-space performance and impedances with parallel and serial feedpoint contentions for a W8JK with 44' elements and 22' separation for 30 through 10 meters

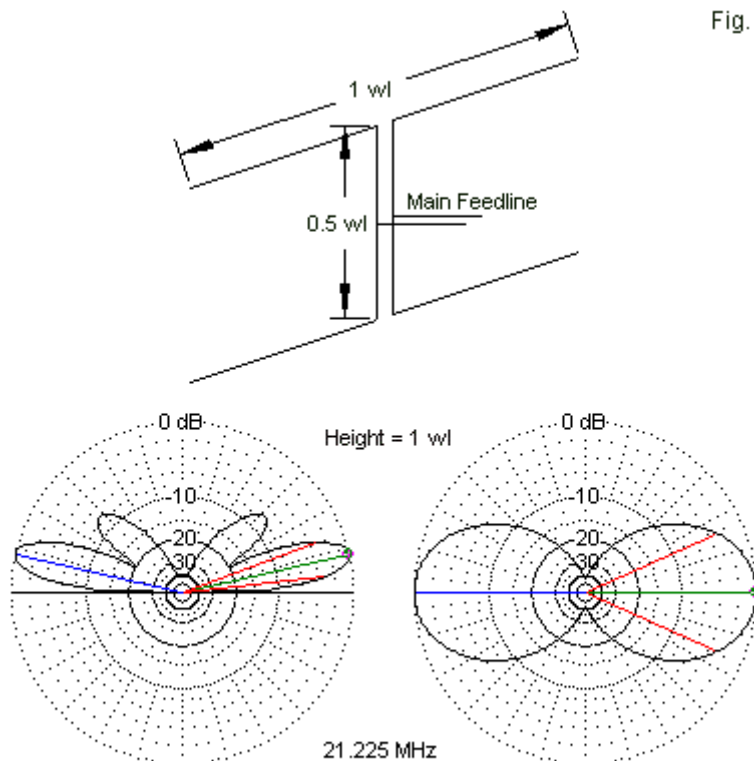
Frequency MHz	Gain dBi	Beamwidth degrees	Parallel Z R +/- jX	SWR 600 $\Omega$	Serial Z R +/- jX $\Omega$	SWR 600
28.5	5.88	32	260 + j675	5.47	1116 + j2781	13.88
24.94	6.15	40	54 + j182	12.13	220 - j736	7.08
21.225	5.91	48	40 - j6	14.84	161 - j21	3.72
18.118	5.76	54	53 - j169	12.25	209 - j668	6.63
14.175	5.60	59	531 - j1017	5.07	2014 - j3982	16.72
10.125	5.54	63	16 + j196	42.34	65 + j785	25.26

As the elements grow shorter while we reduce the operating frequency, the beamwidth grows wider. However, the maximum bi-directional gain remains relatively constant, varying by only 0.6 dB from one end of the operating spectrum to the other. The remaining columns show the feedpoint junction impedance with both parallel and serial feed systems, along with the 600-Ohm SWR as an indicator of probable losses along the main feedline. From 20 through 10 meters, the parallel feed system shows a maximum SWR value of nearly 15:1 at 15 meters, but the other values are lower, with the best values at 10 and 20 meters. However, the SWR value at 30 meters is above 40:1, a condition that promises possibly significant loss and very wide swings of voltage, current, and impedance along the main feedline. In contrast, the series feed system reduces the 30-meter SWR value almost by half, but ends up with higher SWR values on 10 and 20 meters. If we exclude a remote switching system at the main feedline junction with the phasing lines, the potential user is faced with a decision on which

feeding system to use based upon which bands are more important to the station's operating goals.

A second type of array suitable for potential serial feeding is the lazy-H, a broadside array consisting of two elements that are vertically arranged and that provide a bi-directional broadside pattern. **Fig. 4** provides a sketch of a monoband version of the antenna using 1-wavelength elements and a spacing of 1/2-wavelength between the elements. For our sample, the midpoint between the elements, where the phasing lines join, is 1 wavelength above average ground. The difference between the lazy-H and the W8JK--a difference that is crucial to operation--lies in the phasing system. The vertically aligned lazy-H elements are fed in phase.

Fig. 4



General Outline and Elevation and Azimuth Plots  
Lazy-H Broadside Array

Although different in their exact values, the impedance values at the lazy-H feedline junction are similar to those of the W8JK. **Table 4** lists the impedance values for separately sourced phase lines, for a parallel combination, and for a serial combination. The

performance of the array is almost incidental to our purpose in using it, but the lazy-H does show about 1.5-dB higher gain than the same wires and spacing applied to the W8JK, largely as a function of a reduction in the strength of the higher-angle elevation lobes. The TO angle is a degree lower than provided by the W8JK because the effective height of the lazy-H is a small distance above the center point between elements.

Table 4. Modeled Lazy-H performance at 21.225 MHz 1- $\lambda$  above average Ground (at center) with separate, parallel, and serial feedline connections

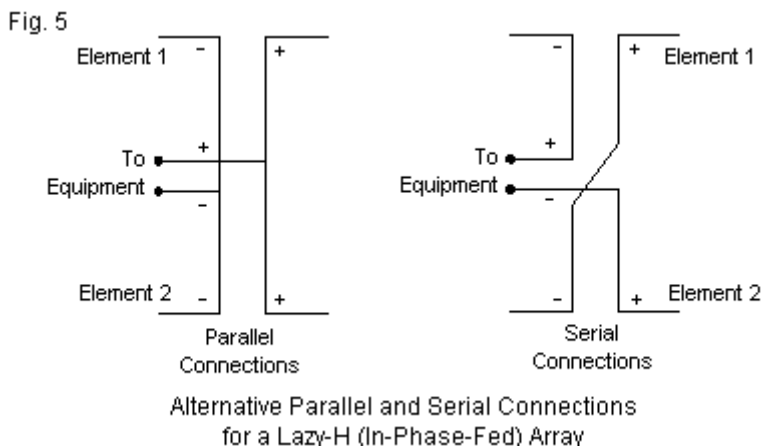
Feed Mode	Gain dBi	TO angle degrees	Beamwidth degrees	Impedance R +/- jX $\Omega$	SWR 600 $\Omega$
Separate	12.87	13	48.6	68 + j11	8.80
Parallel	12.87	13	48.6	34 + j547	17.62
Serial	12.87	13	48.6	136 + j28	4.42

Note: Impedance for separate feedpoints is for each of 2 feedpoints.

Since the lazy-H individual source impedance values are lower than the corresponding W8JK values, the parallel feedpoint system results in a higher 600-Ohm SWR value. The serial feed system creates an SWR values that promises lower losses and narrower impedance excursions along the main feedline, which may result in an easier tuning task, depending upon the exact line length. The serial system for modeling can use the same triangle of short, thin wires used for the W8JK--either centered or at a large distance from the main radiating elements. The only modeling difference related to the phase lines is that both must be either "normal" or



"reversed." Nevertheless, the physical implementation of a serial feedline system will have a quite different appearance, as suggested by the schematic outline in **Fig. 5**.



Unlike the W8JK, the lazy-H radiation properties are not constant as we reduce the operating frequency. Shorter elements and reduced element spacing both reduce gain in the lazy-H, since we are feeding the elements in phase. Consider a pair of 44' lazy-H elements spaced 22' apart vertically in free space. The elements are about 1.25-wavelengths long on 10 meters, with a spacing of about 5/8-wavelength. These conditions optimize gain on 10 meters. On all lower bands, the shorter elements and decreased spacing--as a function of a wavelength--decrease gain. As well, they increase the beamwidth at a faster rate than we saw in the comparable data for the W8JK. **Table 5** shows the data for all

bands from 10 down to 30 meters using series and parallel feed systems.

Table 5. Free-space performance and impedances with parallel and serial feedpoint contentions for a Lazy-H with 44' elements and 22' separation for 30 through 10 meters

Frequency MHz	Gain dBi	Beamwidth degrees	Parallel Z R +/- jX	SWR 600 $\Omega$	Serial Z R +/- jX $\Omega$	SWR 600
28.5	9.79	31	128 + j652	10.76	522 + j2686	25.03
24.94	9.39	40	32 + j153	20.44	126 - j618	9.89
21.225	7.42	51	41 - j43	14.81	162 - j170	4.02
18.118	5.82	60	93 - j225	7.41	365 - j891	5.71
14.175	4.17	70	1080 - j277	1.97	4256 - j1205	7.67
10.125	2.94	80	59 + j160	10.99	235 + j640	5.68

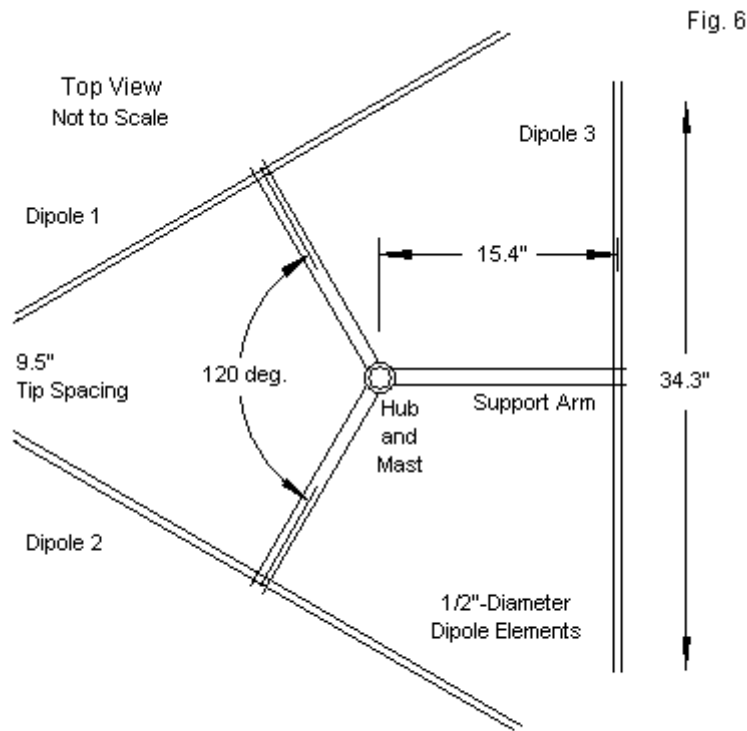
The gain of the lazy-H at 30 meters is marginal in the sense of being less than one dB higher than for a single-wire dipole. However, the array is usable if we can obtain satisfactory feedpoint junction impedance values. With a parallel connection, we find numerous bands with 600-Ohm SWR values above 10:1. Using a series connection, all but one of the bands shows a 600-Ohm SWR value of less than 10:1. However, the single band with a higher value is 10 meters, where the SWR value is very much higher and the losses for any given SWR value are the highest among all of the bands. Like the W8JK, the decision whether to use a parallel or a series connection does not make itself.

We have used very specific examples of both the W8JK and the lazy-H array in providing examples of the required modeling for effective evaluation. One may change the transmission line, the phase line, and even the length of the phase lines in search of a

better combination using either serial or parallel feeding. With a central feedpoint between the elements, the only requirement (besides the W8JK half twist) is that both phase line be identical, including length. However, there is in principle no restriction on the length of the phasing lines. Therefore, one may search for lengths that provide the lowest SWR values relative to the desired main feedline for the bands of highest interest. All of this, of course, rests on the initial premise that one of our goals is to reduce main line losses to a minimum and, almost incidentally, to provide the antenna tuner with the least extreme resistance or reactance conditions at the terminals.

### A Three-Line Serial Feeding Example

Serial feeding is also possible with more than two lines that meet at a junction. Consider a triangle of three dipoles for 2 meters. **Fig. 6** shows some of the details of a prototype modeled and built for an article in *QST*. The elements are 1/2" diameter aluminum on a PVC structure for support. The arm length, the element length, and the spacing between dipole tips are all selected to provide a horizontally polarized omni-directional pattern. The design case used the band center as the design frequency, because the pattern does not change within the confines of 2 meters and the SWR remains low at the final junction with the 50-Ohm main feedline.

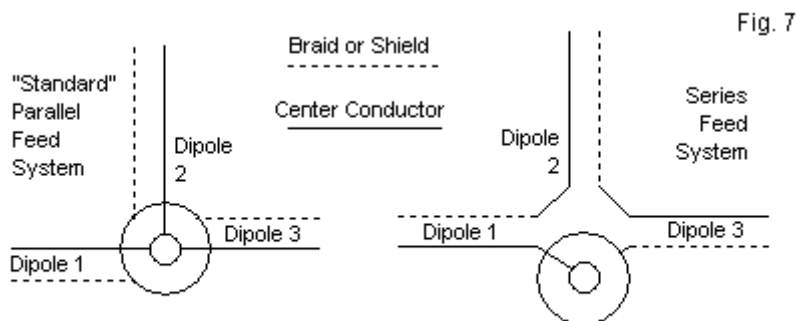


General Outlines of a 2-Meter Triangular 3-Dipole  
Horizontally Polarized Omni-Directional Array

The design is predicated on the fact that a triangle of dipoles, properly spaced, yields the desired omni-directional pattern within perhaps 0.3 dB total variation. As detailed in other documents, the principles of operation differ from the 1961 Big Wheel arrangement. The older antenna creates a circular element with three high

impedance feedpoints. Parallel lines from the feedpoints effect in the  $1/4$ -wavelength distance to the hub an impedance transformation to a low value. At that point, the originators connected them in parallel. The design is highly finicky, since the exact characteristic impedance of the lines and their length determine the hub impedance values.

The revised design actually uses less space than the wheel and can also be configured circularly. We shall omit that version since the question of parallel vs. serial feeding is identical for both straight and circular triangles of dipoles. The key difference between the original wheel and the present design is that the triangle uses independent dipoles. In the arrangement shown, each exhibits a feedpoint impedance very close to 50 Ohms. Therefore, we may run 50-Ohm cables from each dipole to the hub and replicate very closely the impedance at the dipole feedpoints.

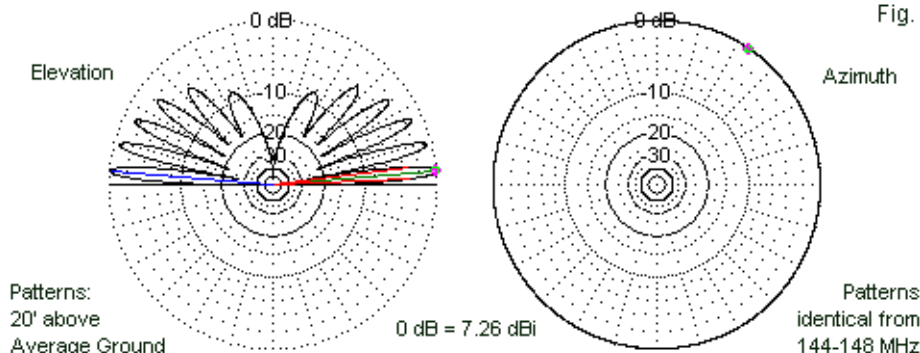


Alternative Methods of Feeding the 3-Dipole Array

Standard treatment of the cables at the hub would be to connect them in parallel, as suggested on the left in **Fig. 7**. The net impedance would be from 15 to 17 Ohms, with some remnant reactance. However, any small reactance at such low impedance values will have a considerable impact upon any matching system that we might try to implement. In contrast, a small reactance in series with a higher impedance will have less impact. Therefore, we selected a series connection system, shown in the right, ensuring that the 50-Ohm lines to each dipole were identical. In the triangular configuration, regardless of the feed system, the builder must ensure the same dipole orientation to obtain the circular pattern. The modeling technique is identical to the one applied to the triangles, except that in this case, we form a square of very short, very thin wires, either at the hub of the triangle or at a considerable distance from the radiating elements.

The net impedance at the hub is about 150 Ohms, usually with a bit of reactance. However, the reactance is rarely more than 10% to 15% of the resistance value. Therefore, one may use a 1/4-wavelength section of cable from the series junction to the main feedline. In this case, RG-62 93-Ohm line proved nearly ideal, with the length adjusted to center the SWR curve in the 2-meter band. **Fig. 8** shows the modeled (and the tested) results of the exercise.

Fig. 8



Representative Elevation and Azimuth Patterns and 50-Ohm SWR Curve  
3-Dipole Triangle at 20' above Average Ground

The triangular antenna system appears only to establish that there is no practical limit to the number of identical feedlines that one may set into a serial configuration. However, when working under these simplifications, identity of line length and element structure are essential to ensure equal current at the feedpoints of the elements. Where an array requires unequal current magnitude and phase angle at each feedpoint, the modeler needs to do

considerable advanced calculation, since series connections rest on voltage division.

## **Conclusion**

Our goal has been to note the considerations that apply to modeling a series line assembly. Since the idea of such a method of feeding antennas is usually foreign to radio amateurs, we have provided some concrete examples that contrast parallel and series feeding methods. When an application calls for series feeding, there are ways to accomplish the modeling task for pre- and post-construction design evaluation. In most cases, adding a triangle or a square to the model will do the job.



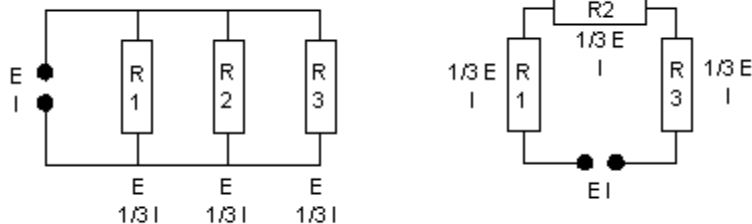
## Chapter 146: Unequal Serial Feedline Connections

In the preceding episode, we examined the modeling of series feedline connections at the source of a model. We looked at a few examples of arrays that used both 2-line and 3-line combinations to familiarize ourselves with both the modeling techniques that we need and with the differences between parallel and series connections of feedlines.

The arrays that we examined had something in common, regardless of the connection. Each individual transmission-line termination had the same impedance. Therefore, we were able to use a simplified set of calculations, outlined in **Fig. 1**. For a parallel connection of individual termination impedances at each feedline, the net impedance was  $1/N (Z)$ , where  $N$  is the number of lines connected and  $Z$  is the impedance of the individual connection. Because we used a series representation of the impedance ( $R \pm jX$  Ohms), we could arrive at the net impedance by handling the resistance and reactance values individually.

$$R1 = R2 = R3 \text{ (or } X1 = X2 = X3 \text{ or } Z1 = Z2 = Z3)$$

Fig. 1

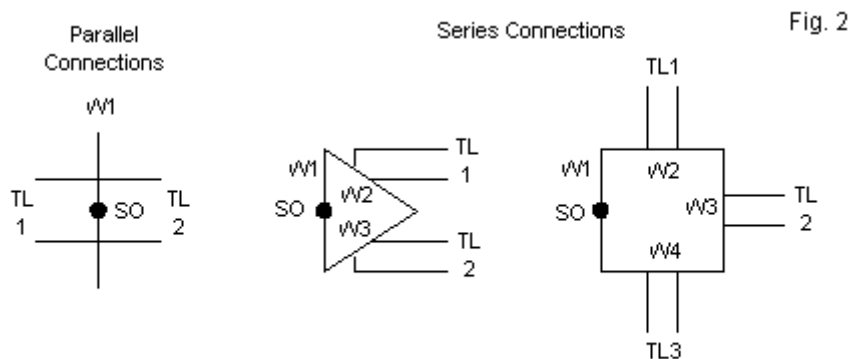


Basic Difference Between Parallel and Series Connections

The series connection presented us with no more difficult an arithmetic task than the parallel connection. For three identical impedance values in series, the net impedance is the sum of the individual impedances, that is,  $N(Z)$ . With the impedance values shown as  $R \pm jX$  Ohms, we could simply multiply  $R$  and  $X$  by the number ( $N$ ) of lines being joined in serial fashion.

The two forms in **Fig. 1** contain a reminder that series and parallel connections do have a difference. A parallel connection of feedlines, relative to the source, shows a constant voltage across each line but divides the total source current equally among the individual lines. In contrast, a series connection of feedlines shows the same current at each line, but there is a voltage drop across each line equal to the source voltage divided by the number of equal loads presented by the lines at the junction. These notes, of course, assume a lossless situation, which is consistent with the lossless lines created by the TL facility within NEC. We also assume, in accord with NEC, that the losses associated with the

structure and loading of the elements within the array are equal and therefore do not disturb the basic calculations that rest on the impedance values that appear at the source-end of each transmission line.



Modeling Parallel and Series Connected Feedlines (TL) and Source (SO)

With respect to modeling parallel and series connections, we do encounter a difference, as suggested by **Fig. 2**. On the left is the very simple scheme required within NEC for modeling a parallel set of transmission lines in conjunction with a source. We need a single 1-segment very short, very thin wire--normally at a remote location relative to the radiating elements of the model--in order to join the lines and the source in parallel. The wire can be as short as about 0.001-wavelength. 1-mm (about AWG #20) is a good diameter, and if the program allows it, the wire can be lossless. Some programs, such as EZNEC, allow the specification of a virtual wire that

automatically meets these criteria and does not appear in the graphic view is the antenna.

Creating a series connection among the transmission lines and the source requires a more complex structure, as suggested by the remaining two outlines in **Fig. 2**. For each transmission line and for the source, we require a separate very thin, very short wire. These wires connect in series forming a complete circuit. Hence, two lines plus a source requires a triangle, while 3 lines plus a source requires a square. The construct creates the required series connection among the element. However, the structure has a finite dimension that forms a loop. The consequences are twofold. First, we need to check the average gain test (AGT) score to determine that the construct has not significantly changed the AGT value relative to the value obtained from a parallel connection. With very thin and very short wires in the construction, the AGT value at HF will normally change by no more than 0.001, an acceptable value under virtually all circumstances. Second, the loop formed by the construct will often add inductive reactance to the net impedance as related to the simple sum of the individual impedance values without the construct. The amount is normally small and should not be surprising. However, it may require noting relative to any physical implementation of the model under development.

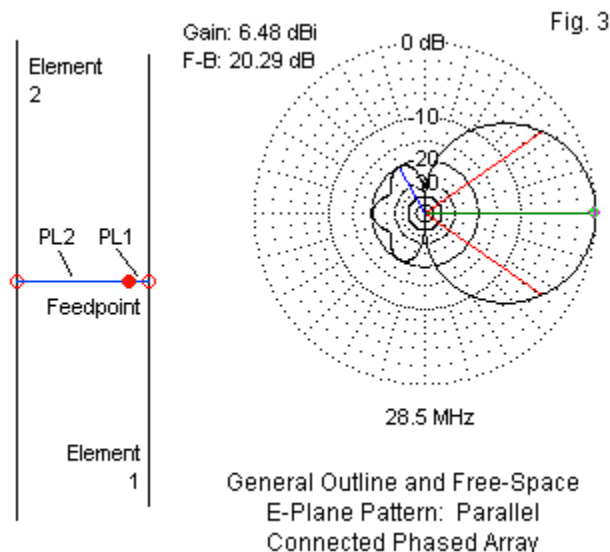
The models that we have so far examined presented equal loads to the junction of lines with the source. At the end of the preceding episode, I indicated that there are many situations in which the lines will not present equal loads. A question arises about how, under these circumstances, we may move from a parallel to a series

connection. The modeling technique will remain the same. We shall switch from a single-wire junction to a more complex series construct of wires. However, to understand what is occurring, we may need to look at modeling practices and at the analysis of behavior of voltage and current under parallel and series connections. In this episode, we shall examine a single example using both types of connections. Our goal is to understand how we can model both ways to obtain a reasonably full analysis and understanding of how and why the two arrays differ.

## **A 2-Element Horizontal Phased Array with Parallel Phaseline Connections with the Source**

Let's consider a 2-element phased array for 28.5 MHz. The design that we shall use emerges from an old design that I once developed to convert a driver-reflector Yagi of good performance of its type to better performance as a phased array, all without altering the elements. The driver and reflector used relatively thin stepped diameter elements so that the whole antenna broke into parts that stored within a PVC boom. The inner section consisted of 0.25" diameter rod, and the total length of the inner sections was 108" (54" each side of the centerline). The outer sections consisted of 0.1875" (3/16") diameter rod. The total length of the driver was 198" (45" per section), while the total length of the reflector was 211.2" (51.6" per section). I spaced the element 57.6" apart. As a Yagi, the array yielded a free-space gain of 6.24 dBi with a front-to-back ratio of 10.88 dB. The design frequency feedpoint impedance was about  $40 + j8$  Ohms, which provided a 50-Ohm SWR of less than 2:1 from 28 to 29 MHz.

Out of curiosity, I developed a phasing harness for the Yagi that improved performance, as shown in **Fig. 3**. Using phasing techniques, the gain increased slightly, but the front-to-back ratio jumped by 10 dB. The Yagi configuration is limited to using only the geometry of the antenna elements to obtain its results. Adding a phase lines allows a broader control of the current magnitude and phase angle values on the individual elements to increase at least some of the performance values.

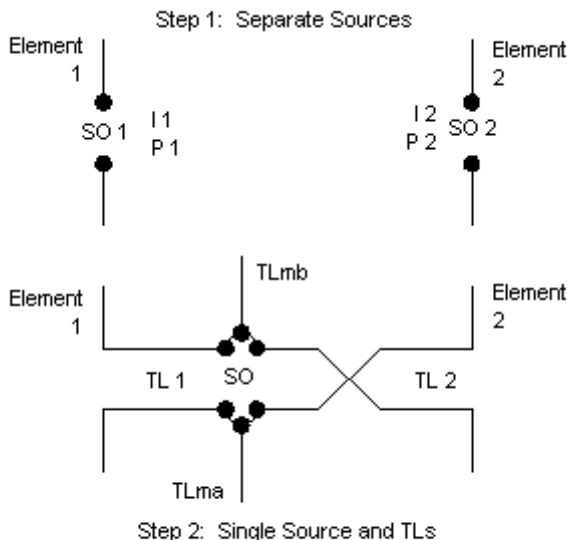


As the outline shows, the phasing system consists of two lines, one from each element, to a main feedline junction. Essentially, we may analyze all 2-element phased arrays on this model, even though

some--like the well-known ZL-Special--used a zero length line from the forward element to the feedline junction. In this design, the forward phasing line consists of 6" of 50-Ohm, 0.78 VF cable, while the rearward line uses the same cable, but with a 64" length. The electrical lengths of these cables, of course, are the physical lengths divided by the velocity factor (VF).

We may develop a fuller understanding of the phased array in the present (and, by extension, any other) design by using two models of the antenna and doing some external calculations. **Fig. 4** shows the outlines of the two models. The upper model establishes the relative current magnitude and phase angle on the two elements required to produce the required performance (as listed in **Fig. 3**). Normally, we assign a current magnitude of 1.0 and a phase angle of zero on the forward element and then find the current magnitude and phase angle required for the rear element. The arrangement of lines used to establish phasing conditions must meet these requirements to obtain the listed performance. (At this point, we shall not concern ourselves with the resulting impedance at the junction of the phase lines in the lower portion of **Fig. 4**, although we shall eventually work with that detail.) Our fundamental question is the conditions that must exist at the junction of the two phase lines to obtain correct element phasing when we use the standard parallel connection of the lines and the source. In this and many other cases, the rearward line (TL2) has a half twist to effect a 180-degree phase shift relative to the junction or to the element phasing that would obtain with a normal line.

Fig. 4



Two-Model Method for Analyzing a 2-Element Phased  
Array Using a Parallel Connection of Phase Lines

Every transmission line (including those in phase-line service) transforms the impedance at the load end to another value at the source end. If the line happens to match the load, the impedance is constant along the line, but any difference between the line characteristic impedance ( $Z_0$ ) and the load impedance ( $Z_L$ ) results in a different impedance values at the source end except for lines that are exactly a multiple of  $1/2$ -wavelength electrically. What amateurs often forget is that the current and voltage also undergo transformation along the line, and they are more critical to the



phased array's performance than the impedance. Voltage and current undergo only one transformation per 360 degrees of electrical change.

The required conditions for proper performance of a phased array include establishing the desired relative current magnitude levels and the required phase angle difference at the two elements. The junction end of the line also has conditions. A parallel connection divides the source current between the two lines. Each line's share of the current must result in the desired ratio of current magnitude and the desired difference in phase angle at the element ends of the line. In addition, the transformations along the line must result in identical voltage magnitudes and phase angles at the junction of the two lines with the source. Very often, we can obtain these conditions, but the combination of parallel voltage and current magnitudes and phase angles results in an unusable or at least a highly undesirable feedpoint impedance. Therefore, with available lines, the designer's options are limited. For example, a combination calling for a total physical length that is less than the spacing between elements would be unusable. As well, we cannot simply change the spacing, since a phased array is a combination of parasitic and directly fed energy at each element. Therefore, for the required performance, changing the element spacing would require a different ratio of current magnitude and an altered phase angle difference to arrive at the specified performance.

To illustrate the required conditions, we can use the standard equations for impedance, voltage, and current transformation down a transmission line from load to source, that is, the junction end of

each line. We shall let  $Z_0$  be the characteristic impedance of the line at the design frequency, while  $Z_L$  is the load impedance and  $Z_s$  is the source end impedance. The script "l" is the electrical length of the line in either degrees or radians, according to the calculator's preferred measurement method.

$$Z_s = Z_0 \frac{\frac{Z_L}{Z_0} \cos l + j \sin l}{\cos l + j \frac{Z_L}{Z_0} \sin l}$$

To calculate the voltage at the source end of the line, where  $E_L$  is the load voltage and  $E_s$  is the source voltage, we can use a comparable standard equation.

$$E_s = E_L \cos l + j I_L Z_0 \sin l$$

The current calculation, where  $I_L$  is the load current and  $I_s$  is the source current, also uses a standard equation.

$$I_s = I_L \cos l + j \frac{E_L}{Z_0} \sin l$$

All of these equations are the versions for lossless lines, the type that appear in the NEC TL system. Therefore, any external calculations based on these equations should yield results that closely coincide with the NEC reports, especially if we are using

NEC data for the input values. The calculations require separating and recombining the real and imaginary portions of the equations, a task well-suited to a spreadsheet or a utility program. TLD and TLW are suitable programs, although they include loss factors. However, the short length of the lines should make any differences inconsequential.

The result of applying these equations to the situation of a modeled phased array allows us to examine how the arrays do their work. **Table 1** provides relevant calculation results for the parallel junction version of our phased array. Note that the input voltage and current for the rearward line have been phase shifted by 180 degrees to account for the half-twist in that line.

Table 1. 2-element phased array: parallel connected lines

	Element 1	Element 2
Step 1 Values		
Relative current magnitude	1.0 @ 0°	0.867 @ 135.97°
Element impedance	34.66 + 20.86 Ω	22.71 + j 7.05 Ω
Element power	34.66 W	17.06 W
Step 2 Calculation Input Values		
Element impedance	34.66 + 20.86 Ω	22.71 + j 7.05 Ω
Element current	1.0 @ 0°	0.867 @ -44.03° *
Element voltage	40.45 @ 31.04°	20.61 @ -26.79° *
Calculation Output Values		
Junction voltage	<b>43.47 @ 37.63°</b>	<b>43.46 @ 37.63°</b>
Junction current	0.928 @ 4.88°	0.407 @ 22.52°
Junction impedance (Z)	45.84 @ 32.75°	106.93 @ 15.12°
Junction impedance (R +/- jX Ω)	38.56 + j24.80	103.23 + j27.88
Net parallel impedance (R +/- jX Ω)	28.07 + j13.13 Ω	
Reported impedance from NEC models	28.77 + j14.94 Ω	

\*Note: Phase angles of voltage and current adjusted by both the required displacement and the 180° twist.

The boldface entry for the calculated voltage values at the junction of lines shows the identity (within a very close approximation) of voltage, with the current being split between the two lines. The net impedance is simply the parallel combination of the two impedance values. The calculation shows a very close coincidence with the reported feedpoint impedance from the NEC model. This should come as no surprise, since NEC makes calculations very similar to these in the course of a core run for the model with phase lines as TL command functions.

The resulting impedance may seem troublesome, since it is neither resonant nor convenient to common matching systems. Had the

impedance been close to resonance at about 25 Ohms, we might have applied a common equation to construct a 1/4-wavelength matching section. A 35.5-Ohm line (composed of RG-83 or of two parallel sections of 70-Ohm line) would have yielded a 50-Ohm final impedance value.

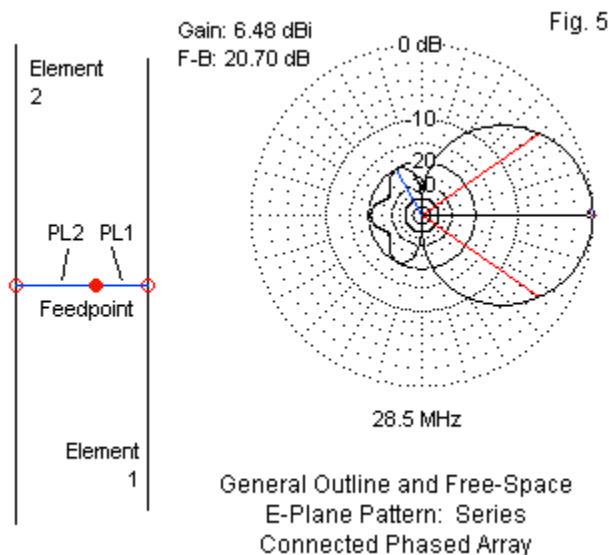
$$Z_s = \frac{Z_0^2}{Z_L} \quad Z_0 = \sqrt{Z_L Z_s}$$

Most amateurs forget that the special formula for exact 1/4-wavelength sections is only a single point along a spectrum of slowly changing impedance values. Therefore, we can create sections that are longer or shorter than 1/4-wavelength to approximate the exact match. A quarter-wavelength at the design frequency is about 103" with a physical length that is the electrical length value times the lines velocity factor. In this case, we need a much shorter length of line. For a VF of 0.66, 34" will do, while for a VF of 0.78, 40" will provide a resonant feedpoint impedance of about 58 Ohms.

The array, then, is quite usable, although I am not here recommending its use. Rather, the phased array with its parallel connections of feedlines and the feedpoint serves as a good example of its type.

## A 2-Element Horizontal Phased Array with Series Phaseline Connections with the Source

For every parallel solution to a design challenge, there should also be a series solution. Therefore, let's use the same set of elements and see if we can develop a series phaseline and feedpoint connection. My purpose is not to claim that one or the other array is superior, but only to show what a series set of connections will entail. The final design for the revised array appears in outline form in **Fig. 5**, along with a free-space E-plane pattern. The gain and front-to-back data on the graphic show the near identity of performance between the new array and its parallel cousin.



The basic outline shows that the feedpoint is not located in the same position as in the case of the parallel junction. The earlier system used 70" of total 50-Ohm, VF 0.78 line divided into a 6" forward section and a 64" rearward section (with its half twist). The new system uses a total of 79" of the same line, with a 25" forward section and a 54" rearward length (again, with a half twist). The new phasing lines are not identical in any way to the old ones, nor are they a mirror image of the old system. Series connections answer to a different set of conditions relative to parallel connections.

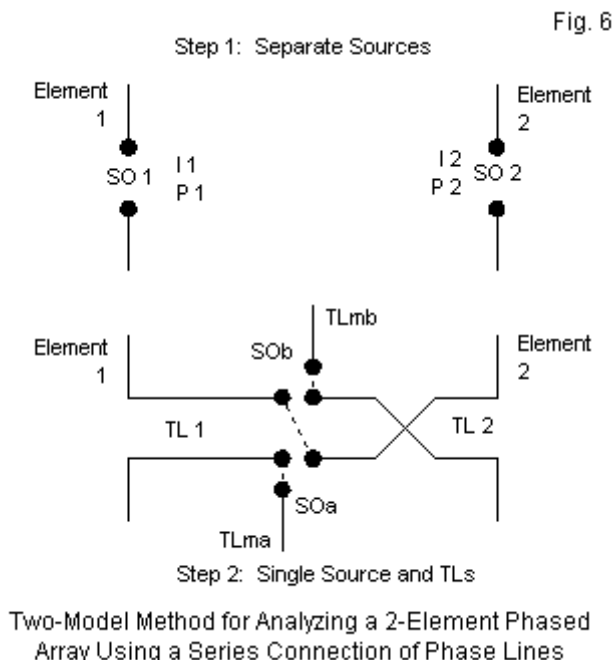


**Fig. 6** shows the two steps through which we shall proceed in hopes of obtaining a better understanding of the series connections. The lower portion of the graphic shows the feedpoint junction area. I could have avoided the double crossing of wires in the schematic representation, but the cross in TL2 is a reminder that the rear line receives a half twist. The junction area of the diagram shows the required connections to obtain a set of series junctions among the lines and the source.



The key to analyzing the series situation is the understanding the each line creates a voltage drop across its transformed version of the element load. Therefore, the current through each of the source ends of the lines is the same. The actual element currents may differ in magnitude and phase angle, but the lines must be of the right length for the characteristic impedance so that the current magnitudes and phase angles at the junction are the same. We may go through the same set of calculations that we used for the parallel connection array to check our work and establish the correct condition at the feedpoint. **Table 2** provides the results of those external calculations. Once more, the initial rear element voltage and current phase angles have been adjusted for the half-twist and its 180-degree alteration of the phase angle between the source and load ends of TL2.

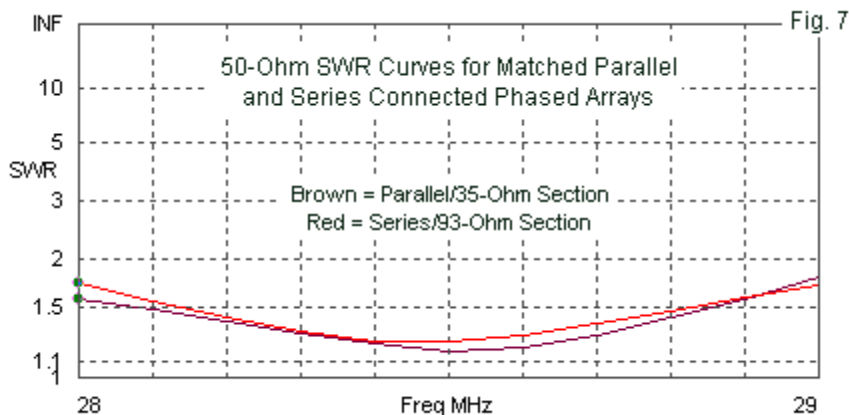
Table 2 2-element phased array: series connected lines

	Element 1	Element 2
Step 1 Values		
Relative current magnitude	1.0 @ 0°	1.048 @ 136.07°
Element impedance	27.50 + 30.09 Ω	33.17 + j 14.57 Ω
Element power	27.50 W	36.32 W
Step 2 Calculation Input Values		
Element impedance	27.50 + 30.09 Ω	33.17 + j 14.57 Ω
Element current	1.0 @ 0°	1.048 @ -43.93° *
Element voltage	40.76 @ 47.58°	37.91 @ -20.22° *
Calculation Output Values		
Junction voltage	55.57 @ 64.06°	55.70 @ 28.02°
Junction current	<b>0.655 @ 23.09°</b>	<b>0.654 @ 23.07</b>
Junction impedance (Z)	84.79 @ 40.96°	85.15 @ 4.97°
Junction impedance (R +/- jX Ω)	84.03 + j58.59	84.83 + j7.37
Net parallel impedance (R +/- jX Ω)	148.86 + j62.96 Ω	
Reported impedance from NEC models	149.40 + j82.12 Ω	

\*Note: Phase angles of voltage and current adjusted by both the required displacement and the 180° twist.

The boldface entry is for the current, which shows a very close coincidence of values. The net impedance at the feedpoint is simply the sum of the individual impedance values. The resistive component shows a tight alignment with the value reported by the NEC model. The model shows a higher reactance than we obtain from the calculations. However, the calculations do not include the triangular loop that creates the series connections. If we remodel the array for a separate source for each phase line, we obtain from NEC impedance values of 64.3 + j55.6 and 84.3 + j7.1 Ohms, for a net series impedance of 148.6 + j62.7 Ohms, very close to the calculated value. Although the connection triangular loop may seem small, it is significant.

Neither of the two versions of the phased array is directly suited to the use of a 50-Ohm main feedline. We raised the impedance of the parallel connected version by the use of a section of 35-Ohm cable, usually constructed from two parallel sections of 70-Ohm cable. Even though the matching section cable impedance is not the geometric mean between the array impedance and the main line impedance, we found a length that provided a satisfactory 50-Ohm SWR. Similarly, we may use a 93-Ohm cable (such as RG-62 with a VF of 0.84) to serve as a matching section for the series connected version of the array. The array impedance is not perfect for use with a 1/4-wavelength of this cable, but a slightly longer cable (108" physically, 128.5" electrically) provides a satisfactory design-frequency resonant impedance (40.9 Ohms).



In fact, both versions of the array, with the proper matching section, provide complete coverage of the first MHz of 10 meters with well under a 2:1 SWR value. Since both arrays also provide essentially the same performance in all vital categories, performance cannot be the deciding factor in selecting which version to use. Of course, these notes are not necessarily recommending either version for actual use.

Careful exploration of both series and parallel connected models can uncover other differences that might impact a selection. Both forms of the array undergo a considerable range of front-to-back values across the defined 1-MHz passband. However, the parallel-connected version shows a much higher change of gain from one end of the passband to the other: 0.88 dB. In contrast, the series connected version varies by only 0.17 dB across the same spread. Despite the gain stability advantage of the series connected version, the parallel-connected form may be simpler to construct. The phaseline system may use available coaxial cable connectors to affect all junctions, both with the elements and at the main junction of the phase lines.

## **Conclusion**

The goal of these notes has been to show the modeling techniques necessary to replicate in NEC a series connection of feedlines and a source in cases more complex than those shown in the preceding episode. We selected a 2-element phased array that required two phase lines constructed using the TL facility. Since the two elements required different terminal current magnitude and phase

angle values to obtain the desired performance, the parallel and the series pairs of phase lines proved to be quite different. The differences stemmed in large part from the fact that parallel connections divide current, while series connections divide voltage. Although NEC provides output data that is both reliable and useful in both cases, we resorted to external calculations to show that both systems established the conditions appropriate to each type.

The external analysis was largely post-facto, that is, applied after finding the correct phase line values, including the characteristic impedance and the length. In this case, the element geometry was given, but any number of other geometries is possible. Since the process depends upon setting realistic performance goals in terms of the gain and the front-to-back ratio for any given geometry, I am not aware of any system for automatically calculating such phase lines. A systematic search among available line  $Z_0$  values and length combinations within NEC remains one of the fastest routes to a reasonable design.

## Chapter 147: Warnings and Errors: What Does NEC Do and What Should You Do?

**N**ewer modelers often encounter situations in which a model aborts a core calculation run and simply returns an error notation. Some implementations of NEC, such as EZNEC, try to prevent the core run by pre-detecting the modeling error (or bad modeling practice), locating it, and labeling it to provide the modeler with a guide as to what should be changed. Other implementations of NEC, such as GNEC, provide pre-run checks within the antenna view system, but the modeler need not examine this facility before ordering the core to perform its calculations. Still other implementations provide no other error identifications other than what may appear in the NEC output report.

In fact, when a run aborts, the first place that a modeler should look is in the NEC output file. Unfortunately, newer modelers fail to realize that NEC produces an output report even for an aborted run, and it identifies errors and warning that fall within its stock of checks. NEC-2 makes only a few checks and reports on very few errors. Some implementations of NEC have expanded the checklist. Therefore, any existing facilities that a program makes available should become a regular part of the modeler's pre-run routine. NEC-4's checking system is far more elaborate, but as we shall see, it is by no means complete, and some warning and error conditions may require considerable hunting to find.

These notes will examine a few kinds of error and warning conditions. The goals interlace, since we sometimes presume that

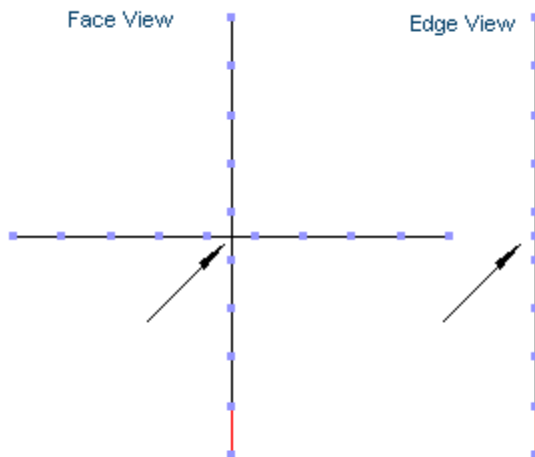
some NEC limits are the same throughout. So in the process of providing a few samples error and warning cases, we can also distinguish among a few ways in which NEC applies different limiting standards to models.

Note that we shall push NEC of its limits on purpose. Therefore, the existence of a full output report on a model does not necessarily mean that the model follows good modeling practices. Reliable NEC output reports generally require us to stay well within the program's limits.

*Case 1: Crossed wires meeting at other than a segment or wire junction:* Our first case is a clear violation of NEC rules. In the model below, the two wires cross and join in the middle of the center segment of each wire. **Fig. 1** shows the view of the situation.

```
CM crossing wires
CE
GW 1 9 0 0 0 0 0 .25 .001
GW 2 9 -.125 0 .125 .125 0 .125 .001
GE 0 0 0
FR 0 1 0 0 299.7925 1
EX 0 1 1 00 1 0
EN
```

Fig. 1



Case 1: Wires Crossing at Other Than a Segment  
or a Wire Junction

NEC-2 will run this model without comment. However, NEC-4 may abort the run, depending on the setting of the GE command. Even if the model runs in accord with the user's instructions, the output report will return the error message in **Fig. 2**. The three lines are essentially encapsulated in the first line, but the segment-check feature aims for completeness.



NEC-4 Warning

Fig. 2

SEGCHK: ERROR - SEGMENTS 5 AND 14 INTERSECT AT A MIDPOINT

SEGCHK: WARNING - THE CENTER OF SEGMENT 5 IS WITHIN THE VOLUME OF SEGMENT 14

SEGCHK: WARNING - THE CENTER OF SEGMENT 14 IS WITHIN THE VOLUME OF SEGMENT 5

NEC Output Report of Crossing-Wire Condition (NEC-4 Only)

The second entry in the GE command dictates whether NEC-4 aborts the run in the presence of errors along or in the presence of either errors and/or warnings. **Fig. 3** shows the GNEC set-up screen with explanations for the options to run or to abort in the center section. I have added the numbers that will appear in the command line for each user selection. NEC-2 does not have anything corresponding to the NEC-4 GE options.

Regardless of which option you choose, referring to the output file is necessary to understand what error or warning is at work and hence what may be at fault with a model. Errors and warning applicable to the geometry (wire) structure of the model appear at the very beginning of the output report, immediately after the core's interpretation of the geometry commands through the GE command.

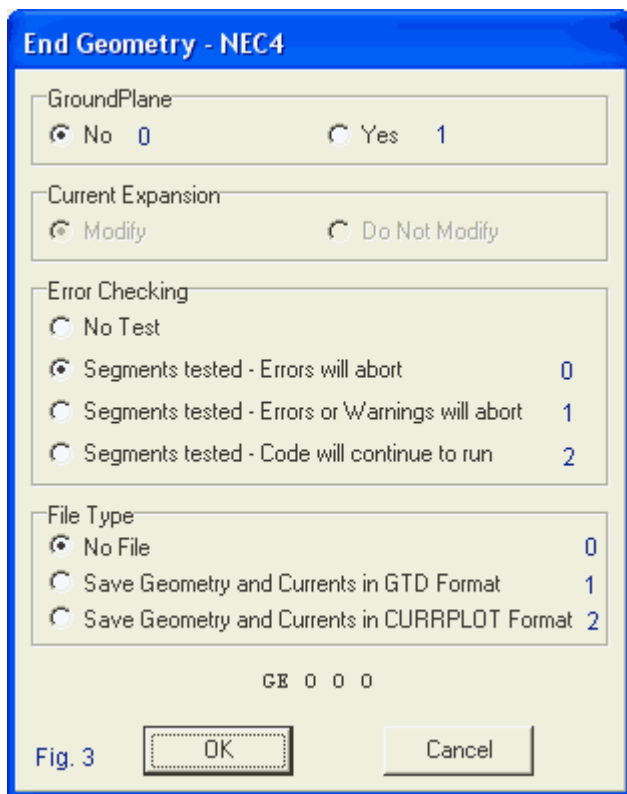


Fig. 3

There is a distinction between error and warning messages. "When segment testing is requested. . . , error messages are printed [in the output report] for illegal segment intersections and warning messages are printed for violations of the thin-wire approximation. An illegal intersection is indicated when the minimum separation of the segments at a point other than at the segment ends is less than

$10^{-3}$  times the length of the shorter of the two segments. A violation of the thin-wire approximation is indicated when the minimum separation of non-connected segments is less than the sum of their radii. A warning message is also printed if the center of a segment is within the volume of another segment." (p. 27, NEC-4 Manual) This latter warning sets up a limit to the angle at which two wires may meet based upon both the radius and the segment lengths in each wire. These are not the totality of warnings that may appear in a NEC-4 output report.

*Case 2: The interpenetration of parallel wires:* When two wires are separated by less than the sum of their radii, we generically refer to them as interpenetrating. In other words, even though their axes are separate, their surfaces are not. The following model samples this condition with parallel wires. The sum of the radii is 0.012 m, but their axes are separated by only 0.01 m. **Fig. 4** shows the outline of the situation and the set of warnings generated by NEC.

```
CM interpenetrating wires
CE
GW 1 9 0 0 0 0 0 .25 .006
GW 2 9 .01 0 0 .01 0 .25 .006
GE 0 0 0
FR 0 1 0 0 299.7925 1
EX 0 1 1 00 1 0
EN
```

```

SEGCHK: WARNING - SEGMENTS 1 AND 10 ARE PARALLEL AND SEPARATED BY LESS THAN THE SUM OF THEIR RADII
SEGCHK: WARNING - SEGMENTS 2 AND 11 ARE PARALLEL AND SEPARATED BY LESS THAN THE SUM OF THEIR RADII
SEGCHK: WARNING - SEGMENTS 3 AND 12 ARE PARALLEL AND SEPARATED BY LESS THAN THE SUM OF THEIR RADII
SEGCHK: WARNING - SEGMENTS 4 AND 13 ARE PARALLEL AND SEPARATED BY LESS THAN THE SUM OF THEIR RADII
SEGCHK: WARNING - SEGMENTS 5 AND 14 ARE PARALLEL AND SEPARATED BY LESS THAN THE SUM OF THEIR RADII
SEGCHK: WARNING - SEGMENTS 6 AND 15 ARE PARALLEL AND SEPARATED BY LESS THAN THE SUM OF THEIR RADII
SEGCHK: WARNING - SEGMENTS 7 AND 16 ARE PARALLEL AND SEPARATED BY LESS THAN THE SUM OF THEIR RADII
SEGCHK: WARNING - SEGMENTS 8 AND 17 ARE PARALLEL AND SEPARATED BY LESS THAN THE SUM OF THEIR RADII
SEGCHK: WARNING - SEGMENTS 9 AND 18 ARE PARALLEL AND SEPARATED BY LESS THAN THE SUM OF THEIR RADII

```

NEC-4 Warning of Parallel Interpenetrating Wires

Wire Radii: 0.006  
C-C Spacing 0.01

Case 2: Wire Interpenetration: Outline and NEC-4 Warning

Fig. 4

The outline of the parallel wires shows two distinct wires and does not reveal the interpenetration. Most (but not necessarily all) graphic representations of models use simple lines connecting the wire end coordinates. They normally do not show the wire thickness. Therefore, the outline may not show an error or a warning condition.

Note that these are warnings and not an error. Therefore, it is possible to set up the GE command to allow this model to run, while still trapping errors with an abort of the run. However, the results of the run will not be reliable. Indeed, merely increasing the separation of the wires to eliminate the warning list may not be enough separation to yield a reliable model. For close spacing that does not result in interpenetration of wires, the average gain (AGT) test is still the most important first-order test of model reliability.

*Cases 3a and 3b: Angularly approaching wires:* If two wires approach each other at an angle, it is possible to incur warnings of interpenetration at the narrow end of the angle. The following model, in which the wires meet at the "top", is such a case. **Fig. 5** on the left shows the outline with a distinct junction of the wires at one end.

CM interpenetrating wires

CE

GW 1 9 0 0 0 0 0 .25 .006

GW 2 9 .013 0 0 0 0 .25 .006

GE 0 0 0

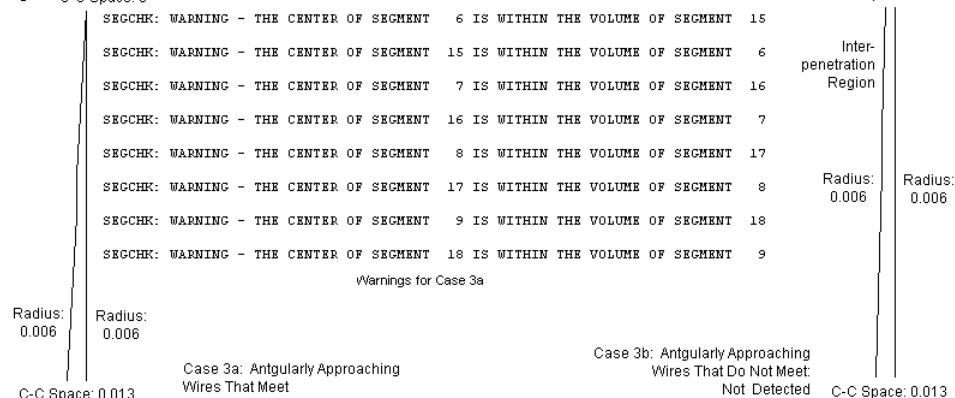
FR 0 1 0 0 299.7925 1

EX 0 1 1 00 1 0

RP 0 181 1 1000 -90 90 1.00000 1.00000

EN

Fig. 5 C-C Space: 0



Because the wires are not parallel, the warning message differs from the previous case. The top four segments of each wire

interpenetrate to the degree where the center of the listed wire is within the volume, that is, inside the radius, of the noted segment of the adjacent wire. This condition normally results in errors in the current calculations for the affected wire segments. (Also note that the error messages use the absolute segment number rather than the tag number and the relative segment number.)

We may modify the case just slightly so that the wires do not join at the ends. We need modify only 1 of the 2 GW entries.

```
GW 1 9 0 0 0 0 0 .25 .006
GW 2 9 .013 0 0 .007 0 .25 .006
```

The revision results in the outline at the right of **Fig. 5**. The close center-to-center (C-C) spacing of the wires at the top indicates, by reference to the wire radii, that we certainly have wire segment interpenetration for at least two or three segments. However, because the wires are not parallel and do not meet at the end, NEC-4 shows no warnings. Wherever wires come into close proximity, the AGT test is a necessary step in model evaluation. Despite the seeming simplicity of the revised model, its AGT score is 0.937, meaning a gain error that approaches -0.3-dB. In most instances, model revision to improve the AGT score would be advisable.

If the implementation of NEC applies additional checks to the model, the situation might well be detected and reported. For example, some implementations take wire radius into consideration for all geometry situations. Such a system would report the

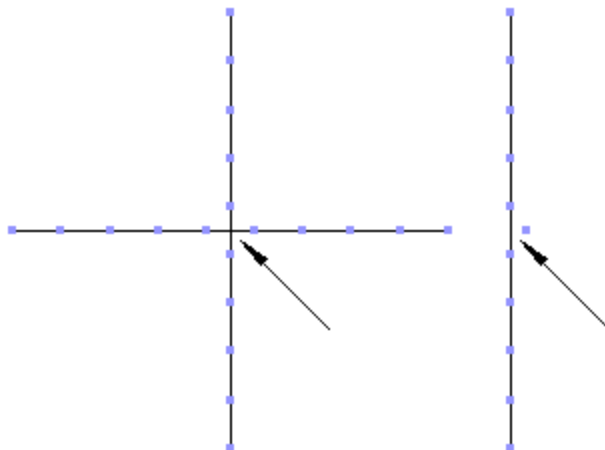
interpenetration and either prevent a core calculation run or advise a model revision.

*Case 4: Crossing interpenetrating wires:* Although NEC-4 will not detect the situation of case 3b, it will detect wires that cross without touching at mid-segment while in a condition of surface interpenetration. The following model, with wires at right angles to each other, illustrates the condition.

```
CM interpenetrating wires
CE
GW 1 9 0 0 0 0 0 .25 .006
GW 2 9 -.125 .01 .125 .125 .01 .125 .006
GE 0 0 0
FR 0 1 0 0 299.7925 1
EX 0 1 1 00 1 0
EN
```

The wire axes are separated by 0.010 m while the radii are both 0.006. Hence there is a 0.002-m interpenetration at the crossing point, that is, relative to the center segments of both wires. **Fig. 6** shows the outline and the warning. The warning message is specific to this type of modeling situation. As usual, the outline uses a single wire along the axis of each wire and therefore does not itself reveal the interpenetration.

Fig. 6



SEGCHK: WARNING - SEGMENTS 5 AND 14 CROSS AT A  
MIDPOINT WITH SEPARATION LESS THAN THE SUM OF  
THEIR RADII

#### Case 4.: Crossing Interpenetrating Wires

All of the errors and warnings that we have so far illustrated show themselves in the form of messages that occur immediately following the core's interpretation of the geometry entries. Although we have been using very simple cases with only GW entries, it is possible to incur "hidden" errors or warnings by the use of some of the other geometry commands. CW, GM, GX, GR, and GA all create wire segments that may or may not be in the clear relative to other wires in the geometry structure. Therefore, reference to the



output report is essential to ensure that the overall structure meets the NEC guideline limits.

*Case 5: Interpenetration insulated sheaths:* Not all warnings and errors involve the geometry commands. Errors and warnings that concern control commands do not occur in the geometry section of the output report. Rather, they occur in the report section directly relevant to the command interpretation. As a result, we may easily overlook them and miss an unintended modification to the model.

The following model sets up two crossing wires that are--with respect to the GW commands--separated enough to pass all tests. The wire radii are 0.001-m, while the separation is 0.01-m. However, the subsequent IS commands set up two sheaths, each with a radius of 0.006-m. Therefore, the sheaths interpenetrate at the crossing point between wires.

```
CM interpenetrating wires-IS
CE
GW 1 9 0 0 0 0 0 .25 .001
GW 2 9 -.125 .01 .125 .125 .01 .125 .001
GE 0 0 0
IS 0 1 1 9 1 1e-10 .006
IS 0 1 1 9 1 1e-10 .006
FR 0 1 0 0 299.7925 1
EX 0 1 1 00 1 0
RP 0 181 1 1000 -90 90 1.00000 1.00000
EN
```

The 0.002-m interpenetration of insulating material may seem innocuous. However, as shown in **Fig. 7**, the warning advises

otherwise. The interpenetration of sheaths results in one of the sheath commands being ignored, which modifies the model relative to the modeler's original intent to have two insulated wires.

Fig. 7

```

- - - WIRE SHEATH PARAMETERS - - -

      SEGMENTS      RELATIVE      CONDUCTIVITY      SHEATH RAD.
TAG  FROM  THRU  PERMITTIVITY  (MHOS/M)      (M)

      1      1      9  1.00000E+00  1.00000E-10  6.00000E-03
      1      1      9  1.00000E+00  1.00000E-10  6.00000E-03

INSET: WARNING - OVERLAPPING SHEATH SPECIFICATIONS.  LAST ONE WAS USED.

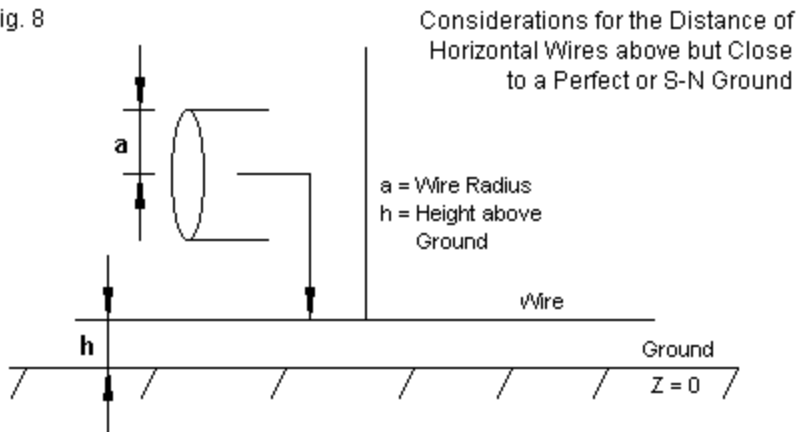
```

#### Case 5: Crossing Wires with Only Interpenetrating Sheaths (IS)

The warning appears only in the section of the output report devoted to the IS command. Unless an implementation of NEC uses an error checking system sufficiently extensive to report such problems before a core run, a careful reading of the output report may be the only way of catching the difficulty.

*Case 6: Horizontal wires close to but above ground:* The NEC-2 manual is quite explicit about the limits of a wire's height (z-coordinates) when the wire is not vertical. As shown in **Fig. 8**, the NEC-2 Manual, Section 3. Modeling Structures Over Ground, specifies that for a wire of radius  $a$  and height  $h$  to the wire axis,  $(h^2 + a^2)^{1/2} > (\text{about}) 10^{-6}$  wavelength. It also notes that  $h$  should be several times the radius for the thin-wire approximation to be valid.

Fig. 8



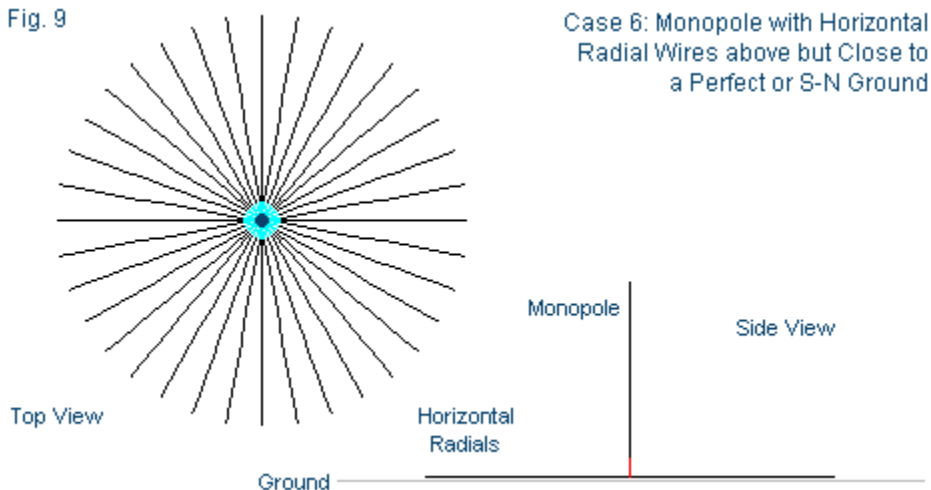
In the user guide for the GE command, the manual also states, "If the height of a horizontal wire is less than  $10^{-3}$  times the segment length, I1 equal to 1 will connect the end of every segment in the wire to ground. I1 should then be -1 to avoid this disaster." I1 is the first digit of the GE command (where a zero means free space or no ground at all). A 1 means that there is a ground plane and that the currents on segments touching the ground in the X-Y plane are interpolated to their images below the ground and the charge at the wire base is zero. In contrast, -1 results in no current expansion modification so that the current on wires touching ground go to zero at ground or  $Z=0$ .

The situation sounds straightforward until we pose the question of when a horizontal wire is close enough to ground to incur the difference between setting GE at 1 or at -1. The options are the

surface of the wire, as defined by its Z-coordinate plus the radius of the wire, or the axis of the wire, that is, its Z-coordinate alone. The warnings that emerge from the various cases of interpenetration might strongly suggest the first option to some, although the manual is not explicit on the matter.

Therefore, I set up a test model consisting of 36 horizontal radials with a simple monopole, as shown in **Fig. 9**. The wire radius is 0.001 m. The segment length for a radial is 0.025 m, while the segment length for the monopole is 0.0239 m. (At the test frequency, 1 m = 1 wavelength.)

Fig. 9



The basic model appears below. The initial height is 0.003 m above ground. This places the horizontal radial wires along their axes at 3

times the wire radius, a rough meeting of the injunction that the value of  $h$  be several times the value of  $a$ . The height also easily meets the minimum value of  $h$  and  $a$  taken together.

#### CM GR Radials for Monopole

CE

GW 1 10 0 0 .003 .25 0 .003 .001

GR 1 36

GW 37 10 0 0 .003 0 0 .243 .001

GE 1 2 0

GN 2 0 0 0 13.0000 0.0050

FR 0 1 0 0 299.7925 1

EX 0 37 1 00 1 0

RP 0 181 1 1000 -90 90 1.00000 1.00000

EN

I then gradually lowered the height of the entire assembly in small steps. Among the more important steps is a height of 0.0011 m. This height would be the last allowable height if NEC faulted the model when the horizontal wire surfaces touched ground. A height of 0.001 m would place the radial wire surfaces in contact with ground. The next height, 0.0009 m would count as a definite penetration of the wire surface into ground. A height of 0.00002 m would place the horizontal wire axes just below the limit of being greater than 1/1000 of the segment length above ground.

The question becomes at what height the model shows a fault with  $GE = 1$  and with  $GE = -1$ . I ran the sequence of models in both NEC-2 and NEC-4 to see what kinds of error conditions might appear with each core. The results appear in **Table 1**.

Table 1. Series of NEC models with horizontal wires above but close to ground ( $Z=0$ )

H (m=wl)	NEC-4			NEC-2		
	Gn dBi	Theta °	R+/-jXΩ	Gn dBi	Theta °	R+/-jXΩ
0.003	0.46	63	32.2 – j1.8	0.52	63	31.9 – j1.0
0.002	0.53	63	31.9 – j2.9	0.56	63	31.7 – j2.0
0.0015	0.58	63	31.9 – j2.3	0.60	63	31.9 – j1.3
0.0011	0.63	62	32.0 – j1.7	0.63	63	32.2 – j0.6
0.001	0.64	62	32.1 – j1.4	0.63	62	32.3 – j0.4
0.0009	0.65	62	32.2 – j1.2	0.64	62	32.4 – j0.2
0.0005	0.70	62	32.7 – j0.2	0.68	62	32.9 + j0.7
0.0002	0.76	62	32.9 + j0.5	0.72	62	33.2 + j1.2
with GE = +1						
0.00002	no-run: segment 1 in ground plane			no-run: segment 1 in ground plane		
0.0	no-run: segment 1 in ground plane			no-run: segment 1 in ground plane		
with GE = -1						
0.00002	0.81	62	32.7 + 0.7	0.76	62	32.9 + j1.2
0.0	-2.97	63	42.4 – j96.6	0.77	62	33.0 + j1.4

Note: Wire radius 0.001 m ( $\lambda$ ); monopole segment length 0.0239 m ( $\lambda$ ); radial segment length 0.025 m ( $\lambda$ )

All heights from 0.003 m down to 0.0002 m produce no error reports in either NEC-2 or NEC-4 with GE set to 1. Moreover, the sequence of gain, theta-angle, and impedance values are quite sensible. In fact, both cores, although they return very slightly different numbers, show the same trends in all three categories. The progressions of both source resistance and source reactance are parallel throughout the progression. These results do not mean that pressing the base of the monopole and the radials downward represents good modeling practice, since the height no longer meets the height-to-wire-radius recommendation. It merely records the fact that nothing disastrous occurs.

With  $GE = 1$ , the lowest two entries record the fact that the cores of both NEC-2 and NEC-4 abort the run and show an error (not a warning) message, as indicated in the table. Since I have only a limited number of NEC-2 cores, it is not clear whether the error report using that core originally came with the core or whether the implementation (NSI) added the message. The NEC-4 core message apparently is inherent to the core as issued.

With  $GE = -1$ , both cores allow the full run with no error reported. When the wire axis is as close as 0.00002 m from the ground, both cores record sensible additions to the progression of values for higher values of  $Z$ . However, at  $Z=0$ , only the NEC-2 core records a seemingly sensible result, while the NEC-4 core result is not an extension of the progression of values in the table.

In both settings for the  $GE$  command, the models fall well below guidelines for good modeling practice and do not represent values for  $h$  that anyone should recommend for virtually any wire radius. Nevertheless, they allow one kind of answer to our inquiry into whether NEC uses the surface or the axis of the wire in determining when an error has occurred with  $GE = 1$ . The answer is that it uses the wire axis. Those who create implementations of either NEC-2 or NEC-4, of course, are free to alter this limit by applying run-abort messages or other flags to indicate when some part of a model lies outside the limits of recommended modeling practices. EZNEC, for example, applies the implicit  $Z$ -coordinate of the lowest point on a wire's surface to determine when the wire is too close to ground.

Vertical and sloping wires, of course, can legitimately reach ground or have a terminating Z-coordinate of zero. Both types of wires are useful in NEC-2 with a perfect ground. For a sloping wire, NEC ignores the wire's surface penetration below ground. Likewise, when penetrating below ground in NEC-4, the wire must reach  $Z=0$  at a segment junction or end, which includes a wire end. A new segment takes up the below-ground portion of the wire in either case. Again, NEC ignores the angular penetration of the segment either above or below ground.

*Conclusion:* We have examined a number of error and warning conditions that can arise in NEC, especially NEC-4, with reference to messages and actions taken by the cores themselves. We have had several goals. The first has been to show the conditions under which NEC will return an error or warning message. Most, but not all, such messages are built into NEC-4 alone, which has an internal segment-checking system. For the most part, NEC-2 lacks the system and may let such models run.

When NEC aborts a run--or even when it does not--we need to know where to find the error. The NEC output report is the locus of such reports. Reports relating to the basic geometry of the wire structure occur at the very beginning of the report. However, examining every section of the report is useful, since it may catch warning relating to control commands that can modify a model relative to one's initial intentions. The IS-command case well illustrated the need for close scrutiny of the report. That was our second goal.



The final aim was to clarify some of the error and warning reports and when they occur and do not occur. The wire penetration of sloping but unjoined wires was a case in point that showed the limitations of the segment-checking system. The monopole + radial model in Case 6 allowed us to determine the basis for NEC error reports for horizontal wires that are too close to ground.

Nothing in these notes is a license for any violation of good modeling practice. Applying the average gain test remains the first line of defense against inadequate models, but it only establishes the necessary, not the sufficient conditions of model adequacy. In the end, the final test is a correlation of the model with reliable measurements of physical implementations of the antenna modeled.

***[ THE END OF A 12.25-YEAR SERIES ]***

## Other Publications

We hope you've enjoyed this 7th in a series of volumes of the **Antenna Modeling Notes**. This is the final volume of this series. Together with existing volumes 1 through 7 of this series, you'll find many other very fine books and publications by the author L.B. Cebik, W4RNL and other fine authors in the ***antenneX Online Magazine BookShelf*** at the web site shown below.

---

***A Publication by  
antenneX Online Magazine***

**<http://www.antennex.com/>**

**POB 271229**

**Corpus Christi, Texas 78427-1229**

**USA**

**August 2010**

---

Copyright © 2010 by ***antenneX Online Magazine***. All rights reserved. No part of this book may be reproduced or transmitted in any form, by any means (electronic, photocopying, recording, or otherwise) without the prior written permission of the publisher.

ISBN: 1-877992-59-3

---